

**ISTANBUL TECHNICAL UNIVERSITY ★ EARTHQUAKE ENGINEERING
AND DISASTER MANAGEMENT INSTITUTE**

**VALUE OF INFORMATION OBTAINED USING STRUCTURAL HEALTH
MONITORING OF AN RC BRIDGE SUBJECTED TO SEISMIC HAZARD**



M.Sc. THESIS

Siamak TAHAEI YAGHOUBI

Earthquake Engineering and Disaster Management Institute

Earthquake Engineering Program

Thesis Advisor: Assoc. Prof. Dr. Ufuk YAZGAN

January 2019

**ISTANBUL TECHNICAL UNIVERSITY ★ EARTHQUAKE ENGINEERING
AND DISASTER MANAGEMENT INSTITUTE**

**VALUE OF INFORMATION OBTAINED USING STRUCTURAL HEALTH
MONITORING OF AN RC BRIDGE SUBJECTED TO SEISMIC HAZARD**



M.Sc. THESIS

**Siamak TAHAEI YAGHOUBI
(802141241)**

Earthquake Engineering and Disaster Management Institute

Earthquake Engineering Program

Thesis Advisor: Assoc. Prof. Dr. Ufuk YAZGAN

JANUARY 2019

İSTANBUL TEKNİK ÜNİVERSİTESİ ★ DEPREM MÜHENDİSLİĞİ VE
AFET YÖNETİMİ ENSTİTÜSÜ

DEPREM TEHLİKESİNE MARUZ KALAN BİR BETONARME KÖPRÜ
İÇİN YAPISAL SAĞLIK İZLEME YÖNTEMİYLE ELDE EDİLEN
VERİLERİN DEĞERİ

YÜKSEK LİSANS TEZİ

Siamak TAHAEI YAGHOUBI
(802141241)

Deprem Mühendisliği ve Afet Yönetimi Anabilim Dalı

Deprem Mühendisliği Programı

Tez Danışmanı: Doç. Dr. Ufuk YAZGAN

OCAK 2019

Siamak TAHAEI YAGHOUBI, a M.Sc. student of İTÜ Institute of EARTH QUAKE ENGINEERING AND DISASTER MANAGEMENT SCIENCES student ID 802141241, successfully defended the thesis/dissertation entitled “VALUE OF INFORMATION OBTAINED USING STRUCTURAL HEALTH MONITORING OF AN RC BRIDGE SUBJECTED TO SEISMIC HAZARD”, which he prepared after fulfilling the requirements specified in the associated legislations, the jury whose signatures are below.

Thesis Advisor : **Assoc. Prof. Dr. Ufuk YAZGAN**
Istanbul Technical University

Jury Members : **Assoc. Prof. Dr. Serdar SOYÖZ**
Boğaziçi University

Assoc. Prof. Dr. Barlas Özden ÇAĞLAYAN.....
Istanbul Technical University

Date of Submission : 30 January 2019
Date of Defense : 11 January 2019





To my family,



FOREWORD

It is an honour for me to express my sincere gratefulness to Assoc. Prof. Dr. Ufuk Yazgan, my thesis advisor, whose kind support, patience and deep knowledge were great assets to me throughout this project. I am also keen to thank Dr. Yazgan for what I can name his democratic attitude. This democratic manner and his respect to new ideas encouraged me to go my own way every now and then, experience unforeseen challenges and learn from my mistakes. Dr. Yazgan was always ready to patiently and enthusiastically correct my mistakes and direct me with precious technical recommendations. I feel I was very lucky to have the chance to learn from a researcher who is so interested in science and engineering and always enthusiastic to broaden his horizons. Finally, I must honestly state that without his guidance and assistance this thesis would not have been completed.

January 2019

Siamak Tahaei Yaghoubi
(Civil Engineer)



TABLE OF CONTENTS

	<u>Page</u>
FOREWORD	ix
TABLE OF CONTENTS	xi
ABBREVIATIONS	xv
SYMBOLS	xvii
LIST OF TABLES	xxi
LIST OF FIGURES	xxiii
SUMMARY	xxix
ÖZET	xxxi
1. INTRODUCTION	1
1.1 Bridges and Earthquakes	1
1.2 Consequences of Bridge Failures and Importance of Inspection and Monitoring of Bridges.....	2
1.3 Efforts for Quantifying Value of Information and Its Importance.....	4
1.4 Scope of Research	8
2. BRIDGE STRUCTURE AND ITS MODELLING	11
2.1 Introduction	11
2.2 Geometrical and Structural Properties of the Bridge	11
2.3 Modelling Programme.....	16
2.4 General View of Elek Deresi Bridge Model	16
2.4.1 Calculating mass of the bridge and gravity analysis.....	25
2.4.2 Idealisation of elastomeric bearings.....	27
2.4.3 Idealisation of abutments	30
2.4.3.1 Calculations.....	33
2.4.4 Simulating collision between bridge components	34
2.4.5 Introducing zerolength elements used in the model.....	37
2.4.6 Idealisation of the superstructure	38
2.4.7 Idealisation of bent system.....	41
2.4.7.1 Materials representing axial, shear and torsional force-deformation characteristics.....	43
2.4.7.2 Materials representing moment-curvature characteristics	43
2.5 Determining Properties of Confined and Unconfined Concrete	44
2.6 Moment-Curvature Analysis of Bent System Sections.....	47
2.6.1 Material models for moment-curvature analysis	48
2.6.2 Moment-curvature curves and their idealisations	50
2.7 Calculating Lengths of Strain Penetration and Plastic Hinges.....	56
2.8 Defining Damping Matrix of the Structure	58
2.9 Pushover Analysis	60
2.10 Eigenvalue Analysis and Mode Shapes of Vibration.....	64
3. ESTIMATION OF UNCONDITIONAL SEISMIC HAZARD RISKS	67
3.1 Introduction	67

3.2 Statistical Parameters of Materials	68
3.2.1 Variations in reinforced concrete properties due to changes in steel strengths	69
3.2.2 Moment-curvature analysis results.....	72
3.2.3 Changes in elastic stiffness values with variations in steel properties.....	79
3.2.4 Changes in plastic hinge lengths with variations in steel properties.....	79
3.2.5 Changes to dynamic properties of models as a result of variations in steel properties.....	81
3.3 Seismic Risk Assessment of Elek Deresi Bridge Using the 2000 SAC/FEMA method	83
3.3.1 Introduction	83
3.3.2 Description of the method	83
3.3.3 Hazard curve for Elek Deresi Bridge	86
3.3.4 Specifications of strong ground motion records	88
3.4 Application of the 2000 SAC/FEMA Method to Elek Deresi Bridge Models.	98
3.4.1 Damage levels and limit states	98
3.4.2 Statistical parameters of demand random element.....	100
3.4.3 Determining statistical parameters of capacity random element	101
3.4.3.1 Results of nonlinear dynamic analyses, determining values of constants a and b and dispersion of demand random element (β_D)	104
3.4.3.2 Failure probabilities in terms of different limit states	119
4. DECISION TREE, COST ESTIMATION AND VALUE OF INFORMATION	123
4.1 Introduction	123
4.2 Decision Tree and Its Structure	124
4.3 Monte Carlo Simulation Technique and Its Application to the Problem	127
4.4 Cost Estimations.....	129
4.4.1 Initial construction cost	129
4.4.2 Repair costs for different damage states	132
4.4.3 Retrofitting and resultant costs.....	133
4.4.3.1 Retrofitting	133
4.4.3.2 Steel jacketing for columns and related expenses	133
4.4.4 Indirect costs	135
4.4.5 Annual and life-time failure and damage probabilities in terms of different limit states and damage levels for the as-built structure	135
4.4.6 Annual and life-time failure and damage probabilities in terms of different limit states and damage levels for the retrofitted structure	137
4.4.7 Expected annual costs and optimal alternative for the non-monitored structure.....	142
4.5 Improving the State of Decision Making by Additional Information	146
4.5.1 Application of preposterior analysis to the problem	147
4.5.2 Formulation of the problem.....	148
4.5.2.1 Determining statistical properties of SHM system output	148
4.5.2.2 Estimating probabilities of outcomes from the SHM system	151
4.5.2.3 Updating probability distribution functions of steel	152
4.5.2.4 Cost of monitoring	155
4.5.3 Value of information and value of perfect information	157
4.5.4 Field modal vibration dynamic testing method of bridge substructures by FHWA.....	162
4.5.5 Elastic FE model for modal analysis of bent system	163

4.5.6 Assessing value of information by monitoring fundamental period of the bent system.....	164
5. CONCLUSIONS AND RECOMMENDATIONS.....	173
5.1 Conclusions	173
5.2 Recommendations	175
REFERENCES	177
APPENDICES	181
CURRICULUM VITAE.....	183





ABBREVIATIONS

Caltrans	: California Department of Transportation
CEB	: Comité Euro-International du Béton
DAC	: Central Data Acquisition
DDA	: Damage Detection Algorithm
DDS	: Damage Detection System
EAPA	: European Asphalt Pavement Association
EMV	: Expected Monetary Value
FDOT	: Florida Department of Transportation
FE	: Finite Element
FHWA	: Federal Highway Administration
fib	: Fédération internationale du béton
FIP	: Fédération Internationale de la Précontrainte
HHT	: Hilbert-Huang Transform
km	: Kilometre
MEMS	: Micro Electro-Mechanical System
MSC	: Multispan Continuous
MSSS	: Multi-Span Simply Seated
NDE	: Non-Destructive Evaluation
NDOT	: Nevada Department of Transportation
NDT	: Non-Destructive Test
OpenSees	: Open System for Earthquake Engineering Simulation
PA	: Pushover Analysis
PC	: Precast Concrete
PDF	: Probability Density Function
PEER	: The Pacific Earthquake Engineering Research Center
PS	: Prestressed
RC	: Reinforced Concrete
SHARE	: Seismic Hazard Harmonization in Europe
SHM	: Structural Health Monitoring
TEC	: Turkish Earthquake Code

TF : Modal Transfer Function
TSO : The Stationery Office
USGS : The United States Geological Survey
VI : Value of Information
VPI : Value of Perfect Information
WSN : Wireless Sensor Network



SYMBOLS

\overline{a}_m	: Non- Monitored Structure Alternative
\overline{a}_r	: Non-Retrofitted (As-Built) Structure Alternative
A_{cc}	: Area of Core Concrete
A_e	: Effective Abutment Area
A_e	: Effectively Confined Concrete Area
\hat{C}	: Median Value of Capacity
\hat{D}	: Median Value of Demand
E_c	: Young's Modulus of Concrete
E_{sec}	: Secant Modulus of Confined Concrete
$F_{friction}$: Friction Force
$H_D(d)$: Demand Hazard
I_{gross}	: Moment of Inertia of Un-Cracked Concrete Section
I_{yy}	: Second Moment of Area About Local y Axis
I_{zz}	: Second Moment of Area About Local z Axis
K_{abut}	: Abutment Stiffness
$K_{bearing}$: Bearing Stiffness
K_i	: Initial Stiffness of Embankment Fill Materials
L_C	: Length from the Critical Section to the Point of Contraflexure
L_P	: Plastic Hinge Length
L_{SP}	: Strain Penetration Length
M_N	: Nominal Yield Moment
M_r	: Residual Moment
M_u	: Ultimate Moment
M_y	: First Yield Moment
P_{bw}	: Ultimate Capacity of Abutment
P_f	: Probability of Failure
S_a	: Pseudo-Spectral Acceleration
T_1	: Actual (True) Fundamental Period of the Bridge
T'_1	: Fundamental Period of the Bridge by FE model

V_S	: Coefficient of Variation of Steel Yield Stress
a_i	: Alternative i
a_{opt}	: Optimal Alternative
a_r^*	: Optimal Alternative of Retrofitting or Non-Retrofitting Options
a_β	: Y Intercept of the Regression Line Fitted to Demand Dispersion - S_a points
a_0	: Rayleigh Damping Coefficient
a_1	: Rayleigh Damping Coefficient
b_β	: Slope of Regression Line Fitted to Demand Dispersion - S_a points
d_{bl}	: Diameter of Longitudinal Reinforcing Bars
f'_{cc}	: Ultimate Strength of Confined Concrete in Compression
f'_{co}	: Unconfined Compressive Strength of Concrete
f_u	: Ultimate Stress of Reinforcing Bars
f_y	: Yield Strength of Reinforcing Steel (also shown by s)
f_{ye}	: Yield Strength of Longitudinal Reinforcing Bars
f_{yh}	: Yield Strength of Transverse Reinforcement
h_{bw}	: Back Wall Height
h_{rt}	: Combined Thickness of Rubber Layers of an Elastomeric Bearing
h_s	: Thickness of Steel Shims of an Elastomeric Bearing
h_t	: Thickness of Elastomeric Bearing
k_e	: Confinement Effectiveness Coefficient
k_0	: Idealised Hazard Curve Constant
l_s	: Limit State
w_{bw}	: Back Wall Width
A	: Area
C	: Compressive Force
C	: Capacity
C	: Cost
D	: Demand
G	: Shear Modulus
J	: Torsional Moment of Inertia
L	: Length
$M.F.$: Modification Factor
T	: Twisting Moment

T	: Period
V	: Coefficient of Variation
X	: Material Random Variable
Y	: Model Uncertainty Random Variable
a	: Constant Relating Demand Dispersion to Pseudo-Spectral Acceleration
b	: Constant Relating Demand Dispersion to Pseudo-Spectral Acceleration
c	: Classical Damping Matrix
k	: Constant for Strain Penetration
k	: Classical Damping Matrix
k	: Idealised Hazard Curve Constant
m	: Classical Mass Matrix
n	: Number of Steel Samples Generated
n	: Number of Steel Shims in Elastomeric Bearings
o	: Outcome of the SHM System
s	: Yield Strength of Reinforcing Steel
s	: Yield Strength of Reinforcing Steel (also shown by f_y)
t	: Time (in Years)
u	: Uniformly Distributed Random Number Between 0 and 1
z	: Standard Normal Random Number Generated from u
$\Delta\phi$: Relative Angle of Twist
β_C	: Capacity Dispersion (Natural Logarithm of Standard Deviation of Capacity)
ϵ_{cc}	: Strain at Maximum Confined Concrete Stress
ϵ_{co}	: Strain at Maximum Stress of Unconfined Concrete
ϵ_{cu}	: Ultimate Concrete Compressive Strain
ϵ_s	: Steel Strain
ϵ_{sp}	: Ultimate Strain of Unconfined Concrete
ϵ_{su}	: Ultimate Strain of Transverse Reinforcement
ζ	: Damping Ratio
$\mu_{f'_{co}}$: Mean Unconfined Concrete Strength
μ_{f_y}	: Mean Steel Yield Stress (also shown by μ_s)
μ_s	: Mean Steel Yield Stress (also shown by μ_{f_y})
ρ_s	: Ratio of Volume of Transverse Bars to Volume of Confined Core

$\sigma_{f'_{co}}$: Standard Deviation of Unconfined Concrete Strength
σ_{f_y}	: Standard Deviation of Steel Strength (also shown by σ_s)
σ_{lns}	: Dispersion (Logarithmic Standard Deviation of steel strength)
σ_s	: Standard Deviation of Steel Strength (also shown by σ_{f_y})
σ^2	: Variance
ω_n	: Natural Circular Frequency for the nth Mode
$\phi_{Cracking}$: Cracking Curvature
$\phi_{Spalling}$: Spalling Curvature
$\phi_{Ultimate}$: Ultimate Curvature
ϕ_{Yield}	: Nominal Yield Curvature
ϕ_r	: Post-ultimate Curvature
$\phi_{u,exp}$: Experimental Ultimate Curvature
$\phi_{u,pred}$: Predicted Ultimate Curvature
ϕ_u	: Ultimate Curvature
$\phi_{y,exp}$: Experimental Yield Curvature
$\phi_{y,pred}$: Predicted Ultimate Curvature
ϕ_y	: Nominal Yield Curvature
ϕ'_y	: First Yield Curvature
Φ	: Standard Normal Cumulative Distribution Function
γ	: Factor Applied to Standard Deviation of Steel to Define Various Samples
λ	: Rate of Occurrence of Seismic Events
μ	: Friction Coefficient
ν	: Poisson's Ratio
ϵ	: Error

LIST OF TABLES

	<u>Page</u>
Table 2.1: Summary of materials employed for zerolength elements.....	36
Table 2.2 : Sectional properties used for modelling elements of superstructure.	41
Table 2.3 : Sectional properties of cap beam and column elements.	42
Table 2.4 : Calculated parameters of stress-strain curve for columns and cap beam.	47
Table 2.5 : Bilinear idealisation of moment-curvature analysis results for column and cap beam sections.	53
Table 2.6 : Elastic and gross stiffness values and their ratios.	56
Table 2.7 : Strain penetration and plastic hinge lengths for a sample constructed from concrete of $f'_{co} = 21.75 \text{ MPa}$ and steel of $f_y = 472.41 \text{ MPa}$	57
Table 2.8 : Characteristic values and natural vibration properties corresponding to the first three modes for a model of ($f'_{co} = 21.75 \text{ MPa}$ and steel of $f_y = 472.41$ MPa).	65
Table 3.1 : Statistical parameters of unconfined concrete and reinforcing steel,.....	68
Table 3.2 : Statistical parameters regarding Elek Deresi Bridge materials.....	68
Table 3.3 : Variations in specifications of confined concrete of capbeam section as a result of changes in steel properties.	70
Table 3.4 : Variations in properties of confined concrete of column sections as a result of changes in unconfined concrete and steel properties.	71
Table 3.5 : Moment-curvature analysis results for capbeam and columns sections made from steel with different properties.	78
Table 3.6 : Elastic and gross stiffness values and their ratios for members built from reinforcing bars with differing yield stress values.	80
Table 3.7 : Strain penetration lengths (L_{sp}) and plastic hinge lengths (L_p) for members built from reinforcing bars with differing yield stress values.	81
Table 3.8 : Dynamic specifications of FE models built from materials of different properties.....	82
Table 3.9 : Characteristics of selected strong ground motions.	96
Table 3.10 : Damage levels and their specifications.....	99
Table 3.11 : Statistical properties of experimental to model prediction values at yield and ultimate curvature.....	102
Table 3.12 : Capacity dispersion values for different limit states.....	103
Table 3.13 : Changes in constants a and b in terms of different limit states due to variations in steel strength values.	116
Table 3.14 : Annual probabilities of failure in terms of cracking, yield, spalling and ultimate limit states.	120
Table 4.1 : Sample set of 10 uniformly distributed random numbers, standard normal random values, sample steel strengths and corresponding γ factor.	129
Table 4.2 : Cost estimation list of the bridge.	131

Table 4.3 : Repair cost ratios provided by Basoz and Mander - excerpted from (Padgett et al, 2010).	132
Table 4.4 : Inflation rates for construction of non-residential buildings.....	135
Table 4.5 : Annual probabilities of failure in terms of different limit states and damage probabilities in terms of various damage levels.....	136
Table 4.6 : Life-time probabilities of failure in terms of different limit states and damage probabilities in terms of various damage levels.....	137
Table 4.7 : Modification factors for steel jacketed MSSS concrete bridges,	138
Table 4.8 : Annual and life-time failure probabilities of retrofitted structure in terms of different limit states.	139
Table 4.9 : Annual and life-time damage probabilities of retrofitted structure in terms of different damage levels.	139
Table 4.10 : Example of calculating annual expected costs for as-built, non-monitored structure.	143
Table 4.11 : Example of calculating annual expected costs for retrofitted, non-monitored structure.	144
Table 4.12 : Annual expected costs of the non-monitored as-built and retrofitted structure as a function of initial cost, life-time and significance.	145
Table 4.13 : Sensitivity of estimated expected annual cost to number of steel samples.....	146
Table 4.14 : Sample set of 10 uniformly distributed random numbers, standard normal random values, sample steel strengths, corresponding first modal period from FEM (T'_1) and corresponding natural logarithms of T'_1	149
Table 4.15 : Prior and updated steel strengths for four different SHM outputs	154
Table 4.16 : Cost of wireless and wire-based SHM systems	157
Table 4.17: Annual cost of monitoring for bridges with different life-times.....	157
Table 4.18 : Evaluation of VPI and the maximum allowable budget of monitoring.	160
Table 4.19 : Evaluation of VPI and the maximum allowable budget of monitoring bent system.....	166
Table 4.20 : Comparison of the optimal alternatives selected for the monitored bridge of various significances.....	169
Table 4.21 : Effect of error on value of information.	170

LIST OF FIGURES

	<u>Page</u>
Figure 2.1 : Figurative three dimensional view of Elek Deresi Bridge.	12
Figure 2.2 : Longitudinal view of Elek Deresi Bridge.....	12
Figure 2.3 : Section A-A (bent system - front view).	13
Figure 2.4 : Column section (section B-B) and cap beam section (section C-C).	13
Figure 2.5 : Detail 1(bent system - side view).	14
Figure 2.6 : Detail 2 (abutment side view).	15
Figure 2.7 : Superstructure and substructure at A) Bent location B) Abutment location.....	16
Figure 2.8 : Elek Deresi Bridge analytical model.	18
Figure 2.9 : Elek Deresi Bridge analytical model – left abutment.....	19
Figure 2.10 : Elek Deresi Bridge analytical model – right abutment.	20
Figure 2.11 : Elek Deresi Bridge analytical model – bent cap system.	21
Figure 2.12 : Elek Deresi Bridge analytical model – bent cap system – left abutment side.	22
Figure 2.13 : Elek Deresi Bridge analytical model – bent cap system – right abutment side.	23
Figure 2.14 : Elek Deresi Bridge analytical model – bent cap system – node and element configuration.....	24
Figure 2.15 : Distribution of applied superstructure weight load between elastomeric bearings of bent system and abutments.....	26
Figure 2.16 : Point and distributed loads applied at bent system.....	26
Figure 2.17 : Schematic view of bearing pads in an ordinary bridge and other components.	28
Figure 2.18 : Specifications of the reinforced elastomeric bearing.	29
Figure 2.19 : Elastomeric material for idealisation of elastomeric bearings.	30
Figure 2.20 : Schematic view of a seat-type abutment.	31
Figure 2.21 : Backfill material for idealisation of embankment backfill contribution.	33
Figure 2.22 : (a) Longitudinal pile material for idealisation of longitudinal contribution of piles (b) Transversal pile material for idealisation of transversal contribution piles.....	34
Figure 2.23 : (a) <i>Abutment Pounding Material</i> for superstructure - abutment collision (b) <i>Shearkey Pounding Material</i> for superstructure - shear key collision (c) <i>Deck Pounding Material</i> for superstructure - superstructure collision.....	36
Figure 2.24 : (a) Combined material for <i>element type 3</i> (b) Combined material for <i>element type 4</i> (c) Combined material for <i>element type 5</i>	38
Figure 2.25 : Bridge superstructure geometry and materials.....	39
Figure 2.26 : Equivalent superstructure section for flexure about local y axis.....	40
Figure 2.27 : Equivalent superstructure section for flexure about local z axis.....	41
Figure 2.28 : Backbone curve for bending material.....	44

Figure 2.29 : Stress –strain model proposed by Mander for monotonic loading of confined and unconfined concrete.....	45
Figure 2.30 : Strain and stress distribution in a symmetrical reinforced concrete section.....	47
Figure 2.31 : Material models for (a) Unconfined concrete (b) Confined concrete (c) Reinforcement steel.....	49
Figure 2.32 : Discretisation of column and cap beam sections for fiber modelling.	50
Figure 2.33 : Moment-curvature curve and its bilinear idealisation for bending about local z axis.....	52
Figure 2.34 : Moment-curvature curve of column section and its bilinear idealisation for bending about local y axis ($f'_{co} = 21.75 \text{ MPa}$, $f_y = 472.41 \text{ MPa}$).....	53
Figure 2.35 : Moment-curvature curve of column section and its bilinear idealisation for bending about local z axis ($f'_{co} = 21.75 \text{ MPa}$, $f_y = 472.41 \text{ MPa}$).....	54
Figure 2.36 : Moment-curvature curve of bent capbeam section and its bilinear idealisation for bending about local y axis ($f'_{co} = 21.75 \text{ MPa}$, $f_y = 472.41 \text{ MPa}$).	54
Figure 2.37 : Moment-curvature curve of bent capbeam section and its bilinear idealisation for bending about local z ($f'_{co} = 21.75 \text{ MPa}$, $f_y = 472.41 \text{ MPa}$).	55
Figure 2.38 : Plastic hinges defined for the BWH elements for a model with concrete of $f'_{co} = 21.75 \text{ MPa}$ and steel of $f_y = 472.41 \text{ MPa}$	58
Figure 2.39 : Schematic view of the bridge, exhibiting direction of displacement of left superstructure.	61
Figure 2.40 : Longitudinal displacement of superstructure vs. reaction at abutment.	61
Figure 2.41 : Transversal displacement of superstructure vs. reaction at abutment in transversal direction.	62
Figure 2.42 : Base shear versus displacement of node 4009 in longitudinal direction.	63
Figure 2.43 : Base shear versus displacement of node 4009 in transversal direction.	63
Figure 2.44 : Undeformed and deformed shapes of Elek Deresi Bridge sample under PA in longitudinal direction.	64
Figure 2.45 : Undeformed and deformed shapes of Elek Deresi Bridge bent system under PA in transversal direction.	64
Figure 2.46 : Three dimensional view of natural mode shapes of vibration (a) mode 1 (b) mode 2 (c) mode 3.	66
Figure 3.1 : Moment curvature curves for varying f'_{co} , $f_y = \mu_{fy} (472.41 \text{ MPa})$ (capbeam - local y axis).	73
Figure 3.2 : Moment curvature curves for varying f'_{co} , $f_y = \mu_{fy} (472.41 \text{ MPa})$	73
Figure 3.3 : Moment curvature curves for varying f'_{co} , $f_y = \mu_{fy} (472.41 \text{ MPa})$	74
Figure 3.4 : Moment curvature curves for varying f'_{co} , $f_y = \mu_{fy} (472.41 \text{ MPa})$	74
Figure 3.5 : Response of Elek Deresi Bridge to intensified values of RSN521 record.	75
Figure 3.6 : Moment curvature curves for varying f_y , $f'_{co} = 21.75 \text{ MPa}$	76
Figure 3.7 : Moment curvature curves for varying f_y , $f'_{co} = 21.75 \text{ MPa}$	76
Figure 3.8 : Moment curvature curves for varying f_y , $f'_{co} = \mu_{f'_{co}} (21.75 \text{ MPa})$	77
Figure 3.9 : Moment curvature curves for varying f_y , $f'_{co} = \mu_{f'_{co}} (21.75 \text{ MPa})$	77
Figure 3.10 : Hazard curves for bridge position at $T = 0.5\text{s}$ and 0.75s and interpolated curve for $T = 0.62\text{s}$	87

Figure 3.11 : Interpolated and idealised hazard curves for bridge position at $T = 0.62s$	88
Figure 3.12 : Horizontal ground acceleration and pseudo acceleration spectra for RSN17 record ($\zeta = 5\%$) (a) North – south component (b) East – west component...	89
Figure 3.13 : Horizontal ground acceleration and pseudo acceleration spectra for RSN216 record ($\zeta = 5\%$) (a) North – south component (b) East – west component.	89
Figure 3.14 : Horizontal ground acceleration and pseudo acceleration spectra for RSN291 record ($\zeta = 5\%$) (a) North – south component (b) East – west component.	90
Figure 3.15 : Horizontal ground acceleration and pseudo acceleration spectra for RSN513 record ($\zeta = 5\%$) (a) North – south component (b) East – west component.	90
Figure 3.16 : Horizontal ground acceleration and pseudo acceleration spectra for RSN521 record ($\zeta = 5\%$) (a) North – south component (b) East – west component.	91
Figure 3.17 : Horizontal ground acceleration and pseudo acceleration spectra for RSN551 record ($\zeta = 5\%$) (a) North – south component (b) East – west component.	91
Figure 3.18 : Horizontal ground acceleration and pseudo acceleration spectra for RSN557 record ($\zeta = 5\%$) (a) North – south component (b) East – west component.	92
Figure 3.19 : Horizontal ground acceleration and pseudo acceleration spectra for RSN610 record ($\zeta = 5\%$) (a) North – south component (b) East – west component.	92
Figure 3.20 : Horizontal ground acceleration and pseudo acceleration spectra for RSN671 record ($\zeta = 5\%$) (a) North – south component (b) East – west component.	93
Figure 3.21 : Horizontal ground acceleration and pseudo acceleration spectra for RSN698 record ($\zeta = 5\%$) (a) North – south component (b) East – west component.	93
Figure 3.22 : Horizontal ground acceleration and pseudo acceleration spectra for RSN742 record ($\zeta = 5\%$) (a) North – south component (b) East – west component.	94
Figure 3.23 : Horizontal ground acceleration and pseudo acceleration spectra for RSN745 record ($\zeta = 5\%$) (a) North – south component (b) East – west component.	94
Figure 3.24 : Pseudo acceleration spectra for north – south components of the 12 strong ground motion records ($\zeta = 5\%$).	95
Figure 3.25 : Pseudo acceleration spectra for east – west components of the 12 strong ground motion records ($\zeta = 5\%$).	95
Figure 3.26 : Damage levels and limit states.	98
Figure 3.27 : Median demand vs. spectral acceleration in terms of yield curvature limit state ($f'_{co} = \mu_{f'co}, f_y = \mu_{fy} - 1.5\sigma_{fy}$).	106
Figure 3.28 : Median demand vs. spectral acceleration in terms of yield curvature limit state ($f'_{co} = \mu_{f'co}, f_y = \mu_{fy} - 0.5\sigma_{fy}$).	106
Figure 3.29 : Median demand vs. spectral acceleration in terms of yield curvature limit state ($f'_{co} = \mu_{f'co}, f_y = \mu_{fy} + 0.5\sigma_{fy}$).	107
Figure 3.30 : Median demand vs. spectral acceleration in terms of yield curvature limit state ($f'_{co} = \mu_{f'co}, f_y = \mu_{fy} + 1.5\sigma_{fy}$).	107
Figure 3.31 : Median demand vs. spectral acceleration in terms of ultimate curvature limit state ($f'_{co} = \mu_{f'co}, f_y = \mu_{fy} - 1.5\sigma_{fy}$).	108
Figure 3.32 : Median demand vs. spectral acceleration in terms of ultimate curvature limit state ($f'_{co} = \mu_{f'co}, f_y = \mu_{fy} - 0.5\sigma_{fy}$).	108
Figure 3.33 : Median demand vs. spectral acceleration in terms of ultimate curvature limit state ($f'_{co} = \mu_{f'co}, f_y = \mu_{fy} + 0.5\sigma_{fy}$).	109
Figure 3.34 : Median demand vs. spectral acceleration in terms of ultimate curvature limit state ($f'_{co} = \mu_{f'co}, f_y = \mu_{fy} + 1.5\sigma_{fy}$).	109
Figure 3.35 : Median demand in terms of cracking limit state vs. S_a for models made from steel of various yield strengths (f_y).	110

Figure 3.36 : Median demand in terms of yield limit state vs. Sa for models made from steel of various yield strengths (f_y).	110
Figure 3.37 : Median demand in terms of spalling limit state vs. Sa for models made from steel of various yield strengths (f_y).	111
Figure 3.38 : Median demand in terms of ultimate limit state vs. Sa for models made from steel of various yield strengths (f_y).	111
Figure 3.39 : Dispersion of demand in terms of yield curvature limit state vs. Sa and linear approximation ($f'_{co} = \mu_{f'co}$, $f_y = \mu_{fy} - 1.5\sigma_{fy}$).	112
Figure 3.40 : Dispersion of demand in terms of yield curvature limit state vs. Sa and linear approximation ($f'_{co} = \mu_{f'co}$, $f_y = \mu_{fy}$).	112
Figure 3.41 : Dispersion of demand in terms of yield curvature limit state vs. Sa and linear approximation ($f'_{co} = \mu_{f'co}$, $f_y = \mu_{fy} + 1.5\sigma_{fy}$).	113
Figure 3.42 : Dispersion of demand in terms of ultimate curvature limit state vs. Sa and linear approximation ($f'_{co} = \mu_{f'co}$, $f_y = \mu_{fy} - 1.5\sigma_{fy}$).	113
Figure 3.43 : Dispersion of demand in terms of ultimate curvature limit state vs. sa and linear approximation ($f'_{co} = \mu_{f'co}$, $f_y = \mu_{fy}$).	114
Figure 3.44 : Dispersion of demand in terms of ultimate curvature limit state vs. Sa and linear approximation ($f'_{co} = \mu_{f'co}$, $f_y = \mu_{fy} + 1.5\sigma_{fy}$).	114
Figure 3.45 : Linear approximation of dispersion of demand in terms of yield curvature limit state vs. Sa curves for models with various steel yield strengths (f_y).	115
Figure 3.46 : Linear approximation of dispersion of demand in terms of ultimate curvature limit state vs. Sa curves for models with various steel yield strengths (f_y).	115
Figure 3.47 : Variations of constants a and b in terms of cracking and yield curvature limit states with γ ($f_y = \mu_{fy} + \gamma\sigma_{fy}$).	117
Figure 3.48 : Variations of constants a and b in terms of spalling and ultimate curvature limit states with γ ($f_y = \mu_{fy} + \gamma\sigma_{fy}$).	117
Figure 3.49 : Variations of constants a_β and b_β in terms of cracking and yield curvature limit states with γ ($f_y = \mu_{fy} + \gamma\sigma_{fy}$).	118
Figure 3.50 : Variations of constants a_β and b_β in terms of spalling and ultimate curvature limit states with γ ($f_y = \mu_{fy} + \gamma\sigma_{fy}$).	118
Figure 3.51 : Probability of failure in terms of a) Cracking limit state b) Yield limit state c) Spalling limit state d) Ultimate limit state and the fitted lines for models made of differing steel properties ($f_y = \mu_{fy} + \gamma\sigma_{fy}$).	121
Figure 4.1 : The decision tree.	125
Figure 4.2 : Schematic view for calculating probability of damage level 3.	127
Figure 4.3 : a) Retrofitted bridge column by full height steel jacketing technique b) Circular steel jacketing of a circular column c) Elliptical steel jacketing of a rectangular column.	134
Figure 4.4 : Regression lines for FE models made from three differing steel strengths and steel jacketed model in terms of cracking curvature limit state.	140
Figure 4.5 : Regression lines for FE models made from three differing steel strengths and steel jacketed model in terms of yield curvature limit state.	140
Figure 4.6 : Regression lines for FE models made from three differing steel strengths and steel jacketed model in terms of spalling curvature limit state.	141

Figure 4.7 : Regression lines for FE models made from three differing steel strengths and steel jacketed model in terms of ultimate curvature limit state.	141
Figure 4.8: $f_y - T_1'$ curve and the regression line.	148
Figure 4.9 : Lognormal cumulative distribution function of SHM system outputs and the process for approximating $p_o[o_k]$	152
Figure 4.10 : Estimated probabilities of SHM system outputs ($p_o[o_k]$) monitoring fundamental period of structure T_1).	152
Figure 4.11 : Prior and updated CDFs of steel for different SHM outputs.	154
Figure 4.12 : Prior and updated CDFs of steel by different SHM outputs.	155
Figure 4.13 : Three dimensional view of the first natural mode shape of bent system.	163
Figure 4.14 : $f_y - T_1'$ curve of the bent system and the regression line.	164
Figure 4.15 : Estimated probabilities of SHM system outputs ($p_o[o_k]$) monitoring fundamental period of bent system.	165
Figure 4.16 : Prior and updated CDFs of steel by different SHM outputs from monitoring the bent system ($\sigma_{nc} = 2.0\%$).	168
Figure 4.17 : Prior and updated CDFs of steel by different SHM outputs from monitoring the bent system ($\sigma_{nc} = 3.0\%$).	171
Figure 4.18 : Prior and updated CDFs of steel by different SHM outputs from monitoring the bent system ($\sigma_{nc} = 4.0\%$).	171



VALUE OF INFORMATION OBTAINED USING STRUCTURAL HEALTH MONITORING OF AN RC BRIDGE SUBJECTED TO SEISMIC HAZARD

SUMMARY

This study deals with assessing value of information obtained from structural health monitoring (SHM) of a two span reinforced concrete bridge inspected for possible structural deficiencies. The structure is subjected to seismic hazard and the question to be answered is whether or not the SHM system should be installed and maintained. An answer to this question has been sought in Chapters 2 to 4 of this study.

Chapter 2 mainly deals with studying structural properties of the bridge, establishing the proper FE model and carrying out gravity, pushover and eigenvalue analyses.

First, structural properties of the bridge have been studied. Different components of the structure (elastomeric bearings, shear keys, etc.) along with reactions of abutment backfill soil and piles have been idealised. Collisions between superstructure and abutments, superstructure and shear keys and deck poundings have been taken into consideration. A three dimensional FE model of the bridge has been constructed in OpenSees using the mentioned idealisations and structural details. Moment-curvature analyses of member sections have been carried out and outputs have been idealised. Pushover analysis of the structure has been performed for controlling performance of idealised elements and studying behaviour of the bent system. An eigenvalue analysis of the structure has been made and mode shapes of vibration have been drawn.

Chapter 3 is mainly devoted to calculation of unconditional probabilities of failure using the SAC/FEMA (2000) method.

For this purpose, statistical specifications of constructing materials have been studied. Yield strength of reinforcing steel has been distinguished as the proper model uncertainty variable after examining moment-curvature results of several models made from varying steel and concrete properties. Moment-curvature analysis results, lengths of plastic hinges and other structural specifications caused by changes in steel properties have been investigated. A number of FE models have been constructed using varying steel strengths. Hazard curve for bridge location has been obtained and idealised linearly. A set of twelve strong ground motion records have been selected to be used in the time history analysis procedure. Five damage levels and four limit states have been defined for classification of intensities of damages caused by seismic loadings. Dispersion values regarding capacity and demand random variables have been estimated. Dispersion value for capacity has been obtained by defining it as a function of model and material variables. Demand dispersion values for various models have been assessed by a number of nonlinear dynamic analyses. Employing the 2000 SAC/FEMA method, annual failure probabilities in terms of different limit states have been estimated using demand and capacity dispersions and properties of the idealised hazard curve. Relationship between failure probabilities and reinforcing steel strength values has been studied. It is identified that a linear relationship can be established between the two parameters.

Chapter 4 mainly investigates value of information obtained from an SHM system and feasibility of such a monitoring.

First, a decision tree has been established as a tool for solving the decision making problem. The decision making process has been assumed to be composed of two stages. At the first stage, it is decided if the SHM system should be installed and maintained. In the second stage, it is decided if the structure is in need of retrofitting.

For assessing expected annual costs of non-monitored alternative, a number of steel samples have been generated using Monte Carlo sampling method. Annual probabilities of failure in terms of defined limit states have been estimated for each steel realisation using the relationship between steel strength and failure probabilities obtained in Chapter 3. Damage probabilities in term of different damage levels have been calculated based on the assessed failure probabilities. Steel jacketing has been studied and distinguished as the proper retrofitting measure. Expenses associated with initial construction, repair and jacketing along with the indirect costs arising from socio-economic side effects of the damaged bridge have been taken into account. Feasibility of retrofitting the non-monitored structure has been determined by the maximum expected monetary value (EMV) criterion. It has been distinguished that feasibility of retrofitting is a function of structures initial construction cost, significance and expected service period.

Expected annual cost of the monitored bridge has been evaluated using principles of preposterior analysis. For this purpose, first, the fundamental period of the structure has been selected as the monitoring parameter. Expenses associated with monitoring have been studied. Steel strengths have been updated using a suitable range of possible SHM system outcomes. Afterwards, expected annual cost of the monitored bridge has been estimated using probability of each outcome and costs related to the optimal alternative chosen between retrofitting and non-retrofitting options. Value of the acquired information from monitoring is evaluated by comparing expected annual costs of the monitored and non-monitored alternatives. It has been observed that the maximum budget that can be allocated to monitoring is a function of modelling and measurement errors, initial construction cost, expected life-time and significance of the bridge. It has also been realised that even for relatively low errors, the maximum amount of resources allocatable to monitoring is less than the estimated monitoring expenses.

As the second try, the fundamental period of bent system has been selected as the monitoring parameter. It has been noticed that value of obtained information increases as a result of monitoring the bent system.

DEPREM TEHLİKESİNE MARUZ KALAN BİR BETONARME KÖPRÜ İÇİN YAPISAL SAĞLIK İZLEME YÖNTEMİYLE ELDE EDİLEN VERİLERİN DEĞERİ

ÖZET

Köprüler, ulaşım sistemlerinin önemli bir bileşenidir. Ancak, bu yapılar genellikle birçok doğal ve insan kaynaklı afetin (sel, fırtına, gemi ve ağır taşıt kazası vb.) tehditi altındadır. Köprülerin maruz kaldıkları doğal afetlerden biri de deprem tehlikesidir. Köprüler genellikle sıradan yapılara kıyasla daha az hiperstatik olmaları nedeniyle sismik sarsılmaya karşı daha hassaslardır. Ayrıca, sıklıkla olumsuz zemin koşullarına sahip sahalarda (koylar, nehirler vb.) inşa edilirler.

Eğer bir köprü çökerse veya ciddi şekilde hasar görürse, ortaya çıkacak doğrudan ve dolaylı ekonomik kayıplar, önemli mertebelere ulaşabilir. Büyük bir köprünün çökmesi çok sayıda can kaybına neden olabilir ve ilgili bölge haftalar, aylar hatta yıllar boyunca ulaşım sorunlarıyla karşı karşıya kalabilir. Köprünün yeniden yapılması veya hasar görmüş köprünün onarımı, önemli seviyede kaynak ihtiyacı doğurabilir. Köprülerin karayolu ağlarına olan önemi ve kapanmaları veya göçmelerinden dolayı ortaya çıkan doğrudan ve dolaylı maliyetleri nedeniyle, servis ve aşırı yükler sırasında uygun işlevselliklerini sağlamak için yapısal durumlarının düzenli olarak incelenmesi önemlidir. Köprülerin her zaman yalnızca afetlerden dolayı çökmezler. Bazen köprüler, ilgili yapısal sorunları yeterince erken tespit edilip önlem alınmazsa servis yükleri altında da göçebilir. Köprü denetimi için başlıca iki yöntem vardır: görsel ve aletsel. Eğitimli uzmanlar tarafından yapılan düzenli görsel incelemeler, köprü durumunun genel değerlendirmesinde sıklıkla kullanılan bir yöntemdir. Ayrıca, otomatik sistemler tarafından tespit edilmesi zor veya maliyetli olan bazı kusurları tespit etmek için görsel denetleme yararlı olabilir. Bunlara rağmen, görsel denetlemenin birçok kısıt ve eksiklikleri vardır. Örneğin, bazı köprü bileşenleri erişilemez veya görüleyen noktalarda olabilir. Köprülerin yapısal durumun değerlendirilmesinde sıklıkla kullanılan bir başka yaklaşım da yapısal sağlık izleme (YSİ) sistemlerinin kullanılmasıdır. Tipik bir yapısal sağlık izleme sisteminde, sensörler köprü bileşenlerinden veriler (örneğin, titreşimler, gerginlikler vb.) toplar. Ham veriler daha sonra merkezi bir istasyona iletilir. Bu merkezde YSİ programları hasarın tespitinde faydalı olabilecek bilgileri tespit eder. Bu bilgilere dayanarak gerekli kararlar uzmanlar tarafından alınır. Ancak, bir köprünün bir izleme sistemi ile donatılmış olması, elde edilen verilerin uygun bir şekilde kullanıldığı anlamına gelmez. Aslında, köprü yöneticilerinin kurulu izleme sistemlerinin sonuçlarından bağımsız olarak da sıklıkla karar verebilmektedirler. Bir diğer önemli husus, izleme sistemine harcanan maddi kaynağın, ondan elde edilebilecek verilerin değerini karşılayıp karşılamamasıdır. Ek olarak, izleme araçlarının yüksek fiyatına göre, köprüyü böyle bir sistemle donatmak için tahsis edilebilecek maksimum bütçe için yaklaşık bir değerlendirme yapılmalıdır.

Bu çalışma, olası yapısal kusurları kontrol eden, iki açıklıklı betonarme köprünün yapısal sağlık izlemesinden (YSİ) elde edilen verilerin değerlendirmesiyle ilgilidir. Yapı sismik tehlikeye maruz kalmaktadır ve cevaplanması gereken soru YSİ sisteminin maddi

açından fayda-maliyet analizinin yapılmasıdır. Bu sorunun cevabı çalışmanın Bölüm 2 - 4 içerisinde araştırılmıştır.

Bölüm 2 temel olarak köprünün yapısal özellikleri, uygun sonlu eleman modelini oluşturulması, düşey yükler, statik itme analizi ve modal analiz sonuçlarını içermektedir. İlk olarak, köprünün yapısal özellikleri incelenmiştir. Köprü kenar ayağı toprak dolgusu ve köprü kazıkları tepki kuvvetleri ile birlikte yapının bileşenleri (elastometrik mesnetler vs.) modellenmiştir. Tabliye ve kenar ayakları, tabliye ve deprem takozları ve iki tabliye arasında oluşan çarpma etkisi modelde göz önüne alınmıştır. OpenSees'te söz konusu modellemeler ve yapısal detayları kullanılarak köprünün üç boyutlu bir sonlu eleman modeli oluşturulmuştur. Eleman kesitlerinde moment-eğrilik analiz yapılmıştır ve sonuçlar idealize edilmiştir. Yapının statik itme analizi, idealize edilmiş elemanların performansını kontrol etmek ve sistemin davranışını incelemek için yapılmıştır. Yapının modal analizi yapılmıştır ve titreşim modu şekilleri elde edilmiştir.

Bölüm 3, özellikle SAC/FEMA (2000) yöntemini kullanarak YSİ sisteminin olmadığı durum için çökme olasılıklarının hesaplanmasına ayrılmıştır. Bu amaçla, yapı malzemelerinin istatistiksel özellikleri incelenmiştir. Donatının akma dayanımı, farklı donatı ve beton özelliklerinden yapılan çeşitli modellerin moment eğrilik sonuçları incelendikten sonra uygulama kapsamında göz önüne alınacak rassal değişken belirlenmiştir. Moment-eğrilik analiz sonuçları, plastik mafsallı uzunlukları ve donatı çeliği dayanımına bağlı olarak değişen diğer yapısal özellikler incelenmiştir. Çeşitli çelik dayanımları için bir dizi sonlu eleman modeli oluşturulmuştur. Köprü konumu için sismik tehlike eğrisi elde edilerek, doğrusal model ile olarak idealleştirilmiştir. Zaman artımı yönteminde kullanılmak üzere 12 deprem ivme kaydı seçilmiştir. Sismik yüklerin neden olduğu hasarın sınıflandırılması için beş hasar seviyesi ve dört limit durumu tanımlanmıştır. Kapasite ve talep rassal değişkenlerine ilişkin logaritmik standart sapma değerleri belirlenmiştir. Kapasite için logaritmik standart sapma değeri model ve malzeme değişkenlerinin bir fonksiyonu olarak tanımlanmıştır. Çeşitli modeller için talep logaritmik standart sapma değerleri doğrusal olmayan dinamik analizlerle elde edilmiştir. 2000 SAC / FEMA yöntemini kullanarak, talep ve kapasite logaritmik standart sapma değerleri ve idealleştirilmiş sismik tehlike eğrisinin özellikleri vasıtasıyla farklı limit durumları açısından yıllık çökme olasılıkları tahmin edilmiştir. Çökme olasılığı ile donatı dayanımı arasındaki ilişki incelenmiştir ve iki parametre arasında doğrusal bir ilişki kurulabileceği tespit edilmiştir.

Bölüm 4'te esas olarak bir YSİ sisteminden elde edilen verilerin değerini ve böyle bir sistemin kurulumunun fizibilitesi incelenmiştir. İlk olarak, bir karar ağacı oluşturulmuştur. Karar verme sürecinin iki aşamadan oluştuğu varsayılmıştır. İlk aşamada, YSİ sisteminin kullanıp kurulmayacağına karar verilir. İkinci aşamada, yapının güçlendirmeye ihtiyacı olup olmadığına karar verilir. YSİ sistemine sahip olmayan yapı için yıllık olası hasar maliyetleri Monte Carlo simülasyonu kullanılarak belirlenmiştir. Tanımlanan limit durumları açısından çökme yıllık olasılıkları, Bölüm 3'te elde edilen çelik dayanımı ve çökme olasılıkları arasındaki ilişkiyi kullanarak her çelik dayanımı için tahmin edilmiştir. Çalışma kapsamında, çelik mantolama ile güçlendirme tekniği göz önüne alınmıştır. Çalışmada, hasar gören köprünün sosyo-ekonomik yan etkilerinden kaynaklanan dolaylı oluşan maliyetleriyle birlikte ilk inşaat, onarım ve mantolama için gereken tahmini maddi kaynaklar dikkate alınmıştır. YSİ sistemine sahip olmayan yapının güçlendirilmesinin fizibilitesi, maksimum beklenen parasal değer (BPD) kriteri ile belirlenmiştir. Güçlendirme fizibilitesinin yapıların ilk inşaat maliyeti, önemi ve beklenen hizmet süresinin bir fonksiyonu olduğu belirlenmiştir.

YSİ sistemine sahip köprünün beklenen yıllık maliyeti, Bayes teoremi esas alınarak öncül-sonsal (pre-posterior) analizler ile değerlendirilmiştir. Bu amaçla, ilk olarak, temel

yapı serbest titreşim periyod, sağlık izleme parametresi olarak seçilmiştir. Sağlık izleme ile ilgili maliyetler incelenmiştir. YSI sistemine sahip köprünün beklenen yıllık maliyeti, her bir hasar durumunun ilgili olasılığı göz önüne alınarak, en düşük toplam beklenen yıllık maliyete karşılık gelen güçlendirme kararı için ilgili maliyetler kullanılarak tahmin edilmiştir. Sağlık izleme sisteminden elde edilen verilerin değeri, izlenen ve izlenmeyen alternatiflerin beklenen yıllık maliyetleri karşılaştırılarak elde edilmiştir. Sağlık izleme için ayrılacak maksimum bütçenin, modelleme ve ölçüm hatalarının, ilk inşaat maliyetinin, beklenen kullanım ömrünün ve köprünün öneminin bir fonksiyonu olduğu gözlemlenmiştir. Ayrıca incelen köprü için, sağlık izleme sistemi için tahsis edilmesi uygun olan maksimum kaynak miktarının tahmini izleme maliyetlerinden daha az olduğu fark edilmiştir.

İkinci denemede, köprünün orta ayağını oluşturan çerçeve sisteminin serbest titreşim periyodu temel denetleme parametresi olarak seçilmiştir. Bu durumda, sistemin sağlığının izlenmesi sonucu elde edilen verinin beklenen değerinin arttığı gözlemlenmiştir.





1. INTRODUCTION

1.1 Bridges and Earthquakes

Bridges are crucial components of any transportation system. They span gaps and carry roads over several obstacles (rivers, valleys, etc.). The word bridge is a generic term and the exact name might differ with the object the structure is crossing over and type of road it carries. For instance, a Viaduct is a bridge carrying a motorway over several obstacles whereas an Underpass is a bridge carrying a railroad over a motorway (Yashinsky, 1998).

Bridges are generally under threat by many natural and man-made hazards (floods, storm surges, vessel and heavy vehicle impacts, etc.). One of the natural hazards that bridges might be subjected to in seismic prone areas is earthquake hazard. Bridges are generally more susceptible to seismic shakings than ordinary structures. One reason for this is that they are simpler structures with less redundancy in comparison to ordinary structures (Priestley et al, 1996). Another reason is that they frequently cross areas like bays and rivers with poor soil conditions (Priestley et al, 1996). The fact that bridges are generally long structures is another factor that adds to their susceptibility as they might be subjected to different soil conditions at different locations. A discussion on relatively poor performance of RC bridges during 1989 Loma Prieta, 1994 Northridge and 1995 Kobe earthquakes and possible earthquake damages to different bridge components can be found in (Priestley et al, 1996). In this reference, subjects like flexural and shear failures of bridge components, unseating, pounding, etc. are presented. California Department of Transportation (2006), has also prepared a collection containing photos of bridges and bridge components damaged during different earthquakes around the world along with a description of corresponding damage type and its severity classification. Among many other earthquake events, one can also find photos related to Erzincan 1992, Adana-Ceyhan 1998, İzmit 1999 and Düzce 1999 earthquakes which recently shook Turkey.

1.2 Consequences of Bridge Failures and Importance of Inspection and Monitoring of Bridges

If a bridge collapses or gets severely damaged, direct and indirect economic losses might be significant to the society by its failure or closure. Many lives can be lost by collapse of a major bridge and the district might face traffic problems for weeks, months or even years to come. As an example, disastrous failure of Cypress Street Viaduct in Oakland, California during the 1989 Loma Prieta earthquake caused 42 deaths and 108 injuries (Yashinsky, 1998). Moreover, it took 1.2 billion dollars and 9 years to replace the failed structure with a new one (Jackson, 1998). Many other expenses and problems can arise as well because of demolishing efforts of a collapsed major bridge, the debris produced by these efforts and its environmental effects (Yashinsky, 1998). Barth (1993), reports some of these demolishing endeavours after the 1989 Loma Prieta earthquake. For instance, he reports that 8,000 tons of reinforcing steel and 50,000 cubic yards of concrete had to be recycled as a result of demolition of Embarcadero Viaduct damaged by the mentioned hazard.

Due to the discussed importance of bridges to road networks and direct and indirect costs imposed by their closure or failure, regular inspection of their condition is significant to ensure their proper functionality during service and extreme loads. It is important to note that bridges do not always fail as a result of major hazards. Sometimes bridges can fail even as a result of regular service loads if their problems are not recognised early enough.

In the U.S., importance of monitoring condition of bridges gained public attention after collapse of Silver Bridge in West Virginia in 1967 which resulted in deaths of 46 people (Dündar et al, 2015). Other bridge failures have occurred afterwards in the U.S. and all over the world. Collapse of I-35W Bridge in Minneapolis, U.S. in 2007 and Çaycuma Bridge in Zonguldak, Turkey in 2012 which both occurred under service loads are examples of recent bridge collapses (Agdas et al, 2016; Dündar et al, 2015). The stated events were both catastrophic; however, these are just some examples of many other bridge failures all over the world. For instance, as stated in a Federal Highway Administration (FHWA) report, 73 bridges were destroyed only in 1985 in Pennsylvania, Virginia and West Virginia as a result of floods (Olson et al, 2005).

There are mainly two methods for bridge inspection: visual and instrumental. Periodic visual inspections are common in many countries and are performed by trained experts

at certain intervals (Dündar et al, 2015). Visual inspection is a valuable means of general evaluation of bridge condition and detecting certain defects that are difficult or costly to distinguish by automated systems. Superstructure cracks are examples of these kinds of defects (Agdas et al, 2016). Nonetheless, in spite of its worth, visual inspection has many limitations and shortcomings. These drawbacks are discussed in many resources in which importance of automated systems for data acquisition is discussed. Agdas et al (2016) cite a classification of concerns regarding visual inspection from an FHWA report (Moore et al, 2001). These concerns are classified as due to: 1) timing, 2) interpretability and 3) accessibility. Concerns regarded with timing originate from discrete nature of visual inspections. Interpretability issues are due to the fact that assessment of bridge damages may differ from person to person and standard to standard. Accessibility concerns are the most important of all and originate from the simple fact that some components of bridges are not reachable or visible.

Concerns similar to those discussed in the above have called for development of non-destructive evaluation (NDE) methods and structural health monitoring (SHM) systems. SHM systems are rooted in NDE methods; however, they represent a separate field nowadays (Agdas et al, 2016). SHM is composed of four fundamental elements. 1) measurements by sensors (strain gauges, accelerometers, etc.) or other instruments. 2) assessment of the structure. 3) identification of the damage and 4) decision making (Alampalli and Ettouney, 2008). In a typical SHM system, sensors collect different sorts of data (vibrations, strains, etc.) from bridge components. The raw data is then transmitted to a central station where SHM programmes are used to extract information which reflects damages. Based on this information the proceeding decisions are made by experts (Cao and Liu, 2016).

From one point, SHM can broadly be categorised as short-term and long-term monitoring (Cao and Liu, 2016). Short-term monitoring is generally employed during periodic inspections or after hazard events. For instance, after an earthquake, flood or vessel impact accident, data might be collected to control condition of the bridge or certain bridge components. Data collection procedure during a short-term monitoring does not generally take more than a few hours and the collected information gets processed later at the engineering office. Consequently, it is a sort of off-line diagnosis (Cao and Liu, 2016). Long-term monitoring systems on the other hand, may be deployed on the structure for months, years or even decades for continuous controlling of

structural integrity. The collected data from long-term SHM systems are reported almost instantly (Cao and Liu, 2016). Hence, this is a real-time monitoring approach.

From another point, SHM systems can be categorised as wire-based and wireless systems. Use of wire-based systems has a longer history and they have been deployed on many bridges all over the world. Drawbacks of wire-based systems are cost, labour and deployment time associated with long cables (a wire-based system might have kilometres of cables) and central data acquisition system (DAC) they need (Cao and Liu, 2016). Moreover, such a system generally requires conduits and AC power supply which add to the expenses (Agdas et al, 2016).

Because of the discussed restrictions with wire-based systems, wireless systems have gained great popularity in recent years particularly as a result of progresses in fields of wireless data transmission and Micro Electro-Mechanical System (MEMS) (Zhu et al, 2018). By eliminating the need for long cables and conduits, wireless systems are generally more cost efficient. Moreover, using a wireless sensor network (WSN), it is possible to achieve finer monitoring and greater measurement accuracy (Cao & Liu, 2016).

Wire-based or wireless, SHM systems can guarantee continuous inspection of bridges and provide decision makers with various sorts of information. This information might concern foundation settlements, deformations of bridge members, dynamic properties of the bridge, wind speed, seabed elevations, etc. However, this does not completely eradicate the necessity for visual inspections. According to Agdas et al. (2016), a hybrid system composed of visual and instrumental inspections might be the optimal health monitoring approach.

Finally, it is worth to state that in addition to controlling structural fitness, SHM has other applications like making design codes and standards, optimisation of inspection and maintenance strategies and prototype development (Faber and Thöns, 2014).

1.3 Efforts for Quantifying Value of Information and Its Importance

SHM systems have been deployed on many sorts of infrastructures since the second half of twentieth century (Faber and Thöns, 2014). Bridges were the first structures which got equipped with SHM systems (Faber and Thöns, 2014). However, the fact that a bridge is equipped with a monitoring system does not necessarily mean the obtained data is being utilised in a proper manner. As a matter of fact, there are some reports

stating that bridge managers frequently make decisions regardless of outcomes of the deployed monitoring systems (Pozzi et al, 2010; Zonta et al, 2014). This is because bridge managers/owners are generally concerned about results of their decisions and tend to trust their common sense more than automated damage detection results which are naturally affected by measurement errors and modelling uncertainties (Pozzi et al, 2010; Zonta et al, 2014). This calls for a rational, well organised method for determining when to make actions (close the bridge for visual inspections, rehabilitate the structure, etc.) if monitoring outputs indicate a potential problem with the structure. Another important issue is to know whether or not the spent monetary resource on the monitoring system is worth data that can be obtained from it. In other words, according to high price of monitoring instruments, there must be an approximate assessment available of the maximum budget that can be allocated to equipping the bridge with such a system.

These questions can be answered using principles of decision theory (Bayesian preposterior analysis) and concept of value of information (VI); as described for example by Ang and Tang (1984).

The described issues are studied by Pozzi et al (2010) with the aim of establishing a framework for evaluating impact of SHM data on bridge management. Although this is not very common for a chapter which is expected to provide only an introduction to the problem, their work and formulations will be described in a relatively detailed manner here. This is because of simplicity of their assumptions corresponding to the decision making process which make their work a good starting point for more complicated problems.

Pozzi et al (2010) have used a cable-stayed bridge with two towers equipped with monitoring instruments (the Bill Emerson Memorial Bridge over Mississippi River) as their case study. The considered hazard is earthquake loading and to make things simple, only two possible states for bridge conditions have been considered by the authors: damaged state (D) and undamaged state (U) which represent mutually exclusive and collectively exhaustive events. It is assumed that after the earthquake, the bridge is standing but, it might be inconspicuously damaged (D) or undamaged (U). Also, only one damage index (x) by the SHM system has been assumed to be available which is stiffness at a critical location. Moreover, only two decision alternatives have been considered as responses to SHM system outputs: 1) to do nothing 2) to close the bridge and run further inspections. Relative expenses regarded with closing the bridge and performing inspections (C_I) and undershooting costs imposed by a possibly damaged

structure if no action is taken (C_{US}) were calculated (costs by putting the society in jeopardy, possible injuries, etc.). They assumed that the SHM system is reporting results about condition of one of the critical locations regarding maximum moments developed during seismic loadings (a tower column – cap beam connection). For detecting damages, they utilised two sequential neural networks after training them by using responses of healthy and manifold scenarios of damaged structures. They used a white noise to sensor responses to represent modelling, measurement and neural network uncertainties and a white noise force to the ground motion record they had employed.

They estimated probability distributions and related parameters of $PDF(x|D)$ and $PDF(x|U)$ by means of Monte Carlo simulating method. For the prior probability of damage, $prob(D)$, they used a value of 30%. This probability represents the bridge manager perception of damage of the critical location after an earthquake. Finally, they calculated the updated probability of damage, $PDF(D|x)$, using Bayes theorem and probability distributions of $PDF(x|D)$ and $PDF(x|U)$.

The authors assumed that the bridge manager acts rationally. Consequently, he/she should always choose the alternative with minimum costs. If cost of *doing nothing* in absence of monitoring data is defined by $C_N = C_{US} \times prob(D)$, then cost of the optimal alternative in absence of monitoring results must be $C^* = \min(C_I, C_N)$.

By calculating cost of *doing nothing* and *inspection* alternatives given monitoring output x as $C_{N|x} = C_{US} \times prob(D|x)$ and $C_{I|x} = C_I$, the cost of optimal alternative given x can be calculated as $C_{neat}^*(x) = \min(C_{I|x}, C_{N|x})$ and $C_{neat}^* = \int_0^\infty C_{neat}^*(x) \times PDF(x)dx$ which is the expected cost of decision making based on the information acquired from the SHM system. It is clear that $PDF(x)$ can be calculated as

$$PDF(x) = PDF(x|D) \times prob(D) + PDF(x|U) \times prob(U) \quad (1.1)$$

Now, value of information can be defined as $VI = C_{neat}^* - C^*$. This value indicates the maximum budget that can be allocated to structural monitoring. Moreover, knowing monitoring output x , the manager must take action if $C_{I|x}$ is smaller than $C_{N|x}$. In other words, the manager does not act when $prob(D|x)$ is greater than $prob(U|x)$; he/she acts when cost of inspection is less than cost of staying idle. This is considered the appropriate economic criterion for manager's intervention.

The problem with bridge managers' reluctant attitude to use monitoring data is studied also by Zonta et al (2014). In the mentioned study, researchers took use of the described

framework by Pozzi et al, (2010) and generalised it by considering multiple damage scenarios and remedial actions. Their case study structure was a pedestrian bridge instrumented for educational purposes (the Streicker Bridge at Princeton University campus). At first, they assumed only one hazard scenario which was collision of a heavy vehicle with bridge arch and outcomes of only one strain gauge at bridge mid-span. After formulating the problem for this simple case, estimating the corresponding costs and probabilities and deriving the relation for value of monitoring information, they provided a discussion on some cases of extreme prior perceptions about bridge state. The two extreme cases were an over concerned bridge manager and a manager who strongly believes that the bridge is invulnerable. They numerically showed that if the manager has such prior strong perceptions about bridge condition, no monitoring data can change his/her mind and value of monitoring information becomes zero as a result. Afterwards, they generalised their methodology and derived equations considering several damage scenarios, remedial measures and life-time monitoring for calculating life-cycle monitoring value of information that might justify investment on SHM systems for bridge owners.

Faber and Thöns (2014), have studied value of information by an SHM system monitoring growth of fatigue cracks of an offshore platform. The concept of decision/event tree has been discussed and a decision tree for objectives of their research has been developed. It has been shown that how the obtained information can be used for optimising inspection and maintenance strategies. This is important because underwater inspections of offshore platforms are both risky and costly. Researchers conclude that usage of SHM systems can result in a considerable life cost reduction both for low and high fatigue failure probabilities which shows merits of monitoring for both new and existing platforms.

Omenzetter et al (2016), have carried out a research on quantifying monitoring information in terms of reduction of risks raised by failures of buildings as a result of earthquake hazard. They have developed a decision tree for their problem and considered costs corresponding to building damage, casualties, monitoring and interruption of usage. Their research involves a study of effects of prior sustaining damage probabilities on monitoring information value. They conclude that the most economic monitoring case is not for buildings with very small or very high prior damage risks but, it is for buildings with intermediate prior damage likelihoods. Performance of different damage detection techniques in the Bayesian preposterior analysis platform of

the research and role of damage extent threshold has been studied and a criterion for the optimal threshold has been proposed. Joint usage of SHM systems and visual inspections has also been formulated for utilisation in pre-posterior analysis.

Thöns et al (2018) have developed a framework using which value of damage detection information (utility gain) can be quantified. The proposed approach uses damage detection system (DDS) data in order to update reliability and risks of structures. In the mentioned approach, vibration monitoring is assumed to be the damage detection method, structural system and the corresponding DDS get modelled and a subspace-based damage detection algorithm (DDA) is introduced. Non-destructive test (NDT) methods have been used for assessment of DDS performance considering the information processing algorithms, measurement and human errors and discretising the system into a number of components with discrete damage states. Probabilities of detection (indication) and no-indication given damage states are calculated and used for updating performance of the structure and calculating performance of DDS. Value of bridge monitoring information problem has been studied numerically using an example of a truss bridge which is expected to undergo a severe deterioration.

1.4 Scope of Research

This study deals with value of information obtained from monitoring a multi-span simply seated (MSSS) concrete bridge threatened by seismic loadings. Feasibility of equipping the bridge with a monitoring system is the subject that will be studied. In the following:

Chapter 2 is dedicated to studying structural properties of the bridge and developing the finite element model of the structure. Utilised material models, elements, assumptions and the simulating programme will be introduced. Gravity, pushover and eigenvalue analyses will be performed and mode shapes will be plotted in this chapter.

Chapter 3 aims to calculate unconditional probabilities of failure using the 2000 SAC/FEMA method. Steel yield strength will be determined as the proper uncertain parameter for the model. Properties of structural steel might be affected by corrosion as studied for example by Xia et al (2013). In this reference, it is stated that both the relative apparent yield and ultimate¹ strengths of reinforcing bars decrease as a result of

¹ Apparent stress is defined as load capacity of a reinforcing bar divided by its uncorroded cross-sectional area (Xia et al, 2013).

corrosion. Moreover, probability of usage of substandard steel by the constructor or variations in steel properties due to production procedure is another issue. Defined limit states and damage levels will be introduced and in the end, a linear relation will be set between failure probabilities in terms of different limit states and steel strength values. In Chapter 4, decision making process and the decision tree will be presented. Direct and indirect costs of bridge damage or failure will be calculated and the optimal alternative will be selected between options of retrofitting the bridge or keeping it in its as-built state using maximum expected monetary value (EMV) criterion and prior failure properties. It will be observed that the optimal alternative varies due to initial construction cost, expected life-cycle and significance of the bridge. In the next step, prior failure probabilities will be updated using SHM system information. The expected annual cost of the monitored bridge will be calculated and will be compared with the expected annual cost of the non-monitored structure. Value of monitoring information will be calculated from these two values.



2. BRIDGE STRUCTURE AND ITS MODELLING

2.1 Introduction

This chapter is dedicated to introduction of the bridge under study and its modelling details and assumptions. Geometrical and structural attributes of the bridge will be discussed in Section 2.2. In this section, structural drawings of the bridge along with some complementary descriptions will be presented. In Section 2.3 modelling programme will be introduced and its advantages will be discussed in brief. Section 2.4 is meant to give a complete insight of the constructed FE models. Details including idealised material properties, modelled bridge components, employed elements, etc. will be introduced in this section. In Section 2.5, Mander's stress-strain model, Mander (1983), will be introduced and properties of confined and unconfined concrete for a model constructed from materials of mean strength properties will be determined. In Section 2.6 moment-curvature analysis theory will be briefly discussed. Analysis responses and their bilinear idealisations will also be presented for a model with materials of mean strength properties. In Section 2.7 length of plastic hinges will be calculated. In Section 2.8 damping matrix of the structure will be defined for usage in response history analyses which will be performed subsequently in Chapter 3. Push over analysis of the bridge will be discussed in 2.9 and finally, three initial natural mode shapes of the structure will be plotted in Section 2.10 after performing an eigenvalue analysis.

2.2 Geometrical and Structural Properties of the Bridge

The name of the bridge that is considered as the case-study bridge in this thesis is Elek Deresi Bridge. It is a two span reinforced concrete bridge located in Boyabat/Sinop and selected from an inventory of ordinary bridges on Turkish roads studied by Avşar (2009).

Avşar has provided a list of 52 ordinary bridges and their important structural properties in his dissertation. From the mentioned inventory, Elek Deresi Bridge has been identified as the most appropriate one for simulation purposes of this research. One

reason for this selection is that structural attributes of Elek Deresi Bridge correspond well with the provided general drawings in the report by Avşar (2009). For instance, only two other bridges (Çarsak and Bitlis Çayı-7 bridges) in the inventory have a superstructure width equal to the one illustrated in drawings of the mentioned report. Moreover, Elek Deresi Bridge is the only non-skewed bridge among the three mentioned bridges. A bridge with a zero skew angle is more preferable as it makes modelling procedure more convenient.

Geometrical and structural details important for purposes of this study have been generated from those provided by Avşar (2009). Figure 2.1, Figure 2.2, Figure 2.3, Figure 2.4, Figure 2.5 and Figure 2.6 present these details.

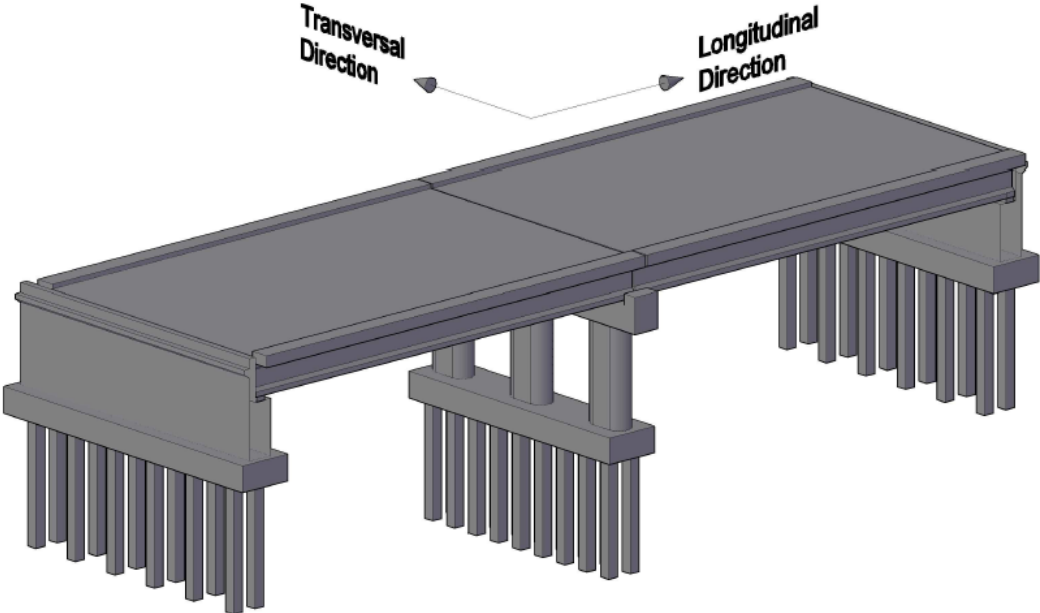


Figure 2.1 : Figurative three dimensional view of Elek Deresi Bridge.

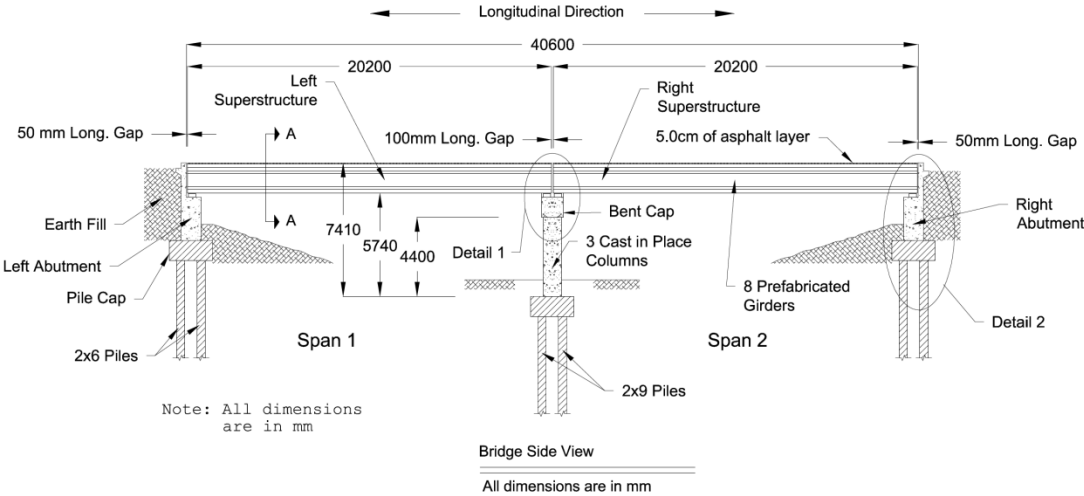


Figure 2.2 : Longitudinal view of Elek Deresi Bridge.

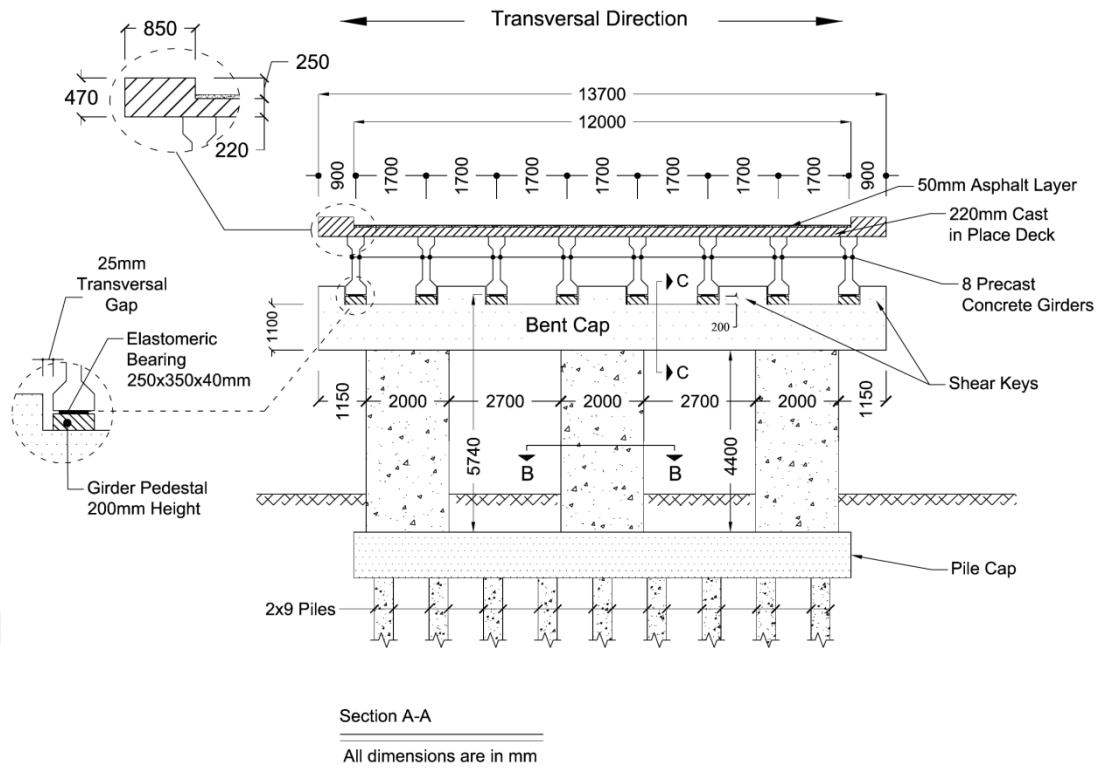


Figure 2.3 : Section A-A (bent system - front view).

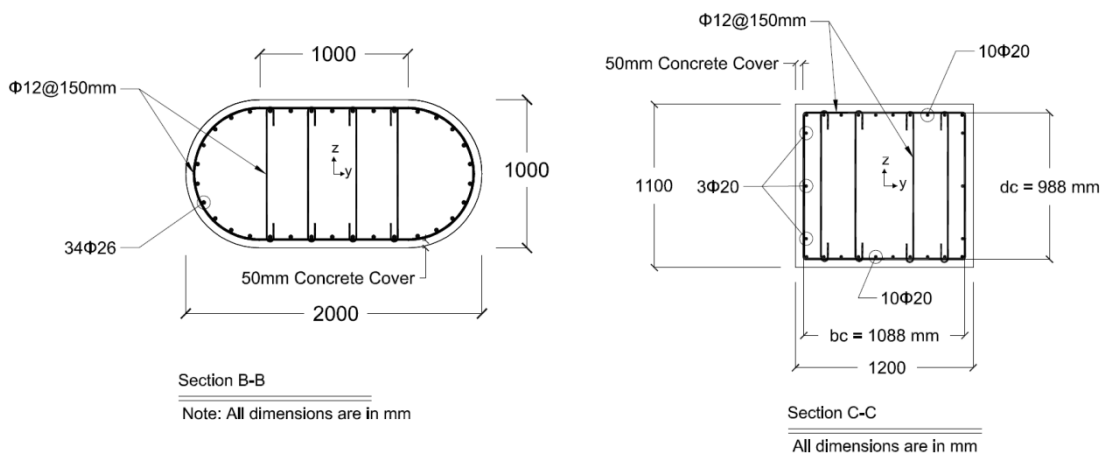
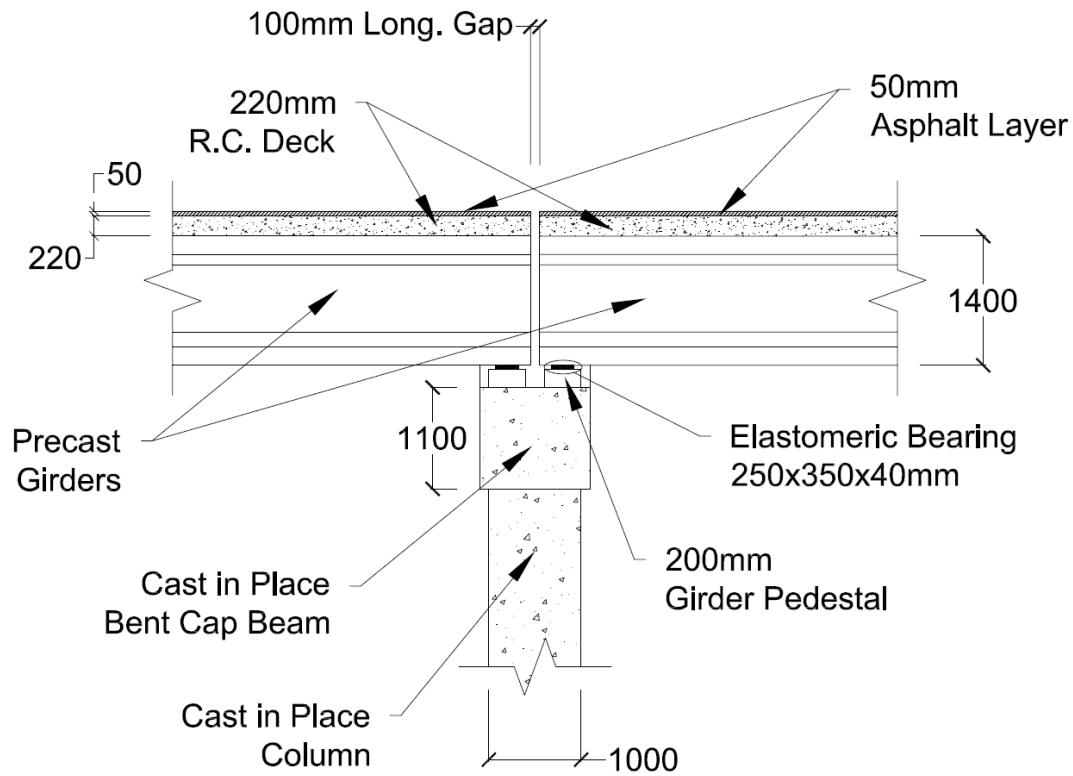


Figure 2.4 : Column section (section B-B) and cap beam section (section C-C).



Detail 1

Note: All dimensions are in mm

Figure 2.5 : Detail 1(bent system - side view).

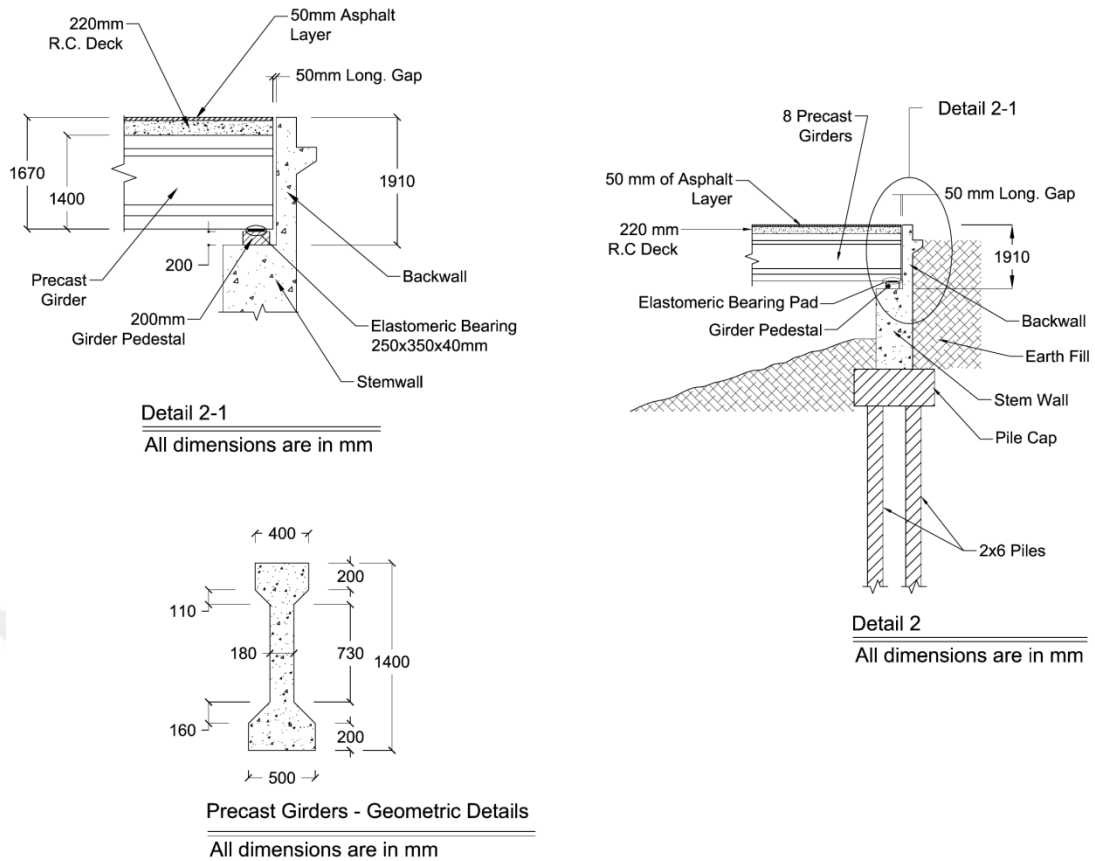


Figure 2.6 : Detail 2 (abutment side view).

As it can be seen from figures presented, Elek Deresi Bridge can be categorised as a non-skewed bridge with multiple columns and multiple spans (considering that it has three columns and two spans). It can also be classified as a Multi Span Simply Seated (MSSS) concrete bridge.

Structures of bridges studied by Avşar (2009) (including Elek Deresi Bridge) are composed of substructures and superstructures (Figure 2.7 presents this terminology). Substructure is the weight supporting part of the bridge and is referred to columns, abutment, foundation, piles or other similar components (Caltrans, 2006). The bent system might be composed of just one column if the bridge is a single-column bridge or of two or more bent columns and a bent cap beam if the bridge is a multi-column one. Substructure of the bridge under study is made of cast in place concrete but the superstructure is composed of eight precast prestressed girders and a cast in place deck. C25 concrete grade has been used for constructing cast in place parts whereas prefabricated girders have been constructed from C40 concrete class. S420 steel grade has been used for all reinforcements.

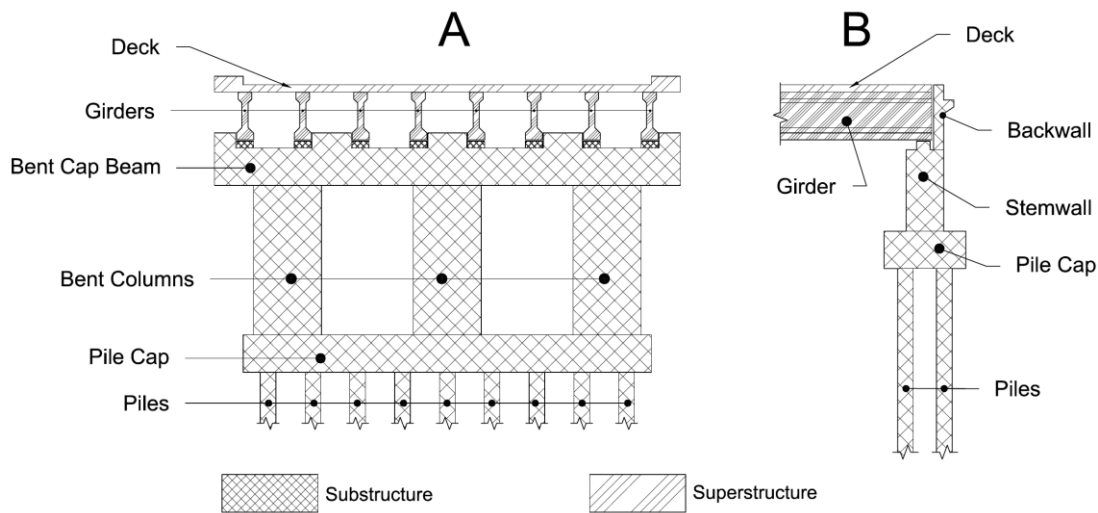


Figure 2.7 : Superstructure and substructure at A) Bent location B) Abutment location.

2.3 Modelling Programme

The simulating programme used in this research is OpenSees¹ (McKenna et al, 2010). OpenSees stands for The Open System for Earthquake Engineering Simulation. It is an open-source software framework developed by Pacific Earthquake Engineering Research Center² and can be used for modelling and analysing structures against seismic loadings. This programme has a large library of elements, materials, solution algorithms and solvers and is able to perform nonlinear static and transient analysis. In addition to the mentioned advantages, there are also other motivations for choosing OpenSees as the modelling programme for this research. For instance, frequent nonlinear transient analyses with various scaling factors need to be performed in this study. This can be performed pretty easily with OpenSees.

2.4 General View of Elek Deresi Bridge Model

Figure 2.8 to Figure 2.14 present analytical model of Elek Deresi Bridge developed for purposes of this study. In Figure 2.8, the complete model has been presented. In Figure 2.9 to Figure 2.13 closer views and more details have been provided. As can be observed in these figures, a three dimensional model has been constructed so that a better simulation of bridge behaviour could be achieved. Figure 2.14 presents combination of nodes and elements of simulated bent system.

¹ <http://opensees.berkeley.edu/index.php>

² <http://peer.berkeley.edu/>

Mass of the structure (calculated later in Subsection 2.4.1) has been introduced to the model as lumped in nodes along structural elements. There are also nodes in the model with no mass as can be seen in Figure 2.14. Nodes without mass have been used for defining zeroLength elements. These elements have been widely used for sampling purposes throughout this study. OpenSees zeroLength elements are elements with no length and can be defined by introducing two nodes with identical positions to the programme. For instance, in Figure 2.9 nodes 1000 and 1001 which have identical coordinates with node 2000 have been introduced to the programme for defining zeroLength elements 100 and 101. In this study, zeroLength elements with different material properties assigned to them have been employed for simulating embankment backfill and pile action, friction resistance, collisions of bridge components, etc. These elements and idealised material properties assigned to them will be discussed in detail in Subsections 2.4.2, 2.4.3, 2.4.4 and 2.4.5. Although zeroLength elements were identified as very useful for sampling purposes of this research, employing them imposed some additional nodes as can be seen in Figure 2.14.

According to Caltrans (2006), superstructures of Ordinary Standard Bridges are expected to remain elastic during earthquakes. Consequently, damages to the superstructure are not considered in this study. Moreover, as it is discussed in Subsection 2.4.6, the superstructure is simulated using elastic elements. However, the bent systems might experience nonlinearities as a result of strong ground motions and damages are expected to occur in its components. For this purpose, elements capable of modelling nonlinearities are used for simulation of bent cap beam and columns as discussed in Subsection 2.4.7. Bridge footing is assumed to be rigid and columns are presumed fixed at their end points to the foundation (constrained in all directions).

In Figure 2.14 a more detailed view of analytical model of the bent system is demonstrated. Rigid elements have been employed at column – bent cap beam joints for the reason that connection zones are stiffer than the rest of cap beam or columns. Avşar (2009), cites results of a research by Wilson (2002) stating that stiffness of rigid elements should not be selected more than 100 times greater than stiffness of adjacent elements. This is because a greater stiffness value might cause convergence problems during analysis. In this study, stiffness of rigid elements has been selected 25 times greater than stiffness of non-rigid elements. Rigid elements have also been used at superstructure ends as can be seen in Figure 2.8, Figure 2.9, Figure 2.10, Figure 2.11, Figure 2.12 and Figure 2.13.

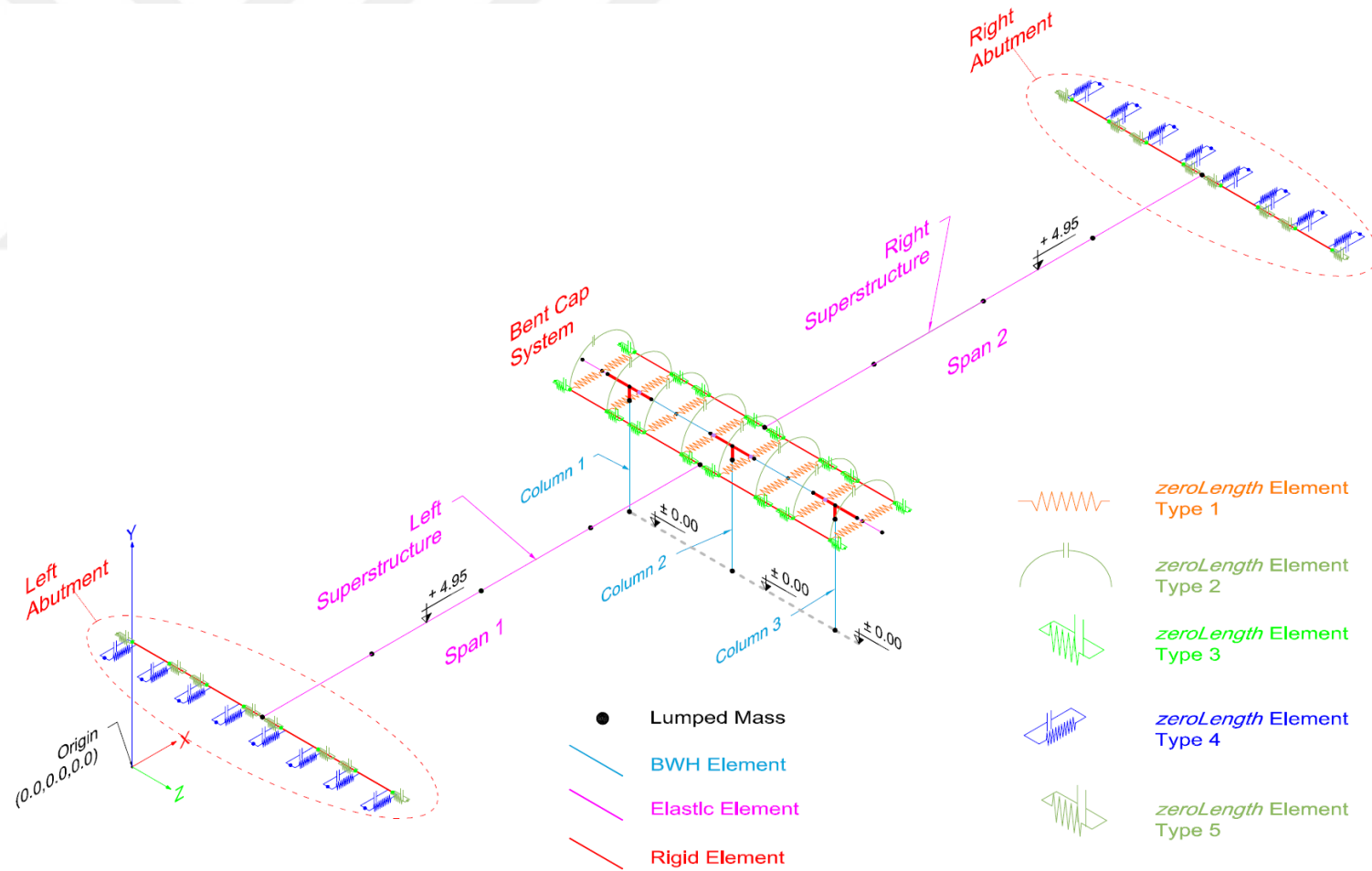


Figure 2.8 : Elek Deresi Bridge analytical model.

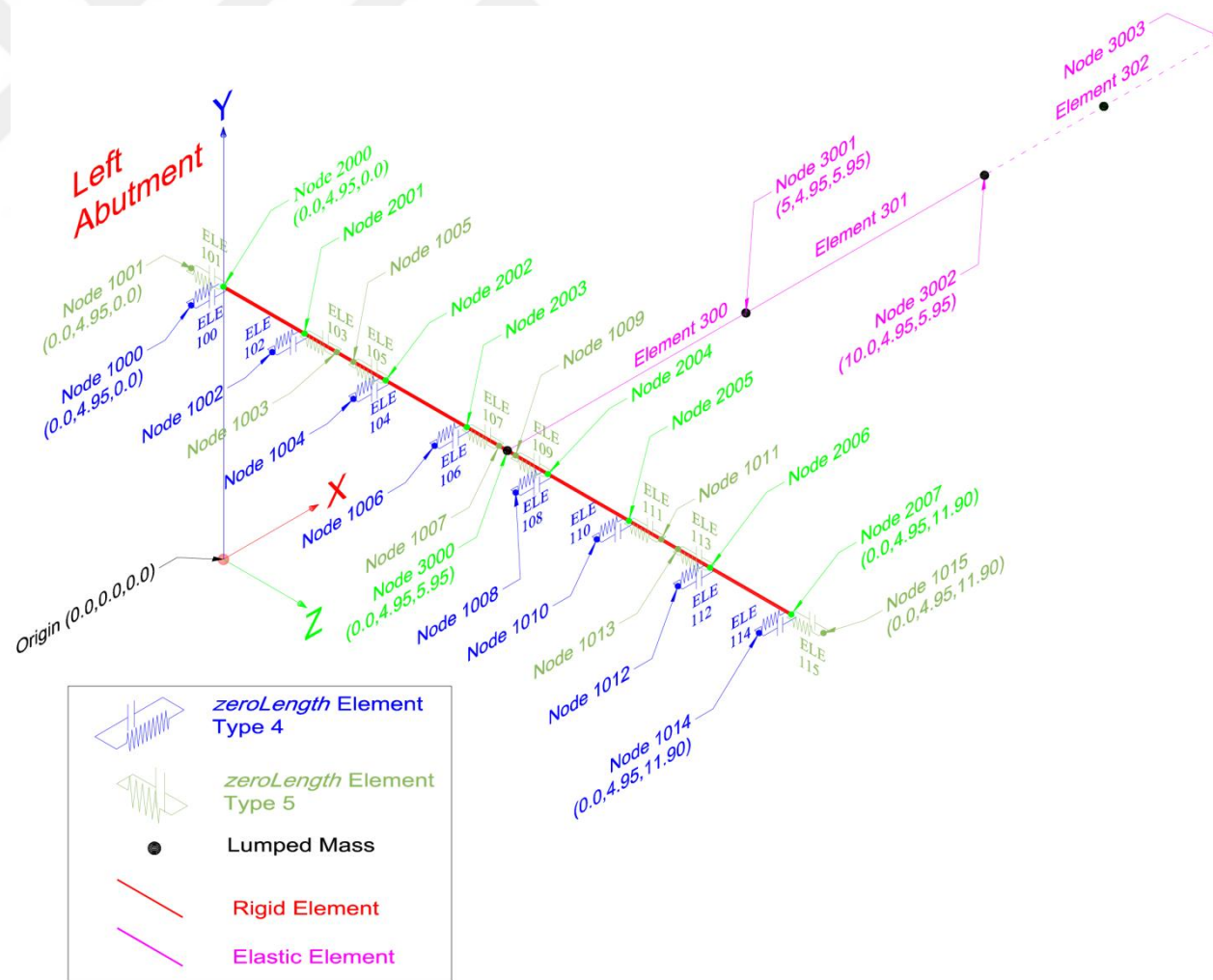


Figure 2.9 : Elek Deresi Bridge analytical model – left abutment.

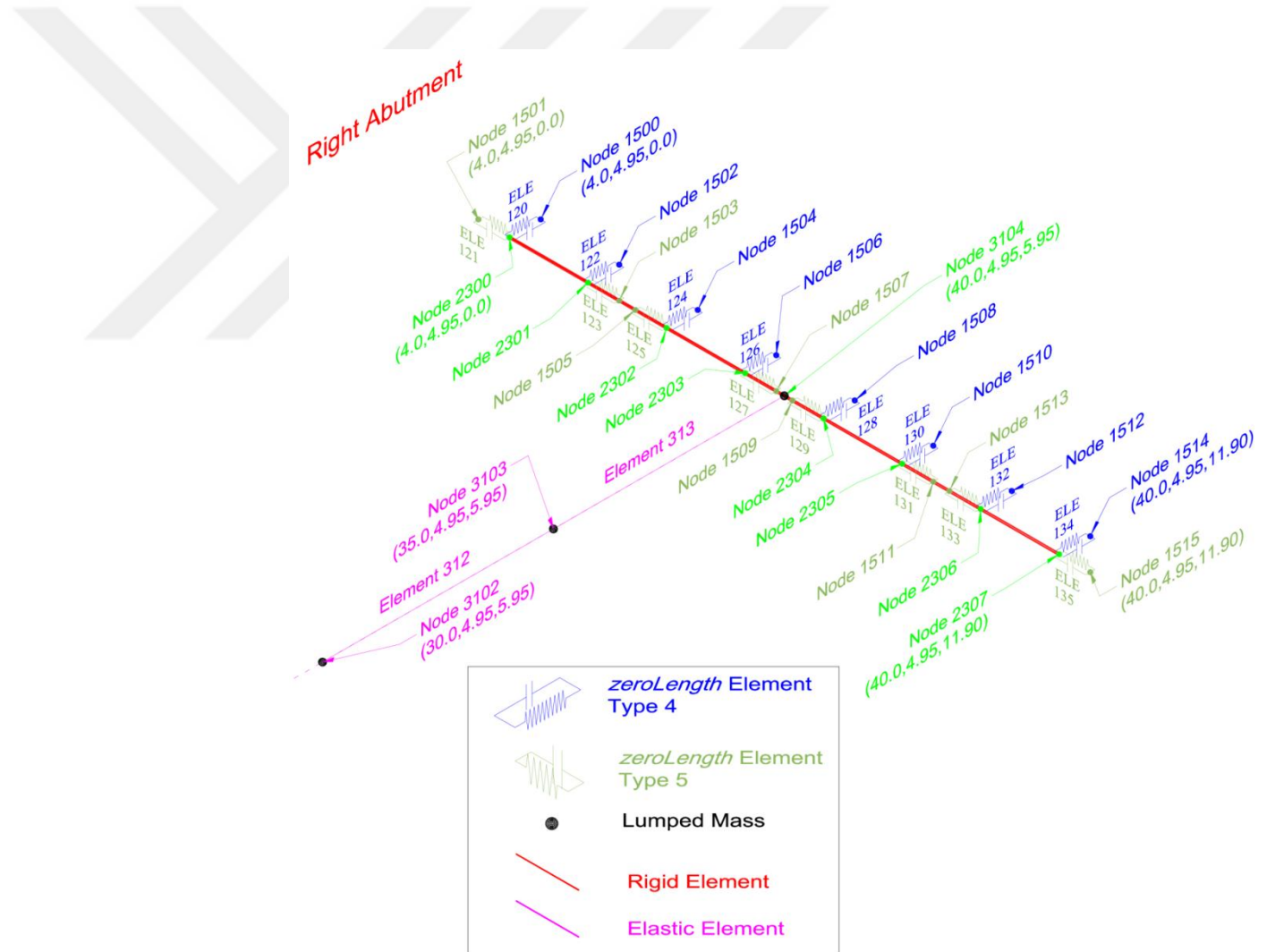


Figure 2.10 : Elek Deresi Bridge analytical model – right abutment.

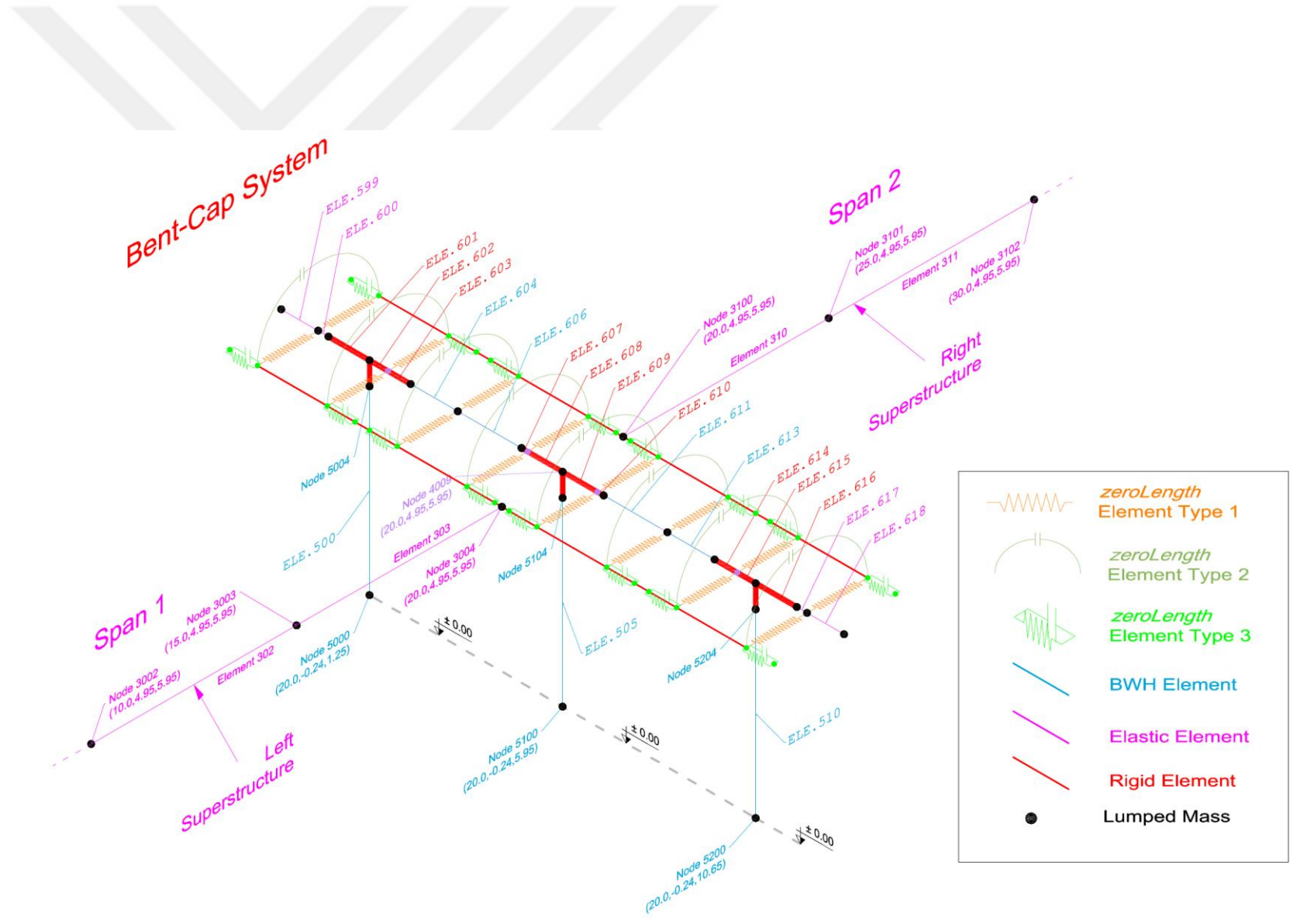


Figure 2.11 : Elek Deresi Bridge analytical model – bent cap system.

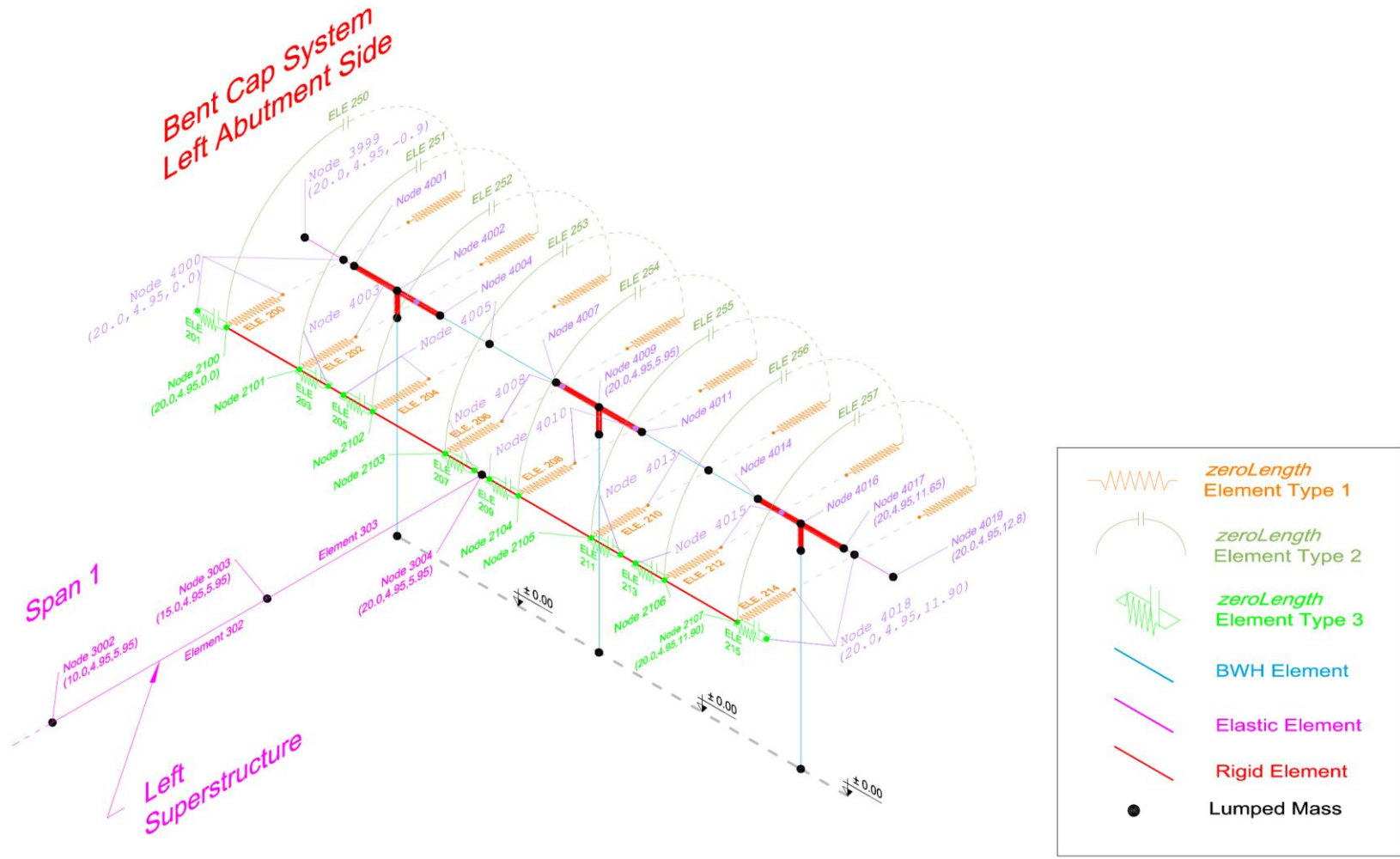


Figure 2.12 : Elek Deresi Bridge analytical model – bent cap system – left abutment side.

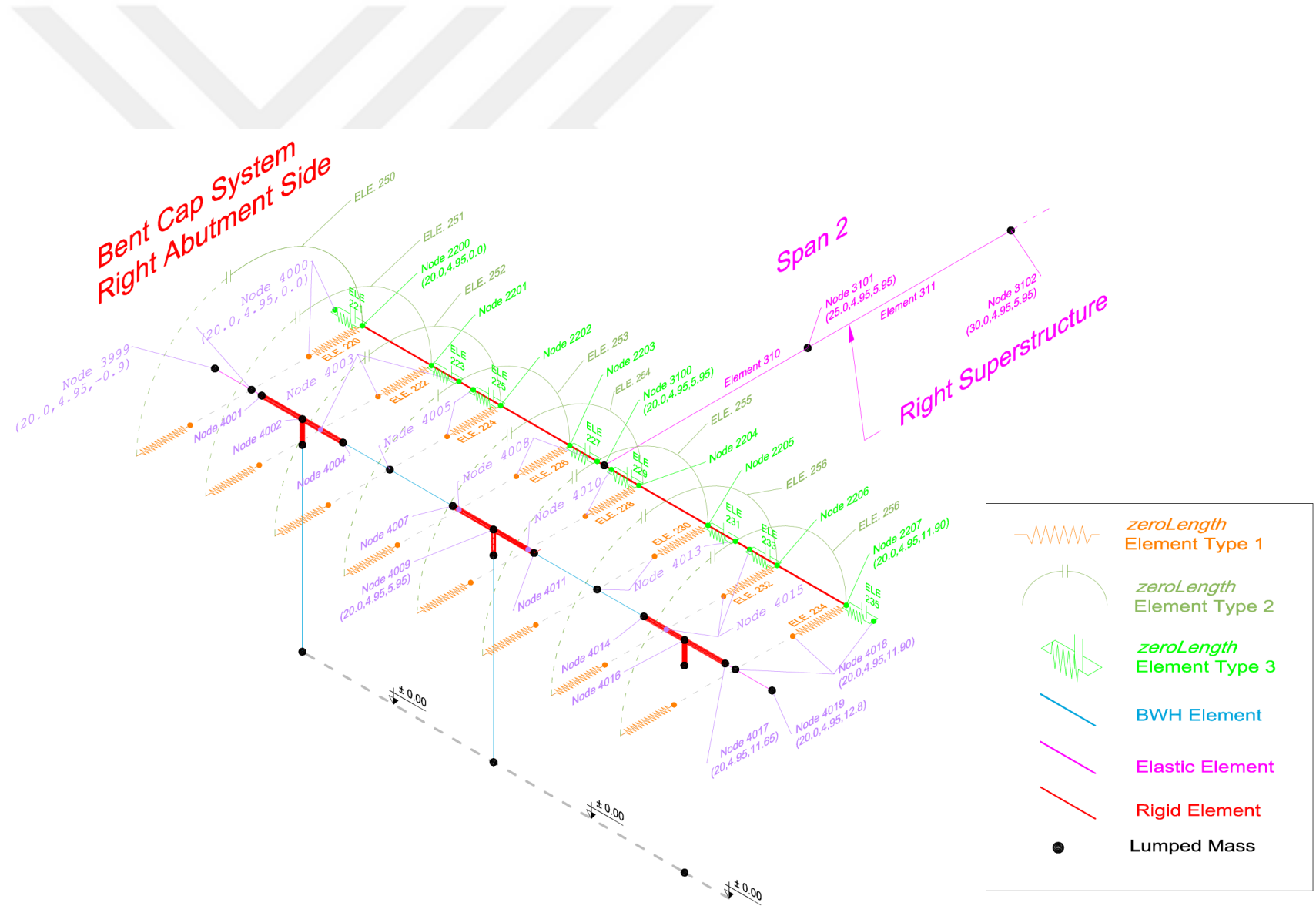


Figure 2.13 : Elek Deresi Bridge analytical model – bent cap system – right abutment side.

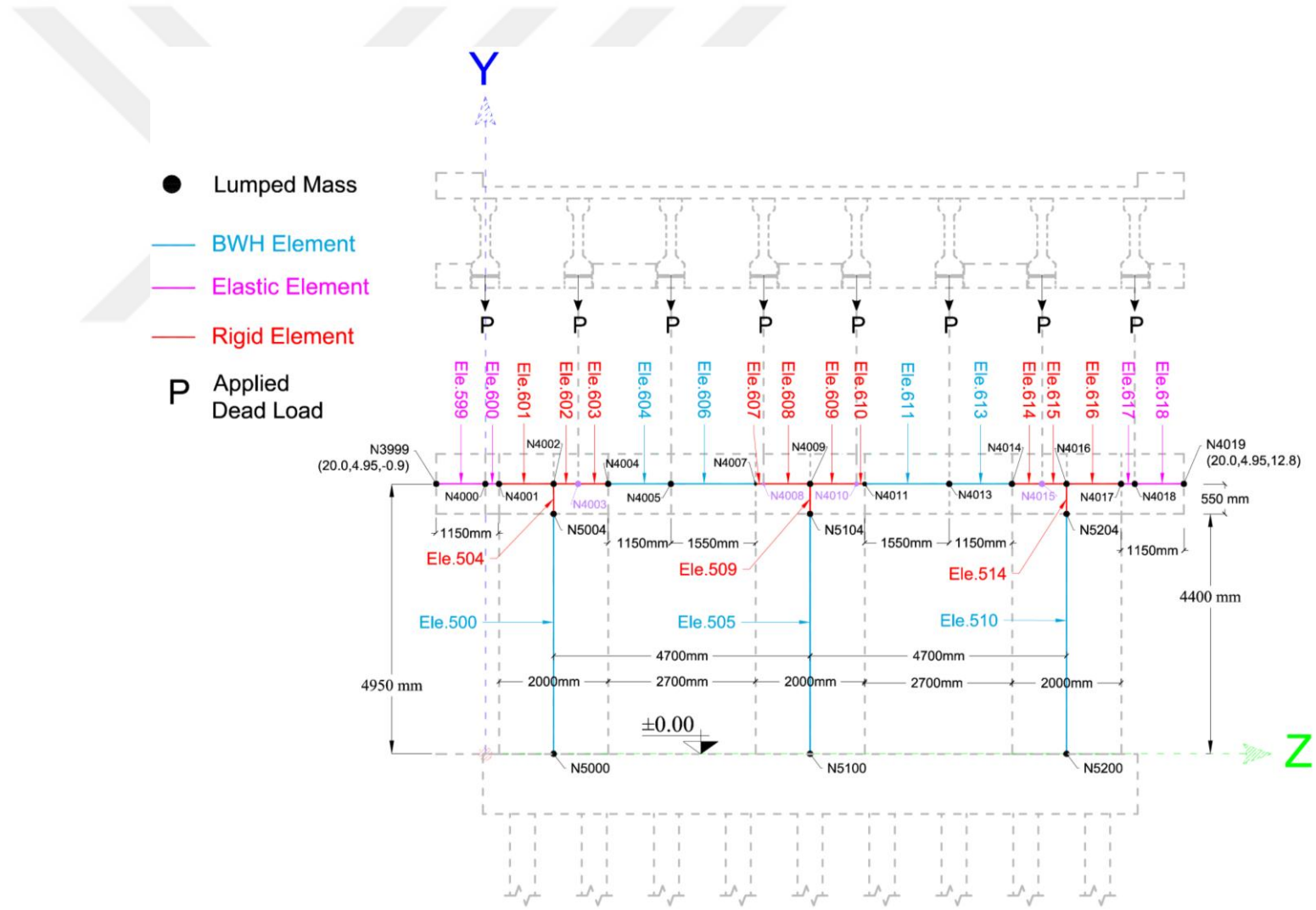


Figure 2.14 : Elek Deresi Bridge analytical model – bent cap system – node and element configuration.

2.4.1 Calculating mass of the bridge and gravity analysis

Only dead load of bridge components has been considered for analysing seismic response of the structure. Geometric properties and dimensions of bridge components have been presented previously in Section 2.2. Based on those drawings, mass of bridge components can be calculated. A 50mm thickness has been assumed also for the bituminous pavement covering the RC deck as this is the common trend in Turkey (EAPA¹, 2013). Results of bridge mass calculations are as follows.

- Superstructure: 730,000 kg = 730 Tons
- Columns: $3 \times 19,635 = 58,905$ kg
- Bent Cap Beam: 56,900 kg.

Thus, total bridge mass must approximately be 846,000 kg or 846 Tons. It is seen that superstructure mass is about 86~87 percent of the total mass.

Gravity analysis of the structure has been performed by defining point loads and uniformly distributed loads. Point loads have been used for introducing weight of the superstructure to the FE model. As the bridge has zero longitudinal slope and considering that each superstructure rests on 16 bearing pads (8 pads at each abutment and 8 pads at bent system), magnitude of the load applied to each bearing has been assumed to be 1/16 of superstructure weight. The described weight load distribution has been exhibited in Figure 2.15. According to the mentioned considerations, weight of the superstructure has been applied as point loads to nodes defined at bearing pad positions. These nodes are labelled as N4000, N4003, N4005, N4008, N4010, N4013, N4015 and N4018 at bent system as can be seen in Figure 2.16. Weights of columns have also been considered as point loads. Half of column weight has been applied at each column end (nodes 5000, 5004, 5100, 5104, 5200 and 5204). Weights of bent cap beam elements have been introduced to the model as uniformly distributed loads as illustrated in Figure 2.16. OpenSees *load* and *eleload* commands have been respectively employed for introduction of described point and distributed loads.

¹ European Asphalt Pavement Association

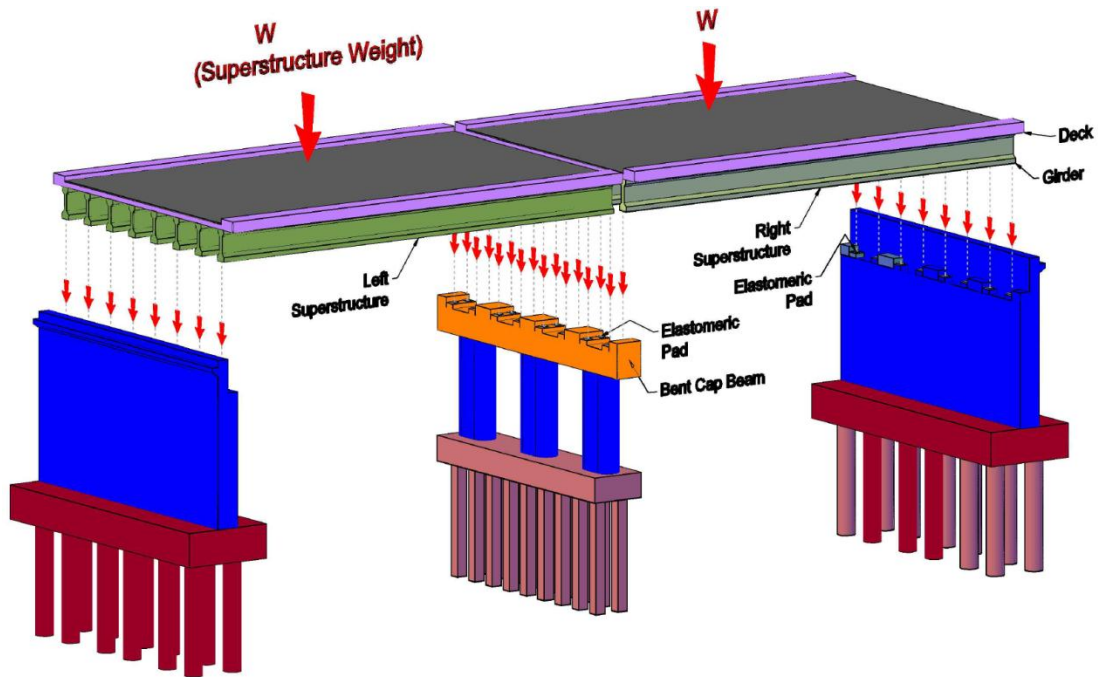


Figure 2.15 : Distribution of applied superstructure weight load between elastomeric bearings of bent system and abutments.

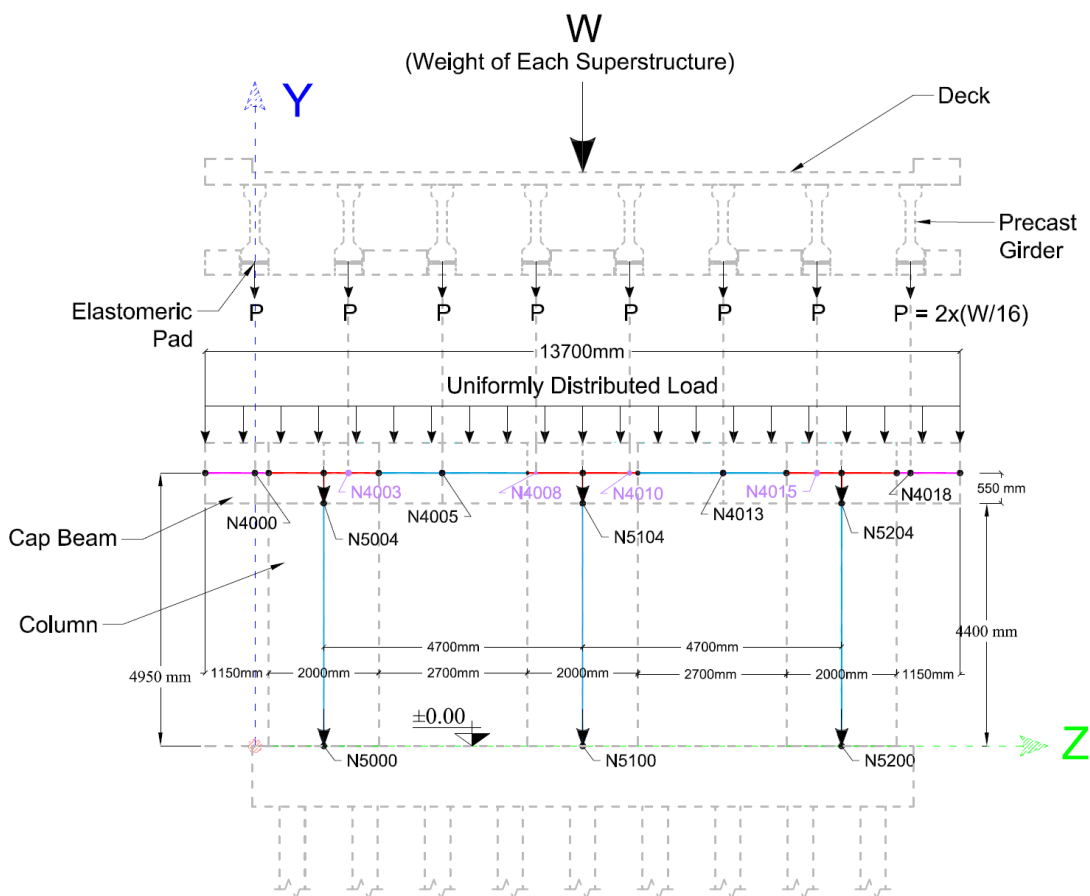


Figure 2.16 : Point and distributed loads applied at bent system.

2.4.2 Idealisation of elastomeric bearings

Bearings are used in bridges for facilitating transfer of loads (particularly traffic loads) from superstructure to substructure. Various types of bearings have been utilised in bridges around the world. One simple bearing type which has been used in Elek Deresi Bridge and other ordinary bridges studied by Avşar is elastomeric bearing (Avşar, 2009). According to Chen and Duan, (2014) those elastomeric bearings which are manufactured from altering layers of rubber with steel plates vulcanised to them are called reinforced elastomeric bearings². The elastomer of bearings is either natural rubber or neoprene which is a family of synthetic rubbers (Chen and Duan, 2014). Sometimes plain elastomeric blocks are used when loadings are small. However, these rubber blocks are not appropriate for heavy loads because they might bulge excessively under great pressures (Chen and Duan, 2014). To meet this deficiency, plain elastomeric pads are reinforced with steel plates (shims). Using this technique, vertical deformations of bearings remain limited (Chen and Duan, 2014).

Figure 2.17 schematically presents placement of reinforced elastomeric bearing pads employed in Elek Deresi Bridge. In contrary to some other types of bearings, elastomeric bearing pads allow the superstructure to move or rotate in all directions (Ramberger, 2002). Sometimes, elastomeric pads are fixed by restraining steel constructions to transmit shear forces (Ramberger, 2002). Nonetheless, elastomeric pads used in Elek Deresi Bridge and other ordinary bridges studied by Avşar (2009) are unanchored ones; which means they are not attached to sub- or superstructure by any device. Hence, the only force that opposes sliding of superstructure over pads is the friction force between superstructure girders and bearings. As well, the only force that stops pads from sliding is the friction between them and concrete surfaces.

² They are also called sometimes laminated elastomeric bearings.

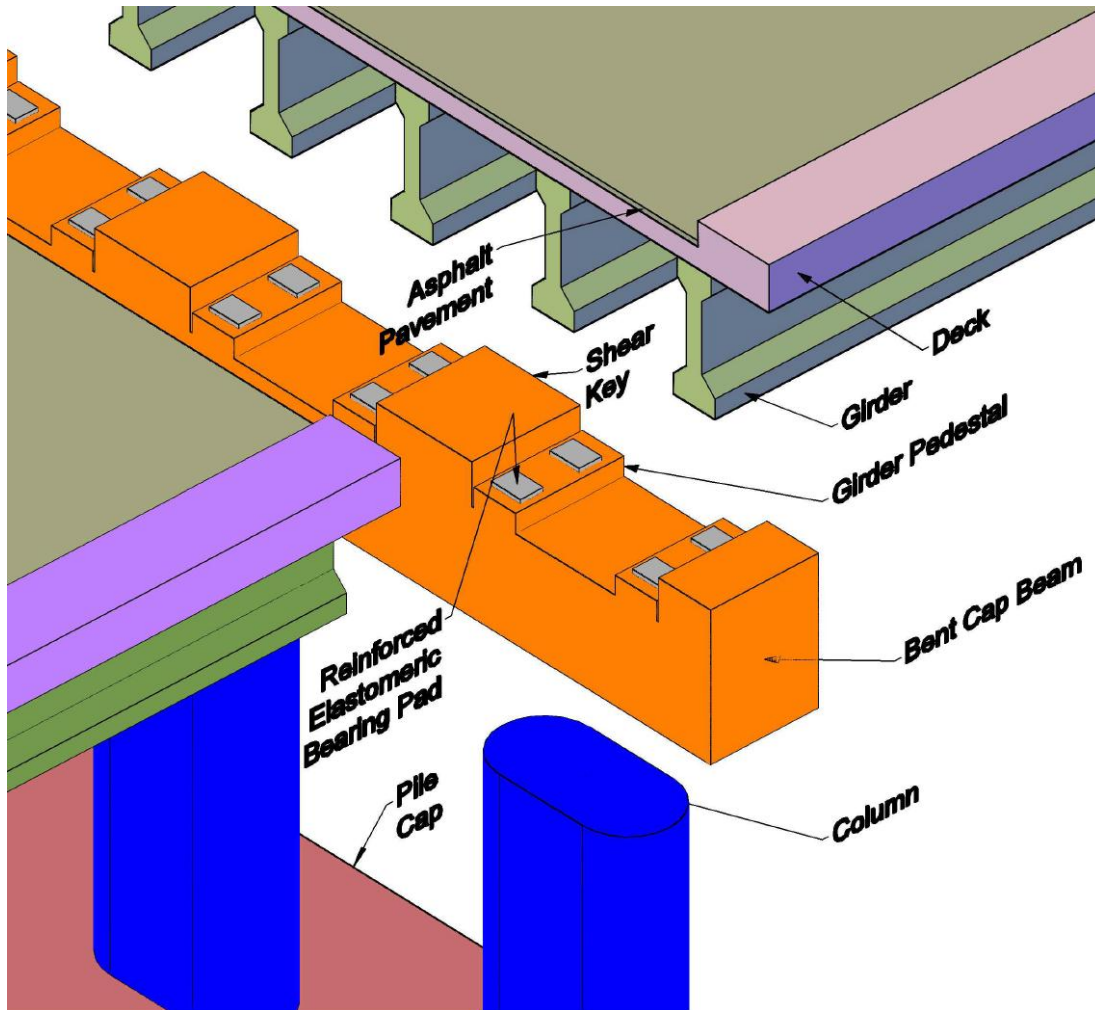


Figure 2.17 : Schematic view of bearing pads in an ordinary bridge and other components.

The relation for estimating friction force (F) is $F = C \times \mu$; in which C stands for compressive force and μ is friction coefficient between pad and concrete surface (Ramberger, 2002). The friction force increases linearly by displacement of superstructure. The ultimate retaining force that can be sustained by bearings can be estimated as 0.4 times the compressive force ($F_{friction} = C \times 0.4$) (Avşar, 2009). As soon as $F_{friction}$ is attained, no extra retaining force is applied by the bearing. Although the compressive force (C) might change during a real earthquake, an average value equal to dead load applied by the superstructure has been considered for it. This is because approximating the frictional force due to an alternating compressive load is pretty impractical (Avşar, 2009).

The material used by Avşar (2009) for characterising elastomeric bearings is Elastic-Perfectly Plastic Material. The relation for initial stiffness of this material has been provided by Avşar (2009) as can be seen in equation (2.1).

$$K_{bearing} = \frac{G \times A}{h_{rt}} ; h_{rt} = h_t - n \times h_s \quad (2.1)$$

In equation (2.1) G is the shear modulus of bearing (1.1 MPa), A is the area of bearing, h_t is thickness of bearing, h_s is thickness of steel plates (shims) and n is the number of shims.

Details provided by Avşar (2009) for bearings used in ordinary bridges with three columns (including Elek Deresi Bridge) are exhibited in Figure 2.18. Moreover, Avşar (2009) reports a value of 350mm for bearing length and a value of 250mm for bearing width.

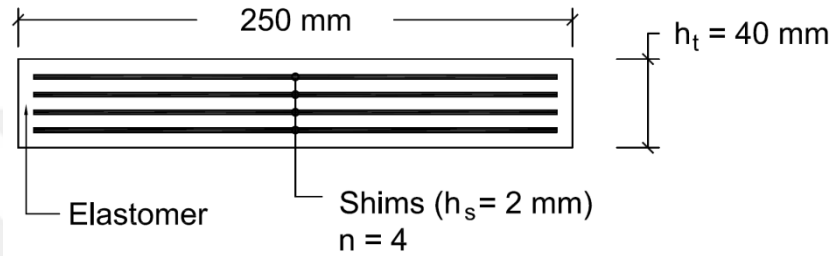


Figure 2.18 : Specifications of the reinforced elastomeric bearing.

Using the mentioned values, h_{rt} (combined thickness of rubber layers) is calculated as 32 mm and bearing stiffness ($K_{bearing}$) as 3.0 KN/mm.

As mentioned previously in Subsection 2.4.1, total mass of superstructure is approximately 730 Tons. Hence, the average compressive load applied to each pad can be calculated as $\frac{730 \times 1000 \times 9.81}{4 \times 8} = 224 \text{ KN}$ and $F_{friction} = 0.4 \times 224 = 89.6 \text{ KN}$.

The material model employed for sampling elastomeric bearings has bilinear behaviour and is named Steel01Material (Figure 2.19). This material will be called *Elastomeric Material* hereafter. A strain hardening ratio equal to 10^{-3} has been introduced to the idealised material after displacement corresponding to $F_{friction}$ (29.9mm) is reached. This minor strain hardening ratio contributes to stability of model in case a shear force greater than the combined force that bearings can sustain³ is applied to the superstructure. This is because expansion gaps allow the superstructure to move freely once the elastomeric pads reach their ultimate capacity. The displacement may continue till the moving superstructure impacts with abutment back wall, shear keys or superstructure of other span.

³ Any force greater than $16 \times F_{ult}$, in which 16 is the number of bearings for left or right superstructure.

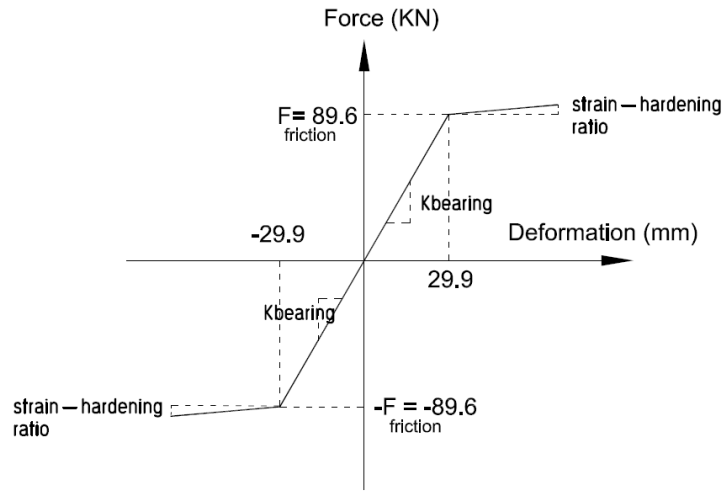


Figure 2.19 : Elastomeric material for idealisation of elastomeric bearings.

2.4.3 Idealisation of abutments

Bridge abutments have functions like sustaining vertical and horizontal loads applied by the superstructure, connecting the superstructure to the main carriageway or to the ground and retaining the backfill soil. Numerous types of abutments have been used in different bridges. The abutment type of Elek Deresi Bridge and other ordinary bridges studied by Avşar (2009) is seat-type abutment. Seat abutment is a type of abutment that is constructed separately from the superstructure (Chen and Duan, 2014)). The superstructure seats on the abutment afterwards, in a way that superstructure loads can be transferred to the abutment through bearings (Figure 2.20 provides a schematic view of seat abutment). Consequently, this approach differs from monolithic (end diaphragm) abutment technique in which abutments are constructed integral with the superstructure (Chen and Duan, 2014). Back wall, stem wall, wing walls and footing are main components of a seat-type abutment (Caltrans, 2006). Back wall and stem wall dimensions that are required for modelling purposes of this study can be observed in Figure 2.6.

Abutments and their backfill soil contribute to structure's stiffness. For estimating this contribution, Avşar (2009) has used a pretty simple technique proposed by Caltrans (2006) which provides a bilinear approximation for abutment stiffness. One reason for selecting this simple approach is that detailed information about backfill material properties of every studied bridge by Avşar (2009) is not available. Hence, soil-structure interactions could not be taken into account. In the following, embankment stiffness and ultimate strength in longitudinal and transversal directions for active and passive soil pressures will be calculated using the mentioned approach.

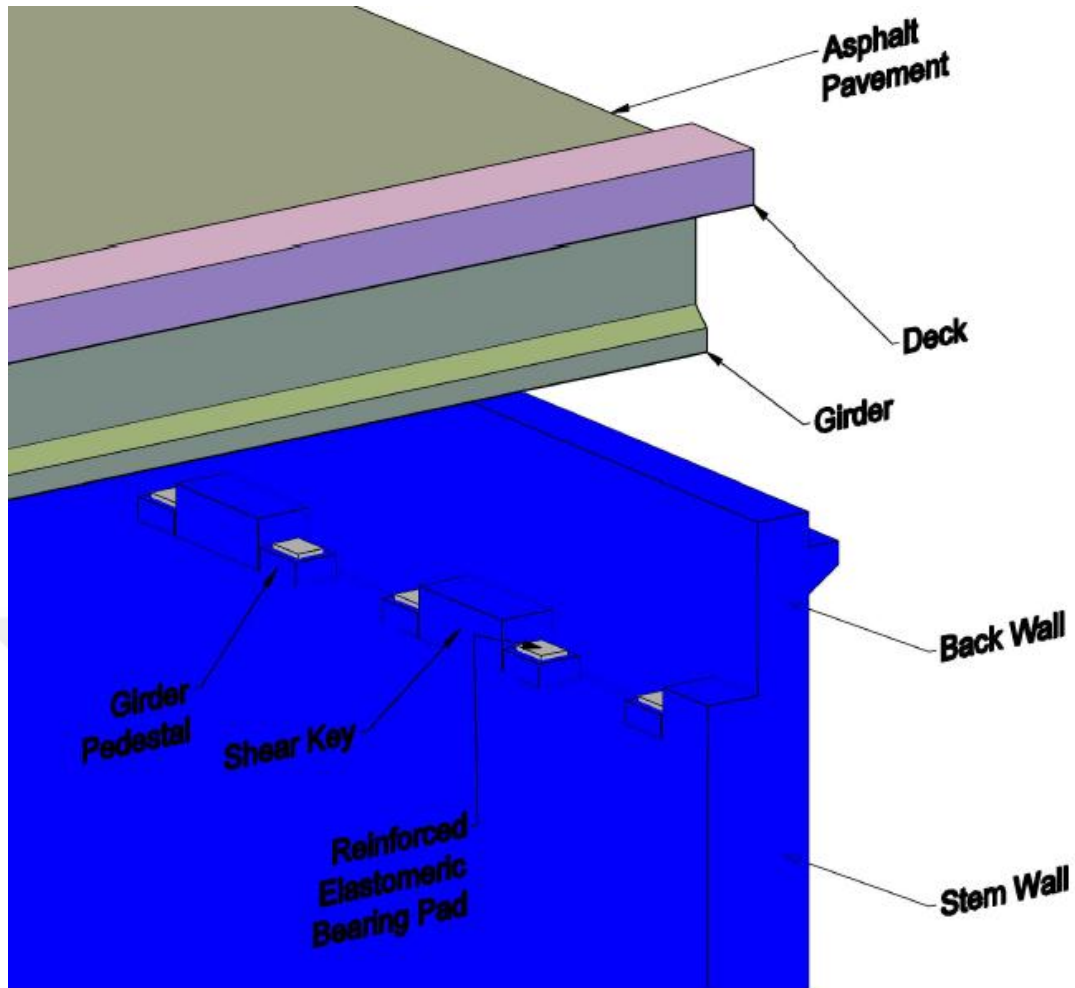


Figure 2.20 : Schematic view of a seat-type abutment.

a- Longitudinal direction - passive case

In passive case (stage when abutment is exerting force to embankment fill and pushing it inside), initial stiffness of embankment fill materials (K_i) is specified by equation (2.2), (Caltrans, 2006).

$$K_i = 11.5 \frac{KN/mm}{m} \quad (2.2)$$

This value can be used in equation (2.3) for calculating abutment stiffness (K_{abut}). In equation (2.3), w stands for back wall width and h stands for back wall height.

$$K_{abut} = K_i \times w \times \left(\frac{h}{1.7} \right) \quad (2.3)$$

Ultimate abutment strength can be obtained from equation (2.4). However, according to Avşar (2009), the maximum passive pressure of 239 KPa appearing in equation (2.4) must be multiplied by 1.5 to account for dynamic and seismic loadings. Hence, the final relation for ultimate capacity of abutment (P_{bw}) is obtained from equation (2.5).

$$P_{bw} = A_e \times 239 \text{ kPa} \times \left(\frac{h_{bw}}{1.7}\right) (m, KN) \quad (2.4)$$

$$P_{bw} = A_e \times 368 \text{ kPa} \times \left(\frac{h_{bw}}{1.7}\right) (m, KN) \quad (2.5)$$

In equations (2.4) and (2.5), A_e is the effective abutment area. For seat abutments, this value can be obtained from equation (2.6) in which h_{bw} and w_{bw} are respectively back wall height and width.

$$A_e = h_{bw} \times w_{bw} \quad (2.6)$$

In passive case, contribution of piles to bridge stiffness must also be taken into account. A conservative estimate of (7.0 KN/mm) per pile has been suggested by Caltrans (2006) for stiffness. For ultimate strength of piles, Avşar (2009) has used a value of 119 KN/pile.

b- Longitudinal direction - active case

For active case (the stage when the embankment fill exerts force to the abutment and pushes it towards bridge columns) contribution of backfill soil is disregarded. Consequently, only pile contribution has been taken into consideration. Pile contribution in active and passive cases is identical and can be considered as described before.

c- Transversal direction

For transversal direction, contribution of wing walls and the soil behind them has been ignored. Again, similar to active case, in longitudinal direction only pile contribution has been taken into account. Values for this contribution are as described previously (7.0 KN/mm per pile for stiffness and 119 KN per pile for ultimate strength).

Height of girder pedestals also influence estimation of abutment stiffness by altering back wall height. According to directions by Florida Department of Transportation (FDOT) (2018), girder pedestal height at bent cap beam must be greater than 4 inches. Also, because of aesthetic reasons, pedestal height should not be greater than 12 inches (FDOT, 2018). Taking into account the mentioned recommendations, an average height of 200mm has been assumed for all bridge pedestals. Moreover, number of abutment piles is also important for estimating abutment stiffness using the approximate method described in the above. Using schematic figures by Avşar (2009), 12 piles have been considered for each abutment.

2.4.3.1 Calculations

h (back wall height) = 1.91 m

w (back wall width) = 12 m

Using equations (2.2) and (2.3): $K_{abut} = 11.5 \times 12 \times \left(\frac{1.91}{1.7}\right) \cong 155 \frac{KN}{mm}$

Using equation (2.6): $A_e = 1.91 \times 12 = 22.92 m^2$

By equation (2.5): $P_{bw} = (1.91 \times 12) \times 368 \times \left(\frac{1.91}{1.7}\right) \cong 9'500 KN$

Eight zeroLength elements have been employed at each bridge end for simulating superstructure interaction with abutments. As a result, the calculated abutment stiffness and ultimate strength values must be divided by 8. By these considerations, material properties used for simulating embankment fill contribution in longitudinal direction (called *Backfill Material* hereafter) has been exhibited in Figure 2.21. As can be observed from this figure, stiffness of each element is $\frac{155}{8} = 19.375 \frac{KN}{mm}$ and ultimate strength of each element is $\frac{9500}{8} = 1'187.5KN$. The material used is Elastic-Perfectly Plastic Compression Gap Material. A gap material was selected because embankment backfill starts applying forces on the superstructure only when the 50.0 mm in between expansion gap has been closed.

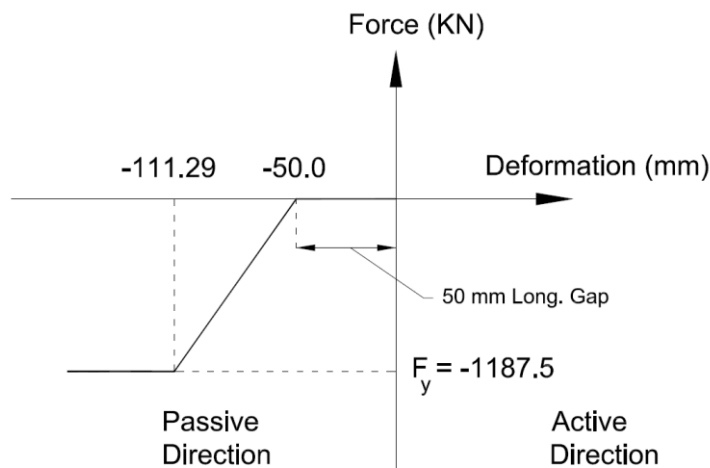


Figure 2.21 : Backfill material for idealisation of embankment backfill contribution.

Pile contribution in both longitudinal and transversal directions has also been idealised by Elastic-Perfectly Plastic Compression Gap Materials. Nonetheless, in longitudinal direction, idealised piles start functioning after superstructure impacts with embankment (the 50.0 mm expansion gap closes) whereas in transversal direction they start working when superstructure impacts with shear keys (the 25.0 mm expansion gap closes).

Again, as eight zeroLength elements have been employed at each bridge end in both transversal and longitudinal directions and 12 piles have been considered for the model, stiffness and ultimate strength of each zeroLength material must be modified. This results in stiffness of each element as $(12 \times 7 \text{ KN/mm})/8 = 10.5 \text{ KN/mm}$ and ultimate strength of each element as $(119 \times 12)/8 = 178.5 \text{ KN}$. After now on, the material used for idealisation of contribution of piles in longitudinal direction will be called *Longitudinal Pile Material* and the material for characterising pile contribution in transversal direction will be called *Transversal Pile Material* (see Figure 2.22).

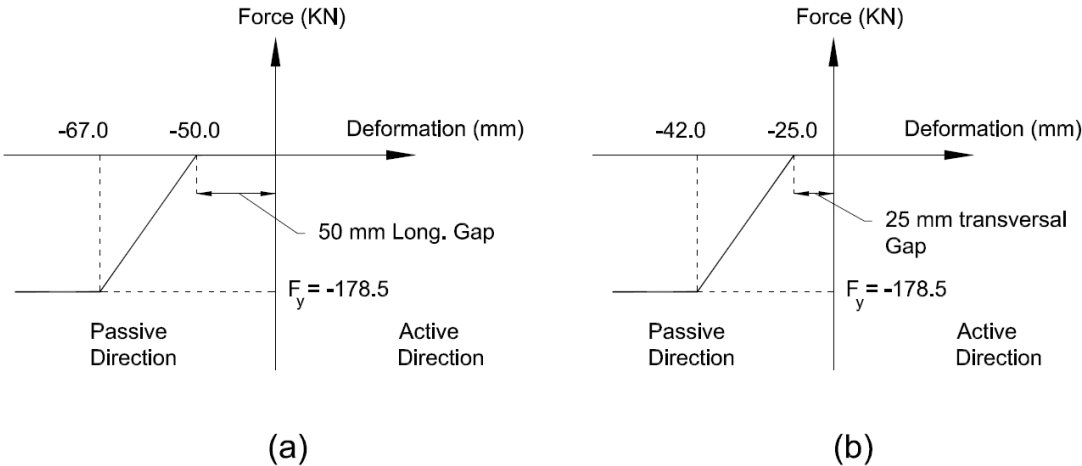


Figure 2.22 : (a) Longitudinal pile material for idealisation of longitudinal contribution of piles (b) Transversal pile material for idealisation of transversal contribution piles.

2.4.4 Simulating collision between bridge components

The bridge under study consists of gaps between its components which are known as expansion gaps. An expansion gap can be defined as the area between adjacent superstructures or superstructure and abutment (TSO, 2007). These gaps are necessary to make up for superstructure displacements, expansions and contractions. Apart from seismic loadings, superstructure of a bridge might move, rotate or change size because of several reasons such as foundation settlements, temperature changes, dynamic loads, traffic loads, etc. (Jones, 2011). Gaps are required for accommodating these movements and size alterations.

As mentioned before, there is no rigid attachment between superstructure and substructure of the bridge under study. Consequently, the superstructure can float over substructure as soon as it gets subjected to a shear force greater than resistance capacity due to friction between superstructure and bearing pads. In longitudinal direction, superstructure collides with abutment if its movement is great enough (impact case 1).

In transversal direction, superstructure may collide with bent system or abutment shear keys (impact case 2). Another instance (impact case 3) is collision of superstructures of two spans with each other. In impact case 1 (superstructure – abutment impact), the 50 mm longitudinal expansion gap needs to get closed. Impact case 2 (superstructure – shear key impact) occurs upon closure of 25 mm in-between transversal gap. Finally, for occurrence of impact case 3 (superstructure – superstructure impact), the 100 mm gap between the two spans must be closed.

Once more, zeroLength elements have been employed for simulating above-mentioned pounding behaviours. Similar to zeroLength elements used for idealisation of embankment backfill and piles, Elastic-Perfectly Plastic Compression Gap Material model has been employed. Avşar (2009) recommends values for stiffness and ultimate strength of back wall and shear keys and their ultimate strengths. For abutment back wall, suggested shear and flexural stiffness is 150 KN/mm and suggested ultimate strength is 250 KN (Avşar, 2009). Nonetheless, similar to abutment earth fill and pile simulation, both stiffness and strength values have been modified (divided by 8). This is because eight elements have been utilised for modelling impacts at superstructure ends. For each shear key, recommended shear and flexural stiffness and ultimate strength are 3,400 KN/mm and 1,600 KN (Avşar, 2009). For impact case 3, peak stress and modulus of elasticity values of the zeroLength element have been chosen equal to ultimate compressive strength and Young's modulus of the concrete used for construction of prefabricated girders (40.0 N/mm^2 and $29,725 \text{ N/mm}^2$ respectively). This is because the superstructure will be modelled by an equivalent section made of C40 grade concrete as will be described in Subsection 2.4.6. From now on, the idealised material employed for characterising collision between superstructure and abutment will be called *Abutment Pounding Material*, the material used for characterising collision between superstructure and shear keys will be called *Shearkey Pounding Material* and the material used for characterising collision between decks will be called *Deck Pounding Material*. Figure 2.23 represents properties of these three idealised materials.

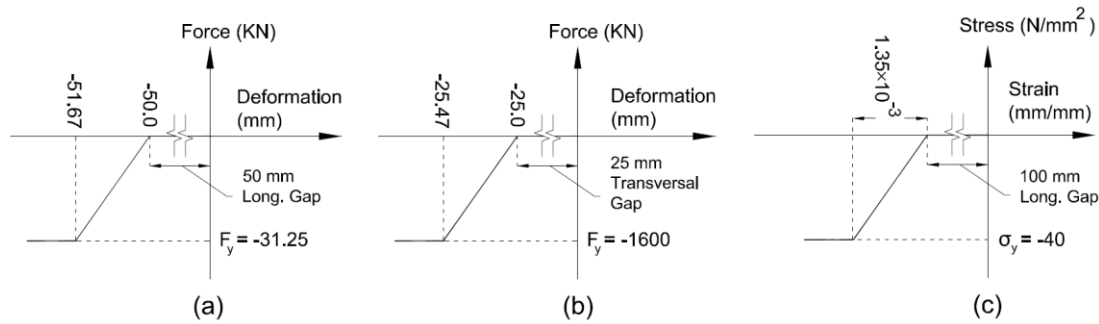


Figure 2.23 : (a) *Abutment Pounding Material* for superstructure - abutment collision (b) *Shearkey Pounding Material* for superstructure - shear key collision (c) *Deck Pounding Material* for superstructure - superstructure collision.

Table 2.1 summarises material models assigned to zeroLength elements, their applications and properties.

Table 2.1: Summary of materials employed for zerolength elements.

	Application	Type	Stiffness (KN/mm)	F _y (KN)
<i>Elastomeric Material</i>	Elastomeric Bearings	Steel01	3.0	89.6
<i>Backfill Material</i>	Embankment Fill	Elastic-Perfectly Plastic Compression Gap Material	19,375	1,187.5
<i>Longitudinal Pile Material</i>	Pile - Long. Direction	Elastic-Perfectly Plastic Compression Gap Material	10.5	178.5
<i>Transversal Pile Material</i>	Pile - Transversal Direction	Elastic-Perfectly Plastic Compression Gap Material	10.5	178.5
<i>Abutment Pounding Material</i>	Abutment Back Wall	Elastic-Perfectly Plastic Compression Gap Material	18.75	31.25
<i>Shearkey Pounding Material</i>	Shear Key	Elastic-Perfectly Plastic Compression Gap Material	3,400	1,600
<i>Deck Pounding Material</i>	Across Superstructures	Elastic-Perfectly Plastic Compression Gap Material	29,725 (N/mm ²)	40.0 (N/mm ²)

2.4.5 Introducing zerolength elements used in the model

Altogether, five types of *zeroLength* elements have been used in Elek Deresi Bridge FE model using idealised material properties discussed previously. This subsection describes types and specifications of employed zeroLength elements.

zeroLength Element Type 1: This element works in longitudinal direction and has been employed for simulating frictional resistance between elastomeric bearing pads of bent system and superstructure. *Elastomeric Material* has been assigned to this element. Ultimate strength of this element is 89.6KN which is the ultimate strength of *Elastomeric Material*.

zeroLength Element Type 2: This element works in longitudinal direction and has been employed for simulating impacts between two superstructures due to closure of 100 mm in between expansion gap. *Deck Pounding Material* has been assigned to this element.

zeroLength Element Type 3: This element works in transversal direction. It is used for simultaneous sampling of 1) frictional resistance between elastomeric pads and superstructure 2) impacts between superstructure and bent cap shear keys. A combined parallel material consisting from *Elastomeric Material* and *Shearkey Pounding Material* has been assigned to this element. Ultimate strength of this element is 120.85 KN which is sum of ultimate strength of *Elastomeric Material* and *Abutment Pounding Material*.

zeroLength Element Type 4: This element works in longitudinal direction. It has been used for simultaneous modelling of 1) frictional resistance between abutment bearings and superstructure girders 2) embankment backfill action 3) pile action in longitudinal direction 4) collision between superstructure and embankment. A combined material made up of *Elastomeric Material*, *Backfill Material*, *Longitudinal Pile Material* and *Abutment Pounding Material* has been assigned to this element. Ultimate strength of this element is 1,486.85 KN which is sum of ultimate strength of its composing materials.

zeroLength Element Type 5: This element works in transversal direction. It has been used for simultaneous modelling of 1) frictional resistance between abutment elastomeric bearings and superstructure girders 2) pile function in transversal direction 3) collision between superstructure and shear keys of embankment. A combined material made up of *Elastomeric Material*, *Transversal Pile Material* and *Shearkey Pounding Material* has been assigned to this element. Ultimate strength of this element is 1868.1 KN which is sum of ultimate strength of its composing materials.

Figure 2.24 schematically presents combined materials assigned to the zeroLength elements.

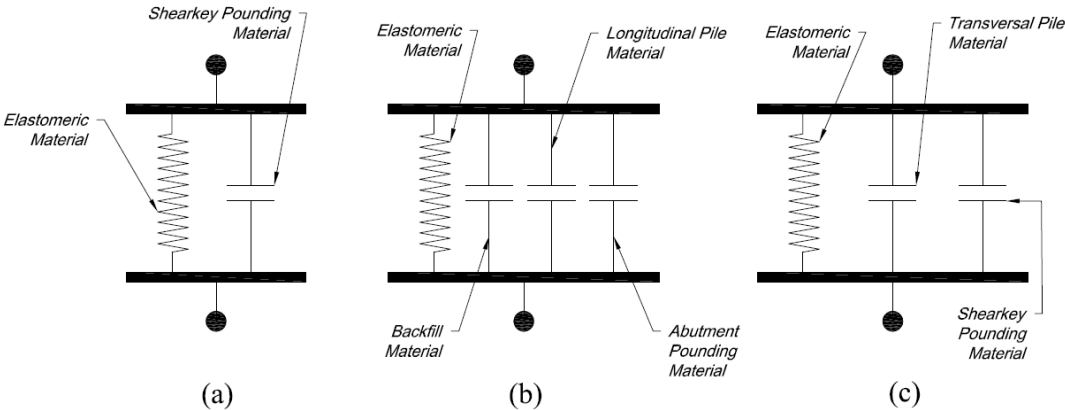


Figure 2.24 : (a) Combined material for *element type 3* (b) Combined material for *element type 4* (c) Combined material for *element type 5*.

2.4.6 Idealisation of the superstructure

As mentioned previously, according to Caltrans (2006), superstructures of ordinary bridges must be strong enough to stay elastic when the bent system reaches its maximum plastic capacity. Moreover, ordinary bridges studied by Avşar (2009), including Elek Deresi Bridge, have been assumed to be in agreement with this guidance. As a result, OpenSees Elastic Beam Column element has been employed for simulating bridge superstructure. The parameters required by OpenSees for introducing this type of element are:

- Cross-sectional area of element
- Young's Modulus
- Shear Modulus
- Torsional moment of inertia of cross section
- Second moment of area about the local axes

The problem with modelling the superstructure by Elastic Beam Column elements is that the superstructure is a composite section made of cast in place deck and prefabricated girders (Figure 2.25). According to Avşar (2009), cast in place deck is made of C25 concrete grade (concrete with unconfined compressive strength of 25 N/mm²) and girders are made of C40 concrete grade (concrete with unconfined compressive strength equal to 40 N/mm²). Consequently, the superstructure cannot be idealised as a homogenous section as it is made of two materials with different material properties.

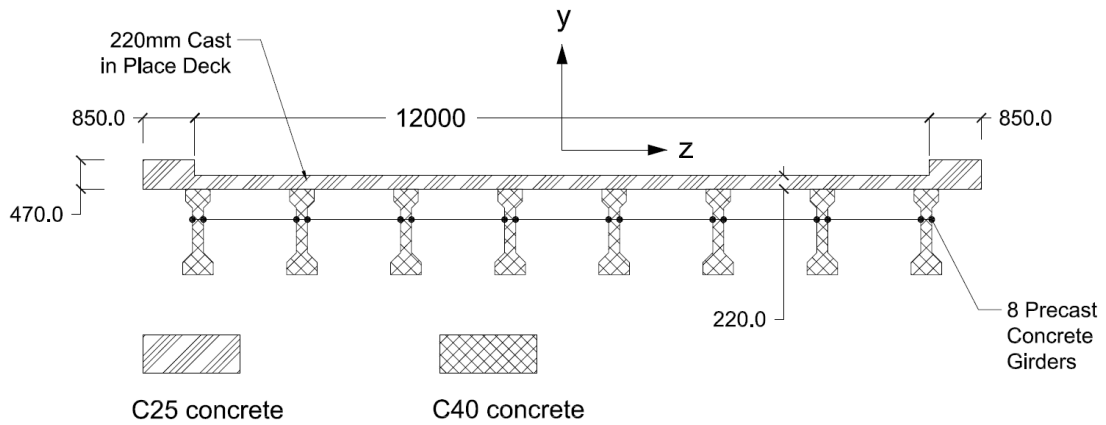


Figure 2.25 : Bridge superstructure geometry and materials.

The problem might be solved by introducing an equivalent section, made homogeneously of C40 concrete class. For this purpose, Young's modulus (E_c) of C25 and C40 concrete are calculated through equation (2.7) (Mander et al, 1988).

$$E_c = 5000\sqrt{f'_{co}} \text{ MPa} \quad (2.7)$$

In equation (2.7) f'_{co} is unconfined compressive strength of concrete. Therefore, Young's modulus of C25 and C40 concrete grades can be calculated as 25,000 MPa and 31,623 MPa respectively.

Second moment of area about local y axis (I_{yy}) of the model element is approximated through an equivalent section as can be observed in Figure 2.26. In this equivalent section, thickness of the original deck has been multiplied by a factor of $E_{C25}/E_{C40} = \frac{25,000}{31,623} = 0.79$ and C40 concrete properties have been considered for the whole section.

I_{yy} of this equivalent section has been calculated as 99.43 m^4 .

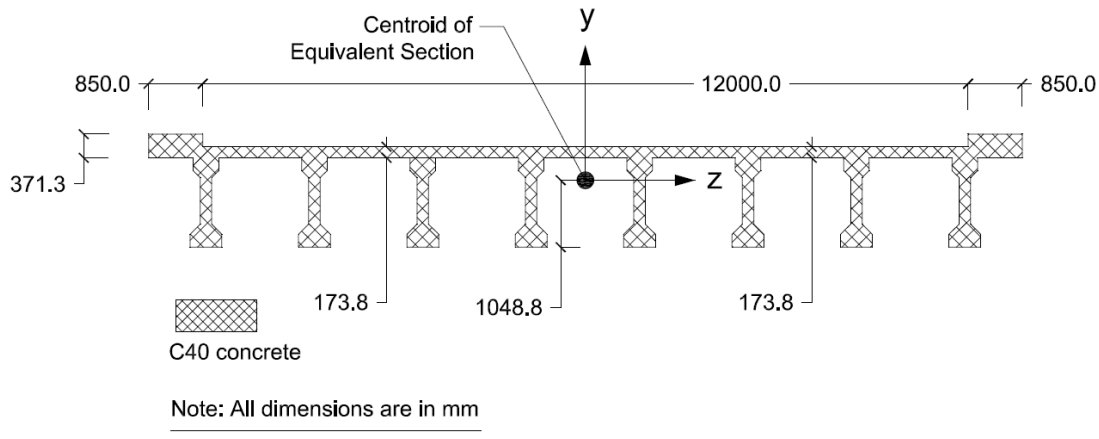


Figure 2.26 : Equivalent superstructure section for flexure about local y axis.

The idea behind this technique is that, assuming an elastic material behaviour, deformations of the modified deck with C40 concrete material equals deformations of the original deck (made of C25 concrete) for a moment causing flexure about local y axis. For flexure about local z axis, the same technique has been utilised. Nonetheless, this time, it is width of the deck that must be adjusted. Hence, the equivalent section is defined as can be seen in Figure 2.27 and I_{zz} (second moment of area about local z axis) of equivalent section is calculated as 1.871 m^4 .

Torsional moment of inertia (J) of discussed equivalent sections can be estimated by SAP2000 programme. This property has been calculated as 0.1297 m^4 for equivalent section exhibited in Figure 2.26 and 0.1474 m^4 for equivalent section presented in Figure 2.27. An average value of 0.138 m^4 has been considered for the modelling purposes.

Shear modulus of C40 concrete is calculated using equation (2.8) (Popov, 1990).

$$G = \frac{E}{2(1 + \nu)} \quad (2.8)$$

In equation (2.8), G is modulus of elasticity in shear, E is Young's modulus and ν is Poisson's ratio (0.2 for concrete).

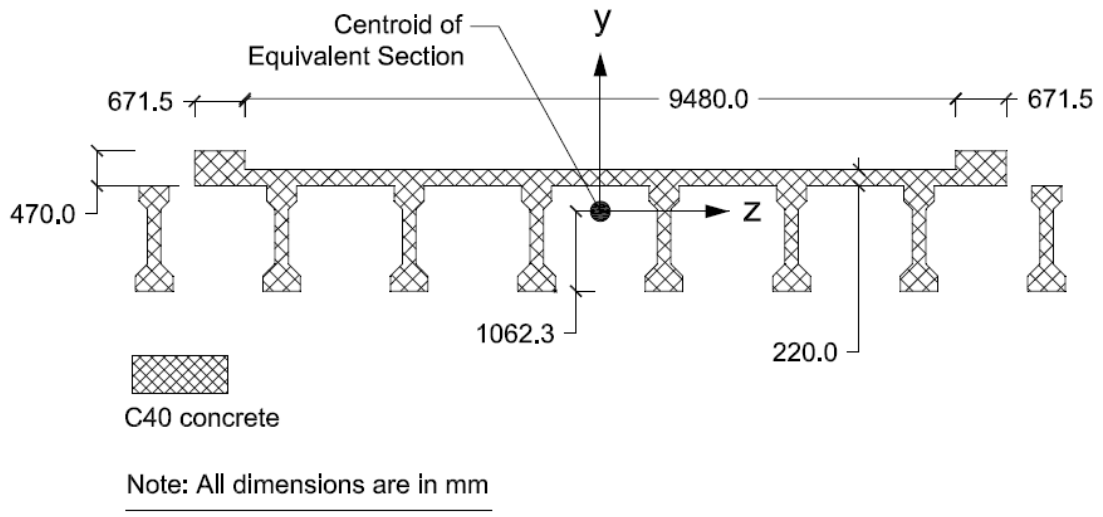


Figure 2.27 : Equivalent superstructure section for flexure about local z axis.

Sectional properties used for elastic modelling of the superstructure have been summarised in Table 2.2. Note that area of the original section represented in Figure 2.25 is 6.62 m².

Table 2.2 : Sectional properties used for modelling elements of superstructure.

Area (m ²)	I_{yy} (m ⁴)	I_{zz} (m ⁴)	J (m ⁴)
5.898	99.43	1.871	0.138

2.4.7 Idealisation of bent system

As mentioned previously, bent system of Elek Deresi Bridge is composed of three columns and a bent cap beam. Contrary to the superstructure, inelastic deformations are expected in bent system components of bridges subjected to strong ground motions. Consequently, elements capable of modelling nonlinearities are required for idealisation of columns and the cap beam. For this purpose, Beam With Hinges Element objects have been employed (Scott and Fenves, 2006). This element allows for considering nonlinearities on the element interior as well as defining length of plastic hinges at element ends. However, beam - column connection zones have been characterised using Elastic Beam Column Elements. Figure 2.14 presents elements considered for simulating bent system components.

Cap beam – column connections have been modelled using Elastic Beam Column Elements. However, Young's modulus of the material assigned to end zone elements has been chosen 25 times greater than adjacent elements to account for higher rigidity at connections. Similar to superstructure elements, sectional properties of the bent system

components must be calculated and assigned to Elastic Beam Column Elements employed at cap beam – column connections. Results of these calculations have been summarised in Table 2.3. Torsional moment of inertia (J) of sections has been calculated using SAP2000 programme.

Table 2.3 : Sectional properties of cap beam and column elements.

	$I_{yy}(m^4)$	$I_{zz}(m^4)$	$J(m^4)$	$I_{yy}(m^4)$
Column Elements	1.785	0.1324	0.4954	0.4029
Cap Beam Elements	1.32	0.1331	0.1584	0.245

For characterisation of non-rigid elements, material properties regarding to all six degrees of freedom have been calculated and aggregated in element sections. This way, a single section force-deformation model can be constructed for each element. The mentioned process and relevant calculations will be discussed in subsections 2.4.7.1 and 2.4.7.2. OpenSees command used for aggregating several material properties in a single section is Section Aggregator command. Using this command, material objects representing axial, torsional and shear force-deformation characteristics as well as materials representing moment-curvatures can be aggregated in one section. Afterwards, this section property can be assigned to particular elements.

Concrete class used in construction of bent systems of the bridge is C25 concrete with characteristic unconfined compressive strength of 25 MPa. Steel used for reinforcement is S420 steel grade with characteristic yield strength of 420 MPa, ultimate strength of 550 MPa and Young's modulus of 200 GPa. Ultimate strain of S420 steel has been assumed to be 0.1 mm/mm according to TEC (2007) and its strain hardening ratio has been considered as 0.0066 which is in agreement with the value used by Avşar (2009). In this study, as it will be discussed in detail in the third chapter, yield stress of reinforcing steel has been selected as the uncertain model parameter. Material strengths for modelling purposes (unconfined compressive strength of concrete and steel yield strength) have been obtained using stochastic simulation. Consequently, different steel properties have been assigned to different models. It will be seen in Section 3.2 that unconfined concrete has a mean strength of 21.75 MPa and reinforcing steel has a mean yield stress of 472.41 MPa.

2.4.7.1 Materials representing axial, shear and torsional force-deformation characteristics

Linear elastic characteristics have been considered for material objects representing axial, shear and torsional force-deformations of bent system non-rigid elements. OpenSees Elastic Uniaxial Material has a linear shape and has been utilised for this purpose.

For the material representing axial force-deformation, stiffness of defined Elastic Uniaxial Material has been considered equal to Young's modulus of concrete. This value was estimated as 2,330 MPa using mean unconfined strength of concrete (21.75 MPa) and equation (2.7). For Elastic Uniaxial Material which represents deformations caused by shearing forces, a stiffness value equal to shear modulus of concrete has been considered utilising equation (2.8). Shear force-deformations along both local axes have been represented by the same material.

Torsional rigidity of bent system elements $T/\Delta\phi$ has been approximated using equation (2.9) (Popov, 1990). This relation is exact for circular shafts assuming that twisting moment remains constant along the member.

$$\frac{T}{\Delta\phi} = \frac{JG}{L} \quad (2.9)$$

In equation (2.9), T is the twisting moment, $\Delta\phi$ is the relative angle of twist, J is torsional moment of inertia, G is shear modulus and L is length of member. Torsional moment of inertia of bent system elements were calculated in Subsection 2.4.7 and are presented in Table 2.3. Torsional rigidity of each element (JG/L) has been introduced as the stiffness of the relevant Elastic Uniaxial Material.

Materials representing axial and shear force-deformations have been considered identical for all non-rigid bent system elements. This is because Young's modulus and shear modulus of concrete are identical for all bent system components (as it will be discussed in the third chapter, it is steel strength that changes for different samples). Nonetheless, as it is evident from equation (2.9), different torsional materials need to be assigned to elements with differing lengths.

2.4.7.2 Materials representing moment-curvature characteristics

Avşar (2009) has used fiber modelling for simulating bent system components of his bridge models. In this study, a uniaxial hysteretic material was selected for representing flexural behaviours of non-rigid elements. Figure 2.28 demonstrates backbone curve of

the defined hysteretic material. Nominal yield curvature (ϕ_y), ultimate curvature (ϕ_u), post-ultimate curvature (ϕ_r), nominal yield moment (M_N), ultimate moment (M_u) and residual moment (M_r) of a reinforced concrete section are parameters required for defining the relative hysteretic material. Post-ultimate curvature (ϕ_r) of the flexural material has been considered as 1.2 times its ultimate curvature (ϕ_u) and the residual moment (M_r) has been considered as 10% of its nominal yield moment (M_N). Procedure and calculations for determining ϕ_y , ϕ_u , M_N and M_u will be discussed in Section 2.6.

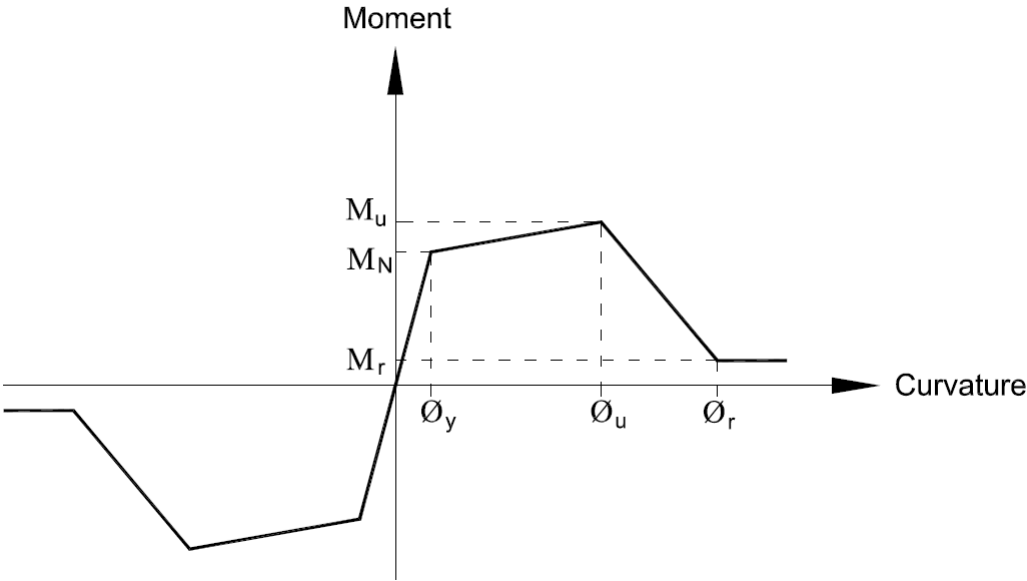


Figure 2.28 : Backbone curve for bending material.

2.5 Determining Properties of Confined and Unconfined Concrete

As discussed in Subsection 2.4.7.2, moment-curvature properties of bent system components are required for determining features of the hysteretic materials used for characterising flexural behaviour of non-rigid bent system elements. Moreover, as will be discussed later, normalised curvature values pertaining to cracking, spalling, yielding and ultimate strength will be used as limit states to categorise damage level of the bridge after a strong ground excitation. All these make moment-curvature analysis of column and cap beam sections necessary. Nevertheless, determining bending moment – curvature relationship of RC sections needs information about confined and unconfined concrete properties. This is because concrete sections confined by transverse reinforcement exhibit higher strength and ductility in comparison to non-confined concrete sections (Mander, 1983; Mander et al, 1988; Priestley et al, 2007). In this

subsection, Mander's stress-strain model will be used for approximating required concrete attributes.

Main features of concrete stress-strain curve based on Mander's model can be observed in Figure 2.29. As it can be seen from this figure, confined concrete is able to sustain greater strains and stresses in comparison to unconfined concrete. Mander's model assumes that section fails when fracture of the first hoop occurs. Strain at first hoop fracture has been represented by ϵ_{cu} .

In Figure 2.29 f'_{co} is ultimate strength of unconfined concrete (21.75 Mpa). ϵ_{co} is strain at f'_{co} and is assumed to be 0.002 mm/mm according to recommendation by Mander et al. (Mander et al, 1988). ϵ_{sp} is ultimate strain of unconfined concrete and can be assumed to be 0.004 mm/mm as denoted by (Priestley et al, 2007). f'_{cc} is ultimate strength of confined concrete in compression and ϵ_{cc} is strain value at f'_{cc} . E_c is Young's modulus of concrete and has been calculated as 23'300 MPa for C25 concrete grade using equation (2.7) and finally E_{sec} is secant modulus of confined concrete at ultimate strength ($E_{sec} = f'_{cc}/\epsilon_{cc}$).

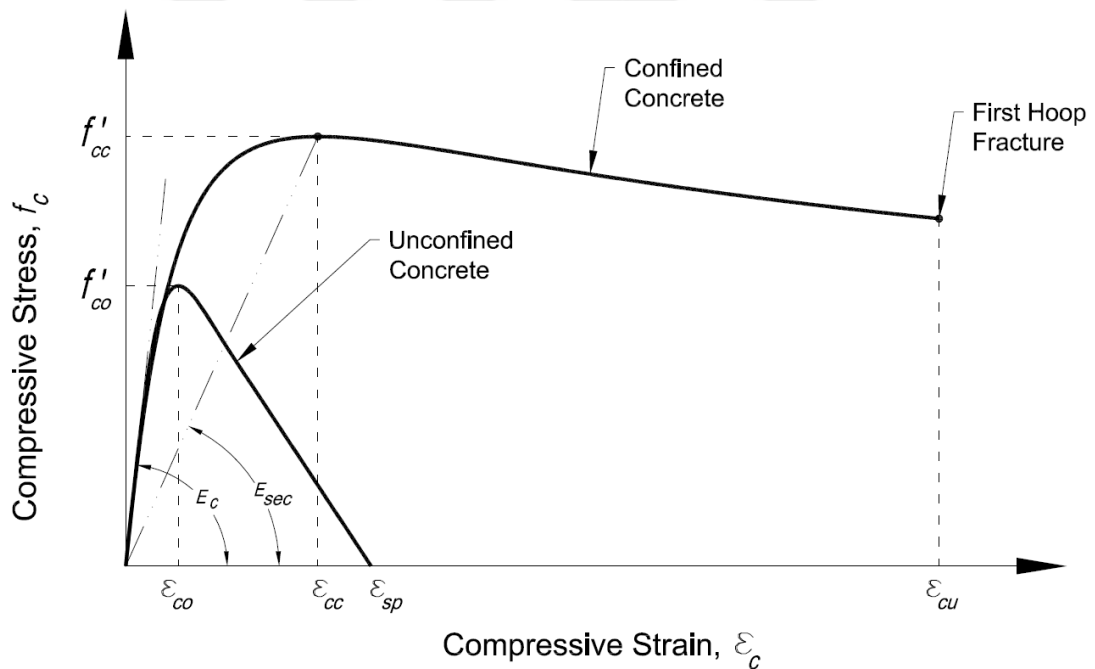


Figure 2.29 : Stress –strain model proposed by Mander for monotonic loading of confined and unconfined concrete.

Effect of transverse reinforcement, has been considered in Mander's model by taking effective confining stresses into account and by defining a parameter called confinement effectiveness coefficient (k_e). This parameter (k_e) can be defined as the ratio of effectively confined concrete area (A_e) to the area of core concrete within centre lines of

perimeter transverse reinforcement bars (A_{cc}) ($k_e = A_e/A_{cc}$). Confinement effectiveness coefficient (k_e), represents how well core of an RC section is confined by taking into account the arching action between longitudinal and transverse reinforcing steel. According to Mander (1983), arching action is assumed to have a second degree parabolic shape with an initial tangent of 45° . The maximum value for k_e is theoretically 1.0 which is for a completely confined section.

Confinement effectiveness coefficient (k_e), might be determined using recommendations by Priestley for rectangular and circular sections. Priestley suggests that values between 0.95 and 1.0 and values between 0.75 and 0.85 should be used respectively for circular and rectangular sections (Priestley et al, 2007). Nonetheless, these directions had better not be applied to columns of the bridge under study as column sections are neither circular, nor rectangular in section; they are rectangular with rounded ends (Figure 2.4). Because of this, direct calculation of A_e , A_{cc} and k_e was performed using a more general approach (Mander, 1983; Mander et al, 1988). By this approach, k_e was approximated as 0.842 for columns and 0.786 for the bent cap beam. Ultimate strength of concrete in compression (f'_{cc}) has been estimated following a six step algorithm described by Mander (1983). Following this algorithm, f'_{cc} has been calculated as about 26.91 MPa for columns and 27.57 MPa for the bent cap beam. Ultimate strain of concrete in compression ϵ_{cu} has been approximated using equation (2.10) which is proposed by Priestley et al (2007).

$$\epsilon_{cu} = 0.004 + 1.4 \frac{\rho_s f_{yh} \epsilon_{su}}{f'_{cc}} \quad (2.10)$$

In equation (2.10), ρ_s is ratio of volume of transverse reinforcement to volume of confined core. This value can be calculated considering steel arrangement details of a section. f_{yh} and ϵ_{su} are respectively yield strength and ultimate strain of transverse steel. Ultimate strain of steel has been considered as constant with a value of 0.1 mm/mm for all models; as mentioned previously in 2.4.7. However, because yield strength of steel varies from model to model, each FE model has its own reinforced concrete properties as will be discussed in subsection 3.2.1. In this section, specifications of the model constructed from steel of mean yield strength ($f_y = 472.41 \text{ Mpa}$) and mean unconfined compressive strength of concrete ($f'_{co} = 21.75 \text{ Mpa}$) have been presented for completeness of discussion (Table 2.4).

Table 2.4 : Calculated parameters of stress-strain curve for columns and cap beam.

	ϵ_{co}	ϵ_{sp}	ϵ_{cc}	ϵ_{cu}	f'_{co} (MPa)	f'_{cc} (MPa)	f'_{cu} (MPa)	E_c (GPa)	E_{sec} (GPa)
Column	0.002	0.004	0.00437	0.0142	21.75	26.91	22.34	23.32	6.15
Cap Beam	0.002	0.004	0.00468	0.0176	21.75	27.58	22.28	23.32	5.89

2.6 Moment-Curvature Analysis of Bent System Sections

Moment-curvature analysis of reinforced concrete sections might be beneficial in various ways such as determining flexural capacity of bending members or to gain a better insight about load-deformation behaviour of sections. As mentioned previously, moment-curvature analysis results of column and cap beam sections have been used in this study for determining properties of hysteretic material models and to specify intensity of damage to the structure as a result of seismic loadings.

Figure 2.30 presents strain and stress distributions in a typical symmetrical RC section subjected to bending. Nomenclature of this figure complies with the one used by Priestley et al (2007).

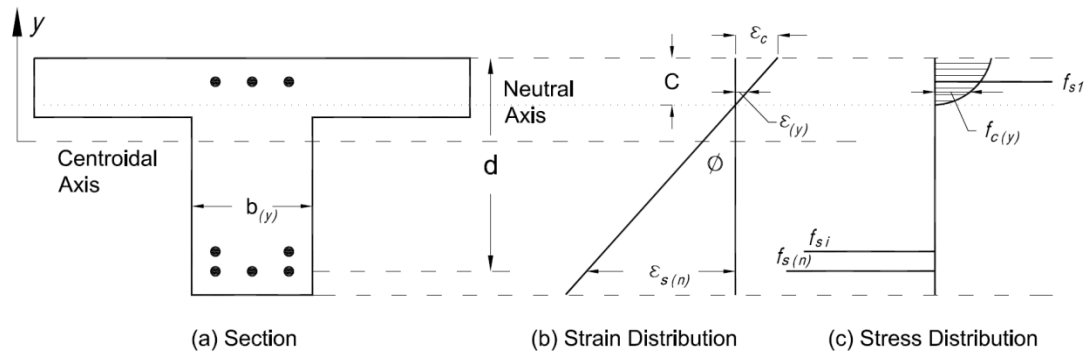


Figure 2.30 : Strain and stress distribution in a symmetrical reinforced concrete section.

According to Priestley et al (2007), tensile strength of concrete can be ignored as RC sections get subjected to reversed loadings during seismic shaking and consequently, cracks usually extend through the entire section. Moreover, tensile strength of concrete has negligible contribution to flexural strength of RC sections. If nonlinear stress-strain relationships of concrete and steel are known as by equations (2.11) and (2.12) and the section presented in Figure 2.30 is subjected to simultaneous effect of axial and flexural loadings, applied axial force (N) might be calculated from equation (2.13) (Priestley et al, 2007).

$$f_{c(y)} = \Phi_c(\varepsilon_{(y)}) \quad (2.11)$$

$$f_{s(y)} = \Phi_s(\varepsilon_{(y)}) \quad (2.12)$$

$$N = \int f_{c(y)} b_{(y)} dy + \sum_1^n f_{si} A_{si} = \int \Phi_c(\varepsilon_{(y)}) b_{(y)} dy + \sum_1^n \Phi_s(\varepsilon_{(y)i}) A_{si} \quad (2.13)$$

In equation (2.13), A_{si} is total area of longitudinal steel in layer i and n is number of layers of reinforcing steel. The applied moment may be specified by equation (2.14) (Priestley et al, 2007).

$$M = \int \Phi_c(\varepsilon_{(y)}) b_{(y)} y dy + \sum_1^n \Phi_s(\varepsilon_{(y)i}) y_i A_{si} \quad (2.14)$$

Then, curvature of the section is given by equation (2.15) (Priestley et al, 2007).

$$\phi = \frac{\varepsilon_c}{c} = \frac{\varepsilon_s(n)}{(d - c)} \quad (2.15)$$

For a known axial force and moment, after determining strain values through equations (2.11), (2.12), (2.13) and (2.14), one needs knowledge about location of the neutral axis in order to specify curvature value by equation (2.15). This might be done through an iterative process generally performed by a computer programme. Priestley et al (2007) provide a 10 step algorithm for this process. In the current research, moment-curvature analyses of sections have been performed by OpenSees.

2.6.1 Material models for moment-curvature analysis

OpenSees fiber modelling was selected for defining sections needed for moment-curvature analysis. This is because by fiber modelling it is possible to consider interaction between applied bending moment and axial force. Moreover, fiber section command has the advantage of allowing the modeller to build a section composed of several uniaxial materials which is favourable for simulating RC sections.

Three types of materials have been employed for sampling bent system sections: one material for unconfined cover concrete, another material for confined core concrete and the third material for reinforcing steel. In order to simulate unconfined cover and confined core concrete, Concrete01 material has been employed. Figure 2.31a exhibits stress-strain curve of a section constructed from Concrete01 material with properties of unconfined concrete subjected to compressive loading. In Figure 2.31b, the same section made of concrete with mean unconfined compressive strength value of (21.75 MPa) and steel with mean yield stress value (472.41 MPa) has been subjected to axial compressive

loading. Specifications attributed to unconfined and confined concrete have been extracted from Table 2.4. Reinforcing steel has been introduced to FE models by employing Steel01 material. Stress-strain curve for this material with mean yield stress value of 472.41 MPa can be observed in Figure 2.31c.

Sections constructed by OpenSees fiber command can be composed of necessary number of fibers for a sufficient degree of accuracy. Each fiber contains a material previously defined by the modeller. Figure 2.32 demonstrates fiber patterns of sections defined for column and bent cap beam sections.

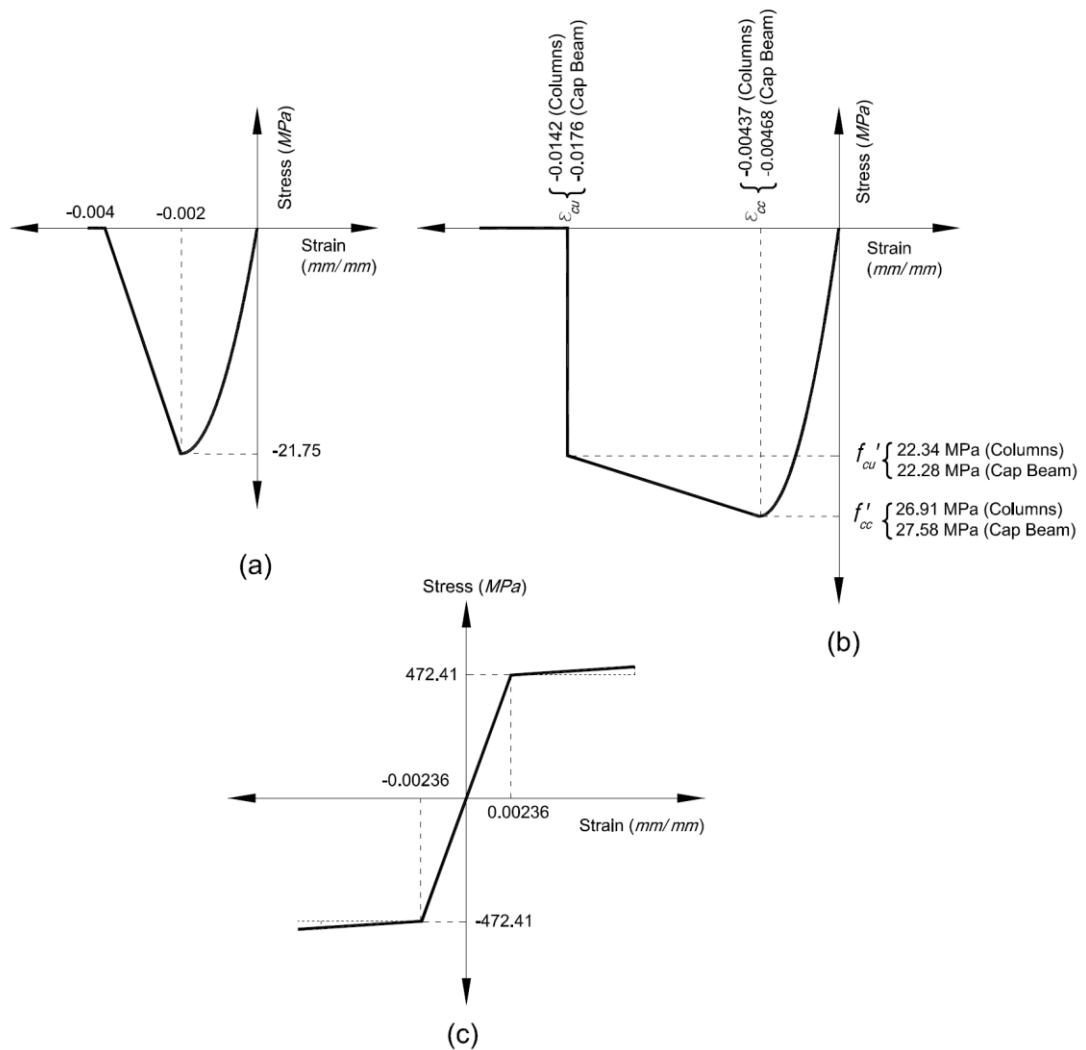


Figure 2.31 : Material models for (a) Unconfined concrete (b) Confined concrete (c) Reinforcement steel.

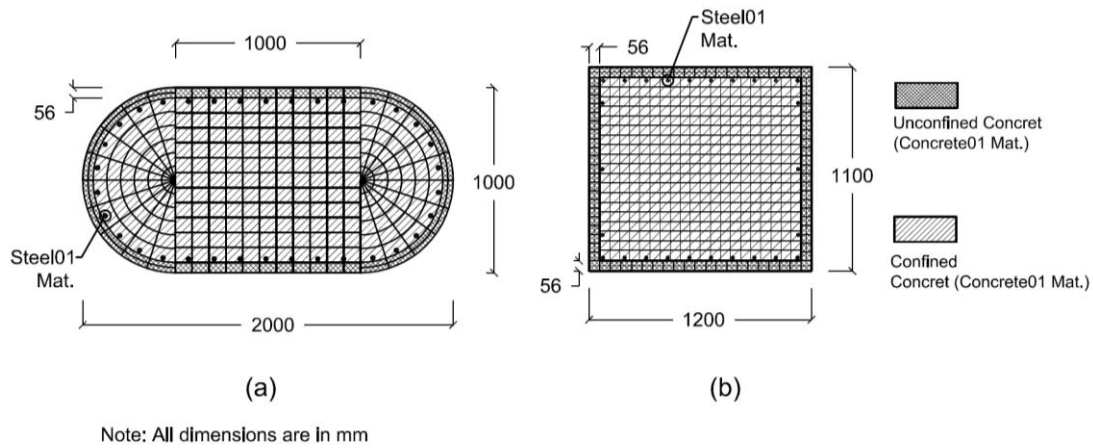


Figure 2.32 : Discretisation of column and cap beam sections for fiber modelling.

2.6.2 Moment-curvature curves and their idealisations

Results of moment-curvature analyses for column and cap beam sections and their linear idealisations for a model made from materials of mean strengths have been presented in this subsection. For moment-curvature analysis of cap beam section, no axial load has been considered. However, for the analysis of column sections the applied compressive load caused by bridge weight must be determined and taken into account. This has been performed through the gravity analysis described in Subsection 2.4.1. Results of the analysis show that middle column of the bridge, sustains a load of about 1,641 KN whereas side columns axial force is about 1,538 KN. Nonetheless, the difference of approximately 100 KN between sustained dead loads is not in a scale to influence moment-curvature responses in a dramatic manner. Because of this, an average value of 1589.5 KN has been considered as the axial load of all three columns for moment-curvature analyses.

Bilinear approximation of concrete moment-curvature responses has the advantage of convenient usage of analysis outputs for engineering purposes. In this research, the approach recommended by Priestley et al (2007) has been utilised for this purpose. The mentioned approach requires three points to get determined according to the moment-curvature response:

- Point No.1 which corresponds to the first yield curvature (ϕ'_y) and moment (M_y)
- Point No.2 which corresponds to nominal yield curvature (ϕ_y) and moment (M_N)
- Point No.3 which corresponds to ultimate curvature (ϕ_u) and moment (M_u)

The abovementioned points have been exhibited in Figure 2.33. For determining point No.1 (first yield point), stress-strain outputs of the moment-curvature analysis for the

reinforcement fiber corresponding to extreme tension (reinforcing steel furthest from the neutral axis) and concrete fiber in extreme compression (concrete fiber furthest from neutral axis) must be studied. If it is observed that rebar strain has reached steel yield strain (e.g. 0.00236 for steel material with mean yield strength) before concrete attaining a strain value of 0.002, then curvature and moment values corresponding to steel yield strain are considered as the first yield curvature and moment (ϕ'_y, M_y). In case strain of the concrete fiber has reached a value of 0.002 before rebar strain attaining steel yield strain then the curvature and moment values corresponding to concrete strain (0.002) are first yield curvature and moment.

For determining point No.2, the same stress-strain outputs will be studied. If it is noticed that strain of rebar at extreme tension has reached the value of 0.015 before extreme compression concrete fiber strain attaining a value of 0.004, the moment corresponding to strain of rebar is considered as nominal moment capacity (M_N). In case it is noticed that strain of extreme compression concrete fiber has reached a value of 0.004 before extreme tension rebar attaining a strain value of 0.015, then the moment corresponding to strain of concrete is considered as nominal moment capacity. After specifying nominal moment capacity (M_N), nominal yield curvature (ϕ_y) must be determined by equation (2.16) (Priestley et al, 2007).

$$\phi_y = \frac{M_N}{M_y} \phi'_y \quad (2.16)$$

For determining point No.3, a procedure similar to the procedure for determining point No.1 needs to be followed; except that ultimate concrete strain and ultimate steel strain values must be considered as limit values. The ultimate strain limit for concrete in compression is ε_{cu} (Table 2.4). For the ultimate strain limit of rebar, a value equal to $\varepsilon_s = 0.6\varepsilon_{su} = 0.06$ has been considered due to recommendations by Priestley et al (2007). As soon as section strain reaches one of these values (ε_{cu} or ε_s), corresponding curvature and moment are respectively considered as the abscissa and ordinate of point No.3.

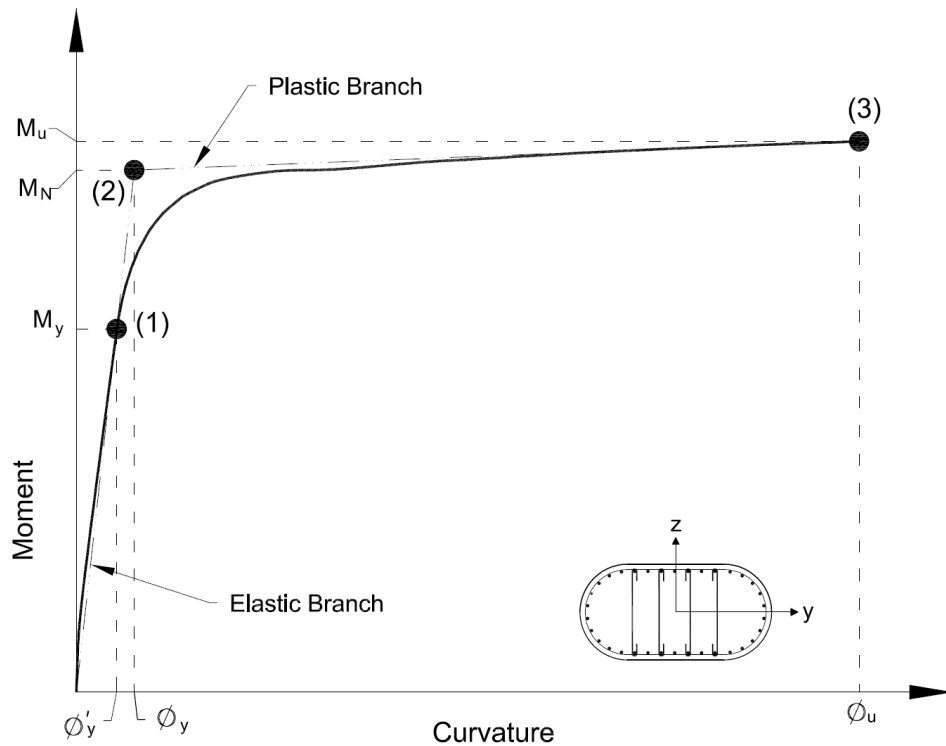


Figure 2.33 : Moment-curvature curve and its bilinear idealisation for bending about local z axis.

Figure 2.34 and Figure 2.35 demonstrate respectively moment-curvature responses of the column section of one of the FE models for bending about local y and z axes. As mentioned before, the model for which results are displayed has been made from concrete with unconfined compressive strength of 21.75 MPa and steel with yield stress of 472.41 MPa. The criterion for ultimate curvature of column sections for bending about both local axes is hoop fracturing. This means that for column sections, extreme compressive concrete fiber attains ultimate strain (ϵ_{cu}) before extreme reinforcing bar in extreme tension attains steel yield strain (ϵ_{su}). Figure 2.36 and Figure 2.37 exhibit moment-curvature curves of cap beam section for bending respectively about local y and z axes. The criterion for ultimate curvature of cap beam for flexure about both local axes is steel yielding. This means that for a cap beam section, reinforcing steel yields before transverse hoops fracture. Analysis results for column and cap beam sections of the mentioned model have been summarised in Table 2.5. A more complete table containing moment-curvature analysis outputs for several models have also been presented in Subsection 3.2.2.

Table 2.5 : Bilinear idealisation of moment-curvature analysis results for column and cap beam sections.

	$\phi'_y(m^{-1})$	M_y (KN.m)	$\phi_y(m^{-1})$	M_n (KN.m)	$\phi_u(m^{-1})$	M_u (KN.m)
Column (Local y axis)	0.00352	3,090.7	0.00462	4,058.65	0.0765	4,381.43
Column (Local z axis)	0.00171	5,075.63	0.0026	7,717.16	0.0335	8,268.04
Bent Cap Beam (Local y axis)	0.00269	1,512.59	0.00346	1,942.93	0.0657	2,108.76
Bent Cap Beam (Local z axis)	0.00244	1,304.94	0.00386	2,068.04	0.06247	2,179.23

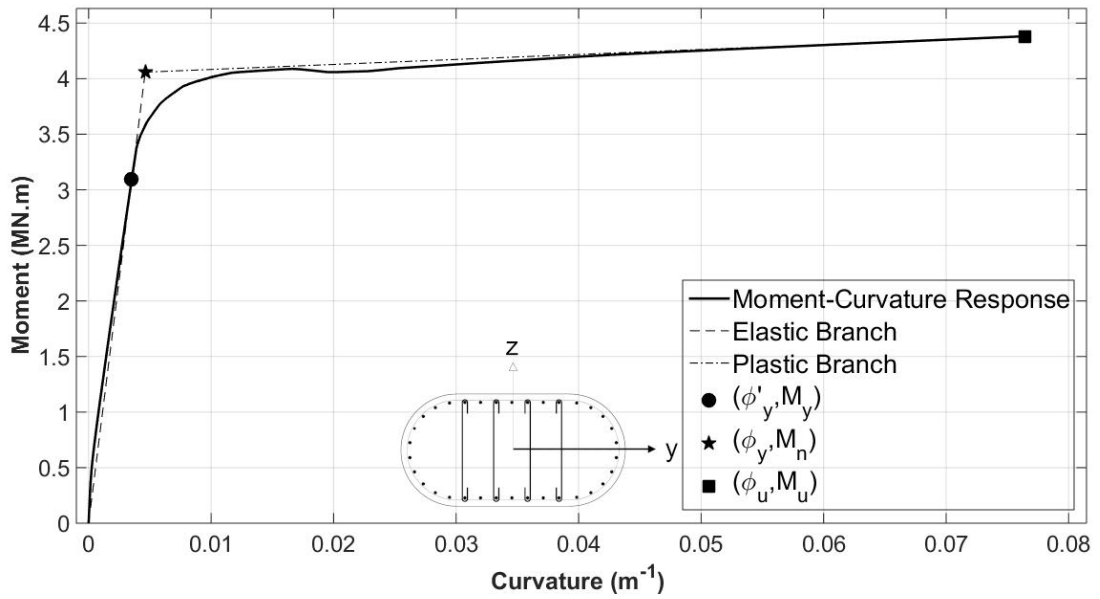


Figure 2.34 : Moment-curvature curve of column section and its bilinear idealisation for bending about local y axis ($f'_{co} = 21.75 MPa$, $f_y = 472.41 MPa$)

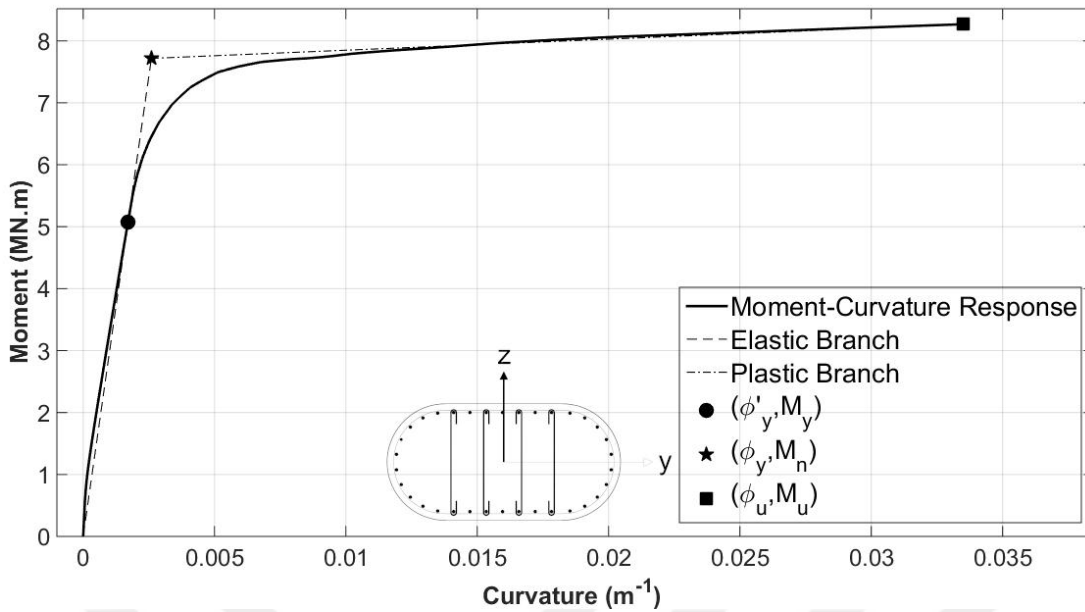


Figure 2.35 : Moment-curvature curve of column section and its bilinear idealisation for bending about local z axis ($f'_{co} = 21.75 \text{ MPa}$, $f_y = 472.41 \text{ MPa}$).

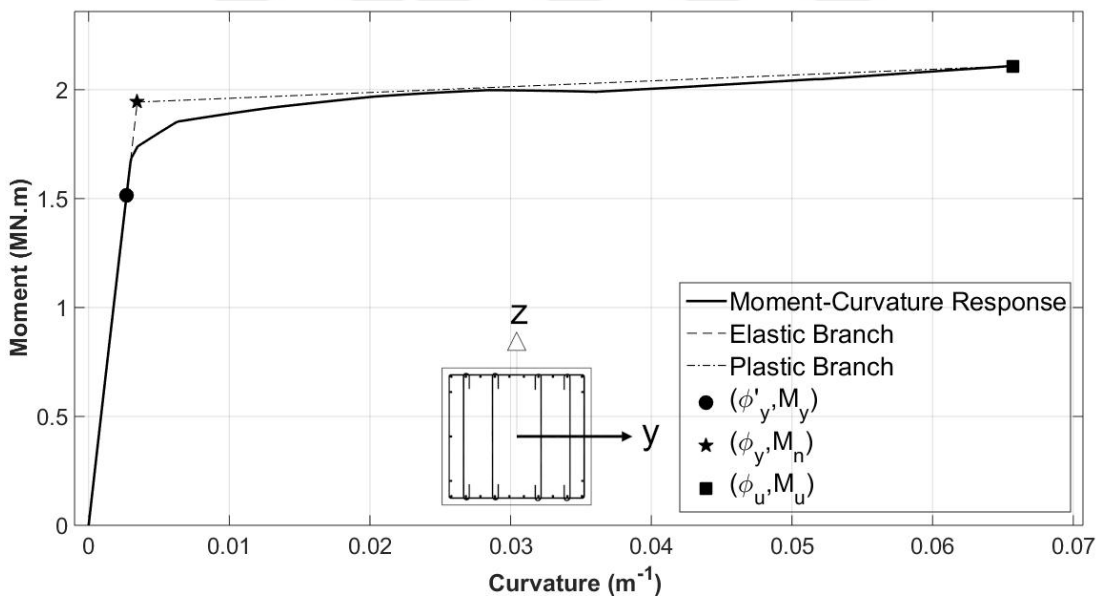


Figure 2.36 : Moment-curvature curve of bent capbeam section and its bilinear idealisation for bending about local y axis ($f'_{co} = 21.75 \text{ MPa}$, $f_y = 472.41 \text{ MPa}$).

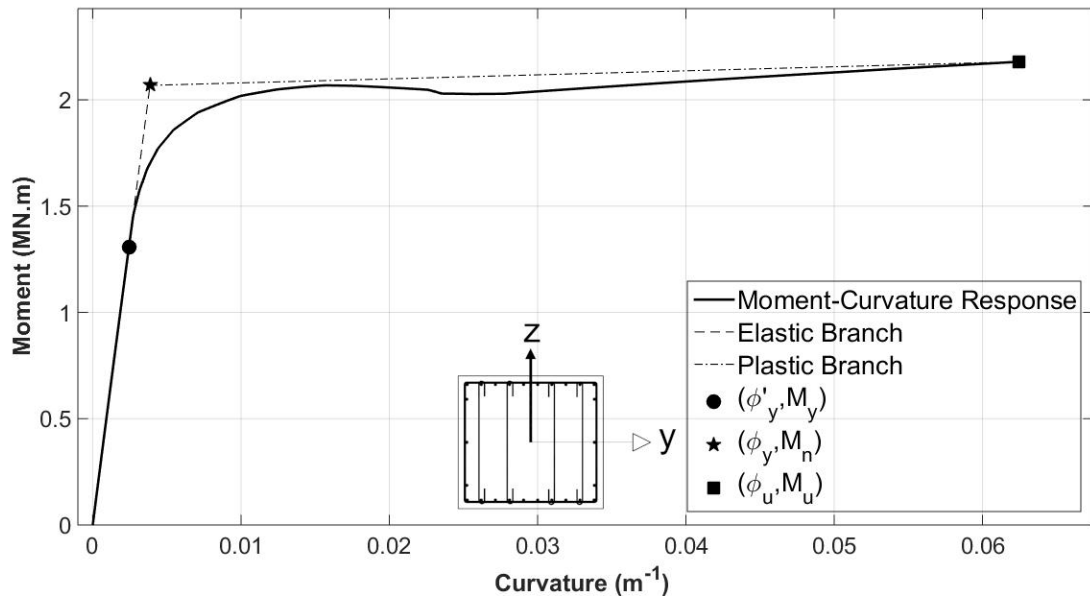


Figure 2.37 : Moment-curvature curve of bent capbeam section and its bilinear idealisation for bending about local z ($f'_{co} = 21.75 \text{ MPa}$, $f_y = 472.41 \text{ MPa}$).

The slope of the elastic branch (presented in Figure 2.33) is called elastic stiffness which corresponds to the stiffness of cracked concrete section (Priestley et al, 2007). This value can be specified using equation (2.17) (Priestley et al, 2007).

$$EI_{el} = \frac{M_y}{\phi_y} = \frac{M_N}{\phi_y} \quad (2.17)$$

Elastic stiffness values have been calculated for column and cap beam moment-curvature analysis results demonstrated in Figure 2.34, Figure 2.35, Figure 2.36 and Figure 2.37. They have also been compared with stiffness values of uncracked section (EI_{gross}) as can be observed in Table 2.6. Young's modulus of concrete and second moment of area values for calculating EI_{gross} can be respectively specified from equation (2.7) and Table 2.3. Table 2.6 is only for a sample constructed from concrete of $f'_{co} = 21.75 \text{ MPa}$ and steel of $f_y = 472.41 \text{ MPa}$. A more complete table contains different elastic stiffness values for various samples made of steel with differing strengths. Such a table will be presented in Subsection 3.2.3.

Table 2.6 : Elastic and gross stiffness values and their ratios.

	$EI_{el}(MN.m^2)$	$EI_{gross}(MN.m^2)$	$\frac{EI_{el}}{EI_{gross}}$
Column (Local y axis)	911	3'310	0.275
Column (Local z axis)	3'115.4	12'385	0.251
Cap Beam (Local y axis)	576.4	3'327.5	0.173
Cap Beam (Local z axis)	550.29	3'960	0.139

2.7 Calculating Lengths of Strain Penetration and Plastic Hinges

Plastic hinge is a concept introduced to make analytical calculations of displacements more realistic by compensating for increased displacements due to tension shift and shear deformations (Priestley et al, 2007). If this concept is not employed, member displacements by calculations become more different from what is experienced in reality because hypotheses like plane-sections are not absolutely correct in the real world. As another example, in real structures, displacements do not fall to zero exactly at column ends or beam faces. Conversely, strains in reinforcing bars under tension exist throughout their development lengths and compressive strains on the side under pressure do not drop abruptly to zero but, disperse steadily in base. This leads to a concept called strain penetration length (L_{SP}) along which curvature is assumed to stay constant and equal to the curvature at the member end (Priestley et al, 2007). The relation recommended by Priestley et al (2007) for strain penetration length is

$$L_{SP} = 0.022f_{ye}d_{bl} \quad (2.18)$$

In which f_{ye} (MPa) and d_{bl} are respectively yield strength and diameter of longitudinal bars. Priestley et al (2007) also recommended equation (2.19) for calculating plastic hinge length for beams and columns.

$$L_p = kL_C + L_{SP} \geq 2L_{SP} \quad (2.19)$$

In equation (2.19), k is calculated as

$$k = 0.2 \left(\frac{f_u}{f_y} - 1 \right) \leq 0.08 \quad (2.20)$$

L_C is defined as the length from the critical section to the point of contraflexure in a member. Although location of contraflexure point alters naturally during seismic loadings for each member, it is assumed in this study that contraflexure points for both column and beam elements are approximately located in the position of their middle

clear lengths. Clear length for columns (from top of footing to bottom surface of cap beam) and for cap beam elements (from one face to the other face) are respectively 4.4m and 2.7m as can be observed in Figure 2.3. By the mentioned assumption for location of point of contraflexure and by considering size of longitudinal bars for columns and cap beam (Figure 2.4), strain penetration length and plastic hinge length values for a sample made from concrete of $f'_{co} = 21.75 \text{ MPa}$ and steel of $f_y = 472.41 \text{ MPa}$ are presented in Table 2.7.

Table 2.7 : Strain penetration and plastic hinge lengths for a sample constructed from concrete of $f'_{co} = 21.75 \text{ MPa}$ and steel of $f_y = 472.41 \text{ MPa}$.

Cap beam Elements	Column Elements
$L_{SP} \cong 185mm$	$L_{SP} \cong 240mm$
$L_p = 370mm$	$L_p = 480 \text{ mm}$

Lengths of plastic hinges have been introduced to Beam With Hinges Elements of FE models. This has been schematically displayed in Figure 2.38 for a model with concrete of $f'_{co} = 21.75 \text{ MPa}$ and steel of $f_y = 472.41 \text{ MPa}$. Certainly, similar to reinforced concrete properties, moment-curvature analysis outputs and elastic stiffness values, strain penetration and plastic hinge lengths differ from model to model because of changes in yield strengths of steel bars. Results presenting such changes are shown in Subsection 3.2.4.

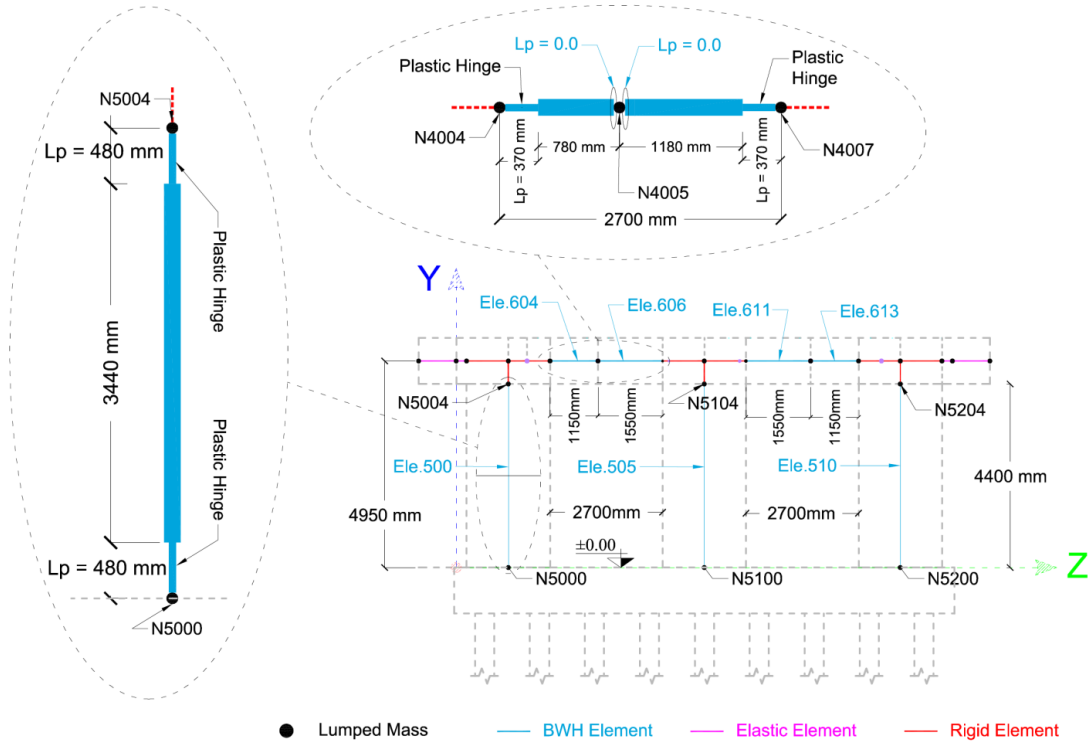


Figure 2.38: Plastic hinges defined for the BWH elements for a model with concrete of $f'_{co} = 21.75 \text{ MPa}$ and steel of $f_y = 472.41 \text{ MPa}$.

2.8 Defining Damping Matrix of the Structure

In current study the bridge model will get subjected to strong transient loads causing severe nonlinearities in bent system components. This makes calculation of damping matrix necessary as described by Chopra (2012). In this study, Rayleigh damping has been utilised for defining damping matrix of the structure as can be seen in equation (2.21) (Chopra, 2012).

$$c = a_0 m + a_1 k \quad (2.21)$$

Where c , m and k are respectively classical damping, mass and stiffness matrices of the structure. Damping ratio for the n th mode (ζ_n) of a system with damping matrix defined in equation (2.21) can be obtained from equation (2.22) (Chopra, 2012).

$$\zeta_n = \frac{a_0}{2} \frac{1}{\omega_n} + \frac{a_1}{2} \omega_n \quad (2.22)$$

In equation (2.22), ω_n is natural circular frequency for the n th mode. Constants a_0 and a_1 can be calculated from equation (2.23) in case damping ratios of mode i and j are known (Chopra, 2012).

$$\frac{1}{2} \begin{bmatrix} 1/\omega_i & \omega_i \\ 1/\omega_j & \omega_j \end{bmatrix} \begin{Bmatrix} a_0 \\ a_1 \end{Bmatrix} = \begin{Bmatrix} \zeta_i \\ \zeta_j \end{Bmatrix} \quad (2.23)$$

Damping ratio has been assumed to have the same value for all modes. Hence, by solving equation (2.23), coefficients a_0 and a_1 can be calculated as can be seen in equation (2.24).

$$a_0 = \zeta \frac{2\omega_i\omega_j}{\omega_i + \omega_j} \quad a_1 = \zeta \frac{2}{\omega_i + \omega_j} \quad (2.24)$$

Natural circular frequency values for required modes of a model structure might be determined using OpenSees *eigen* command. This command is able to solve the characteristic equation of the structure and print out required number of eigenvalues. Natural frequencies are calculated then by taking square root of the printed eigenvalues (Chopra, 2012). For performing the eigenvalue analysis for different FE models, a number of elastic models were built using various steel properties. The mentioned elastic models were established using Elastic Beam Column elements for all bridge components, i.e. rigid elements and superstructure elements were kept as they were, but, BWH elements were replaced by elastic elements. Sectional properties of bent system components were not modified however, the assigned Young's modulus to the elastic cap beam and column elements were calculated from stiffness values discussed in Subsection 2.6.2 (EI_{el}). This is because using Young's modulus of uncracked concrete determined from equation (2.7) is very unrealistic for RC structures subjected to great deformations but, using the described technique, cracked stiffness of components can be considered for analysis purposes.

Eigenvalue analysis results were determined for the first two modes for each FE model. From these values, natural circular frequency values were determined. Results for a model made of mean material properties ($f'_{co} = 21.75 \text{ MPa}$ and $f_y = 472.41 \text{ MPa}$) are as $\omega_1 = \sqrt{100.624} = 10.031 \frac{\text{rad}}{\text{s}}$ and $\omega_2 = \sqrt{127.107} = 11.274 \frac{\text{rad}}{\text{s}}$.

Considering damping ratio (ζ) as 0.05, which is the suggested value for concrete structures by Chopra (2012), we will have $a_0 = 0.5308$ and $a_1 = 4.694 \times 10^{-3}$. Similar coefficients were calculated for each FE model (Subsection 3.2.5) and were used as inputs to OpenSees Rayleigh command. Moreover, according to Chopra (2012), main period of the bridge can be specified from equation (2.25) if natural circular frequency for the first mode is used in the relation.

$$T_n = \frac{2\pi}{\omega_n} \quad (2.25)$$

This way, main period of the bridge is calculated as $T_1 = 2\pi/10.068 = 0.6264 \text{ s}$ for the discussed FE model.

2.9 Pushover Analysis

Pushover analysis is a nonlinear static analysis that is mostly performed when linear elastic analysis is recognised as insufficient for studying the strength capacity and inelastic deformations of a structure (Diotallevi and Landi, 2005). Additionally, pushover analysis might be selected as an alternative to nonlinear dynamic analysis in case dynamic analysis is recognised to be too complicated (Diotallevi and Landi, 2005). In the current study, pushover analysis has been performed for controlling performance of zeroLength elements introduced to the model and for studying variations in base shear values (V_b) as a result of displacements of cap beam in longitudinal and transversal directions.

In Figure 2.39, left superstructure has been pushed towards the left abutment till ultimate strength of zeroLength element Type 4 is achieved. As mentioned in Subsection 2.4.5, zeroLength element Type 4 is a combined element simultaneously representing frictional resistance, action of embankment backfill, action of piles and collision between superstructure and back wall.

The result of this analysis is demonstrated in Figure 2.40. As can be observed in this figure, slope of the response curve increases gently till point No.1 is reached. In this portion of the curve, the only resisting force is friction force caused by movement of left superstructure on bearing pads. The friction force reaches its ultimate value as displacement reaches Point No.1. Then, no extra resistance is applied to the superstructure till the 50mm expansion gap is closed (Point No.2). After this, the resultant reaction from abutment back wall, piles and passive pressure of embankment fill make the curve rise sharply. Slope of the response curve alters once more as soon as point No.3 is reached. This is where abutment back wall attains its ultimate strength. In the same manner, Point No.4 shows the displacement at which piles fail and finally point No.5 shows the displacement at which embankment earth fill fails. The maximum reaction force at point No.5 (1486.85 KN) naturally equals strength capacity of the zeroLength element type 4 as demonstrated in Table 2.1.

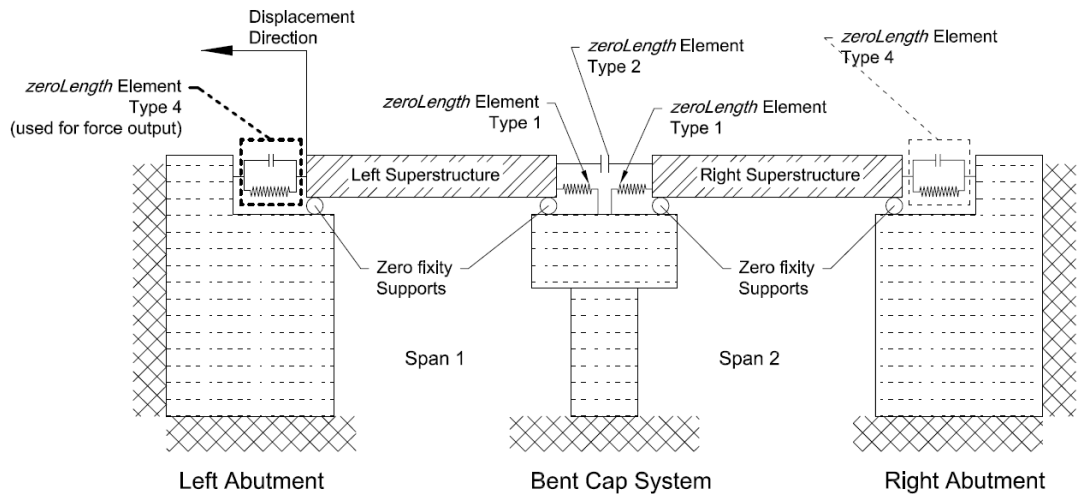


Figure 2.39 : Schematic view of the bridge, exhibiting direction of displacement of left superstructure.

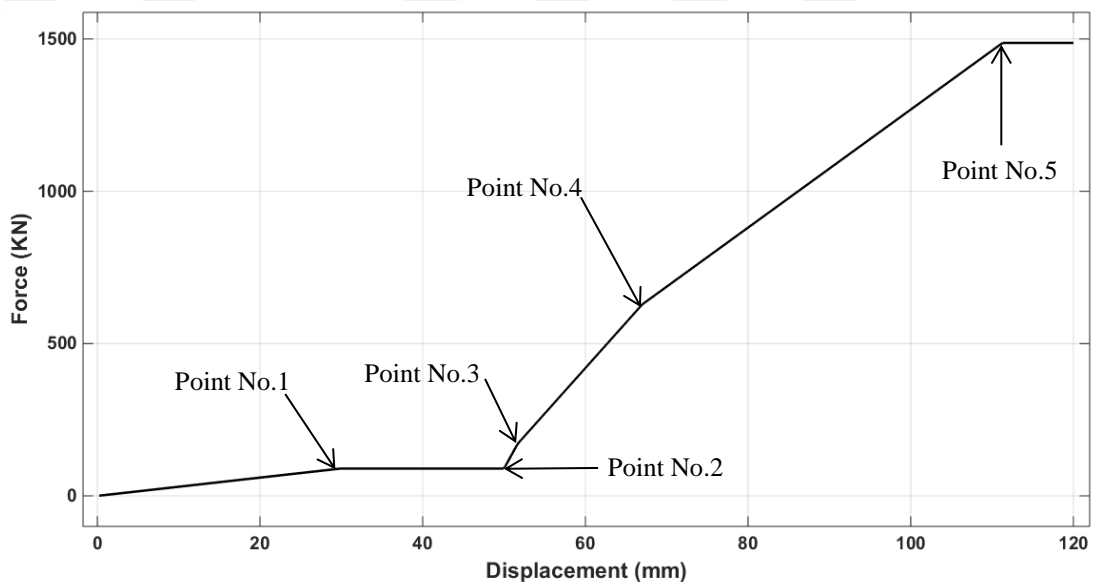


Figure 2.40 : Longitudinal displacement of superstructure vs. reaction at abutment.

Figure 2.41 demonstrates reaction forces for zeroLength Element Type 5 at abutment due to displacement of the superstructure in transversal direction. It is reminded from Subsection 2.4.5 that this element represents simultaneously friction resistance, pile action in transverse direction and collision between superstructure and shear keys. The reaction force due to the friction resistance increases steadily until point No.1. At this point, the 25 mm transversal gap closes and reactions from shear key and piles cause the curve to rise in a sharp manner. Shear key fails at point No.2 and piles fail at point No.3. Once more, the reaction force at point No.3 equals capacity of zeroLength Element Type 5 as demonstrated in Table 2.1.

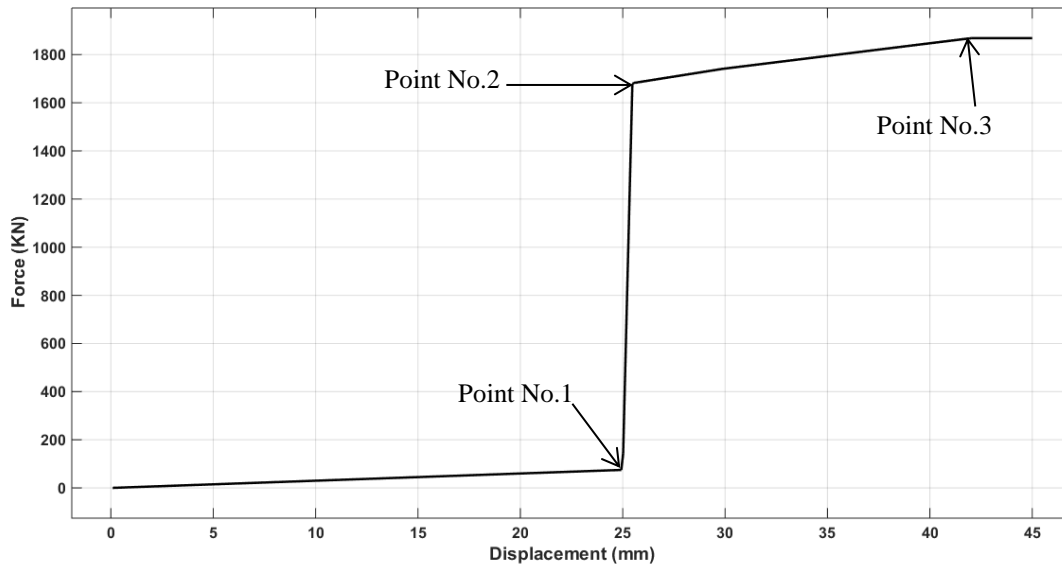


Figure 2.41 : Transversal displacement of superstructure vs. reaction at abutment in transversal direction.

Diagrams presented in Figure 2.40 and Figure 2.41 show that the employed zeroLength elements are behaving in the expected manner.

In addition to Figure 2.40 and Figure 2.41 which exhibit behaviour of zeroLength elements of the bridge under statically growing loads, plots of base shear (V_b) versus displacement of cap beam in longitudinal and transversal directions have been drawn also. Base shear values have been calculated by summing up nodal reactions of nodes 5000, 5100 and 5200 (Figure 2.14) in relative directions. Displacement values correspond to those of node 4009 as it is representing centre of mass of the bent cap beam.

The pushover analysis has been performed using OpenSees displacement control scheme. Three horizontal loads with value of 1.0N are applied at nodes 4002, 4009 and 4016 in longitudinal or transversal directions depending on the degree of freedom for what pushover analysis was run. Real loads at each analysis step get calculated by multiplying the load required for a target deformation by the initial loads (1.0N here). Hence, the introduced 1.0N loads act only as load factors in reality. Target values for displacements of node 4009 (Δ_{N4009}) were increased gradually in several analyses till the model failure occurred because of convergence errors. It might be also worth to mention that several solution algorithms were examined, by gathering them within a while loop, to solve a PA analyses. This is because while sometimes a particular algorithm may experience convergence problems during a nonlinear analysis like PA, another algorithm may come to the result.

By the process described above, plots exhibited in Figure 2.42 to Figure 2.45 have been prepared. Figure 2.42 and Figure 2.43 present base shear (V_b) against Δ_{N4009} respectively in longitudinal and transversal directions for a model made of materials with mean strengths ($f'_{co} = 21.75 \text{ MPa}$ and steel of $f_y = 472.41 \text{ MPa}$). Figure 2.44 is a three dimensional illustration of deformed shape of the bridge FE model under push over analysis in longitudinal direction. Figure 2.45 shows deformed shape of bridge bent system under PA analysis in transversal direction. As mentioned before, nodes 4009, 4002, 4016, 5000, 5100 and 5200 are important nodes for this analysis. For this reason, they have been highlighted in Figure 2.44 and Figure 2.45.

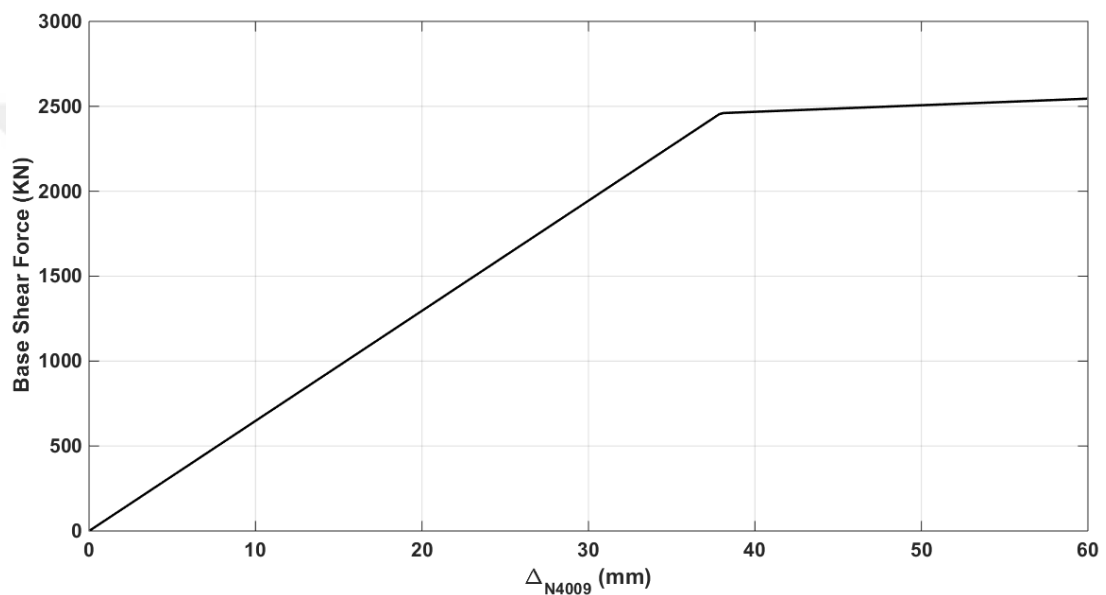


Figure 2.42 : Base shear versus displacement of node 4009 in longitudinal direction.

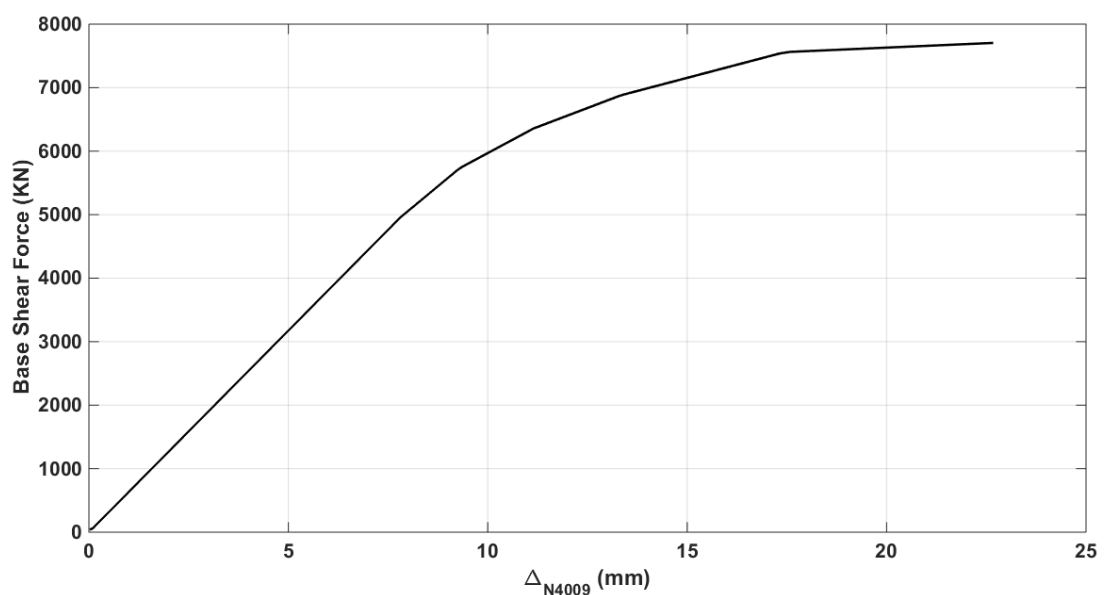


Figure 2.43 : Base shear versus displacement of node 4009 in transversal direction.

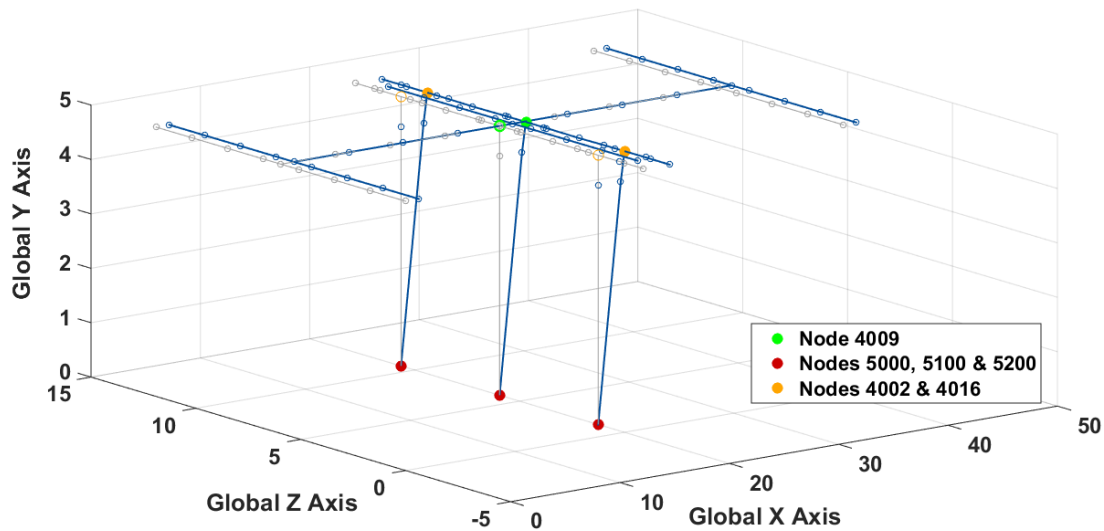


Figure 2.44 : Undeformed and deformed shapes of Elek Deresi Bridge sample under PA in longitudinal direction.

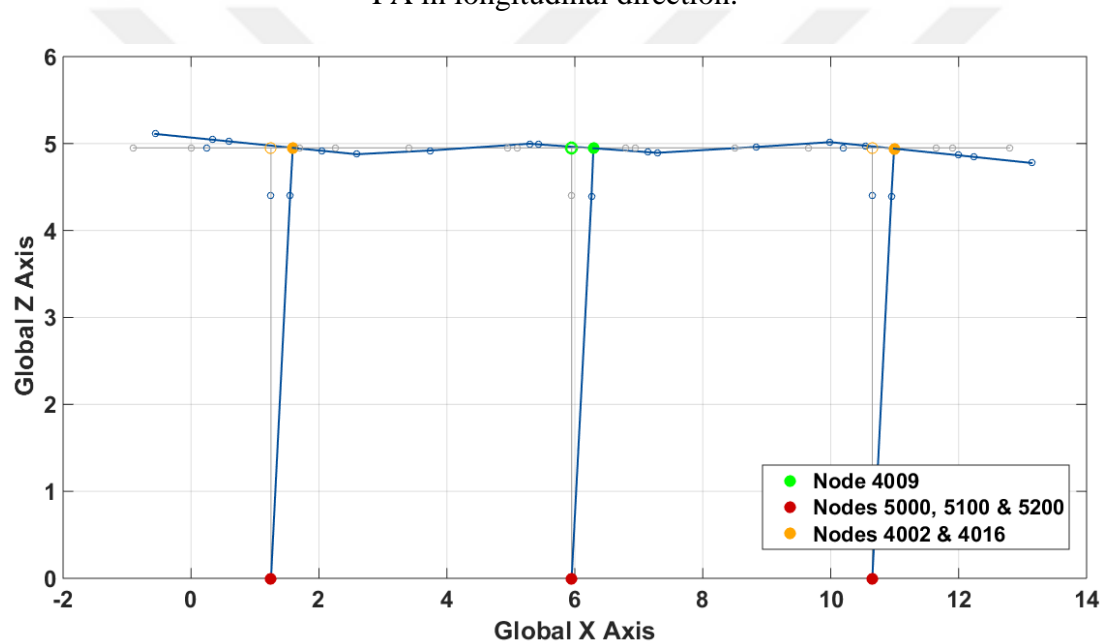


Figure 2.45 : Undeformed and deformed shapes of Elek Deresi Bridge bent system under PA in transversal direction.

2.10 Eigenvalue Analysis and Mode Shapes of Vibration

In this subsection the procedure for performing eigenvalue analysis of the bridge and plotting its mode shapes for the three initial natural modes has been described.

The three initial characteristic values of the FE model constructed from materials with mean strengths ($f'_{co} = 21.75 \text{ MPa}$ and steel of $f_y = 472.41 \text{ MPa}$) are presented in Table 2.8. As mentioned before, they have been calculated using OpenSees *eigen* command. Using those characteristic values, the first three natural circular frequencies,

cyclic frequencies and natural period of vibration of structure have been calculated and presented in the aforesaid table.

Table 2.8 : Characteristic values and natural vibration properties corresponding to the first three modes for a model of ($f'_{co} = 21.75 \text{ MPa}$ and steel of $f_y = 472.41 \text{ MPa}$).

$\omega_1^2 = 100.624 \text{ sec}^{-2}$	$\omega_1 = 10.031 \frac{\text{rad}}{\text{sec}}$	$f_1 = 1.597 \text{ Hz}$	$T_1 = 0.626 \text{ s}$
$\omega_2^2 = 127.107 \text{ sec}^{-2}$	$\omega_2 = 11.274 \frac{\text{rad}}{\text{sec}}$	$f_2 = 1.795 \text{ Hz}$	$T_2 = 0.557 \text{ s}$
$\omega_3^2 = 131.425 \text{ sec}^{-2}$	$\omega_3 = 11.464 \frac{\text{rad}}{\text{sec}}$	$f_3 = 1.824 \text{ Hz}$	$T_3 = 0.548 \text{ s}$

Afterwards, eigenvectors have been recorded at all nodes for translational degrees of freedom (displacements in global X, Y and Z directions). Rotations of non-rigid elements have not been considered in plots of mode shapes. With the aim that the deflected shapes can be effortlessly visible, eigenvector values have been amplified using a scaling factor in the plots. Three dimensional plots of mode shape 1, mode shape 2 and mode shape 3 have been demonstrated in Figure 2.46.

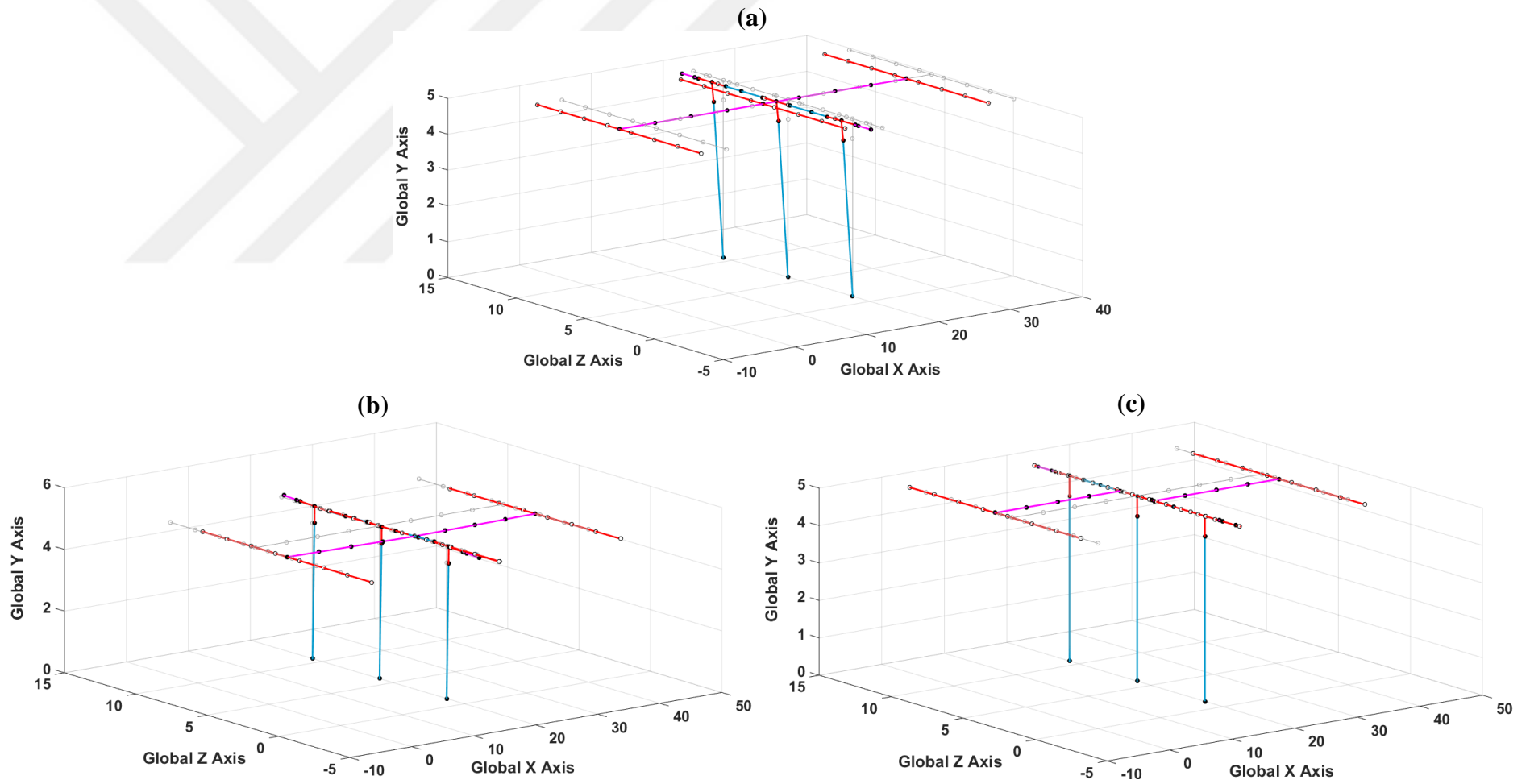


Figure 2.46 : Three dimensional view of natural mode shapes of vibration (a) mode 1 (b) mode 2 (c) mode 3.

3. ESTIMATION OF UNCONDITIONAL SEISMIC HAZARD RISKS

3.1 Introduction

The main objective of this chapter is studying probabilities of failure of various FE models in terms of defined limit states made from different material properties. Moreover, it is of interest to learn whether there exist a relation between material property changes and probabilities of failure. To investigate this, statistical parameters of concrete and reinforcing steel have been studied in Section 3.2. Using values representing statistical specifications of materials, several FE models of the bridge were constructed. As the first trial, steel properties were kept constant and concrete strength was defined as the uncertain model parameter. As the second trial, concrete properties were kept constant and steel strength was altered from model to model. While studying moment curvature curves for different models, it was identified that it is more appropriate to choose steel yield stress as the uncertain parameter. Consequently, variations in reinforced concrete properties, moment-curvature curves, lengths of plastic hinges and other structural properties of the bridge model as a result of variations in reinforcing steel strength are studied in this section. In Section 3.3, the 2000 SAC/FEMA method is introduced as the main approach for estimating unconditional seismic hazard risks to bridge structure. In this section, hazard curves and accelerograms used in the analysis procedure are also presented. Section 3.4 deals with application of the 2000 SAC/FEMA method to the case study bridge problem. Failure limit states and damage levels are defined. Statistical parameters of capacity are determined through defining capacity variable as multiplication of material and model uncertainties. Statistical parameters of demand for each model have been assessed through a number of dynamic nonlinear analyses. The obtained information is used in estimation of probabilities of failure in terms of different limit states for different models. Finally, the relationship between steel yield strength and failure probabilities in terms of the defined limit states has been investigated.

3.2 Statistical Parameters of Materials

Statistical parameters relating to compressive strength of unconfined concrete and steel yield stress have been derived from (Nowak and Collins, 2000). These parameters are as presented in Table 3.1.

Table 3.1 : Statistical parameters of unconfined concrete and reinforcing steel, excerpted from (Nowak and Collins, 2000).

Property	Mean Value	Coefficient of Variation	Standard Deviation
Concrete Compressive Strength			
1 f'_{co} = 3000 <i>psi</i> (20.68 <i>MPa</i>)	2760 <i>psi</i> (19.03 <i>MPa</i>)	0.18	496.8 <i>psi</i> (3.425 <i>MPa</i>)
2 f'_{co} = 4000 <i>psi</i> (27.58 <i>MPa</i>)	3390 <i>psi</i> (23.37 <i>MPa</i>)	0.18	610.2 <i>psi</i> (4.207 <i>MPa</i>)
3 f'_{co} = 5000 <i>psi</i> (34.47 <i>MPa</i>)	4028 <i>psi</i> (27.77 <i>MPa</i>)	0.15	604.2 <i>psi</i> (4.166 <i>MPa</i>)
Reinforcement			
4 Grade 40 yield (275.8 <i>MPa</i>)	45.3 <i>ksi</i> (312.33 <i>MPa</i>)	0.116	5.255 <i>ksi</i> (36.23 <i>MPa</i>)
5 Grade 60 yield (413.7 <i>MPa</i>)	67.5 <i>ksi</i> (465.4 <i>MPa</i>)	0.098	6.615 <i>ksi</i> (45.609 <i>MPa</i>)

For the Elek Deresi Bridge, material specifications of class C25 for cast in place concrete and S420 grade for reinforcing steel has been reported by Avşar (2009). Consequently, utilising Table 3.1, the following values could be obtained for mean and standard deviation of material strengths via interpolation or extrapolation (Table 3.2).

Table 3.2 : Statistical parameters regarding Elek Deresi Bridge materials.

Property	Mean Value	Coefficient of Variation	Standard Deviation
C25 concrete	$f'_{co} = 21.75 \text{ MPa}$	0.18	3.91 <i>MPa</i>
S420 steel	$f_y = 472.41 \text{ MPa}$	0.097	45.91 <i>MPa</i>

As stated before, in order to select one of either concrete or steel strengths as the uncertain parameter, a few models were established using differing material properties. Behaviour of the structure was studied due to alterations in both materials. It was noticed that moment-curvature outcomes are not sensitive to variations in compressive

strength of unconfined concrete (f'_{co}). As the second trial, yield stress of reinforcing bars (f_y) was selected as the uncertain parameter. This time, it was observed that moment-curvature outcomes differ in a more significant manner (this behaviour will be studied in Subsection 3.2.2 where moment-curvature outputs for various analytical models are discussed). As a result of what was said, in the following, only results for models constructed from varying steel strengths have been reported and results relating to samples made of different concrete properties have been ignored. The only exception is for moment-curvature outputs which were found necessary to support the discussion made.

3.2.1 Variations in reinforced concrete properties due to changes in steel strengths

As described in Section 2.5, Mander's (1988) stress-strain model was used for assessing reinforced concrete properties. The results are presented in Table 3.3 and Table 3.4. Values in Table 3.3 correspond to the bent system capbeam whereas values in Table 3.4 correspond to columns.

Table 3.3 : Variations in specifications of confined concrete of capbeam section as a result of changes in steel properties.

Capbeam								
Model	f'_{co} (MPa)	f_y (MPa)	ϵ_{cc}	f'_{cc} (MPa)	ϵ_{cu}	f'_{cu} (MPa)	E_c (GPa)	E_{sec} (GPa)
$f_y = \mu_{f_y} - 1.5\sigma_{f_y}$	21.75	403.54	0.0043	26.84	0.0160	21.50	23.32	6.18
$f_y = \mu_{f_y} - 1.25\sigma_{f_y}$	21.75	415.02	0.0044	26.96	0.0163	21.64	23.32	6.13
$f_y = \mu_{f_y} - 1.0\sigma_{f_y}$	21.75	426.50	0.0045	27.09	0.0165	21.77	23.32	6.08
$f_y = \mu_{f_y} - 0.75\sigma_{f_y}$	21.75	437.98	0.0045	27.21	0.0168	21.90	23.32	6.03
$f_y = \mu_{f_y} - 0.5\sigma_{f_y}$	21.75	449.45	0.0046	27.33	0.0171	22.03	23.32	5.98
$f_y = \mu_{f_y} - 0.25\sigma_{f_y}$	21.75	460.93	0.0046	27.45	0.0174	22.15	23.32	5.94
$f_y = \mu_{f_y}$	21.75	472.41	0.0047	27.58	0.0176	22.28	23.32	5.89
$f_y = \mu_{f_y} + 0.25\sigma_{f_y}$	21.75	483.88	0.0047	27.70	0.0179	22.41	23.32	5.85
$f_y = \mu_{f_y} + 0.5\sigma_{f_y}$	21.75	495.36	0.0048	27.82	0.0182	22.54	23.32	5.81
$f_y = \mu_{f_y} + 0.75\sigma_{f_y}$	21.75	506.84	0.0048	27.94	0.0184	22.66	23.32	5.77
$f_y = \mu_{f_y} + 1.0\sigma_{f_y}$	21.75	518.31	0.0049	28.05	0.0187	22.79	23.32	5.73
$f_y = \mu_{f_y} + 1.25\sigma_{f_y}$	21.75	529.79	0.0050	28.17	0.0190	22.91	23.32	5.69
$f_y = \mu_{f_y} + 1.5\sigma_{f_y}$	21.75	541.27	0.0050	28.29	0.0192	23.04	23.32	5.65

Table 3.4 : Variations in properties of confined concrete of column sections as a result of changes in unconfined concrete and steel properties.

Columns								
Model	f'_{co} (MPa)	f_y (MPa)	ϵ_{cc}	f'_{cc} (MPa)	ϵ_{cu}	f'_{cu} (MPa)	E_c (GPa)	E_{sec} (GPa)
$f_y = \mu_{f_y} - 1.5\sigma_{f_y}$	21.75	403.54	0.00406	26.22	0.0130	21.57	23.32	6.46
$f_y = \mu_{f_y} - 1.25\sigma_{f_y}$	21.75	415.02	0.00411	26.34	0.0132	21.70	23.32	6.41
$f_y = \mu_{f_y} - 1.0\sigma_{f_y}$	21.75	426.50	0.00416	26.45	0.0134	21.83	23.32	6.35
$f_y = \mu_{f_y} - 0.75\sigma_{f_y}$	21.75	437.98	0.00422	26.57	0.0136	21.96	23.32	6.30
$f_y = \mu_{f_y} - 0.5\sigma_{f_y}$	21.75	449.45	0.00427	26.68	0.0138	22.09	23.32	6.25
$f_y = \mu_{f_y} - 0.25\sigma_{f_y}$	21.75	460.93	0.00432	26.80	0.0140	22.21	23.32	6.20
$f_y = \mu_{f_y}$	21.75	472.41	0.00437	26.91	0.0142	22.34	23.32	6.15
$f_y = \mu_{f_y} + 0.25\sigma_{f_y}$	21.75	483.88	0.00443	27.03	0.0144	22.47	23.32	6.10
$f_y = \mu_{f_y} + 0.5\sigma_{f_y}$	21.75	495.36	0.00448	27.14	0.0146	22.59	23.32	6.06
$f_y = \mu_{f_y} + 0.75\sigma_{f_y}$	21.75	506.84	0.00453	27.25	0.0148	22.72	23.32	6.01
$f_y = \mu_{f_y} + 1.0\sigma_{f_y}$	21.75	518.31	0.00458	27.37	0.0150	22.84	23.32	5.97
$f_y = \mu_{f_y} + 1.25\sigma_{f_y}$	21.75	529.79	0.00463	27.48	0.0152	22.97	23.32	5.93
$f_y = \mu_{f_y} + 1.5\sigma_{f_y}$	21.75	541.27	0.00469	27.59	0.0154	23.09	23.32	5.89

3.2.2 Moment-curvature analysis results

Differing material properties naturally result in different moment curvature curves and analysis results. As mentioned before, along with results for varying steel properties, results corresponding to models made of varying concrete properties will be demonstrated in this subsection. A discussion on reasons for selecting steel strength as the uncertainty variable will be provided also.

Figure 3.1, Figure 3.2, Figure 3.3 and Figure 3.4 demonstrate moment curvature curves of sections constructed from concretes with different unconfined compressive strengths but, identical steel properties and geometries. It can be conveniently observed that alterations in concrete properties from 15.88 N/mm^2 to 27.62 N/mm^2 ($f'_{co} = \mu_{f'_{co}} - 1.5\sigma_{f'_{co}}$ to $f'_{co} = \mu_{f'_{co}} + 1.5\sigma_{f'_{co}}$) has a pretty minor effect on moment curvature outputs; particularly when flexure of capbeam about its local y axis is considered (Figure 3.1). This is particularly important as capbeam curvature about its local y axis is generally the parameter which determines failure of Elek Deresi Bridge model under seismic loading. As an instance, Figure 3.5 can be used to determine whether columns or the capbeam have become critical during a transient analysis using an intensified earthquake record. This figure also shows flexure about which local axis of the critical member has gained a greater normalised value. It is observed from the figure that except for the scale factors resulting in $\sqrt{(S_{ax}[T_1]^2 + S_{ay}[T_1]^2)} = 0.3745g$ and $0.4898g$, for what one of the columns have become critical, it has always been bending of the capbeam about its local y axis that has reached the upmost value. Considering this fact, it is predictable that minor variations in capbeam flexure capacity, as exhibited in Figure 3.1 will not influence model behaviour in a serious manner.

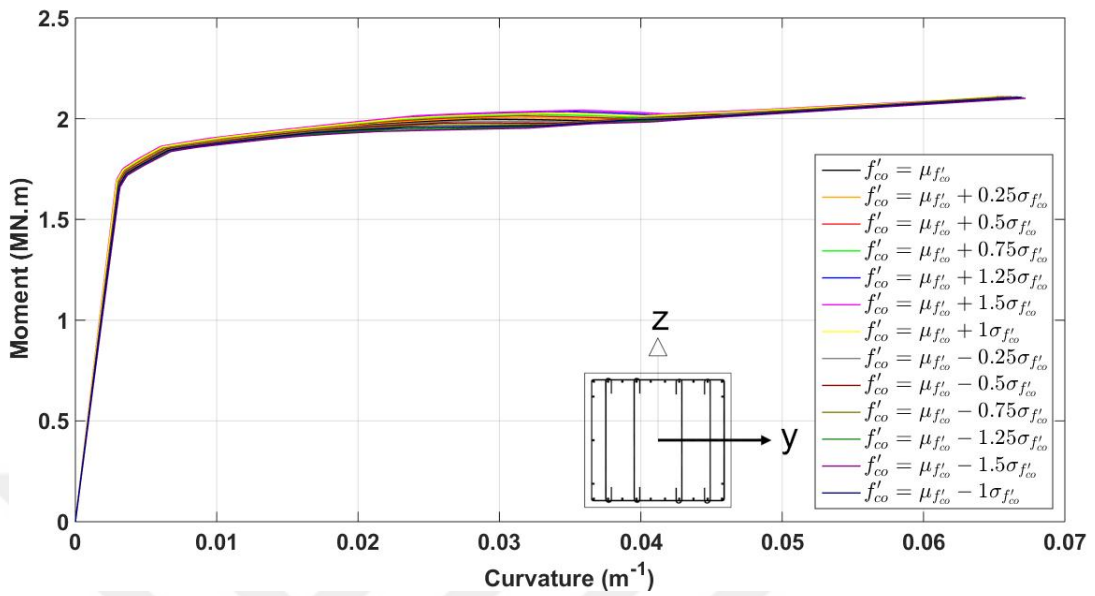


Figure 3.1 : Moment curvature curves for varying f'_{co} , $f_y = \mu_{fy}$ (472.41 MPa) (capbeam - local y axis).

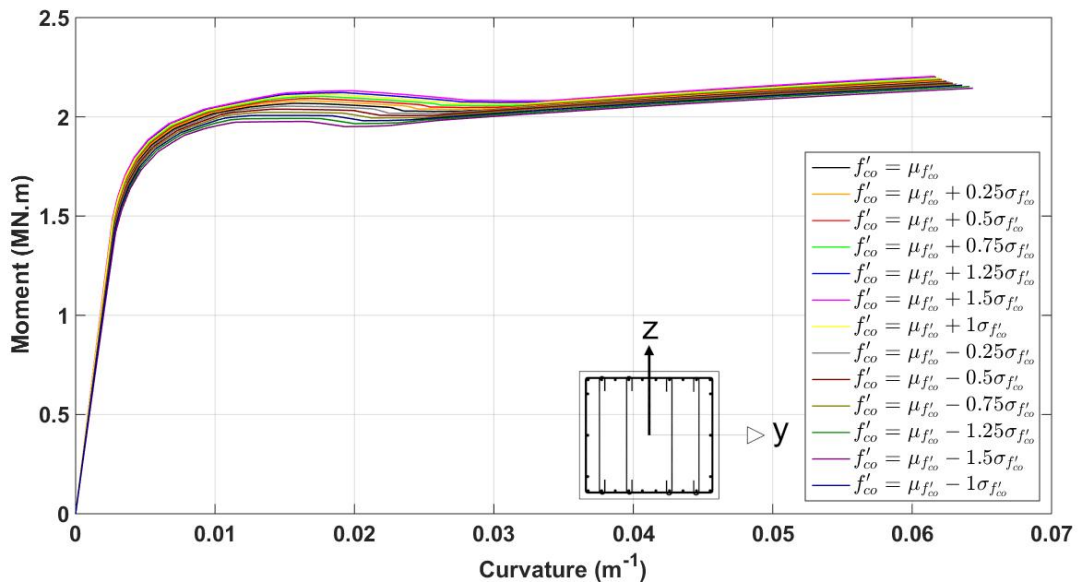


Figure 3.2 : Moment curvature curves for varying f'_{co} , $f_y = \mu_{fy}$ (472.41 MPa) (capbeam - local z axis).

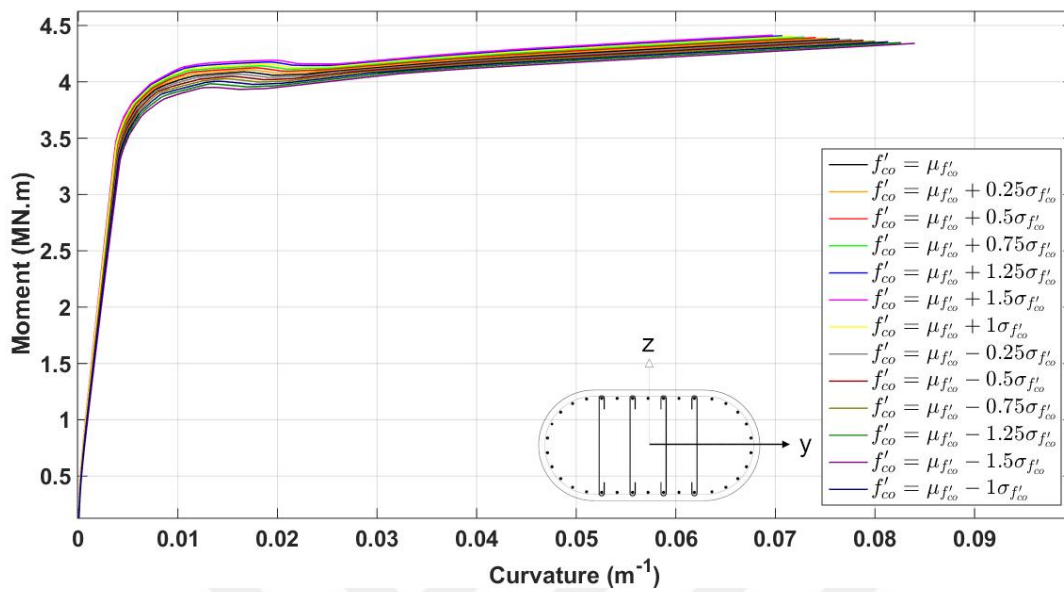


Figure 3.3 : Moment curvature curves for varying f'_{co} , $f_y = \mu_{fy}$ (472.41 MPa) (column - local y axis).

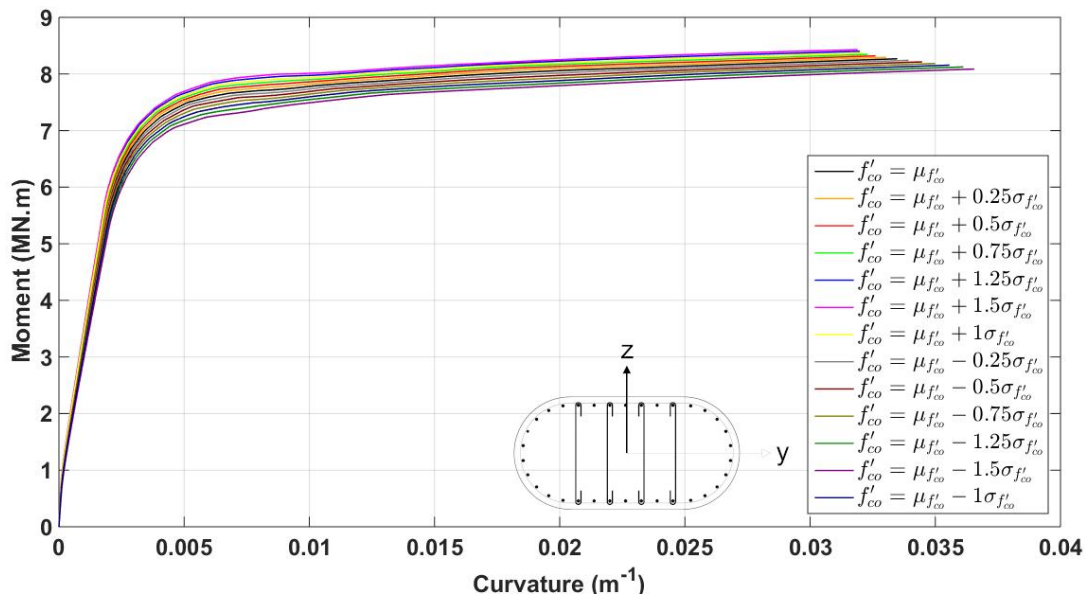


Figure 3.4 : Moment curvature curves for varying f'_{co} , $f_y = \mu_{fy}$ (472.41 MPa) (column - local z axis).

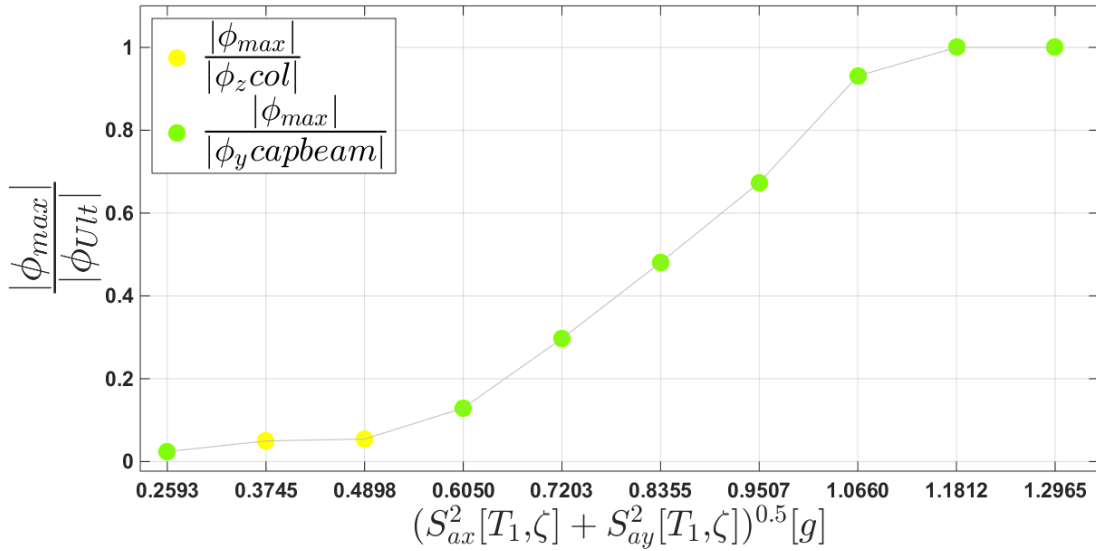


Figure 3.5 : Response of Elek Deresi Bridge to intensified values of RSN521 record.

Figure 3.6, Figure 3.7, Figure 3.8 and Figure 3.9 illustrate variations in moment curvature analyses outcomes due to changes in values of reinforcing bar yield stress. The model sections in mentioned figures have been built from identical geometries and concrete properties however, yield stress of their reinforcing bars vary from 403.54 N/mm² to 541.27 N/mm² as demonstrated in Table 3.3 and Table 3.4 (both longitudinal and transversal reinforcements have the same properties). It is observed that alterations of moment – curvature analyses results are more considerable when steel strength is selected as the uncertainty parameter. Table 3.5 demonstrates results of bilinear idealisations of a number of moment-curvature curves demonstrated in Figure 3.6, Figure 3.7, Figure 3.8 and Figure 3.9. For the sake of brevity, only results corresponding to $\gamma = -1.5, -0.75, 0.0, 0.75$ and 1.5 have been demonstrated. The method used for idealisation of moment-curvature outputs is recommended by Priestley et al. and described in Subsection 2.6.2. Results of bilinear idealisation for a model with mean material strengths presented in Table 3.5 have also been demonstrated previously in Subsection 2.6.

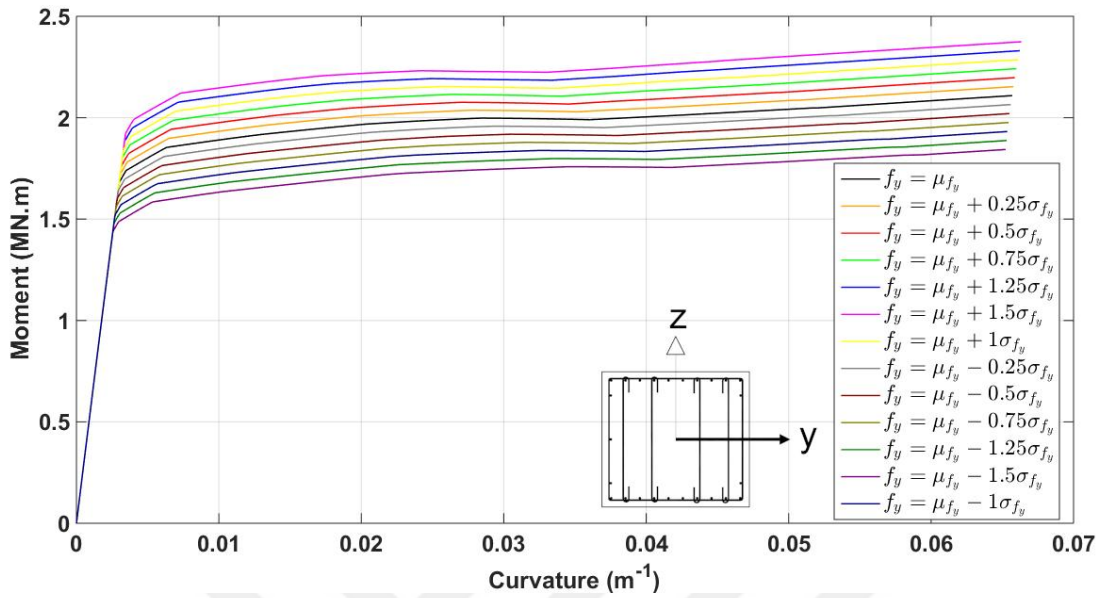


Figure 3.6 : Moment curvature curves for varying f_y , $f'_{co} = 21.75$ MPa (capbeam - local y axis).

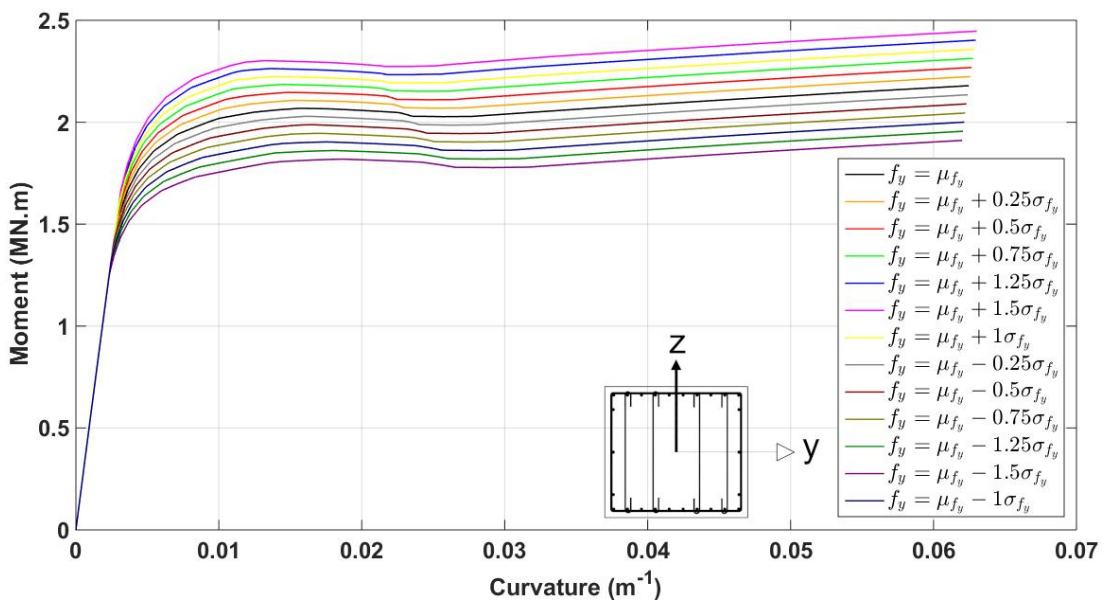


Figure 3.7 : Moment curvature curves for varying f_y , $f'_{co} = 21.75$ MPa (capbeam - local z axis).

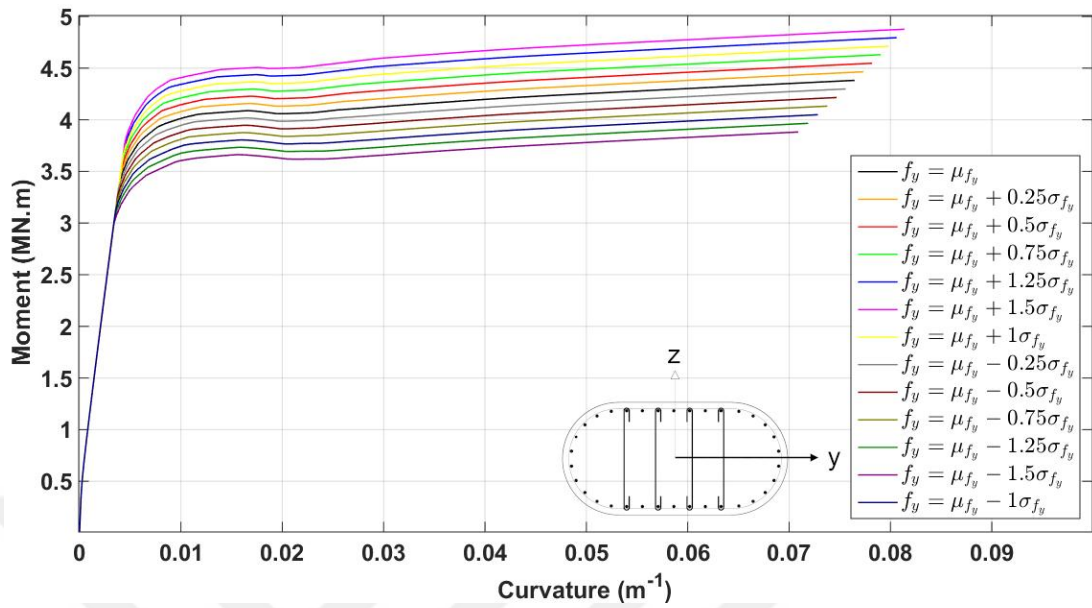


Figure 3.8 : Moment curvature curves for varying f_y , $f'_{co} = \mu_{f'co}$ (21.75 MPa) (column - local y axis).

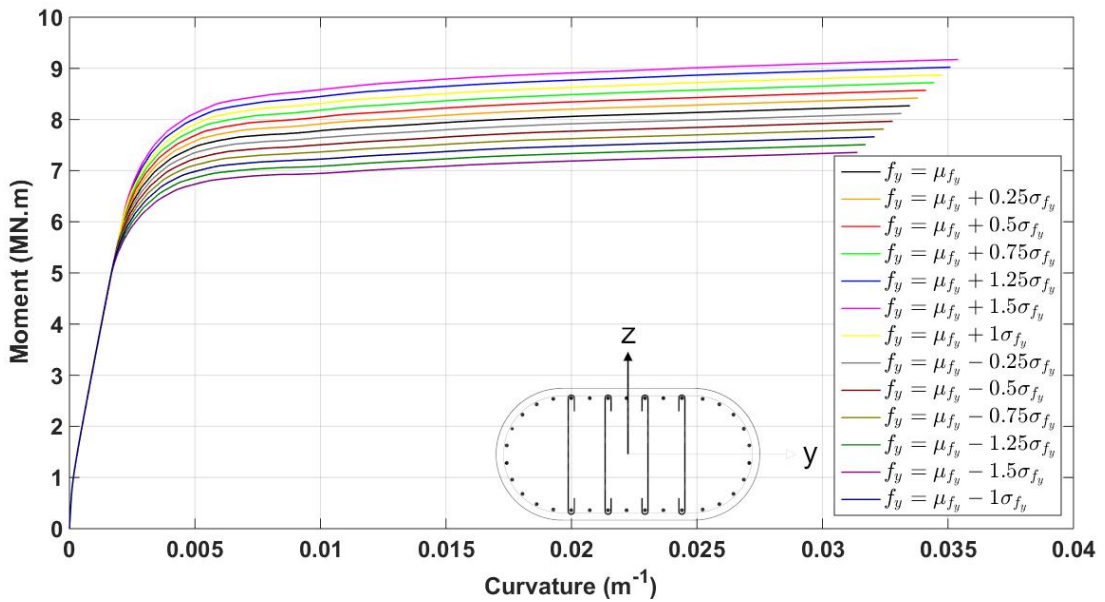


Figure 3.9 : Moment curvature curves for varying f_y , $f'_{co} = \mu_{f'co}$ (21.75 MPa) (column - local z axis).

Table 3.5 : Moment-curvature analysis results for capbeam and columns sections made from steel with different properties.

Model		M_y (KN.m)	ϕ'_y (m^{-1})	M_N (KN.m)	ϕ_y (m^{-1})	M_u (KN.m)	ϕ_u (m^{-1})
$f_y = \mu_{f_y} - 1.5\sigma_{f_y}$	Capbeam (y axis)	1289.37	0.00228	1681.61	0.00298	1843.18	0.0652
	Capbeam (z axis)	1103.33	0.00205	1810.66	0.00336	1910.94	0.0620
	Column (y axis)	2698.53	0.00298	3619.79	0.00399	3881.6	0.0709
	Column (z axis)	4445.17	0.00144	6927.36	0.00225	7355.9	0.0314
$f_y = \mu_{f_y} - 0.75\sigma_{f_y}$	Capbeam (y axis)	1400.700	0.002	1812.160	0.003	1976.010	0.065
	Capbeam (z axis)	1203.560	0.002	1942.810	0.004	2045.090	0.062
	Column (y axis)	2894.340	0.003	3839.290	0.004	4132.090	0.074
	Column (z axis)	4796.630	0.002	7327.700	0.002	7812.610	0.032
$f_y = \mu_{f_y}$	Capbeam (y axis)	1513.13	0.00269	1942.97	0.00346	2108.86	0.0657
	Capbeam (z axis)	1304.94	0.00244	2068.04	0.00386	2179.23	0.0625
	Column (y axis)	3090.69	0.00352	4058.65	0.00462	4381.43	0.0765
	Column (z axis)	5075.63	0.00171	7717.16	0.00260	8268.04	0.0335
$f_y = \mu_{f_y} + 0.75\sigma_{f_y}$	Capbeam (y axis)	1626.91	0.00290	2073.08	0.0037	2241.62	0.0660
	Capbeam (z axis)	1406.93	0.00264	2183.26	0.0041	2313.19	0.0628
	Column (y axis)	3289.2	0.00379	4277.66	0.0049	4629.91	0.0790
	Column (z axis)	5353.34	0.00183	8105.79	0.0028	8721.2	0.0345
$f_y = \mu_{f_y} + 1.5\sigma_{f_y}$	Capbeam (y axis)	1742.75	0.00312	2202.91	0.00394	2374.47	0.0663
	Capbeam (z axis)	1508.98	0.00284	2296.78	0.00432	2446.83	0.0630
	Column (y axis)	3484.33	0.00407	4496.56	0.00525	4876.55	0.0814
	Column (z axis)	5635.47	0.00195	8487.52	0.00293	9172.96	0.0354

3.2.3 Changes in elastic stiffness values with variations in steel properties

Concept of elastic stiffness and its significance for developing elastic models were discussed in Subsection 2.6.2. It was also mentioned that a table demonstrating variations of this parameter with steel properties will be provided later. The current subsection provides such a table for a number of FE models (Table 3.6). Once more, results corresponding to only 6 models have been presented to avoid the table from becoming too large. It is seen that EI_{gross} is the same for all models as concrete properties are constant.

3.2.4 Changes in plastic hinge lengths with variations in steel properties

Variations in yield stress values of reinforcing bars result in changes in strain penetration and plastic hinge lengths. Specifications of plastic hinges for samples made of various steel properties have been calculated by the method recommended by Priestley et al. (2007) and discussed in Section 2.7. These consequences have been summarised in Table 3.7. In the mentioned table, L_{SP} and L_P stand respectively for strain penetration length and plastic hinge length.

Table 3.6 : Elastic and gross stiffness values and their ratios for members built from reinforcing bars with differing yield stress values.

Model		EI_{el} (MN.m ²)	EI_{gross} (MN.m ²)	$\frac{EI_{el}}{EI_{gross}}$
$f_y = \mu_{f_y} - 1.5\sigma_{f_y}$	Column (Local y axis)	906.20	3087.27	0.294
	Column (Local z axis)	3078.52	11551.60	0.267
	Cap Beam (Local y axis)	564.73	3103.59	0.182
	Cap Beam (Local z axis)	539.19	3693.53	0.146
$f_y = \mu_{f_y} - 0.75\sigma_{f_y}$	Column (Local y axis)	891.71	3087.27	0.289
	Column (Local z axis)	3017.34	11551.60	0.261
	Cap Beam (Local y axis)	563.28	3103.59	0.181
	Cap Beam (Local z axis)	537.39	3693.53	0.145
$f_y = \mu_{f_y}$	Column (Local y axis)	878.76	3087.27	0.285
	Column (Local z axis)	2972.32	11551.60	0.257
	Cap Beam (Local y axis)	561.84	3103.59	0.181
	Cap Beam (Local z axis)	535.60	3693.53	0.145
$f_y = \mu_{f_y} + 0.75\sigma_{f_y}$	Column (Local y axis)	866.97	3087.27	0.281
	Column (Local z axis)	2931.79	11551.60	0.254
	Cap Beam (Local y axis)	560.39	3103.59	0.181
	Cap Beam (Local z axis)	533.81	3693.53	0.145
$f_y = \mu_{f_y} + 1.5\sigma_{f_y}$	Column (Local y axis)	856.33	3087.27	0.277
	Column (Local z axis)	2894.41	11551.60	0.251
	Cap Beam (Local y axis)	558.93	3103.59	0.180
	Cap Beam (Local z axis)	532.03	3693.53	0.144

Table 3.7 : Strain penetration lengths (L_{sp}) and plastic hinge lengths (L_p) for members built from reinforcing bars with differing yield stress values.

Model	Capbeam		Column	
	L_{SP} (m)	L_P (m)	L_{SP} (m)	L_P (m)
$f_y = \mu_{f_y} - 1.5\sigma_{f_y}$	0.1776	0.3551	0.2308	0.4617
$f_y = \mu_{f_y} - 1.25\sigma_{f_y}$	0.1826	0.3652	0.2374	0.4748
$f_y = \mu_{f_y} - 1.0\sigma_{f_y}$	0.1877	0.3753	0.2440	0.4879
$f_y = \mu_{f_y} - 0.75\sigma_{f_y}$	0.1927	0.3854	0.2505	0.5010
$f_y = \mu_{f_y} - 0.5\sigma_{f_y}$	0.1978	0.3955	0.2571	0.5142
$f_y = \mu_{f_y} - 0.25\sigma_{f_y}$	0.2028	0.4056	0.2637	0.5273
$f_y = \mu_{f_y}$	0.2079	0.4157	0.2702	0.5404
$f_y = \mu_{f_y} + 0.25\sigma_{f_y}$	0.2129	0.4258	0.2768	0.5536
$f_y = \mu_{f_y} + 0.5\sigma_{f_y}$	0.2180	0.4359	0.2833	0.5667
$f_y = \mu_{f_y} + 0.75\sigma_{f_y}$	0.2230	0.4460	0.2899	0.5798
$f_y = \mu_{f_y} + 1.0\sigma_{f_y}$	0.2281	0.4561	0.2965	0.5930
$f_y = \mu_{f_y} + 1.25\sigma_{f_y}$	0.2331	0.4662	0.3030	0.6061
$f_y = \mu_{f_y} + 1.5\sigma_{f_y}$	0.2382	0.4763	0.3096	0.6192

3.2.5 Changes to dynamic properties of models as a result of variations in steel properties

Variations caused by differing material specifications to dynamic properties of the bridge system have been summarised in Table 3.8. In this table ω_1 and ω_2 are structures first and second natural circular frequencies and T_1 and T_2 are structures first and second natural periods. Moreover, coefficients a_0 and a_1 which are used in defining Rayleigh damping matrix of the system have also been presented for comparison. As it is conveniently seen from this table, fundamental period of the structure (T_1) alters very slightly with changes in steel properties. In other words, T_1 increases by only 0.54% when steel yield strength changes from 403.54 MPa to 541.27 MPa. The main reason for this behaviour is freedom of bridge deck to float over the substructure as a result of the bearing type (elastomeric pads) employed (consulting Figure 2.46a which demonstrates first mode shape of vibration of system could also be helpful).

Table 3.8 : Dynamic specifications of FE models built from materials of different properties.

	ω_1^2 (s ⁻²)	ω_2^2 (s ⁻²)	ω_1 (s ⁻¹)	ω_2 (s ⁻¹)	T ₁ (s)	T ₂ (s)	a ₀	a ₁
$f_y = \mu_{f_y} - 1.5\sigma_{f_y} = 403.54 \text{ MPa}$	101.223	127.211	10.061	11.2788	0.6245	0.55708	0.5318	0.004686
$f_y = \mu_{f_y} - 1.25\sigma_{f_y} = 415.02 \text{ MPa}$	101.099	127.190	10.055	11.2778	0.6249	0.55713	0.5316	0.004688
$f_y = \mu_{f_y} - 1.0\sigma_{f_y} = 426.50 \text{ MPa}$	100.978	127.169	10.049	11.2769	0.6253	0.55717	0.5314	0.004689
$f_y = \mu_{f_y} - 0.75\sigma_{f_y} = 437.98 \text{ MPa}$	100.895	127.155	10.045	11.2763	0.6255	0.55720	0.5312	0.004690
$f_y = \mu_{f_y} - 0.5\sigma_{f_y} = 449.45 \text{ MPa}$	100.811	127.140	10.040	11.2756	0.6258	0.55724	0.5311	0.004691
$f_y = \mu_{f_y} - 0.25\sigma_{f_y} = 460.93 \text{ MPa}$	100.700	127.121	10.035	11.2748	0.6261	0.55728	0.5309	0.004693
$f_y = \mu_{f_y} = 472.41 \text{ MPa}$	100.624	127.107	10.031	11.2742	0.6264	0.55731	0.5308	0.004694
$f_y = \mu_{f_y} + 0.25\sigma_{f_y} = 483.88 \text{ MPa}$	100.520	127.089	10.026	11.2734	0.6267	0.55735	0.5307	0.004695
$f_y = \mu_{f_y} + 0.5\sigma_{f_y} = 495.36 \text{ MPa}$	100.476	127.080	10.024	11.2730	0.6268	0.55737	0.5306	0.004696
$f_y = \mu_{f_y} + 0.75\sigma_{f_y} = 506.84 \text{ MPa}$	100.375	127.063	10.019	11.2722	0.6271	0.55741	0.5304	0.004697
$f_y = \mu_{f_y} + 1.0\sigma_{f_y} = 518.31 \text{ MPa}$	100.278	127.045	10.014	11.2714	0.6274	0.55744	0.5303	0.004698
$f_y = \mu_{f_y} + 1.25\sigma_{f_y} = 529.79 \text{ MPa}$	100.238	127.038	10.012	11.2711	0.6276	0.55746	0.5302	0.004699
$f_y = \mu_{f_y} + 1.5\sigma_{f_y} = 541.27 \text{ MPa}$	100.144	127.021	10.007	11.2704	0.6279	0.55750	0.5301	0.004700

3.3 Seismic Risk Assessment of Elek Deresi Bridge Using the 2000 SAC/FEMA method

3.3.1 Introduction

The 2000 SAC/FEMA Method was originally developed by Cornell et al (2002) for steel moment-resisting frame buildings. The major motivation of its development was unsatisfactory performance of steel moment structures during 1994 Northridge earthquake (Lupoi G et al, 2002). It is an innovative reliability based approach which allows the designer or the analyser to estimate unconditional seismic hazard risk for a particular structure located in a specific earthquake-prone situation. Hence, it has superiority over approaches which calculate risks conditional to occurrence of a specific earthquake event (Lupoi G et al, 2002). This method can be used for probabilistic performance-based design or assessment of structures.

Three random elements are considered in the original method; the ground motion intensity (represented by pseudo-spectral acceleration in the neighbourhood of the first natural period of the structure - S_a), drift *demand* D and drift *capacity* C . Using processes of theory of probability, the method folds the mentioned three random variables together. *Demand* and *capacity* terms in this method are replacements for more conventional terms of *load* and *resistance* terms which are used in force-based design methodology. This is because the 2000 SAC/FEMA method is based on a non-linear, dynamic, displacement-based representation of the behaviour of the structure under seismic loads. Although the original method was developed for steel moment structures, it can be applied to reinforced structures as well (Pinto et al, 2004). Moreover, demand and capacity might be selected as variables other than inter-storey drifts; e.g. section curvatures or chord rotations.

3.3.2 Description of the method

As mentioned earlier, intensity of ground motion is the first of the three random elements considered in the method. It is represented by pseudo-acceleration (S_a) values in the neighbourhood of fundamental period of the structure for damping ratios equal to or greater than 5%. The annual probability that ground motion intensity becomes greater than a certain amount in a location - $H(s_a)$ - can be derived from seismic hazard curves. These curves are prepared by certain agencies and organisations with expertise in

geoscience and can be accessed and modified for annual rate of exceedance as will be discussed in Subsection 3.3.3.

The second random element as mentioned earlier is demand (D) which is conditional on the value of pseudo acceleration (S_a). For the start, the demand hazard curve – $H_D(d)$ - is developed by combining these two random variables (S_a and D) employing the total probability theorem.

$$H_D(d) = P[D \geq d] = \sum_{\text{all } x_i} P[D \geq |S_a = x_i] P[S_a = x_i] \quad (3.1)$$

$H_D(d)$ in equation (3.1) can be interpreted as the annual probability of exceedance of a certain demand value (d). $P[S_a = x_i]$ can be derived from the seismic hazard curve discussed earlier. In continuous form, equation (3.1) can be written as:

$$H_D(d) = \int P[D \geq |S_a = x_i] \left| \frac{dH(x)}{dx} \right| dx \quad (3.2)$$

In equation (3.2) taking absolute of $dH(x)$ is necessary because the hazard curve is always a monotonically decreasing function (annual probabilities of exceedance become smaller as pseudo-spectral accelerations increase). In the third step, demand hazard curve - $H_D(d)$ - is coupled with the third random variable which is the capacity. This is done using the total probability theorem again and the result is annual probability of a certain performance level not being fulfilled (P_f).

$$P_f = P[C \leq D] = \sum_{\text{all } d_i} P[C \leq D | D = d_i] P[D = d_i] \quad (3.3)$$

In equation (3.3), the second term can be determined from $H_D(d)$ presented earlier in equation (3.2). Moreover, it is assumed that demand and capacity are independent random variables and consequently, $P[C \leq D | D = d_i] = P[C \leq D]$. As a result, equation (3.3) in the continuous form appears as follows.

$$P_f = \int P[C \leq D] |dH_D(d)| \quad (3.4)$$

In equations (3.3) and (3.4), P_f does not necessarily stand for probability of total collapse of the structure. As mentioned previously, it merely stands for the probability of a performance level not being fulfilled.

For developing a manageable closed form of equations (3.2) and (3.4) and making calculation of demand from hazard curve and probability of failure feasible, three analytical approximations have been made.

First, it is assumed that seismic hazard curve at the site of the structure can be written as

$$H(s_a) = P[S_a \geq s_a] = k_0 s_a^{-k} \quad (3.5)$$

It is clear that equation (3.5) appears as a straight line if it is drawn as a log-log plot. As the second assumption, it is assumed that demand is a log-normally distributed variable with median \hat{D} and standard deviation of natural logarithm β_D . The latter parameter (β_D) will be called dispersion hereafter which is consistent with the nomenclature used by Cornell et al (2002). Moreover, it is assumed that median demand can be expressed approximately by the following expression.

$$\hat{D} = a(S_a)^b \quad (3.6)$$

In this study, parameters a , b and β_D have been approximated by means of a number of nonlinear transient analyses. The process, considered limit states and number of analyses will be subsequently described in detail. Now, returning to equation (3.2) and considering that demand has been assumed as a log-normally distributed random variable, the first term of equation (3.2) can be re-written as

$$P[D \geq d | S_a = x] = 1 - \Phi \left(\ln \left[\frac{d}{ax^b} \right] / \beta_D \right) \quad (3.7)$$

In equation (3.7), Φ is the CDF⁷ of standard normal distribution. After integration, demand hazard curve can be written in the form of

$$H_D(d) = P[D \geq d] = H[S_a(d)] \exp \left[\frac{1}{2} \frac{k^2}{b^2} \beta_D^2 \right] \quad (3.8)$$

In equation (3.8), $S_a(d)$ is defined as pseudo-spectral acceleration corresponding to drift level d and can be calculated from equation (3.6):

$$S_a(d) = \left(\frac{d}{a} \right)^{1/b} \quad (3.9)$$

The final of the three aforesaid assumptions is that capacity C is also a log-normally distributed random variable with median \hat{C} and dispersion (standard deviation of natural logarithm) β_C . By this final assumption, the first term of equations (3.3) and (3.4) can be written as

$$P[C \leq d] = \Phi \left(\ln \left[\frac{d}{\hat{C}} \right] / \beta_C \right) \quad (3.10)$$

So, the final form of equation (3.2) after substitution of equation (3.10) and integration becomes

⁷ Cumulative Distribution Function

$$P_f = H[S_a(\hat{C})] \exp \left[\frac{1}{2} \frac{k^2}{b^2} (\beta_D^2 + \beta_C^2) \right] \quad (3.11)$$

In equation (3.11), $S_a(\hat{C})$ appearing in the first term is:

$$S_a(\hat{C}) = \left(\frac{\hat{C}}{a} \right)^{1/b} \quad (3.12)$$

In calculations, it is possible to use the original form or linear approximation of the hazard curve as the first term of equation (3.11). Using the linear approximation from equation (3.5), equation (3.11) can be re-written as

$$P_f = k_0 \left(\frac{\hat{C}}{a} \right)^{-k/b} \times \exp \left[\frac{1}{2} \frac{k^2}{b^2} (\beta_D^2 + \beta_C^2) \right] \quad (3.13)$$

3.3.3 Hazard curve for Elek Deresi Bridge

A hazard curve is a diagram which shows probability of exceedance of a certain level of ground shaking at a site within a prescribed time interval. As stated in Section 2.2, Elek Deresi Bridge is constructed on the road from Boyabat to Sinop. Hazard curves for position of Elek Deresi Bridge might be obtained from SHARE⁸ online database for $T = 0.5s$ and $0.75s$ and probability of exceedance in 50 years. Nonetheless, to utilise curves from SHARE database for analysis purposes of this study, they must get converted to 1 year exceedance curves to be in agreement with the 2000 SAC/FEMA method. The approach used for converting probability of exceedance in 50 years to annual probability of exceedance is performed by assuming Poisson probability distribution for seismic events. By this assumption, probability of occurrence of at least one earthquake event within a time interval t can be calculated by equation (3.14), (Baker, 2008).

$$P(\text{at least one event in time } t) = 1 - e^{-\lambda t} \quad (3.14)$$

In which λ is rate of occurrence of seismic events. Taking $t = 50$ and extracting probability values from hazard curves by SHARE, it is possible to calculate λ :

$$P(\text{at least one event in 50 years}) = 1 - e^{-50\lambda} \rightarrow \lambda = \frac{-\ln(1-p)}{50}$$

Using the calculated λ , annual probability of exceedance is evaluated as:

$$P(\text{at least one event in 1 year}) = 1 - e^{-1 \times \lambda} = 1 - e^{-\lambda}$$

⁸ <http://www.share-eu.org/>

Moreover, the main period of Elek Deresi Bridge is about 0.62s for all constructed FE models (Table 3.8). As a result, the curve for $T_1 = 0.62s$ and probability of exceedance in 1 year was derived through interpolation of the curves from SHARE for $T_1 = 0.5s$ and $T_1 = 0.75s$ modified for annual probability of exceedance as described in the above. Results of the described process can be seen in Figure 3.10.

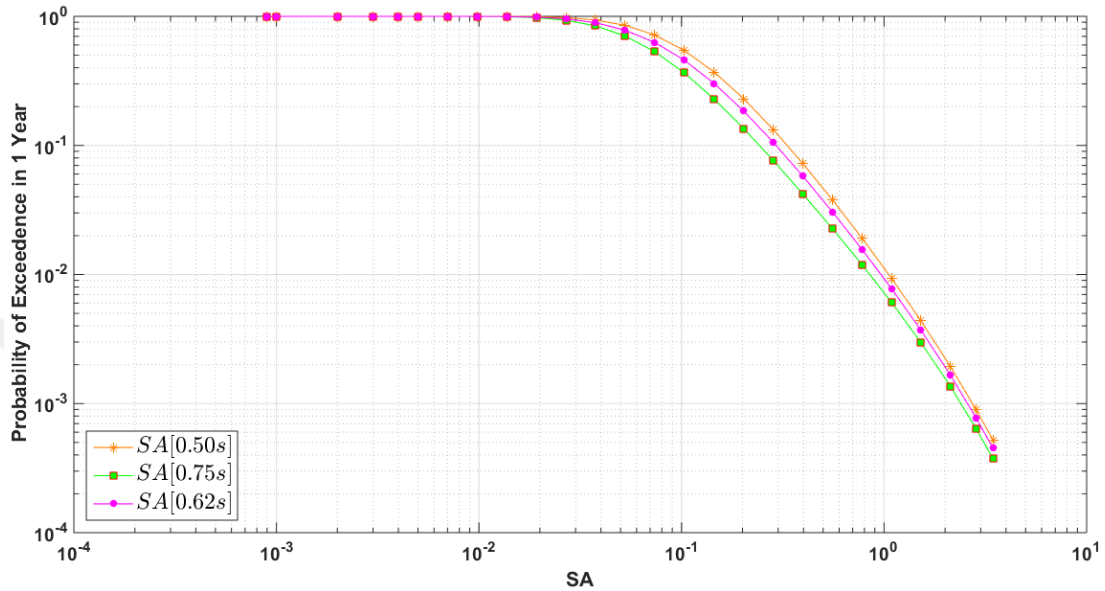


Figure 3.10 : Hazard curves for bridge position at $T = 0.5s$ and $0.75s$ and interpolated curve for $T = 0.62s$.

As the final step, it is noticed that the 2000 SAC/FEMA method defines hazard at the location of a structure by equation (3.5). Hence, the curve resulting from equation (3.5) must be fitted to the curve obtained by interpolation and demonstrated in Figure 3.10. This results in the idealised hazard curve illustrated in Figure 3.11 with equation of $H(S_a) = 1.5574 \times 10^{-4} s_a^{-2.0466}$.

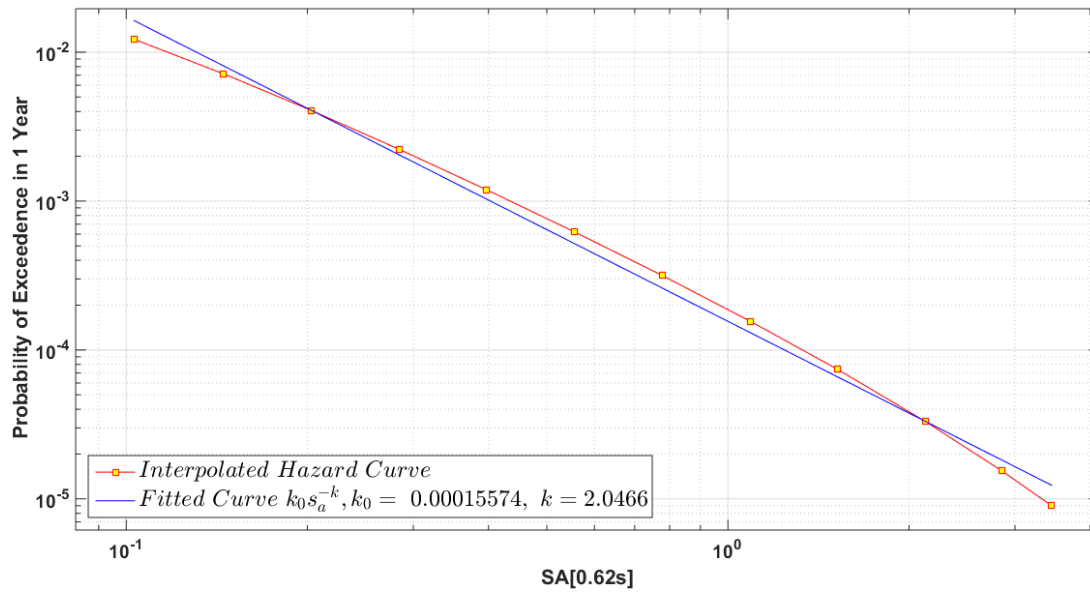


Figure 3.11 : Interpolated and idealised hazard curves for bridge position at T = 0.62s.

3.3.4 Specifications of strong ground motion records

Strong ground motion records used for analysis purposes of this report have been acquired from PEER ground motion data base⁹. Figure 3.12 to Figure 3.23 exhibit accelerograms of records in north-south and east-west directions along with their pseudo acceleration spectra prepared for a 5% damping ratio. In these figures, a red dot specifies value of pseudo acceleration at structures fundamental period which is about 0.62s for all FE models. All pseudo acceleration spectra for north-south and east-west components are also collected respectively in Figure 3.24 and Figure 3.25 for a more convenient view. Table 3.9 summarises some specifications of the selected ground motion records. In this table, information about record ID, earthquake name, event date and registering seismograph station have been acquired from Peer Ground Motion Database. Data relating to location of epicentre, depth and magnitude of the earthquake have been obtained from United States Geological Survey (USGS) webpage¹⁰.

⁹ <https://ngawest2.berkeley.edu/site>

¹⁰ <https://earthquake.usgs.gov/>

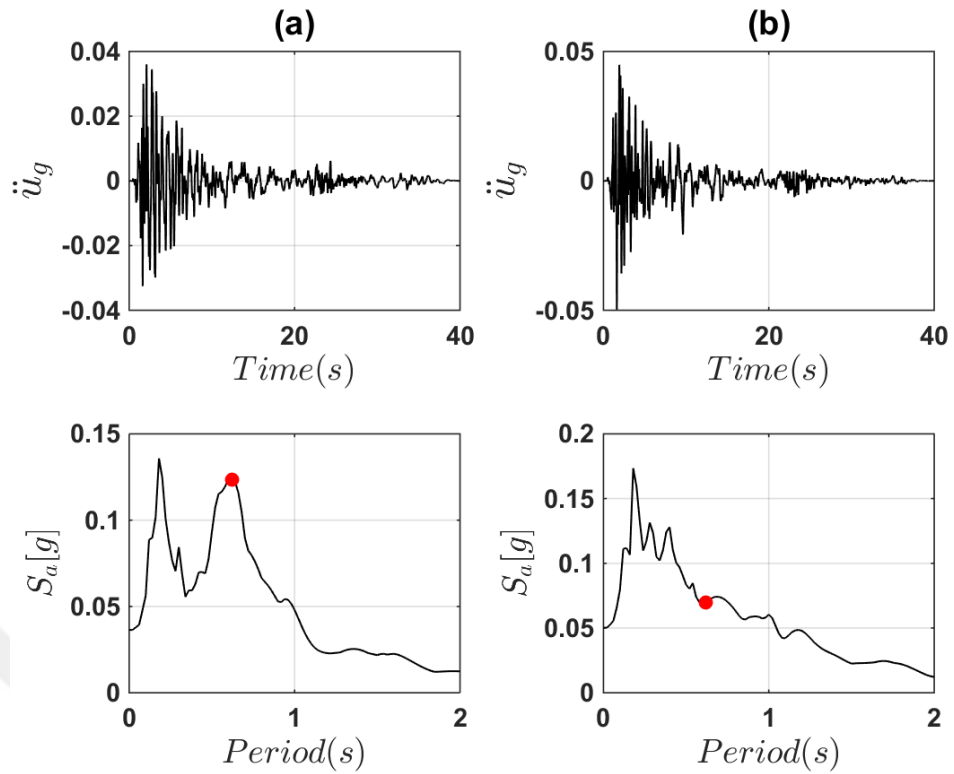


Figure 3.12 : Horizontal ground acceleration and pseudo acceleration spectra for RSN17 record ($\zeta = 5\%$) (a) North – south component (b) East – west component.

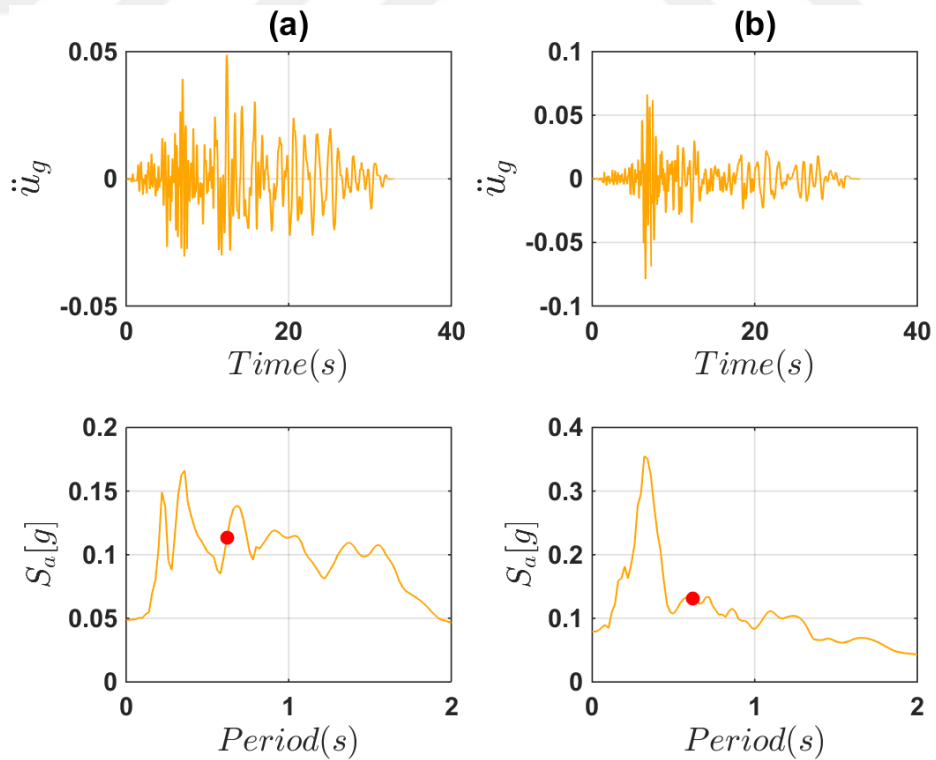


Figure 3.13 : Horizontal ground acceleration and pseudo acceleration spectra for RSN216 record ($\zeta = 5\%$) (a) North – south component (b) East – west component.

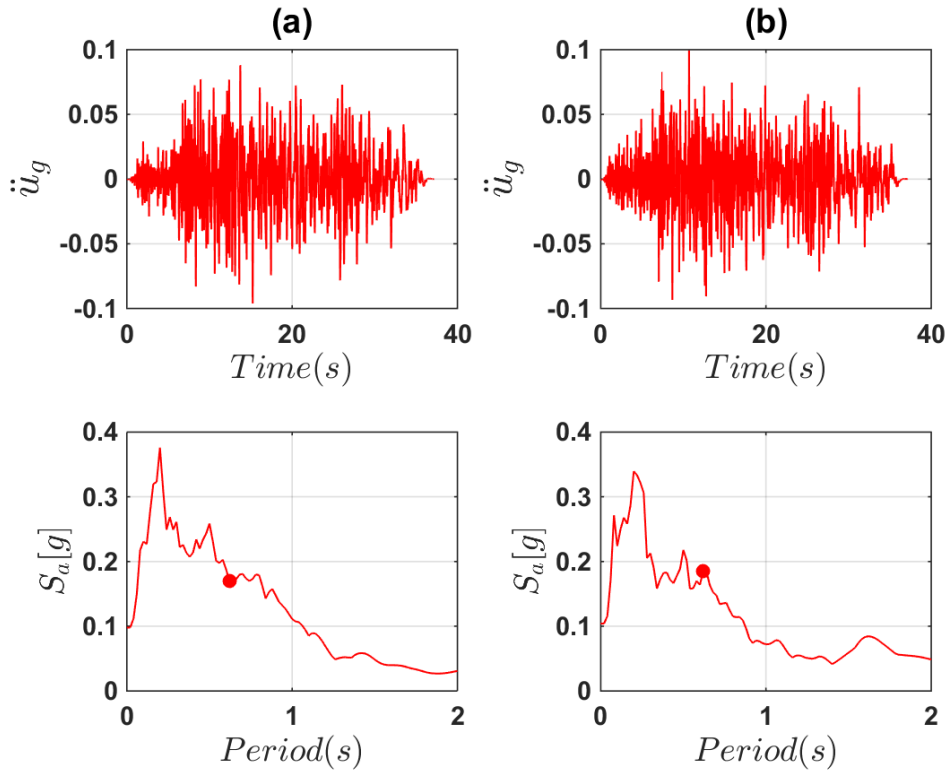


Figure 3.14 : Horizontal ground acceleration and pseudo acceleration spectra for RSN291 record ($\zeta = 5\%$) (a) North – south component (b) East – west component.

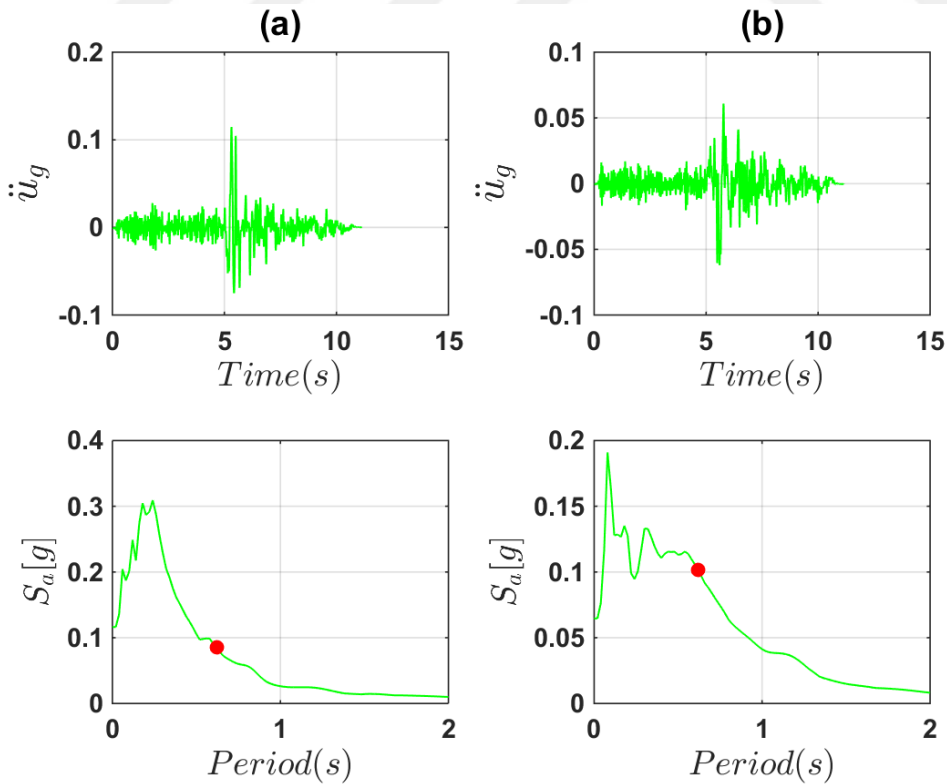


Figure 3.15 : Horizontal ground acceleration and pseudo acceleration spectra for RSN513 record ($\zeta = 5\%$) (a) North – south component (b) East – west component.

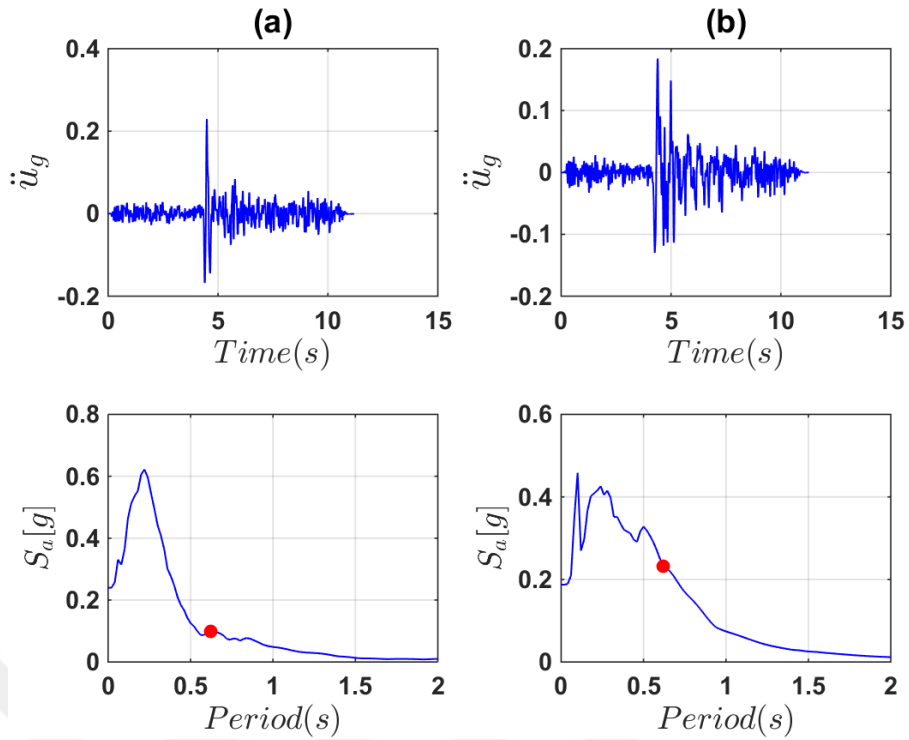


Figure 3.16 : Horizontal ground acceleration and pseudo acceleration spectra for RSN521 record ($\zeta = 5\%$) (a) North – south component (b) East – west component.

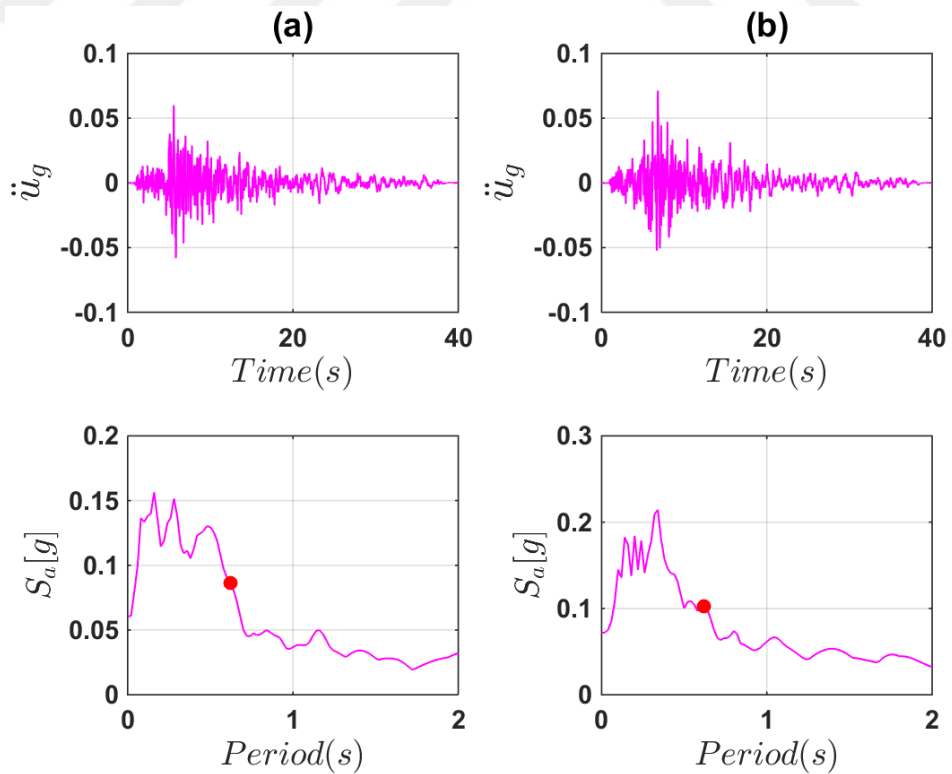


Figure 3.17 : Horizontal ground acceleration and pseudo acceleration spectra for RSN551 record ($\zeta = 5\%$) (a) North – south component (b) East – west component.

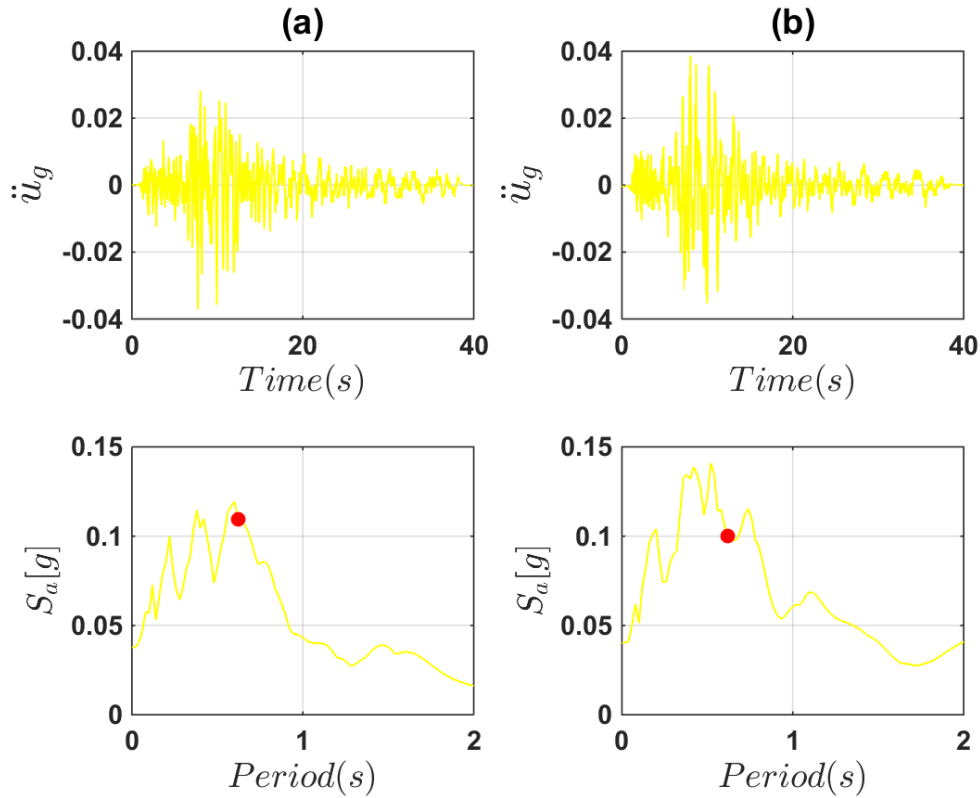


Figure 3.18 : Horizontal ground acceleration and pseudo acceleration spectra for RSN557 record ($\zeta = 5\%$) (a) North – south component (b) East – west component.

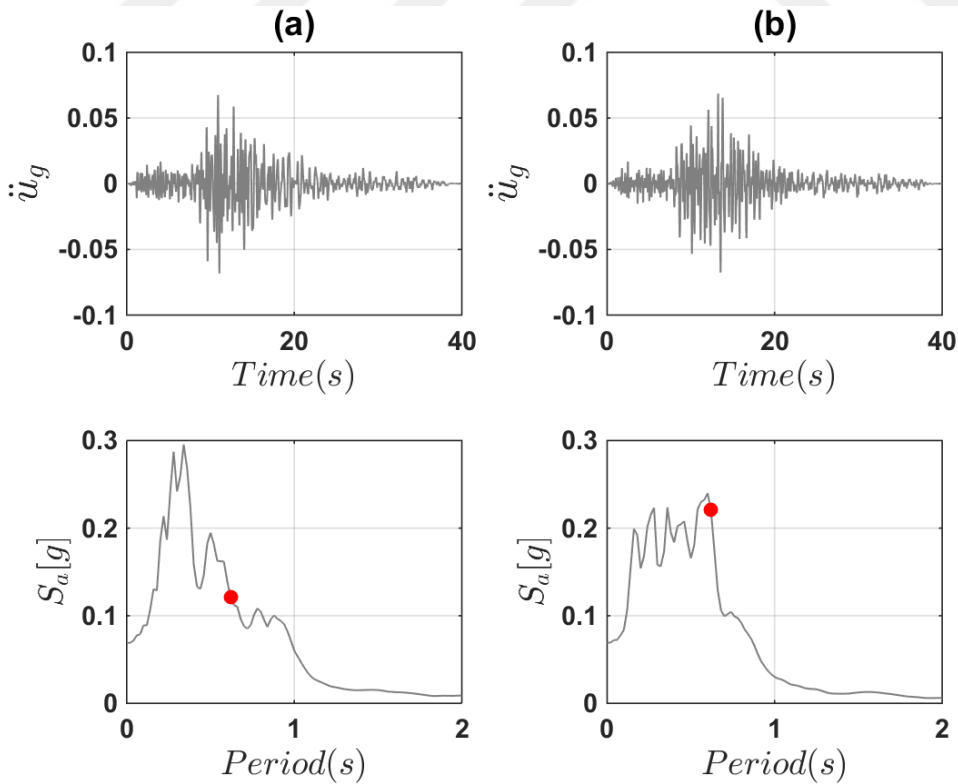


Figure 3.19 : Horizontal ground acceleration and pseudo acceleration spectra for RSN610 record ($\zeta = 5\%$) (a) North – south component (b) East – west component.

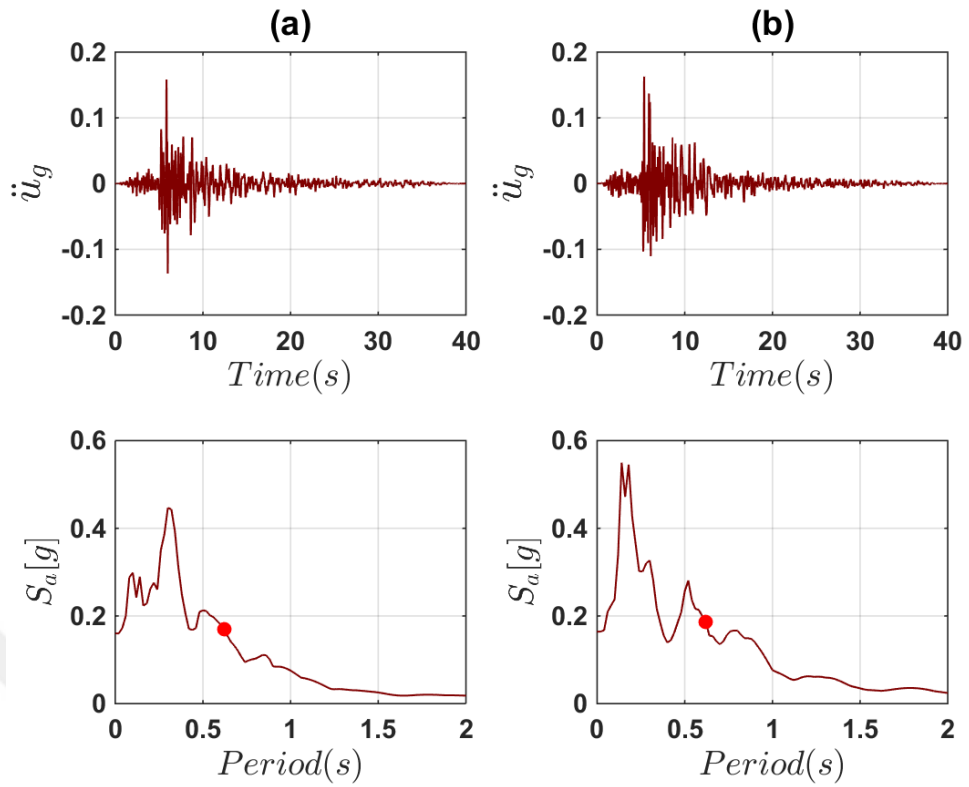


Figure 3.20 : Horizontal ground acceleration and pseudo acceleration spectra for RSN671 record ($\zeta = 5\%$) (a) North – south component (b) East – west component.

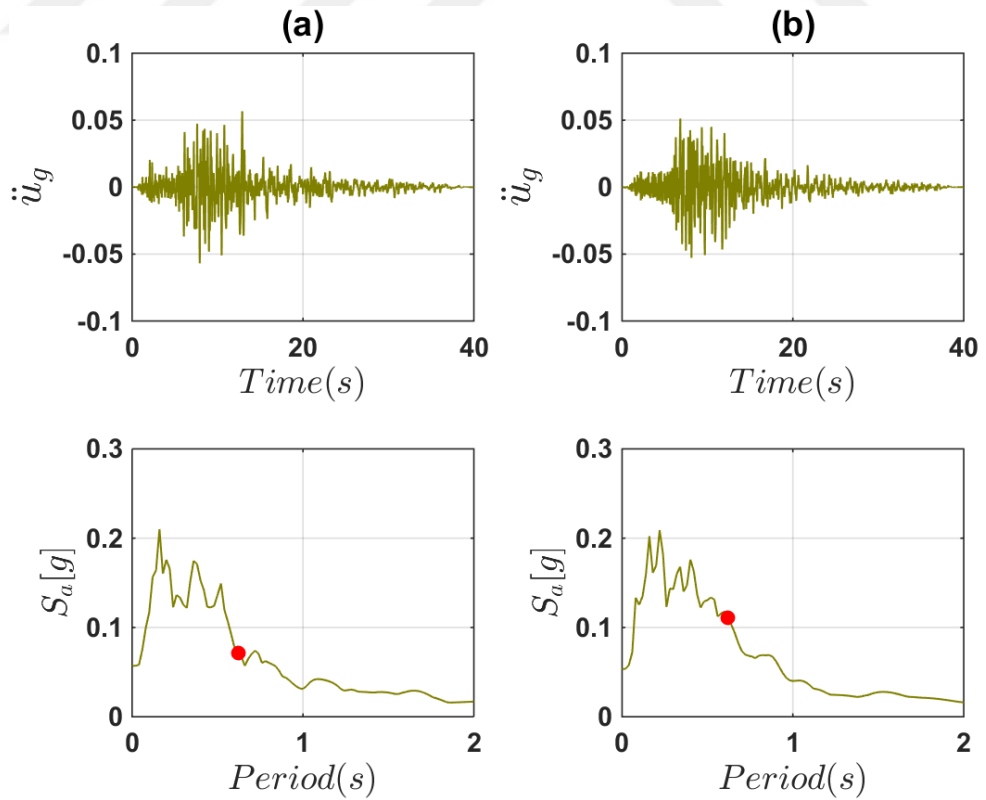


Figure 3.21 : Horizontal ground acceleration and pseudo acceleration spectra for RSN698 record ($\zeta = 5\%$) (a) North – south component (b) East – west component.

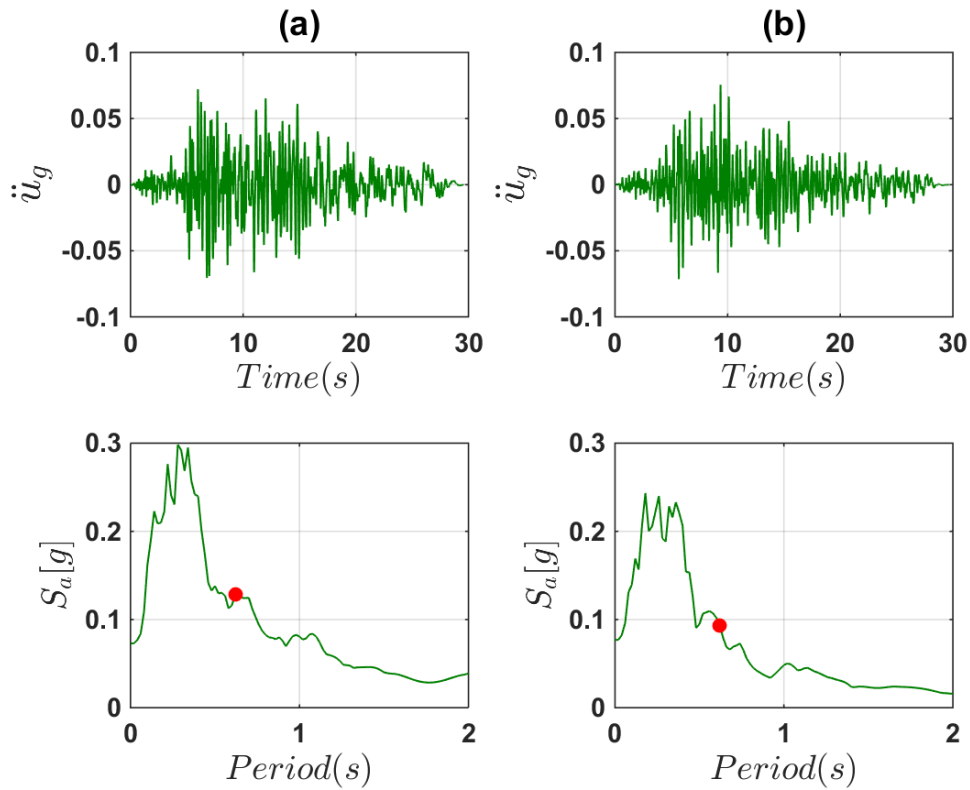


Figure 3.22 : Horizontal ground acceleration and pseudo acceleration spectra for RSN742 record ($\zeta = 5\%$) (a) North – south component (b) East – west component.

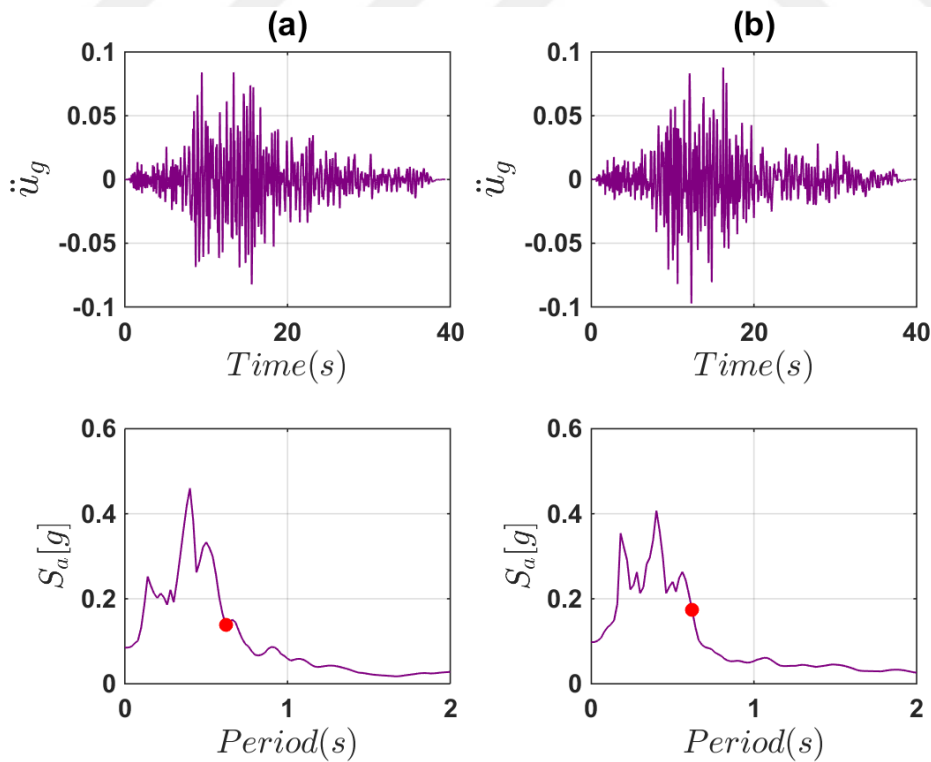


Figure 3.23 : Horizontal ground acceleration and pseudo acceleration spectra for RSN745 record ($\zeta = 5\%$) (a) North – south component (b) East – west component.

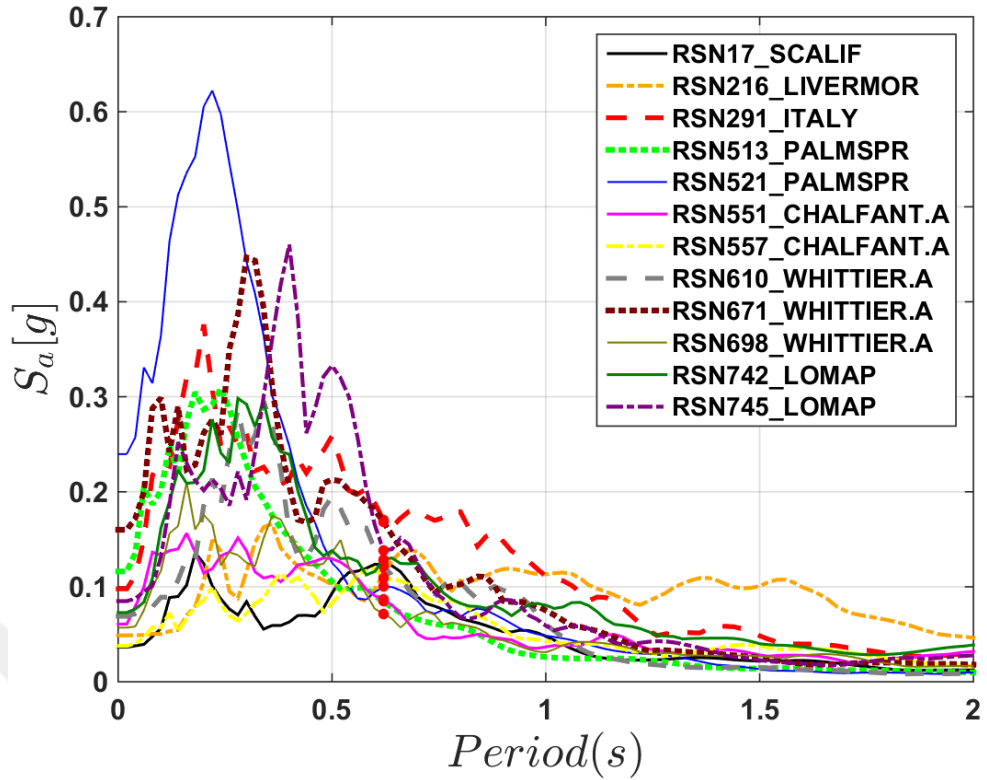


Figure 3.24 : Pseudo acceleration spectra for north – south components of the 12 strong ground motion records ($\zeta = 5\%$).

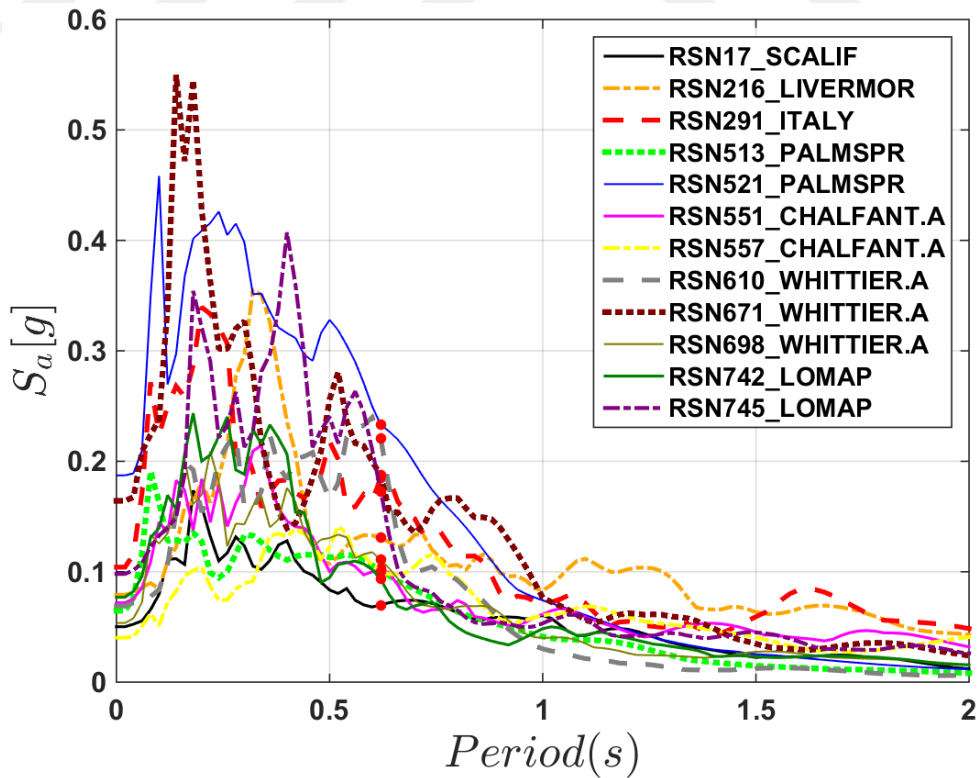


Figure 3.25 : Pseudo acceleration spectra for east – west components of the 12 strong ground motion records ($\zeta = 5\%$).

Table 3.9 : Characteristics of selected strong ground motions.

Record ID and Earthquake Name	Date	Epicentre Location	Depth (km)	Magnitude	Station	$\sqrt{(S_{ax}[T_1]^2 + S_{ay}[T_1]^2)}$
(RSN17) Southern California	22/11/1952	28km NW of Cambria, California (35.723°N,121.328°W)	6.0	6.2 (ml*)	San Luis Obispo	0.14184g
(RSN216) Livermor-01	24/01/1980	Northern California (37.852°N,121.815°W)	11.0	5.8 (mw**)	Tracy – Sewage Treatm Plant	0.15696g
(RSN291) Southern Italy	23/11/1980	Southern Italy (40.914°N,15.366°E)	10.0	6.9 (ms***)	Rionero In Vulture	0.2519g
(RSN513) N. Palm Springs	08/07/1986	Palm Springs, California (34.02°N, 116.76°W)	11.0	6.0 (mw)	Anza Fire Station	0.15076g
(RSN521) N. Palm Springs	08/07/1986	Palm Springs, California (34.02°N, 116.76°W)	11.0	6.0 (mw)	Hurkey Creek Park	0.25344g
(RSN551) Chalfant Valley-02	21/07/1986	Chalfant Valley, California (37.54°N,118.42°W)	10.0	6.2 (mw)	Convict Creek	0.15091g
(RSN557) Chalfant Valley-02	21/07/1986	Chalfant Valley, California (37.54°N,118.42°W)	10.0	6.2 (mw)	Tinemaha Res. Free Field	0.15091g

Table 3.9 (continued): Characteristics of selected strong ground motions.

Record ID and Earthquake Name	Date	Epicentre Location	Depth (km)	Magnitude	Station	$\sqrt{(S_{ax}[T_1]^2 + S_{ay}[T_1]^2)}$
(RSN671) Whittier Narrows-01	01/10/1987	SSW of Rosemead, California (34.061°N,118.079°W)	8.9	5.9 (mw)	Pacoima Kagel Canyon	0.16127g
(RSN698) Whittier Narrows-01	01/10/1987	SSW of Rosemead, California (34.061°N,118.079°W)	8.9	5.9 (mw)	Sylmar – Olive View Med FF	0.16127g
(RSN742) Loma Prieta	18/10/1989	Day Valley, California (37.036°N,121.880°W)	17.2	6.9 (mw)	Bear Valley #1 Fire Station	0.20001g
(RSN745) Loma Prieta	18/10/1989	Day Valley, California (37.036°N,121.880°W)	17.2	6.9 (mw)	Bear Valley #14 Upper Butts Rn	0.20001g

* local magnitude

** moment magnitude

*** surface-wave magnitude

3.4 Application of the 2000 SAC/FEMA Method to Elek Deresi Bridge Models

Procedure of application of the 2000 SAC/FEMA method to the case study bridge will be described in this section.

Geometrical and structural properties of Elek Deresi Bridge, its geographical situation, the hazard curve pertaining to bridge location, linear idealisation of the hazard curve and strong ground motion records employed have been studied in previous sections. Statistical specifications of materials and variations in structural parameters by changes in material properties were also discussed in Section 3.2. In this section, remaining aspects of application of the method will be presented.

3.4.1 Damage levels and limit states

Five damage levels and four limit states have been considered in this study as can be observed in Figure 3.26. More descriptions have been provided in Table 3.10 which has been obtained from (California Department of Transportation, 2006).

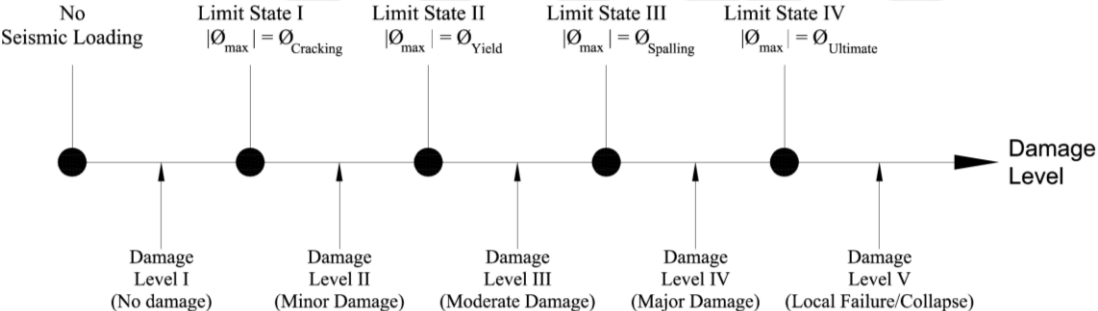


Figure 3.26 : Damage levels and limit states.

Table 3.10 : Damage levels and their specifications
 excerpted from (California Department of Transportation, 2006).

Level	Damage Classification	Damage Description	Repair Description	Socio-Economic Description
I	None	Barely visible cracking	No Repair	Fully Operational
II	Minor	Cracking	Possible Repair	Operational
III	Moderate	Open cracks; onset of spalling	Minimum Repair	Life Safety
IV	Major	Very wide cracks; extended spalling	Repair	Near Collapse
V	Local Failure/Collapse	Visible permanent deformation	Replacement	Collapse

For Limit State I (Figure 3.26), $\phi_{Cracking}$ pertains to the section curvature under which cracks begin to onset. It has been assumed that $\phi_{Cracking}$ for a section is approximately 50% of ϕ_{Yield} which is the nominal yield curvature of section and can be obtained from moment-curvature analysis outputs (Subsection 3.2.2). In the same figure, $\phi_{Spalling}$ that appears in Limit State III is section curvature under which concrete spalling onsets. It is assumed to be two times nominal yield curvature ($\phi_{Spalling} = 2.0 \times \phi_{Yield}$). $\phi_{Ultimate}$ appearing in Limit State IV is the ultimate section curvature and can be obtained from Subsection 3.2.2.

A certain limit state is reached as soon as the maximum absolute curvature over time over the structure during a nonlinear dynamic analysis becomes equal to that limit state. For instance, as long as $|\phi_{max}| < \phi_{Cracking}$ or $|\frac{\phi_{max}}{\phi_{Cracking}}| < 1$, the structure is in Damage Level I state (absolute value is required because of cyclic nature of seismic loading). As soon as $|\phi_{max}| = \phi_{Cracking}$ or $|\frac{\phi_{max}}{\phi_{Cracking}}| = 1$, Limit State I is reached and for greater absolute curvature values, the structure is in states of Damage Level II, III, IV or V. For convenience, hereafter, most of the calculations and analyses will be performed utilising maximum of normalised demand values ($|\frac{\phi_{max}}{\phi_{Limit\ State}}|$).

3.4.2 Statistical parameters of demand random element

As discussed in subsection 3.3.2, demand and capacity in the 2000 SAC/FEMA method are assumed to be random elements with lognormal distributions. Median and dispersion values of demand for each of the FE models constructed with material and structural properties discussed in Section 3.2 has been determined by 10 nonlinear dynamic analyses carried out using the set of 12 accelerograms for the 4 limit states. This will be discussed in detail in Subsection 3.4.3.1. It will be seen that a series of 10 equally incremented, increasing in value, scaling factors has been considered so that the smallest scaling factor is 10% of the largest one. Each of the 12 strong ground motion records has been scaled by this series of scaling factors and introduced as the transient load of the nonlinear dynamic analysis. Median curves of normalised limit state drawn against square root of sum of squares of pseudo spectral accelerations at bridge main period ($\sqrt{(S_{ax}^2[T_1, \zeta] + S_{ay}^2[T_1, \zeta])}$) have been plotted for each FE model. Using these curves (median normalised limit state – pseudo spectral acceleration curves), constants a and b in equation (3.6) have been determined and the regression curves, $\hat{D} = a(S_a)^b$, have been drawn.

As can be observed in Subsection 3.4.3.1, for each scaling factor, dispersion of normalised limit state outputs has been calculated for each model. A straight line has also been fitted to the scattered data points. Following notations used by Pinto and Giannini (2004), this line can be expressed as

$$\beta_D(s_a) = a_\beta + b_\beta \cdot s_a \quad (3.15)$$

Equation (3.15) can be used for approximating dispersion of demand (β_D) at $S_a(\hat{C})$ which is pseudo spectral acceleration value corresponding to the median capacity of the structure with regard to a certain failure mechanism; as can be seen in equation (3.12). Consequently, using equations (3.6) and (3.15) median (\hat{D}) and dispersion (β_D) of demand can be estimated for any S_a value (including $S_a(\hat{C})$ value). In other words, if \hat{C} is known, one can calculate demand median (\hat{D}) at $S_a(\hat{C})$ from equation (3.6) and demand dispersion (β_D) at $S_a(\hat{C})$ from equation (3.15). Hence, statistical specifications of structure capacity will be discussed in the next subsection and median value of capacity (\hat{C}) will be determined.

3.4.3 Determining statistical parameters of capacity random element

It seems to be reasonable to assume medium value of capacity (\hat{C}) in terms of each limit state as 1 considering the nature of normalised demands discussed in Subsection 3.4.1. In other words, it is assumed that a certain limit state is reached as soon as normalised demand equals median capacity value which is 1 ($|\frac{\phi_{max}}{\phi_{Limit\ State}}| = \hat{C} = 1$).

For estimating the logarithmic standard deviation (dispersion), capacity has been assumed as the product of two independent random variables; i.e. material random variable and model uncertainty random variable.

$$C = X.Y \quad (3.16)$$

In equation (3.16), X stands for random variable of material and Y stands for random variable of model uncertainty. It is assumed that both X and Y are lognormal random variables. Statistical parameters of material random variable have been discussed in Section 3.2 and coefficient of variation of steel strength was approximated as 0.097 ($V_{f_{co}} = 0.097$). Standard deviation of steel strength was approximated as 45.91 MPa ($\sigma_{f_y} = 45.91\ MPa$).

Model uncertainty can be considered as the result of incompleteness of available theories for quantifying deformations of RC elements under loadings. In this report, results of a research by Fardis and Biskins (2003) have been utilised for approximating properties of model uncertainty variable. In the mentioned research, several tests have been performed on beams, columns, piers and walls of various sectional geometries for studying their deformations; mainly under monotonic and cyclic lateral loads. Available models used for estimating deformations of RC members were evaluated by comparing their predictions with test results and new empirical relations were proposed by the authors of the mentioned research.

Among the extensive amount of data presented by Fardis and Biskins (2003), of interest here, are those results which deal with yield and ultimate curvatures. For rectangular beams and columns without reinforcement slippage, statistical properties for experimental to model prediction ratio values are presented in Table 3.11.

Table 3.11 : Statistical properties of experimental to model prediction values at yield and ultimate curvature.

Quantity	Number of Data	Mean	Median	Coefficient of Variation
$\frac{\phi_{y,exp}}{\phi_{y,pred}}$	198	1.325	1.275	29.3%
$\frac{\phi_{u,exp}}{\phi_{u,pred}}$	89	0.955	0.545	130.5%

It must be noted that as demonstrated in Figure 2.4, although bent cap beam section of Elek Deresi Bridge is rectangular, its columns do not have rectangular sections. Nonetheless, considering the wide range of specimens tested by Fardis and Biskins (2003), it has been assumed that data presented in Table 3.11 can provide a sound approximation for statistical properties of model uncertainty variable.

For approximating theoretical values of ultimate curvature ($\phi_{u,pred}$), Fardis and Biskins (2003) have used four available models to estimate properties of confined concrete (peak stress f'_{cc} , strain at peak stress ϵ_{cc} and ultimate strain of confined concrete ϵ_{cu}). The mentioned theoretical models are the original Mander model, model of Mander modified by Priestley, the model used by CEB/FIP Model Code 90¹¹ and a variation of the model by Priestley. They have also reported consequences of their works for both monotonically and cyclically loaded specimens. The results cited in Table 3.11 for ultimate curvatures are those that their theoretical ultimate curvatures have been calculated using confined concrete ultimate strain (ϵ_{cu}) based on recommendations by Priestley and their experimental ultimate curvatures have been derived by specimens loaded cyclically. This is because recommendation by Priestley is the approach used in this research (Section 2.5) and the fact that the current study is dealing with seismic loadings which have a cyclic nature.

Accepting the mentioned assumptions, it is possible to estimate dispersion (standard deviation of natural logarithm) of capacity (β_c) using dispersions of material and model uncertainty random variables utilising concepts of product of lognormal random variables as presented in equation (3.17) and definition of standard deviation and its relation with variance reminded by equation (3.18), (Nowak and Collins, 2000).

$$\sigma_{\ln C}^2 = \sigma_{\ln X}^2 + \sigma_{\ln Y}^2 \quad (3.17)$$

¹¹ Comité Euro-International du Béton, 1993

$$\sigma_{lnC} = \sqrt{\sigma_{lnC}^2} \quad (3.18)$$

Variance of natural logarithms of variables X and Y (σ_{lnX}^2 and σ_{lnY}^2) can be calculated by equation (3.19) (Nowak and Collins, 2000).

$$\sigma_{lnZ}^2 = \ln(V_Z^2 + 1) \quad (3.19)$$

In which Z is an arbitrary lognormal random variable, V_Z is coefficient of variation of random variable Z and σ_{lnZ}^2 is variance of natural logarithm of variable Z (lnZ).

Hence, by means of equation (3.19) and using data of Table 3.2, dispersion value of material random variable can be estimated. Considering that steel yield strength is selected as model uncertainty:

$$\beta_{X,f_y} = \sigma_{lnX,f_y} = \sqrt{\ln(V_{f_y}^2 + 1)} = \sqrt{\ln(0.097^2 + 1)} = 0.0969$$

By the same process, dispersion values of model uncertainty in terms of yield and ultimate limit states can be determined using equation (3.19) and data of Table 3.11:

$$\beta_{Y,Yield} = \sigma_{lnY,Yield} = \sqrt{\ln(V_{Y,Yield}^2 + 1)} = \sqrt{\ln(0.293^2 + 1)} = 0.287$$

$$\beta_{Y,Ult} = \sigma_{lnY,Ult} = \sqrt{\ln(V_{Y,Ult}^2 + 1)} = \sqrt{\ln(1.305^2 + 1)} = 0.997$$

Also, recalling that limit states for cracking and spalling have been defined as coefficients of yield limit state ($\Phi_{Cracking} = 0.5\Phi_{Yield}$ and $\Phi_{Spalling} = 2\Phi_{Yield}$), dispersion values of model uncertainty in case of cracking and spalling limit states will be equal to that of yield limit state. In other words,

$$\beta_{Y,cracking} = \beta_{Y,spalling} = \beta_{Y,yield} = 0.287$$

Employing obtained values of material and model dispersions by the described process, dispersion of capacity random variable can be calculated using equation (3.17) and equation (3.18) for different limit states. Table 3.12 summarises these results for steel strength assumed as uncertainty parameter.

Table 3.12 : Capacity dispersion values for different limit states.

Model Uncertainty	$\beta_{C,cracking}$	$\beta_{C,yield}$	$\beta_{C,spalling}$	$\beta_{C,ultimate}$
f_y	0.303	0.303	0.303	1.002

3.4.3.1 Results of nonlinear dynamic analyses, determining values of constants a and b and dispersion of demand random element (β_D)

Using strong ground motion records presented in Section 3.3.4, nonlinear dynamic analyses were performed for bridge models made from varying steel properties. The objective is to determine constants a , b and demand dispersion (β_D) in terms of a certain limit state. Variations of normalised demand versus pseudo spectral acceleration for 4 (out of 13) FE models can be seen in Figure 3.27 to Figure 3.34. The mentioned figures demonstrate demand values in terms of normalised yield limit state ($\frac{\phi_{max}}{\phi_{Yield}}$) and normalised ultimate limit state ($\frac{\phi_{max}}{\phi_{Ult}}$) versus square root of sum of squares of pseudo spectral accelerations at bridge main period ($\sqrt{(S_{ax}^2[T_1, \zeta] + S_{ay}^2[T_1, \zeta])}$) made from steel of varying yield stress values. For the sake of brevity, only results corresponding to 4 (out of 13) models regarding 2 (out of 4) limit states have been demonstrated. Nonetheless, results for all models have been accumulated in Figure 3.35, Figure 3.36, Figure 3.37 and Figure 3.38 which relate respectively to cracking, yield, spalling and ultimate curvature limit states. It is evident from these figures that models made from steel of various strengths behave distinctively when they are imposed to intensified strong ground motion records. In other words, "weaker" models reach their limit states sooner and for a greater number of accelerograms in comparison to "stronger" models. Variations in behaviour of different models can also be observed from Figure 3.39 to Figure 3.44 in which dispersion of demands in terms of normalised yield and ultimate limit states versus $\sqrt{(S_{ax}^2[T_1, \zeta] + S_{ay}^2[T_1, \zeta])}$ have been exhibited for three models ($f_y = \mu_{f_y} + \gamma\sigma_{f_y}$ where γ equals -1.5, 0.0 and +1.5) along with the regression line fitted to the scattered data.

For the case study bridge analysed using the set of accelerograms discussed previously, it is observed that dispersion values of demand - S_a pairs for greater scaling factors are smaller for weaker models. This is because weaker models of the case study bridge behave in a more uniform manner when compared with the stronger samples for larger scaling factors. On the other hand, stronger samples behave more uniformly for small scaling factors, however; variability of their responses grows as they get exposed to intensified accelerograms. This behaviour is easier to notice when Figure 3.45 and Figure 3.46 are observed. In these figures all linear approximations of demand dispersion against pseudo spectral acceleration results have been accumulated for yield

and ultimate curvature limit states. The trend shown is similar for the other two limit states (cracking and spalling curvature) as well; i.e. variability of demand increases for stronger samples with scaling factor while the trend is vice versa for weaker models. Table 3.13 presents values of constants a and b for models made of varying steel properties. Figure 3.47 and Figure 3.48 exhibit information seen in Table 3.13 in form of diagrams. Moreover, a straight regression line has been drawn through the scattered data in order to help recognise the trend. It is obvious from the figures that both constants a and b tend to drop along the fitted line as the samples get stronger. Figure 3.49 and Figure 3.50 demonstrate variations of constants a_β and b_β with steel properties along with a regression line fitted to the data. It is conveniently seen that while a_β - y intercept in equation (3.15) - consistently decreases, b_β - the slope in equation (3.15) - steadily increases with γ which results in increase in dispersion of $D - S_a$ pairs for stronger structures. It is also clear that variability of $D - S_a$ pairs remain almost constant for some models ($f_y = \mu_{f_y} - 0.75\sigma_{f_y}$ and $f_y = \mu_{f_y} - 0.5\sigma_{f_y}$).

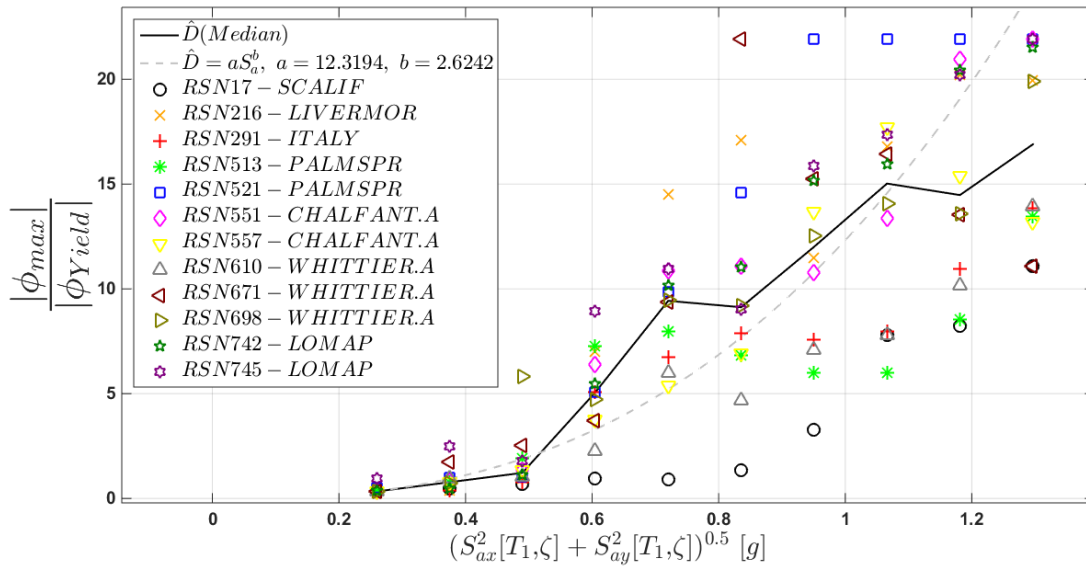


Figure 3.27 : Median demand vs. spectral acceleration in terms of yield curvature limit state ($f'_{co} = \mu_{f'co}$, $f_y = \mu_{fy} - 1.5\sigma_{fy}$).

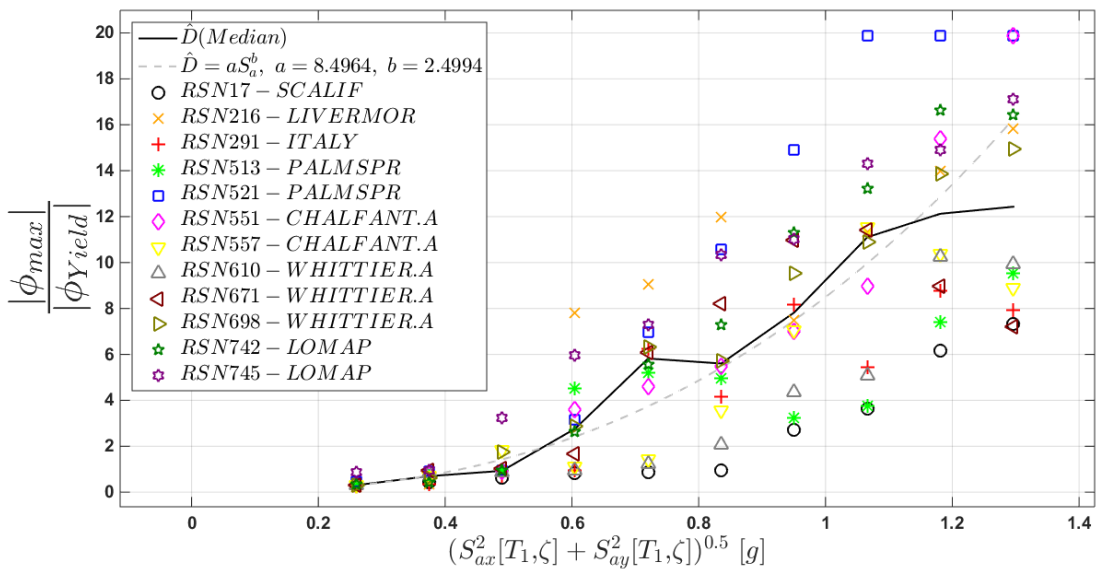


Figure 3.28 : Median demand vs. spectral acceleration in terms of yield curvature limit state ($f'_{co} = \mu_{f'co}$, $f_y = \mu_{fy} - 0.5\sigma_{fy}$).

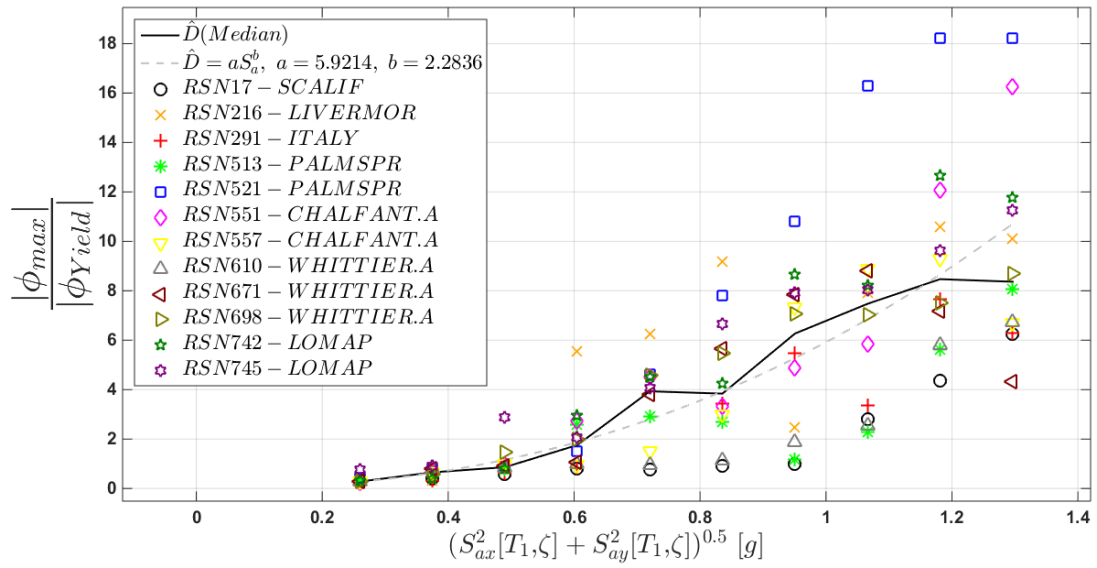


Figure 3.29 : Median demand vs. spectral acceleration in terms of yield curvature limit state ($f'_{co} = \mu_{f'co}$, $f_y = \mu_{fy} + 0.5\sigma_{fy}$).

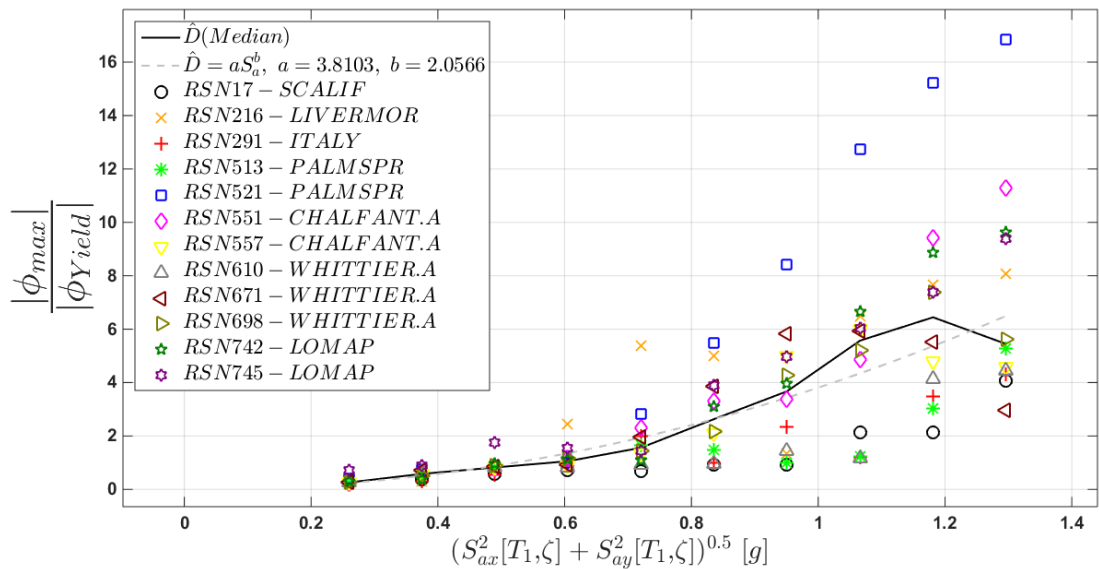


Figure 3.30 : Median demand vs. spectral acceleration in terms of yield curvature limit state ($f'_{co} = \mu_{f'co}$, $f_y = \mu_{fy} + 1.5\sigma_{fy}$).

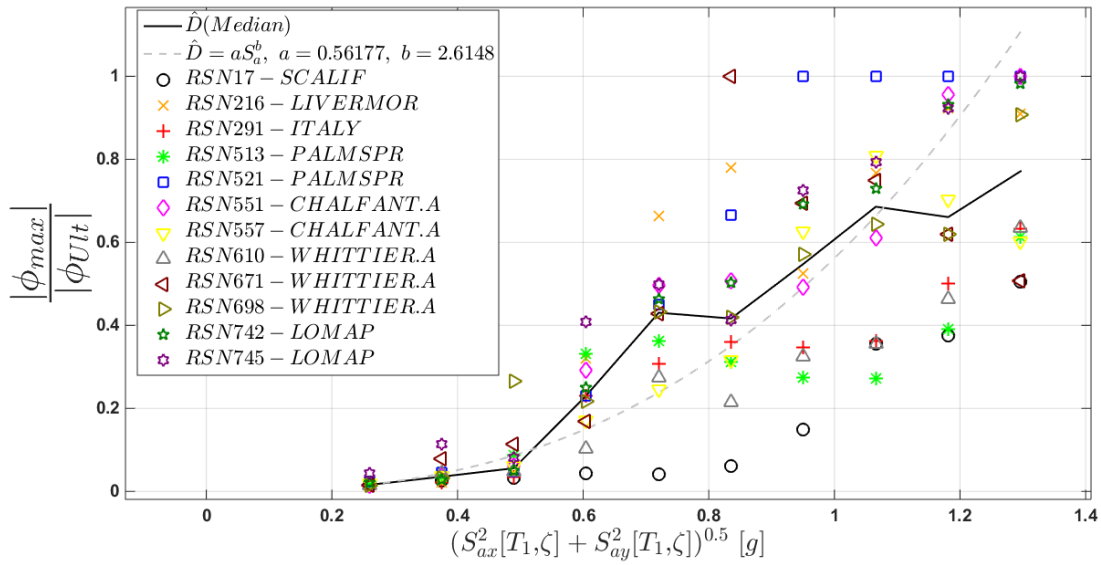


Figure 3.31 : Median demand vs. spectral acceleration in terms of ultimate curvature limit state ($f'_{co} = \mu_{f'co}$, $f_y = \mu_{fy} - 1.5\sigma_{fy}$).

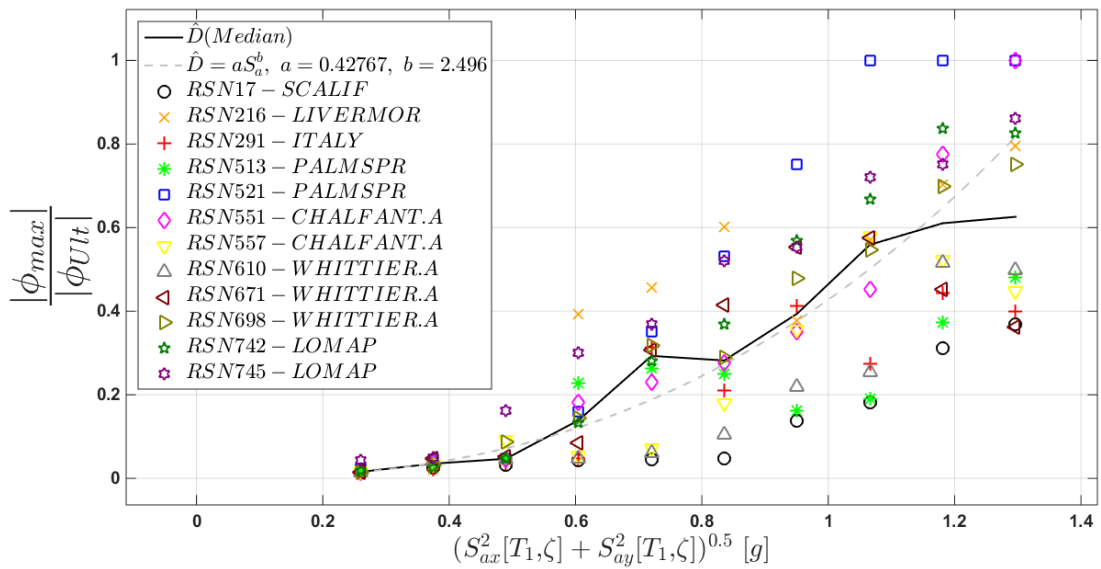


Figure 3.32 : Median demand vs. spectral acceleration in terms of ultimate curvature limit state ($f'_{co} = \mu_{f'co}$, $f_y = \mu_{fy} - 0.5\sigma_{fy}$).

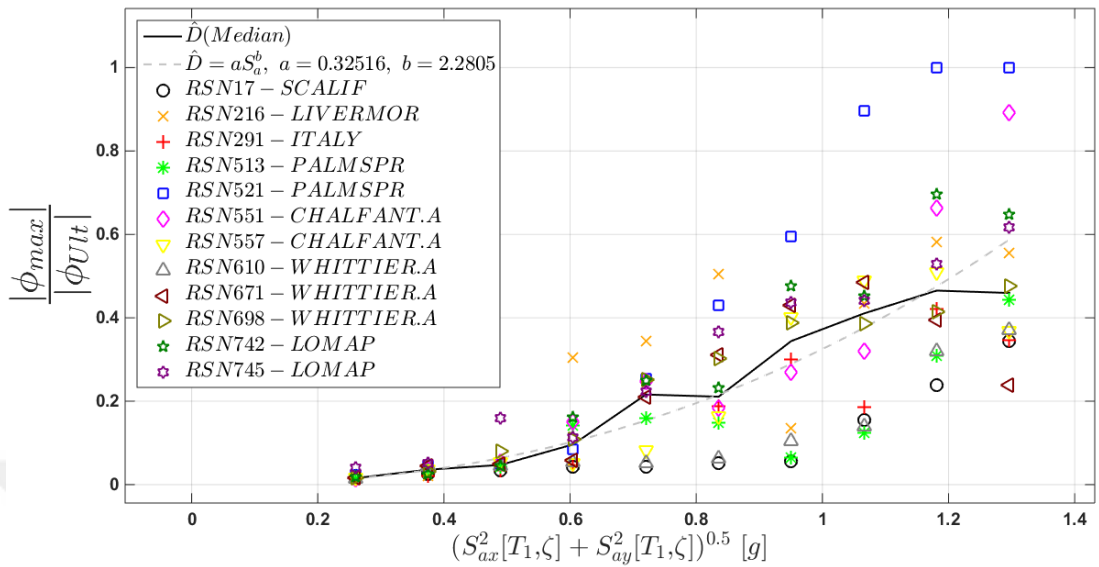


Figure 3.33 : Median demand vs. spectral acceleration in terms of ultimate curvature limit state ($f'_{co} = \mu_{f'co}$, $f_y = \mu_{fy} + 0.5\sigma_{fy}$).

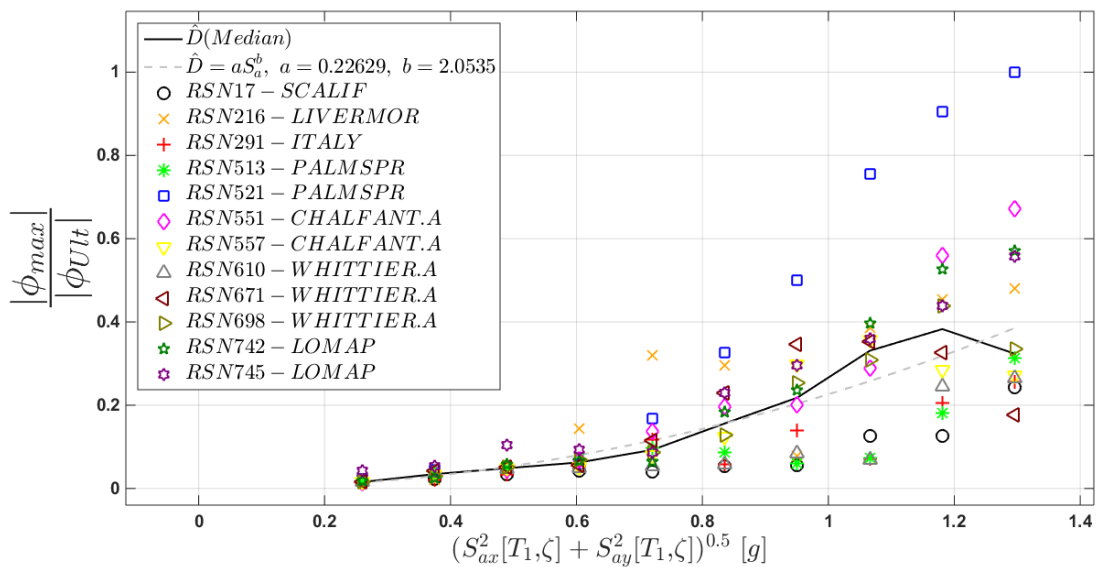


Figure 3.34 : Median demand vs. spectral acceleration in terms of ultimate curvature limit state ($f'_{co} = \mu_{f'co}$, $f_y = \mu_{fy} + 1.5\sigma_{fy}$).

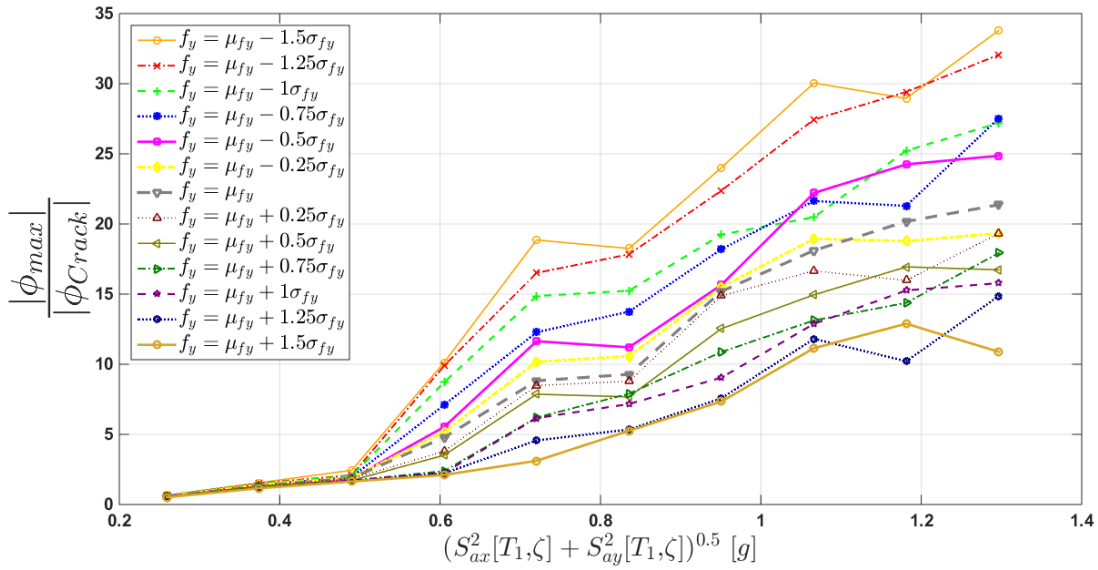


Figure 3.35 : Median demand in terms of cracking limit state vs. Sa for models made from steel of various yield strengths (f_y).

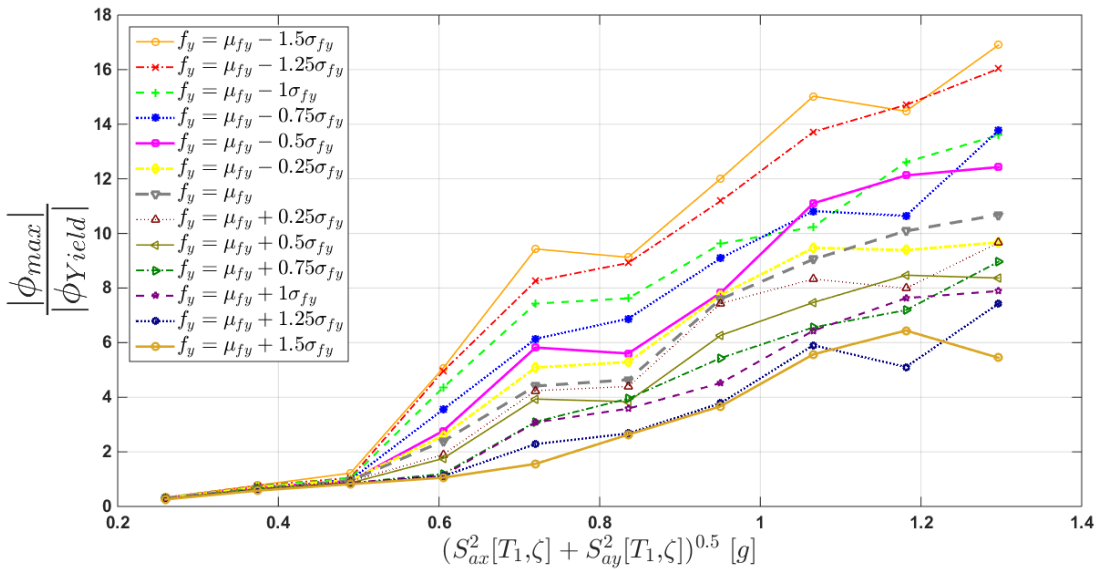


Figure 3.36 : Median demand in terms of yield limit state vs. Sa for models made from steel of various yield strengths (f_y).

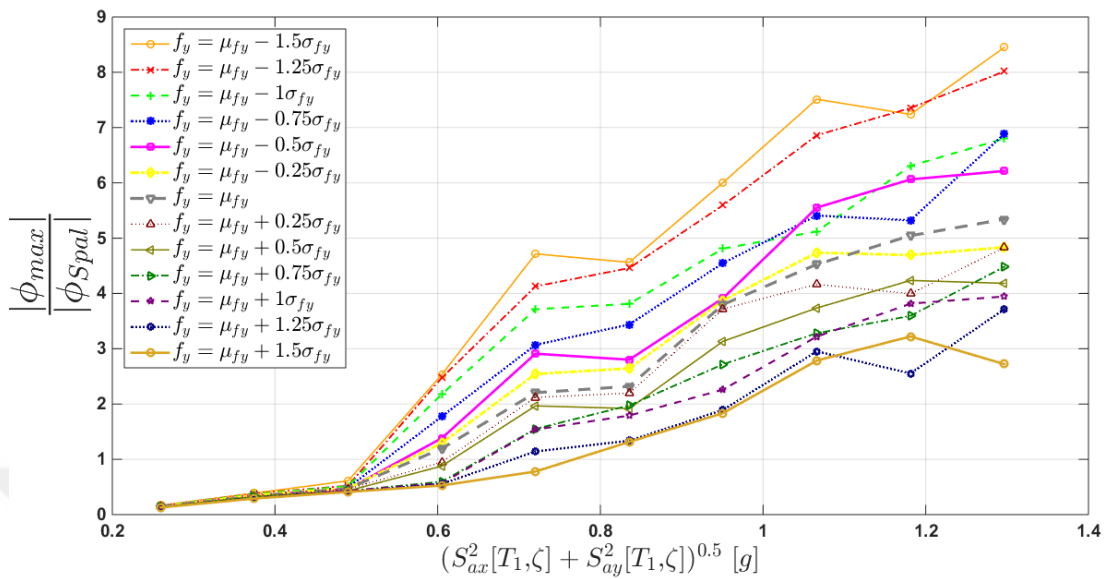


Figure 3.37 : Median demand in terms of spalling limit state vs. S_a for models made from steel of various yield strengths (f_y).

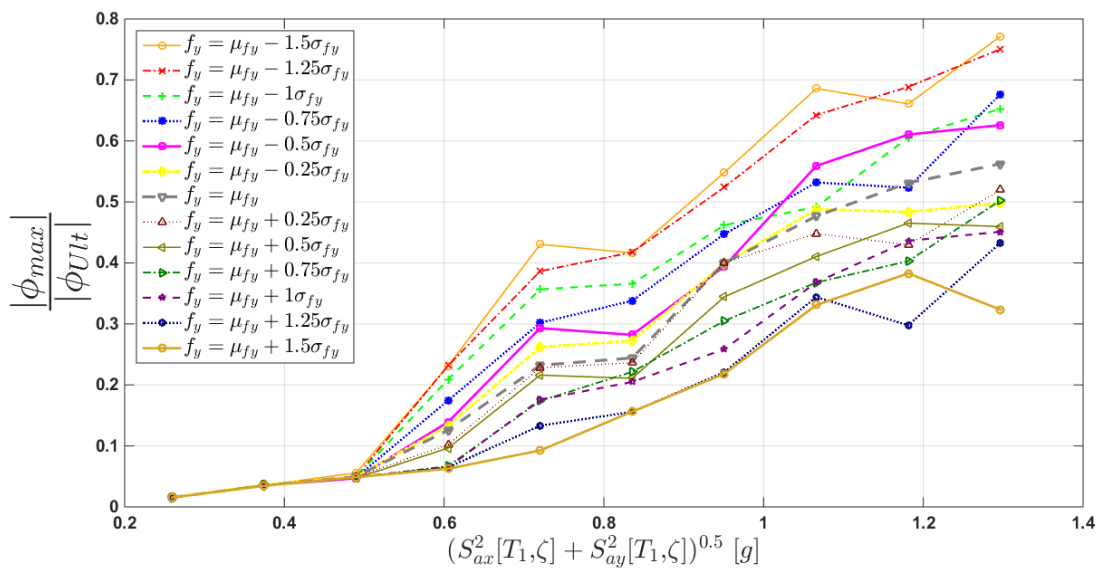


Figure 3.38 : Median demand in terms of ultimate limit state vs. S_a for models made from steel of various yield strengths (f_y).

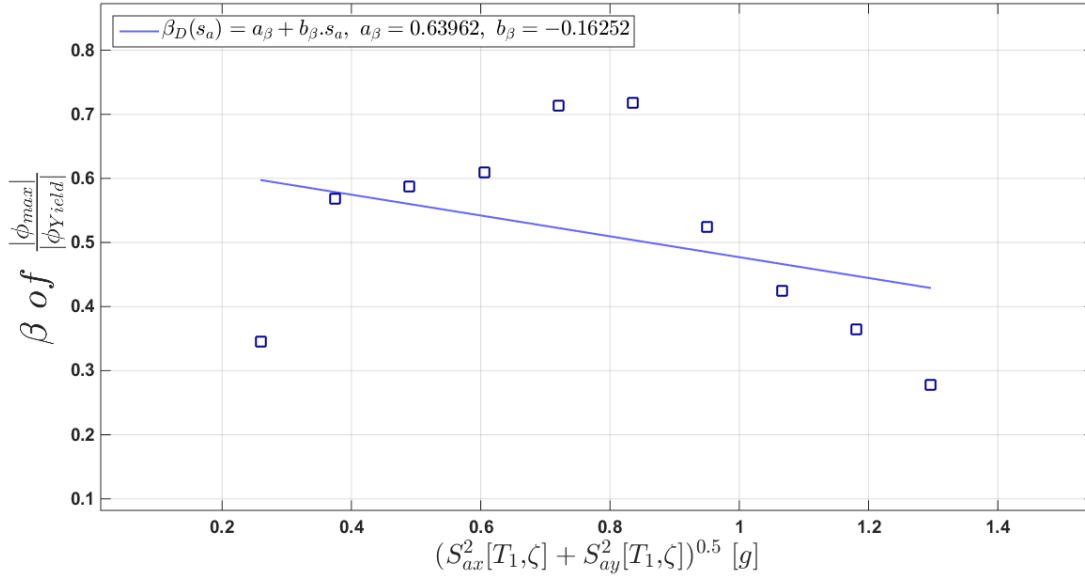


Figure 3.39 : Dispersion of demand in terms of yield curvature limit state vs. S_a and linear approximation ($f'_{co} = \mu_{f'co}$, $f_y = \mu_{fy} - 1.5\sigma_{fy}$).

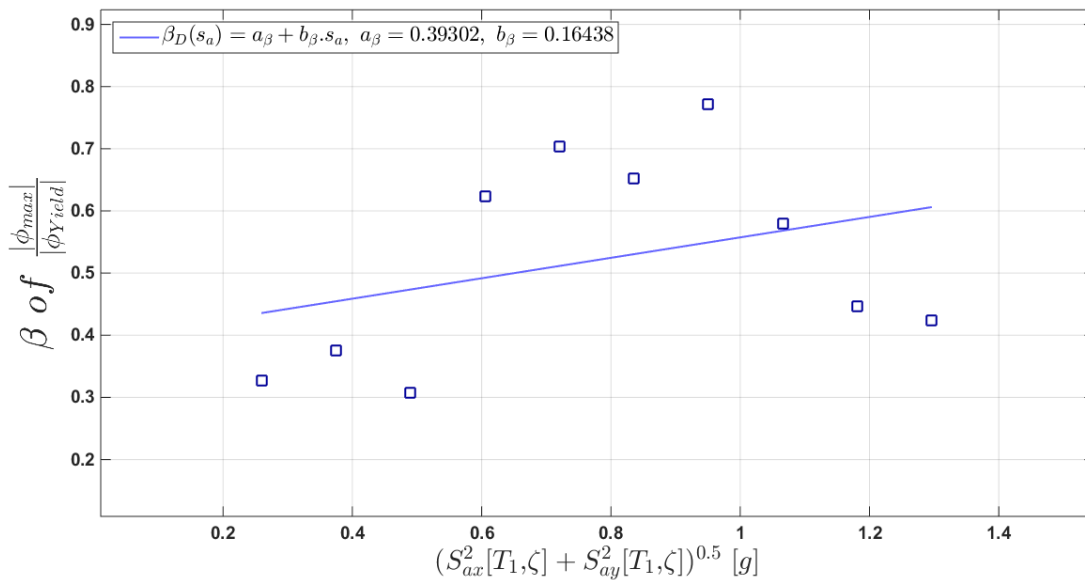


Figure 3.40 : Dispersion of demand in terms of yield curvature limit state vs. S_a and linear approximation ($f'_{co} = \mu_{f'co}$, $f_y = \mu_{fy}$).

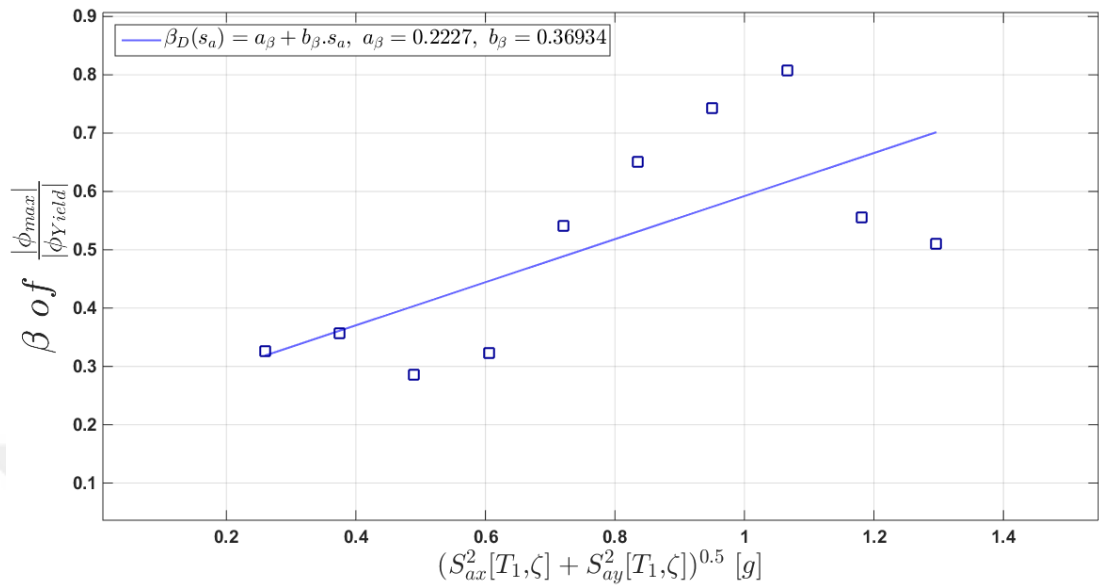


Figure 3.41 : Dispersion of demand in terms of yield curvature limit state vs. Sa and linear approximation ($f'_{co} = \mu_{f'co}$, $f_y = \mu_{fy} + 1.5\sigma_{fy}$).

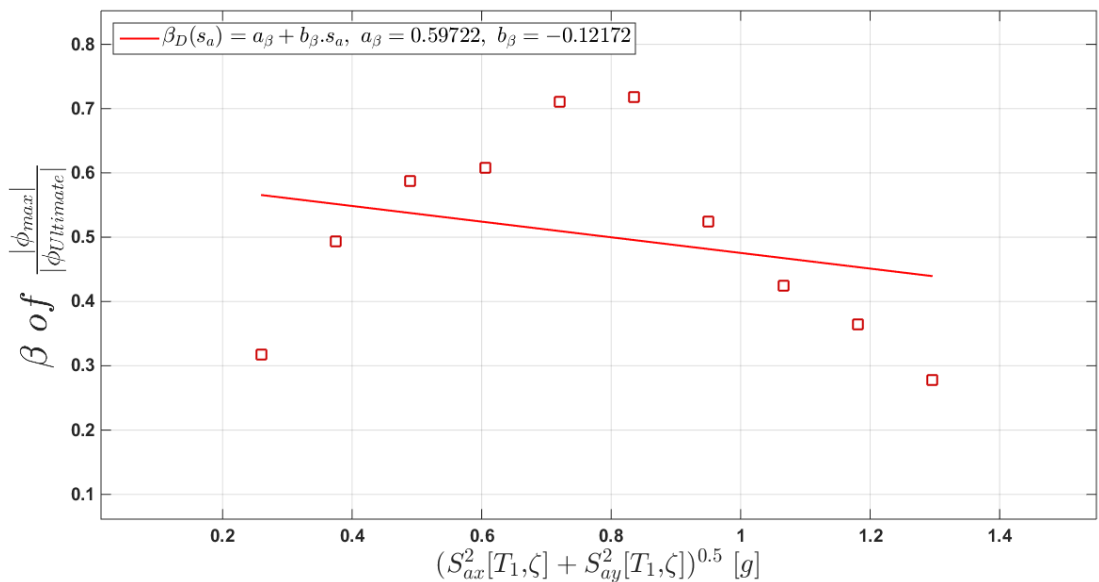


Figure 3.42 : Dispersion of demand in terms of ultimate curvature limit state vs. Sa and linear approximation ($f'_{co} = \mu_{f'co}$, $f_y = \mu_{fy} - 1.5\sigma_{fy}$).

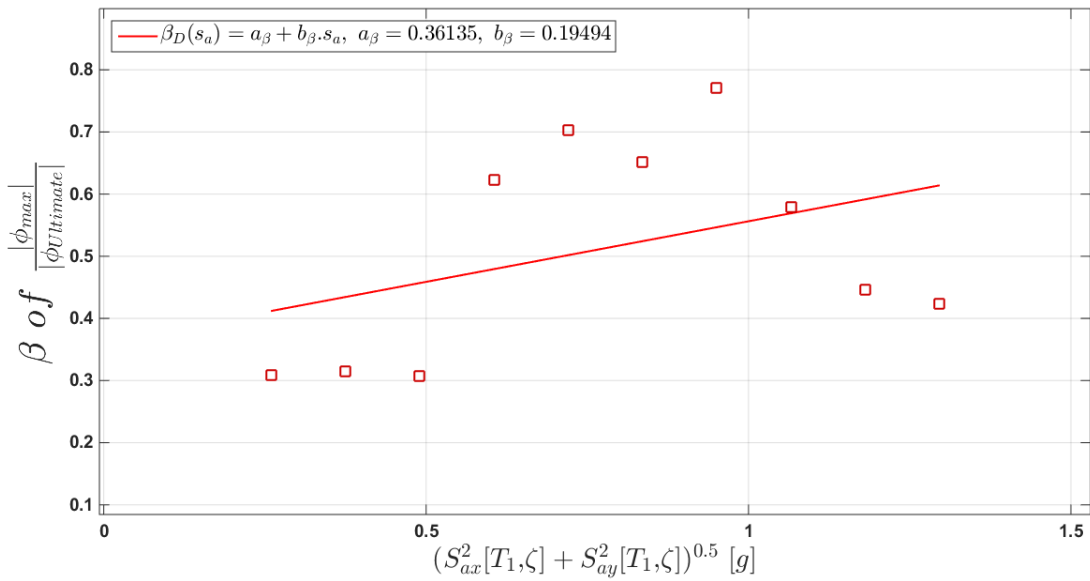


Figure 3.43 : Dispersion of demand in terms of ultimate curvature limit state vs. sa and linear approximation ($f'_{co} = \mu_{f'co}, f_y = \mu_{fy}$).

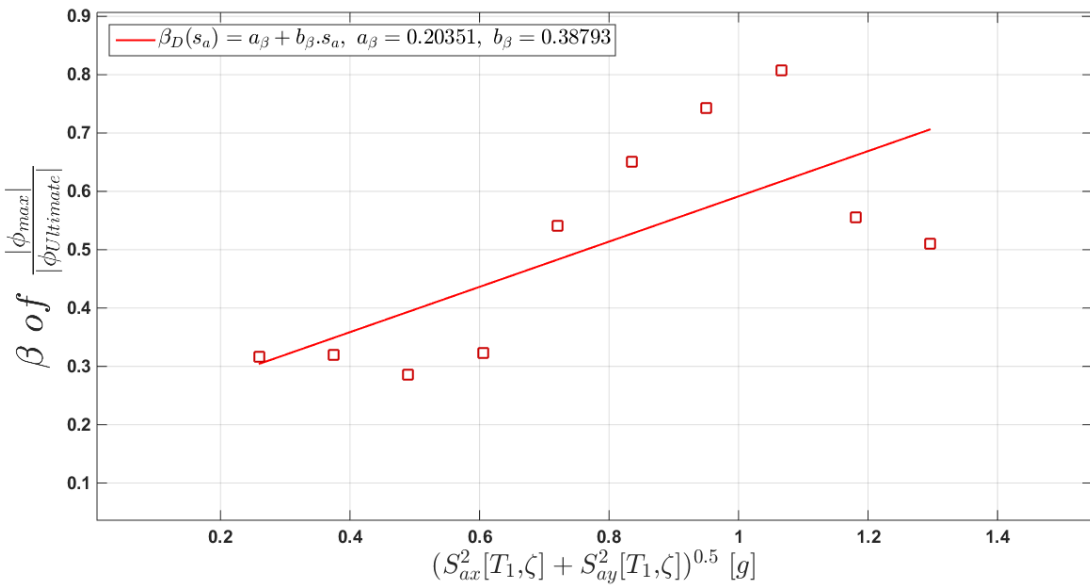


Figure 3.44 : Dispersion of demand in terms of ultimate curvature limit state vs. Sa and linear approximation ($f'_{co} = \mu_{f'co}, f_y = \mu_{fy} + 1.5\sigma_{fy}$).

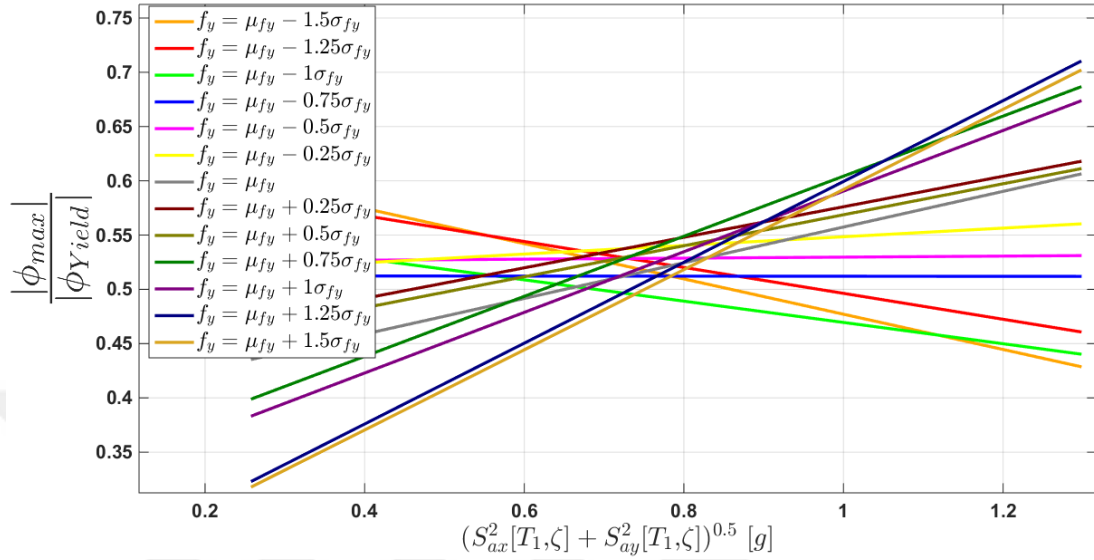


Figure 3.45 : Linear approximation of dispersion of demand in terms of yield curvature limit state vs. Sa curves for models with various steel yield strengths (f_y).

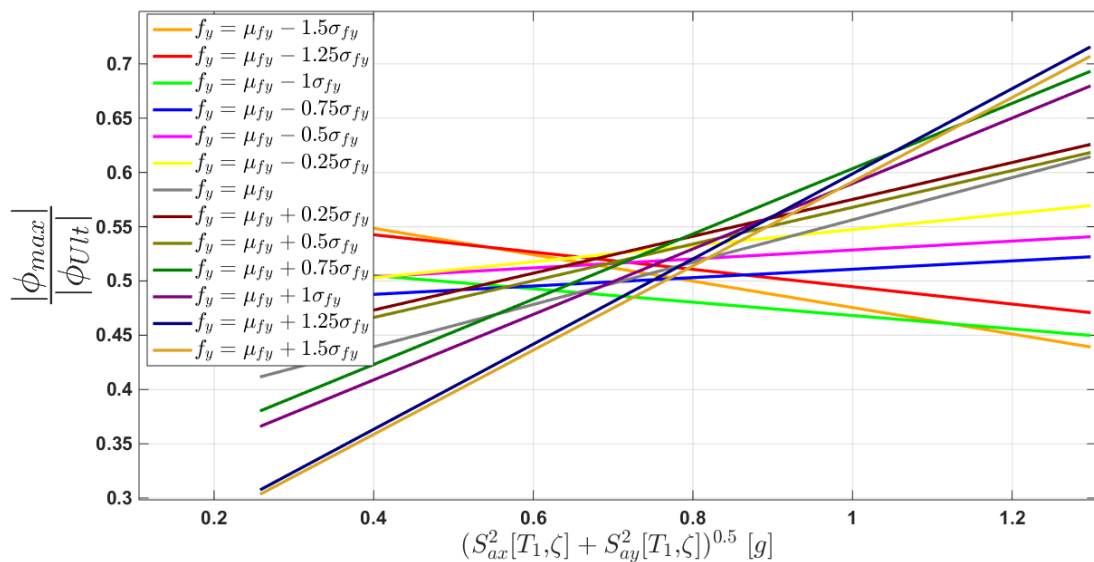


Figure 3.46 : Linear approximation of dispersion of demand in terms of ultimate curvature limit state vs. Sa curves for models with various steel yield strengths (f_y).

Table 3.13 : Changes in constants a and b in terms of different limit states due to variations in steel strength values.

Material Properties	Limit State I ($\frac{\phi_{max}}{\phi_{Cracking}} = 1$)		Limit State II ($\frac{\phi_{max}}{\phi_{Yield}} = 1$)		Limit State III ($\frac{\phi_{max}}{\phi_{Spalling}} = 1$)		Limit State IV ($\frac{\phi_{max}}{\phi_{Ult}} = 1$)	
	a	b	a	b	a	b	a	b
$f_y = \mu_{f_y} - 1.5\sigma_{f_y}$	24.639	2.624	12.319	2.624	6.160	2.624	0.562	2.615
$f_y = \mu_{f_y} - 1.25\sigma_{f_y}$	23.262	2.624	11.631	2.624	5.815	2.624	0.544	2.615
$f_y = \mu_{f_y} - 1.0\sigma_{f_y}$	19.644	2.495	9.822	2.495	4.911	2.495	0.471	2.489
$f_y = \mu_{f_y} - 0.75\sigma_{f_y}$	18.167	2.495	9.083	2.495	4.542	2.495	0.447	2.491
$f_y = \mu_{f_y} - 0.5\sigma_{f_y}$	16.993	2.499	8.496	2.499	4.248	2.499	0.428	2.496
$f_y = \mu_{f_y} - 0.25\sigma_{f_y}$	14.706	2.355	7.353	2.355	3.676	2.355	0.379	2.351
$f_y = \mu_{f_y}$	14.464	2.403	7.232	2.403	3.616	2.403	0.381	2.400
$f_y = \mu_{f_y} + 0.25\sigma_{f_y}$	13.002	2.331	6.501	2.331	3.251	2.331	0.350	2.328
$f_y = \mu_{f_y} + 0.5\sigma_{f_y}$	11.843	2.284	5.921	2.284	2.961	2.284	0.325	2.280
$f_y = \mu_{f_y} + 0.75\sigma_{f_y}$	10.617	2.262	5.309	2.262	2.654	2.261	0.298	2.258
$f_y = \mu_{f_y} + 1.0\sigma_{f_y}$	10.000	2.231	5.000	2.231	2.500	2.231	0.286	2.228
$f_y = \mu_{f_y} + 1.25\sigma_{f_y}$	8.238	2.089	4.119	2.089	2.060	2.089	0.240	2.086
$f_y = \mu_{f_y} + 1.5\sigma_{f_y}$	7.621	2.057	3.810	2.057	1.905	2.057	0.226	2.053

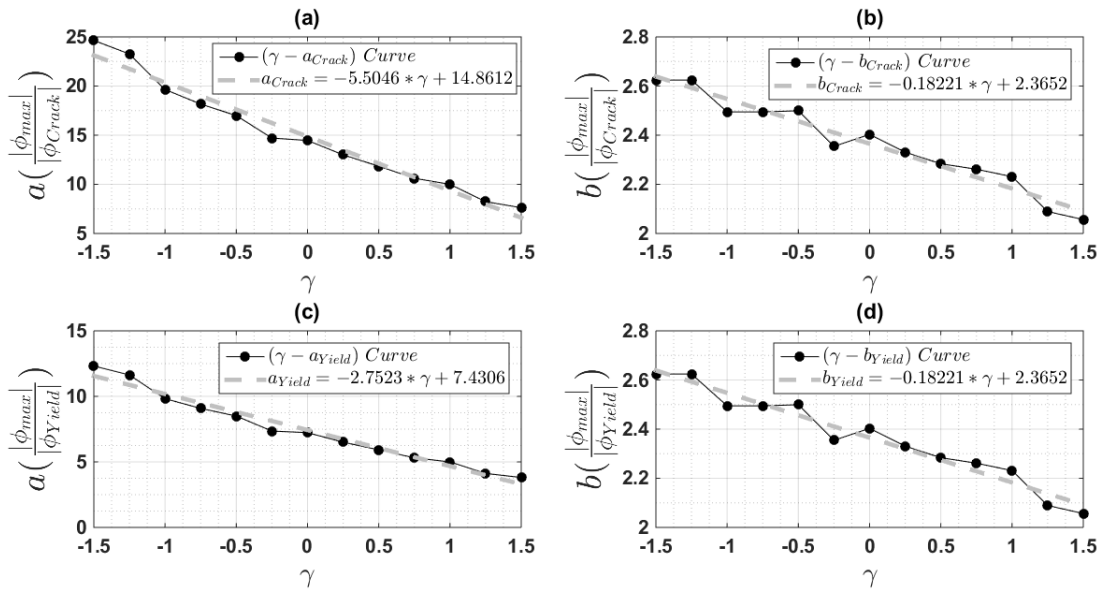


Figure 3.47 : Variations of constants a and b in terms of cracking and yield curvature limit states with γ ($f_y = \mu_{fy} + \gamma\sigma_{fy}$).

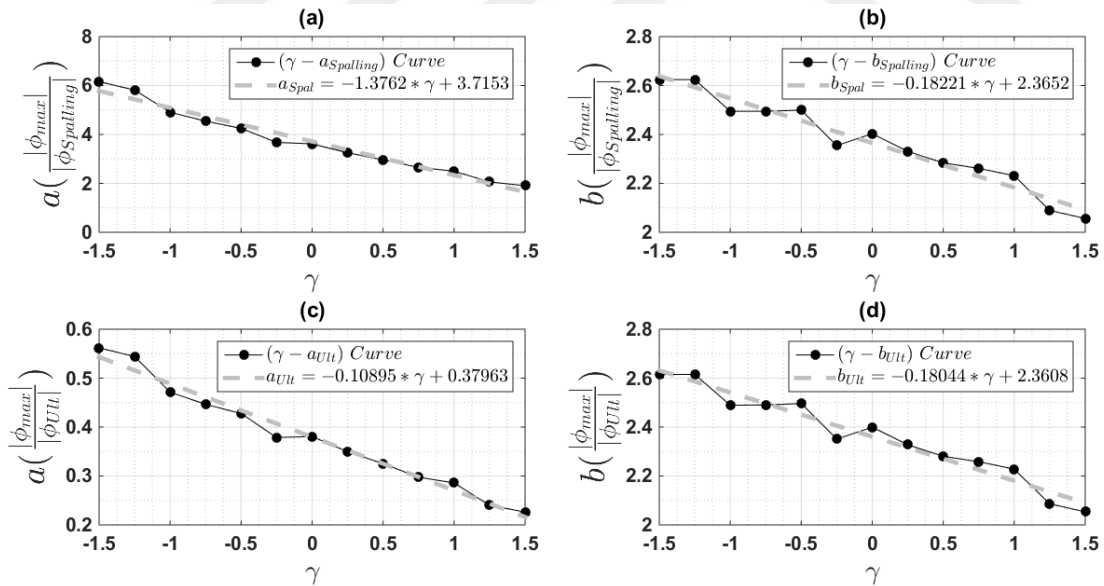


Figure 3.48 : Variations of constants a and b in terms of spalling and ultimate curvature limit states with γ ($f_y = \mu_{fy} + \gamma\sigma_{fy}$).

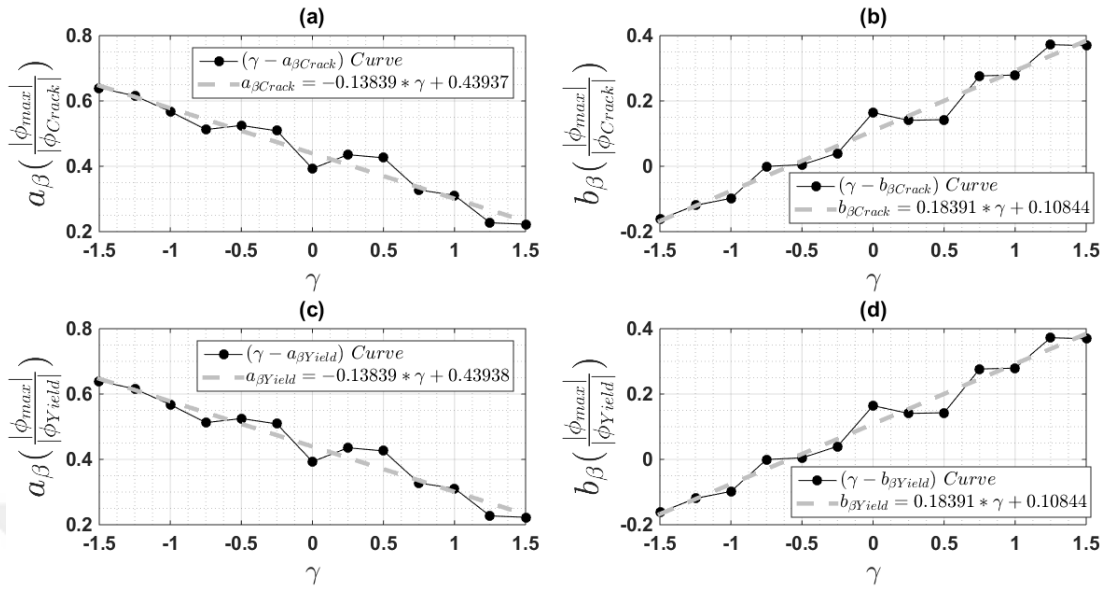


Figure 3.49 : Variations of constants a_β and b_β in terms of cracking and yield curvature limit states with γ ($f_y = \mu_{fy} + \gamma\sigma_{fy}$).

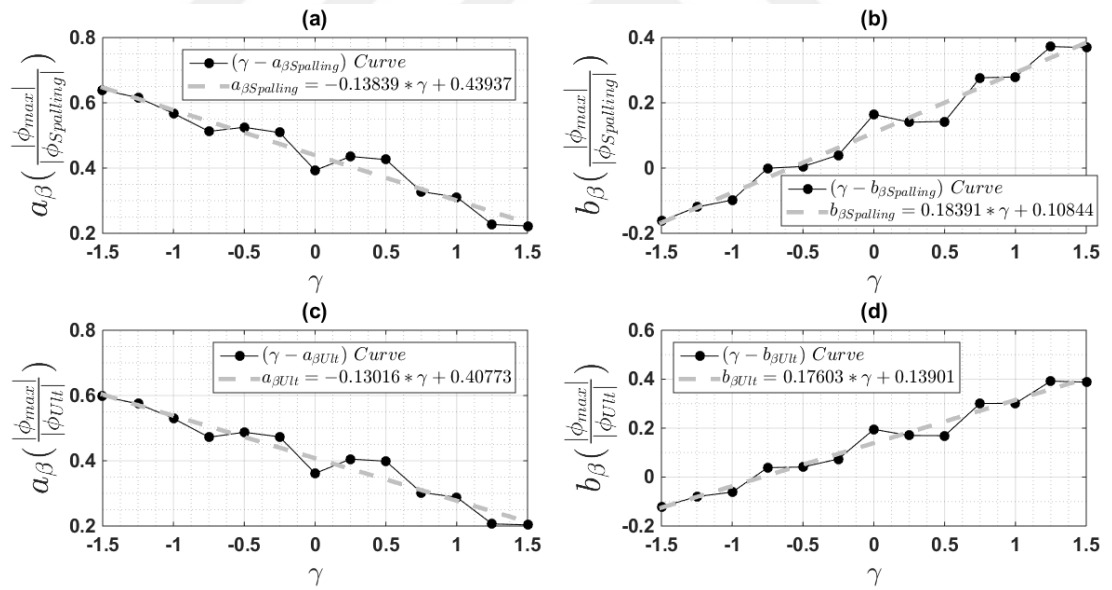


Figure 3.50 : Variations of constants a_β and b_β in terms of spalling and ultimate curvature limit states with γ ($f_y = \mu_{fy} + \gamma\sigma_{fy}$).

3.4.3.2 Failure probabilities in terms of different limit states

Reviewing equations (3.11) and (3.13) which are relations for estimating annual failure probabilities, it is observed that all required parameters have been calculated so far. To be more exact, parameters \hat{C} and β_C have been calculated in Subsection 3.4.3 and parameters β_D , a and b have been calculated in subsection 3.4.3.1 for different limit states. Moreover, parameters k_0 and k which pertain to the power function fitted to the hazard curve according to equation (3.5) have been respectively calculated in Subsection 3.3.3.

In light of discussions made previously and parameters evaluated, annual failure probabilities in terms of the four defined limit states have been calculated for 13 FE models made of varying steel strengths. Calculated results demonstrate variations in annual probabilities of failure with steel yield strength (presented by γ factor) and have been accumulated in Figure 3.51. A straight regression line has also been fitted to each $P_f - \gamma$ curve for providing a better insight into the governing trend. It can be conveniently observed that as a general trend, annual probability of failure drops for stronger structures (those made of stronger reinforcement steel) in an approximately linear manner for all limit states. Table 3.14 reflects also the same information as Figure 3.51 in a tabular format.

Table 3.14 : Annual probabilities of failure in terms of cracking, yield, spalling and ultimate limit states.

Model	Yearly	Yearly	Yearly	Yearly $P_f(\%)$ Ultimate Limit State
	$P_f(\%)$ Cracking Limit State	$P_f(\%)$ Yield Limit State	$P_f(\%)$ Spalling Limit State	
$f_y = \mu_{f_y} - 1.5\sigma_{f_y}$	0.2436	0.1492	0.0928	0.0182
$f_y = \mu_{f_y} - 1.25\sigma_{f_y}$	0.2357	0.1399	0.0882	0.0179
$f_y = \mu_{f_y} - 1.0\sigma_{f_y}$	0.2335	0.1337	0.0812	0.0159
$f_y = \mu_{f_y} - 0.75\sigma_{f_y}$	0.2214	0.1278	0.0743	0.0155
$f_y = \mu_{f_y} - 0.5\sigma_{f_y}$	0.2129	0.1236	0.0696	0.0149
$f_y = \mu_{f_y} - 0.25\sigma_{f_y}$	0.2186	0.1240	0.0685	0.0126
$f_y = \mu_{f_y}$	0.2020	0.1164	0.0654	0.0133
$f_y = \mu_{f_y} + 0.25\sigma_{f_y}$	0.2020	0.1150	0.0640	0.0124
$f_y = \mu_{f_y} + 0.5\sigma_{f_y}$	0.1961	0.1108	0.0612	0.0120
$f_y = \mu_{f_y} + 0.75\sigma_{f_y}$	0.1797	0.1020	0.0568	0.0122
$f_y = \mu_{f_y} + 1.0\sigma_{f_y}$	0.1747	0.0986	0.0546	0.0118
$f_y = \mu_{f_y} + 1.25\sigma_{f_y}$	0.1659	0.0901	0.0484	0.0111
$f_y = \mu_{f_y} + 1.5\sigma_{f_y}$	0.1581	0.0848	0.0449	0.0102

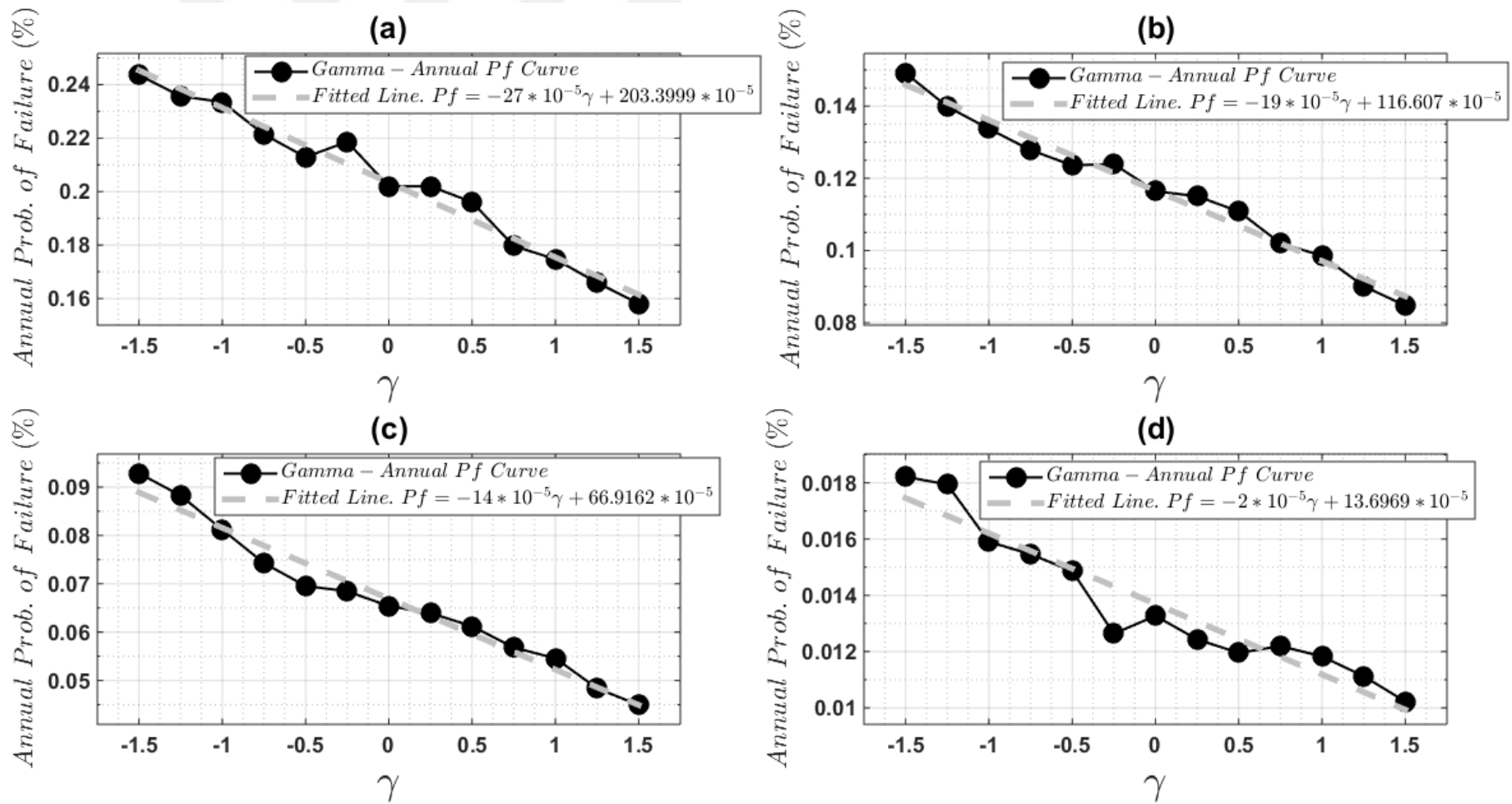


Figure 3.51 : Probability of failure in terms of a) Cracking limit state b) Yield limit state c) Spalling limit state d) Ultimate limit state and the fitted lines for models made of differing steel properties ($f_y = \mu_{fy} + \gamma\sigma_{fy}$).



4. DECISION TREE, COST ESTIMATION AND VALUE OF INFORMATION

4.1 Introduction

In this chapter, a decision tree will be established in Section 4.2 which will help to choose whether or not to retrofit the bridge under study. Additionally, in this section, maximum expected monetary value criterion will be introduced, its application to the problem under study will be presented and probabilities of damage in terms of different damage levels will be formulated. In Section 4.3, Monte Carlo sampling method and its application to the problem will be briefly presented. Section 4.4 discusses non-monitored section of the decision tree. First, an approximate price analysis of the initial construction cost and expenses significant for cost analysis process which include repair, retrofit and indirect costs will be performed in this section. Subsequently, an introduction to retrofitting, evaluation of damage probabilities and expected annual costs of non-monitored structure will be presented.

Section 4.5, is devoted to studying of the monitoring option. First a short description about application of preposterior analysis to the case study problem will be provided in Subsection 4.5.1. Then, the problem will be formulated in Subsection 4.5.2. Monitoring costs will be also discussed in this subsection. Value of information (*VI*) acquired from a system monitoring the fundamental period of structure and value of perfect information (*VPI*) will be studied in Subsection 4.5.3. It will be seen that monitoring is not feasible due to minor variations of the fundamental period with steel properties and need for an extremely sensitive measurement. In Subsection 4.5.4 a field test developed by FHWA for evaluating dynamic specifications of bridge substructures will be introduced. In Subsection 4.5.5, bent system of Elek Deresi Bridge will be analysed and its fundamental period will be estimated. In Subsection 4.5.6, value of information will be assessed assuming that the fundamental period of the bent system is the monitored parameter.

4.2 Decision Tree and Its Structure

A decision tree might be defined as a tool developed for solving general decision problems. A general decision problem could be composed of many alternatives and outcomes. Moreover, additional information might be obtained during the process of decision making or decision makers might be interested in estimating profits and costs of collecting such data to make the best strategy. The decision tree can help decision makers put this probably complicated process into an organised framework.

The decision tree used in this study is exhibited in Figure 4.1. It will be utilised to evaluate value of information obtained from structural health monitoring. The problem is composed of two-stages of decision making. At the first stage a choice is made to whether or not to establish and maintain a structural health monitoring system. If it is chosen not to install an SHM system in the first stage (\bar{a}_m), it will be decided in the second stage if the bridge should be retrofitted. If it is chosen not to retrofit the structure (\bar{a}_r), yield strength of reinforcing steel will control probability of each damage state (branch 1); as it is the uncertainty variable for the FE models constructed in this study. Otherwise if it is chosen to retrofit the structure (a_r), it will be the steel jacketing measure that mostly controls the seismic performance of the bridge; marginalising roll of reinforcing steel properties (branch 2).

In case it is chosen to install an SHM system, additional information provided by it will influence damage probabilities of different damage levels as they will become conditional on this new piece of information. The acquired data from the SHM system might be useful and contribute to choosing between retrofitting and not retrofitting options; nonetheless, installing and maintaining such a system imposes extra costs on the project. Preposterior analysis technique will be used for answering whether or not an SHM system should be established and new information be acquired.

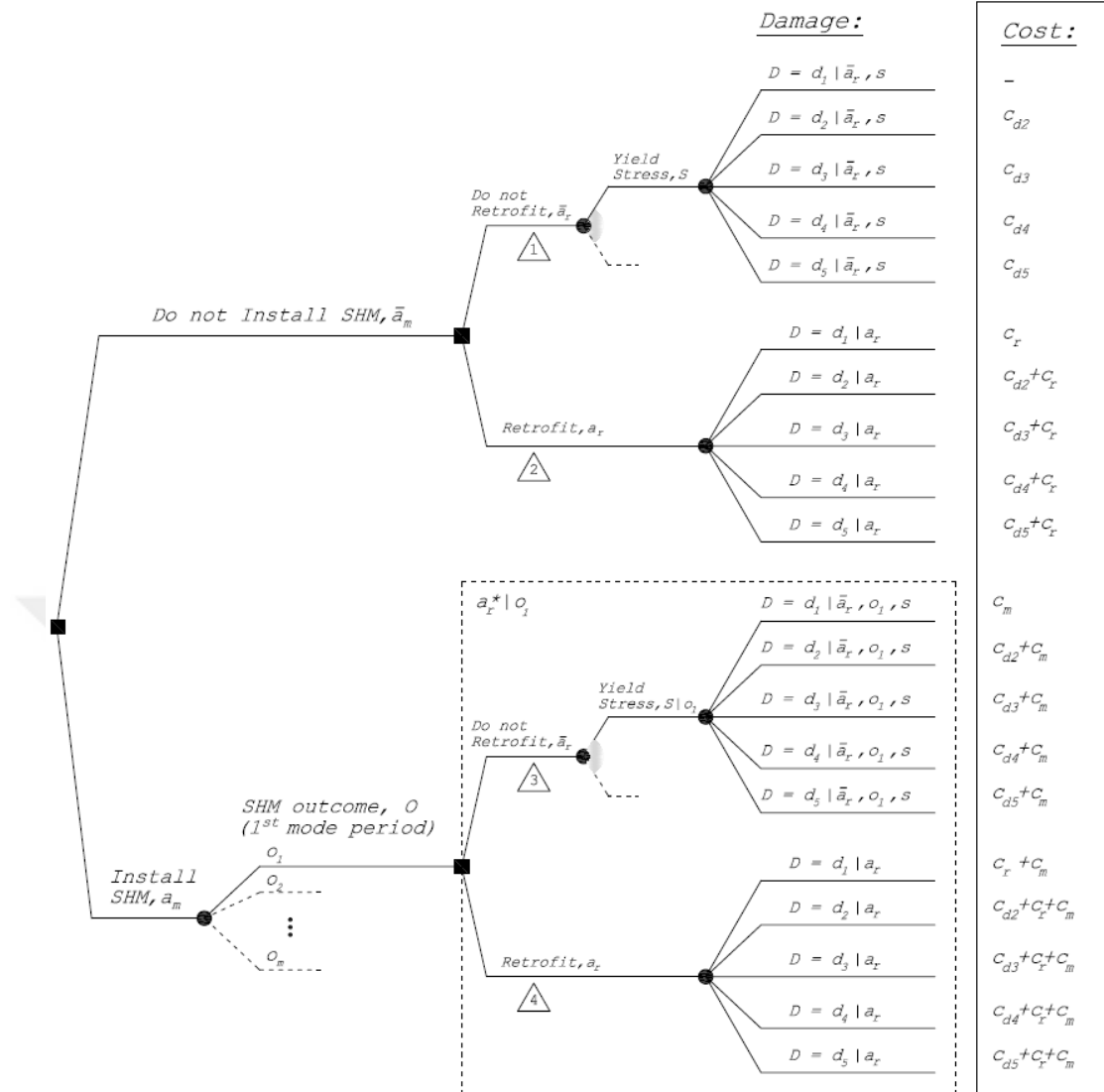


Figure 4.1 : The decision tree.

Considering the options faced in the current problem (establishing or not establishing an SHM system; retrofitting or not retrofitting the structure), there must be a criterion for distinguishing the best choice. Generally the optimal strategy would be the one which results in maximum expected monetary gain or in the case of this study, the minimum expected monetary loss caused by seismic hazard. The maximum monetary gain could be estimated using the Maximum Expected Monetary Value (EMV) Criterion. Following descriptions of EMV Criterion method by Ang and Tang (1984), if c_{dij} is the monetary cost of the j th consequence of alternative i , and p_{ij} is the probability related to this alternative, the expected monetary value of alternative i could be estimated as

$$E(a_i) = \sum_j p_{ij} c_{dij} \quad (4.1)$$

Hence, the optimal alternative would be

$$d(a_{opt}) = \max \sum_j p_{ij} c_{dij} \quad (4.2)$$

It is clear that in equation (4.2) the cost corresponding to the j th consequence of alternative i (c_{dij}), is a negative value. So, $d(a_{opt})$ is the maximum of those negative values or in other words, the minimum of their absolute values. Equation (4.1) can be adjusted for branch 1 of the decision tree exhibited in Figure 4.1 as

$$E[C|\bar{a}_m, \bar{a}_r] = \sum_{j=1}^5 c_{dj} \left(\int p_{D|S} [d_j|\bar{a}_r, s] f_s(s) \right) ds \quad (4.3)$$

In equation (4.3) $p_{D|S} [d_j|\bar{a}_r, s]$ is the annual probability of damage for damage level j given that the structure is not retrofitted and constructed using steel s , identified by its yield strength. Damage probabilities for each of the five previously defined damage levels (no damage, minor damage, moderate damage, major damage and collapse) can be estimated using probabilities of failure for each limit state as follows

$$p_{D|S} [d_j|\bar{a}_r, s] = \begin{cases} 1 - \sum_{j=2}^5 p_{D|S} [d_j|\bar{a}_r, s] & \text{if } j = 1 \\ p_f [ls_{j-1}|\bar{a}_r, s] - \sum_{j+1}^5 p_{D|S} [d_j|\bar{a}_r, s] & \text{if } 2 \leq j \leq 4 \\ p_f [ls_5|\bar{a}_r, s] & \text{if } j = 5 \end{cases} \quad (4.4)$$

Where $p_f [ls_j|\bar{a}_r, s]$ is probability of failure of as-built structure in terms of limit state j . It is reminded that four limit states have been defined corresponding to normalised cracking, yield, spalling and ultimate curvatures. For instance, probability of damage for damage level 3 (moderate damage) can be calculated as:

$$p_{D|S} [d_3|\bar{a}_r, s] = p_f [ls_2|\bar{a}_r, s] - (p_{D|S} [d_4|\bar{a}_r, s] + p_{D|S} [d_5|\bar{a}_r, s])$$

This calculation can also be observed schematically in Figure 4.2.

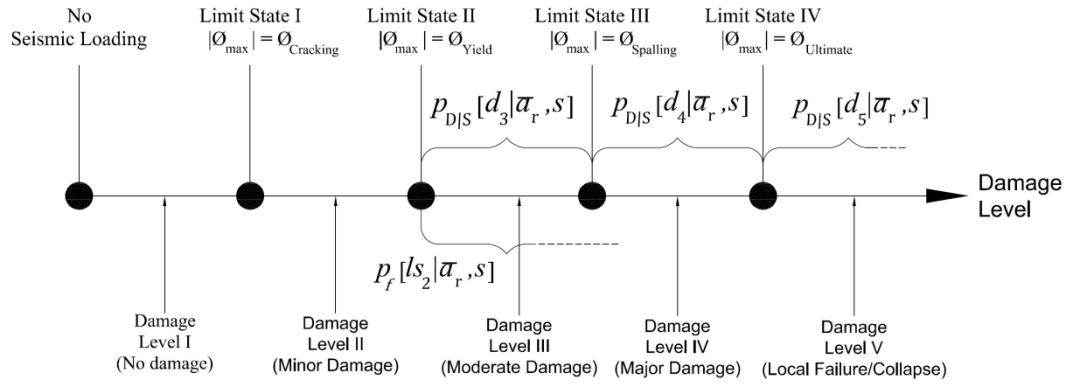


Figure 4.2 : Schematic view for calculating probability of damage level 3.

Failure probabilities in terms of the four limit states were obtained for some steel properties through nonlinear dynamic analyses and the 2000 SAC/FEMA method as described in previous chapter. Moreover, it was shown through Figure 3.51 that relationship between variations of yield strength of reinforcing steel (characterised by factor γ) and failure probabilities in terms of all four limit states could be approximated using a linear regression line. Fitted lines obtained for different limit states may be used for estimating probabilities of failure of as-built structure for a given steel property ($p_f [ls_j | \bar{a}_r, s]$). Afterwards, using equation (4.4), probabilities of damage corresponding to any damage level could be approximated.

By means of the described method for estimating $p_{D|S} [d_j | \bar{a}_r, s]$ and returning once more to equation (4.3), it is observed that the integral appearing in the equation can be approximated by means of numerical methods. This is because the probability distribution of steel which is the second term of the integral has been assumed to be as lognormal with known statistical properties (Table 3.2). The approach used here for solving the integral numerically is the well-known Monte Carlo simulation technique.

4.3 Monte Carlo Simulation Technique and Its Application to the Problem

Monte Carlo simulation is a technique which uses known information (e.g. results from previous tests) to generate new results without need to real physical tests. This method has been examined by many sources in depth; however, a concise introduction provided by Nowak and Collins (2000) is identified to be sufficient for purposes of this study. The "known information" for the case study probabilistic model is probability distribution function of steel (lognormal) and its statistical properties (Table 3.2).

As the first step of Monte Carlo sampling, a set of 1,000 uniformly distributed random numbers between 0 and 1 (u_1, u_2, \dots) was generated (this can be done by many widely available mathematical programmes). As the second step, 1,000 standard normal random numbers (z_1, z_2, \dots) were generated from uniformly distributed random numbers produced in step 1 and using equation (4.5) (Nowak and Collins, 2000).

$$z_i = \Phi^{-1}(u_i) \quad (4.5)$$

In equation (4.5) Φ^{-1} is the inverse of standard normal cumulative distribution function. As the third and final step, a set of 1,000 lognormally distributed samples (s_1, s_2, \dots) was produced using relations between normal and lognormal random variables as can be seen in equations (4.6), (4.7) and (4.8).

$$s_i = \exp[\mu_{lns} + z_i \sigma_{lns}] \quad (4.6)$$

$$\sigma_{lns}^2 = \ln(V_S^2 + 1) \quad (4.7)$$

$$\mu_{lns} = \ln(\mu_S) - \frac{1}{2} \sigma_{lns}^2 \quad (4.8)$$

In equation (4.6), s_i is the yield strength (f_y) of steel sample and μ_S and V_S are respectively mean and coefficient of variation of steel yield stress. It is reminded here that μ_S was estimated as 472.41 MPa and V_S as 0.097. A set of 10 (out of 1,000) uniformly distributed random numbers generated (u_i), corresponding standard normal values (z_i), sample yield strength of steel (s_i) and coefficient γ ($f_y = \mu_{f_y} + \gamma \sigma_{f_y}$) have been demonstrated in Table 4.1.

Returning now to equation (4.3), using the set of steel strength samples, it can be estimated as

$$E[C|\bar{a}_m, \bar{a}_r] \cong \sum_{j=1}^5 c_{dj} \left(\frac{1}{n} \sum_{i=1}^n p_{D|S}[d_j|\bar{a}_r, s_i] \right) \quad (4.9)$$

In equation (4.9), n is number of generated steel samples (e.g. 1,000 in this study as mentioned previously).

Table 4.1 : Sample set of 10 uniformly distributed random numbers, standard normal random values, sample steel strengths and corresponding γ factor.

$0 < u < 1$	z	$s (f_y) (MPa)$	γ
0.610	0.280	483.1	0.234
0.089	-1.347	412.6	-1.302
0.367	-0.340	454.9	-0.381
0.940	1.554	546.7	1.618
0.923	1.424	539.8	1.468
0.261	-0.641	441.9	-0.665
0.265	-0.629	442.4	-0.654
0.780	0.773	506.8	0.749
0.402	-0.248	459.0	-0.292
0.886	1.208	528.6	1.224

4.4 Cost Estimations

Estimating annual expected cost of Elek Deresi Bridge as a result of damages by earthquake hazard and making decisions between possible alternatives (retrofitting or not retrofitting, equipping it with an SHM system or leaving it as it is), requires having an idea about monetary amount of losses related to each damage level. This has been illustrated schematically in the decision tree (Figure 4.1). Costs related to a bridge prone to seismic loadings can be categorised as direct and indirect costs. Direct costs encompass initial cost of construction and cost of repairing a bridge damaged by the hazard. The latter cost increases naturally with severity of the hazard. Indirect costs are related to social and economic side-effects caused by a damaged or failed bridge (e.g. business losses, delays in emergency procedures, etc.). In case the bridge is retrofitted or monitored, related expenses must also enter calculations. In the following, both direct and indirect costs will be estimated and used in the decision making process. Note that all costs are in U.S. dollars. Estimations of monitoring expenses will be performed in Subsection 4.5.2.4.

4.4.1 Initial construction cost

An approximate cost analysis has been performed for estimating initial construction cost of the bridge. For those components that structural details are not available, estimations were performed based on typical drawings, available data for similar bridge components and wherever needed, by engineering judgements. The discussed information voids and resources used to fill them are listed in the below.

- Pile foundation specifications at abutments and bent system:
Each footing has been assumed to be composed of a $2.4\text{ m} \times 12.0\text{ m} \times 1.1\text{ m}$ pile cap and 12.2 m prestressed vertically driven (plumb) pile shafts. Number of piles at each abutment and bent system has been assumed respectively as 12 and 18 and their sectional dimensions as $460\text{ mm} \times 460\text{ mm}$ (18" square piles). Approximate length and sectional dimensions of piles have been obtained from a research by Wang et al (2014). Pile cap width and thickness have been obtained from a research by Padgett et al (2010). In both studies, bridge component dimensions used by the authors are based on statistical data for bridges in the U.S. roadways. Pile cap length has been approximated considering spacing between columns and with the assumption that a single pile cap is carrying all three columns. The discussed assumptions have been illustrated via drawings in APPENDIX A.
- Approximate values for seat abutment dimensions and reinforcement have been obtained from typical drawings and design directions provided by NDOT¹² (2008). Details for wingwalls have been approximated from standard plans provided by California Department of Transportation (Caltrans)¹³. Assumed dimensions for abutments and wingwalls have been exhibited in APPENDIX A.
- Estimated dimensions ($13.7\text{ m} \times 7.5\text{ m} \times 0.45\text{ m}$) and reinforcing for approach slabs have been obtained from directions by the Federal Highway Administration (FHWA).
- A price analysis list provided by Florida Department of Transportation (FDOT, 2018) has been utilised for cost estimation of the bridge. This list has the advantage of providing rough values for some missing data (e.g. approximate amount of superstructure reinforcement). Table 4.2 demonstrates considered items and prices for the year 2018 in a concise format utilising the mentioned price list.

¹² Nevada Department of Transportation

¹³ 2015 STANDARD PLAN D84

Table 4.2 : Cost estimation list of the bridge.

Item No.			Cost per Lin. Foot	Quantity	Price
1	Piling	18" w/Carbon Steel Strands (Driven Plumb)	\$90	2,041.3	\$183,720
			Cost per Cubic Yard	Quantity	Price
2	Substructure Concrete	Concrete	\$850	268.4	\$228,109
			Cost per Pound	Quantity	Price
3	Substructure Reinforcing Steel	Carbon Reinforcing Steel	\$0.90	41,106.8	\$36,996
			Cost per Cubic Foot	Quantity	Price
4	Neoprene Bearing Pads	Composite Neoprene Bearing Pads	\$1,560	19.8	\$30,851
			Cost per Lin. Foot	Quantity	Price
5	Prestressed Concrete Girders	I Beam	\$190	1,060.4	\$201,470
			Cost per Cubic Yard	Quantity	Price
6	Cast-in-Place Superstructure Concrete	Deck Concrete	\$700	180.4	\$126,261
			Cost per Pound	Quantity	Price
7	Superstructure Reinforcing Steel	Carbon Reinforcing Steel	\$0.95	36,976	\$35,128
			Cost per Lin. Foot	Quantity	Price
8	Traffic Railings	Thrie Beam Retrofit	\$180	265	\$47,717
			Cost per Lin. Foot	Quantity	Price
9	Expansion Joints	Strip Seal (at span ends)	\$250	89.9	\$22,474
10		Finger Joint <6" (at bent system)	\$850	45	\$38,205
			Cost per Unit	Quantity	Price
11	Approach Slabs	Cast-in-Place Concrete (per Sq. Yard)	\$400	245.8	\$98,310
12		Reinforcing Steel (per Pound)	\$0.95	23,910	\$22,713
				Total Cost	\$1,071,954
				Cost/sqft	\$179

Using assumptions discussed briefly in the above, initial construction cost of the case study bridge has been estimated to be about \$1,072,000 regarding the year 2018 prices. As the bridge deck is 13.7m (45 foot) in width and 40.6m (133.2 foot) in length, approximate cost per square foot for the bridge is about \$179. However, as it can be understood from Table 4.2, some items such as bridge drainage system, asphalt pavement, etc. have not been taken into account in the price estimation process. Hence, to care for all missing items, an approximate net price of \$200 per square foot (\$1,120,000 total cost) could be a reasonable estimate of the initial construction cost for purposes of this study. This price could be controlled using data by Caltrans which provides a comparative cost list for different types of bridges. For precast/prestressed concrete I girder roadway bridges (PC/PS I girder bridge type) with span length of 50 to 120 foot (15.25-36.6m)¹, reported price by Caltrans for January 2017 varies from \$160 to \$440 per square foot.

4.4.2 Repair costs for different damage states

Padgett et al. (Padgett et al, 2010) have quoted results of a study by Basoz and Mander which could be used for estimating costs of repair pertaining to different damage states (Table 4.3). Ratios seen in Table 4.3 are based on regional construction costs and will be used for approximating expected annual cost of the case study bridge by applying them to the initial construction cost estimated in Subsection 4.4.1.

Table 4.3 : Repair cost ratios provided by Basoz and Mander - excerpted from (Padgett et al, 2010).

Damage State	Best Mean Repair Cost Ratio
Slight	0.03
Moderate	0.08
Extensive	0.25
Complete	1.0 (if $n^* < 3$)
	2.0/n (if $n \geq 3$)

*n = Number of spans

¹ Span length of Elek Deresi Bridge is 20.2m

4.4.3 Retrofitting and resultant costs

4.4.3.1 Retrofitting

If a structure is distinguished as weak due to material, construction or design deficiencies or modifications in design codes and standards, the need for its retrofitting might arise. There is a great number of retrofitting measures that address several components of bridges. Bridge substructure (columns, bent cap beam, abutments and foundations) might be subjected to strengthening as well as the superstructure; e.g. by installing devices for preventing unseating, etc. (fib, 2007). Studying these techniques is out of scope of this research. This section is intended to only provide a basis for retrofitting branches of the decision tree which is discussed in Figure 4.1.

As discussed in Subsection 3.2.2, in the case of the bridge under study, it is almost always the bent cap beam that becomes critical under seismic loadings; i.e. reaches its ultimate bending curvature. Hence, strengthening the cap beam might seem to be the best strategy in the first place. However, it should be noted that retrofitting the cap beam is generally difficult and costly (fib, 2007), (Itani and Liao, 2003). On the other hand, a study by Padgett et al. (2009) shows that steel jacketing of columns of MSSS concrete bridges is particularly effective in reducing probability of moderate or severe damages caused by seismic loadings. The latter strategy might look encouraging considering that strengthening bridge columns is a common and straightforward retrofitting scheme. Consequently, in this subsection, a brief introduction to steel jacketing and related expenses will be provided. Further discussions about the procedure for calculations of failure and damage probabilities and expected costs of the jacketed bridge by seismic loading will be continued in Subsection 4.4.7.

4.4.3.2 Steel jacketing for columns and related expenses

There are many techniques available for retrofitting RC bridge columns; e.g. reinforced concrete jacketing, implementing composite material jackets, precast concrete segment jackets, etc. Among these techniques, steel jacketing (Figure 4.3) has been one of the most popular column retrofitting schemes in recent years (fib, 2007). There are also plenty of scholarly documents studying behaviour of columns retrofitted by this technique. Steel jacketing enhances column ductility as well as its shear and flexural capacities. It can be implemented both for rectangular and circular columns.

Steel jacketing improves column performance in a manner comparable to transverse reinforcing. In other words, it provides core concrete with extra confinement and increases ultimate compressive strength and strain capacity of the member.

The technique for implementing steel jackets has differences for circular and rectangular columns. For circular columns, a cylindrical steel casing is fabricated about the column which has been distinguished to be in danger of premature failure. Size of the steel casing is considered slightly larger than that of the column. After the casing is welded in the construction site, the gap between gets filled with a cement based grout (Figure 4.3b and Figure 4.3c). Generally jacket is terminated above the footing and below the cap beam with a gap of 50 – 100 mm in order to avoid additional strength enhancement of plastic hinges that can be transferred to cap beam or footing (fib, 2007) (Figure 4.3a). For rectangular columns, steel jacketing has been known as being less effective compared to circular columns. This is because confinement of rectangular sections becomes less efficient as column dimensions grow. Yet, steel jacketing can improve performance of rectangular columns considerably using techniques such as Elliptical retrofitting (Figure 4.3c), Built-up steel channels, Stiffened rectangular jacketing and other more recent innovative methods (fib, 2007).

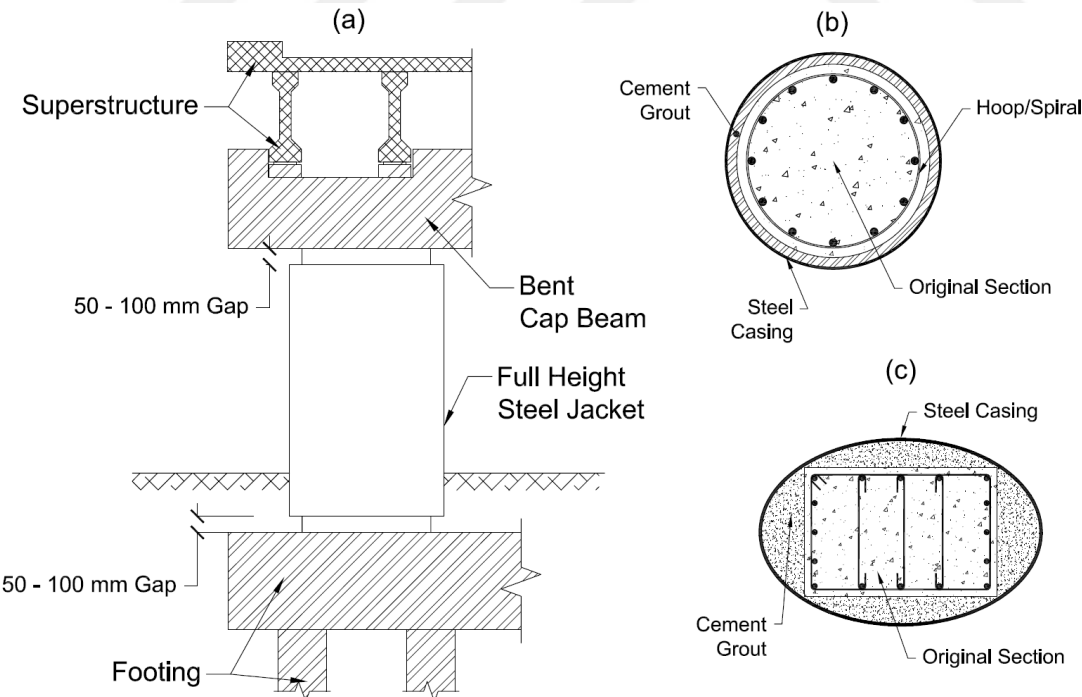


Figure 4.3 : a) Retrofitted bridge column by full height steel jacketing technique b) Circular steel jacketing of a circular column c) Elliptical steel jacketing of a rectangular column.

Costs related to steel jacketing have been obtained from a study by Padgett et al. (2010) which is reported to be about \$6,000 per column. Nonetheless, as the mentioned price relates to the year 2010, it has been adjusted for the year 2018 using inflation rates for construction of non-residential buildings; which differs from inflation rates by Consumer Price Index (CPI). Annual inflation rates for construction of non-residential buildings have been obtained from Turner Actual Cost Index¹. Using values for rates of inflation presented in Table 4.4, cost of steel jacketing has been approximated as \$7,460 for each column for year 2018 (\$22,380 in total for three columns of Elek Deresi Bridge).

Table 4.4 : Inflation rates for construction of non-residential buildings (excerpted from Turner Actual Cost Index).

Year	Inflation Rate (%)
2010	-4.0%
2011	1.6%
2012	2.1%
2013	4.1%
2014	4.4%
2015	4.5%
2016	4.7%
2017	5.0%

4.4.4 Indirect costs

Losses by damages to bridges are not limited to repair or reconstruction costs. Indirect costs caused by increased travel time and accident probabilities, interruptions of economic activities, etc. might be much greater than direct losses. Padgett et al. (2010) have cited results of a research by Applied Technology Council (ATC) indicating that costs caused by travel prolongations are 5-20 times greater than direct losses. They have also used an average value of 13 times direct losses in their study to account for indirect losses. Following their work, all damage costs will be multiplied by a factor of 13 for taking the indirect costs into consideration.

4.4.5 Annual and life-time failure and damage probabilities in terms of different limit states and damage levels for the as-built structure

In order to make use of equation (4.9) and calculate expected cost of the as-built bridge (branch 1 of the decision tree), it is necessary to calculate probabilities of failure in

¹ <http://www.turnerconstruction.com/>

terms of different limit states and probabilities of damage in the course of different damage levels. Annual probabilities of failure in terms of cracking, yielding, spalling and ultimate limit states are shown in Table 4.5 for a set of 10 steel samples. It is seen that Table 4.5 also demonstrates annual damage probabilities in the course of different damage levels (no damage, minor damage, moderate damage, major damage and collapse). These probabilities have been calculated using the discussed failure probabilities employing equation (4.4).

Table 4.5 : Annual probabilities of failure in terms of different limit states and damage probabilities in terms of various damage levels.

s (f_y) (MPa)	$P_f (ls_1 \bar{a}_{rr}, s)$ %	$P_f (ls_2 \bar{a}_{rr}, s)$ %	$P_f (ls_3 \bar{a}_{rr}, s)$ %	$P_f (ls_4 \bar{a}_{rr}, s)$ %	$P_D (d_1 \bar{a}_{rr}, s)$ %	$P_D (d_2 \bar{a}_{rr}, s)$ %	$P_D (d_3 \bar{a}_{rr}, s)$ %	$P_D (d_4 \bar{a}_{rr}, s)$ %	$P_D (d_5 \bar{a}_{rr}, s)$ %
483.1	0.1969	0.1120	0.0635	0.0131	99.803	0.085	0.049	0.050	0.013
412.6	0.2398	0.1420	0.0860	0.0170	99.760	0.098	0.056	0.069	0.017
454.9	0.2140	0.1240	0.0725	0.0147	99.786	0.090	0.052	0.058	0.015
546.7	0.1582	0.0850	0.0432	0.0096	99.842	0.073	0.042	0.034	0.010
539.8	0.1623	0.0880	0.0454	0.0100	99.838	0.074	0.043	0.035	0.010
441.9	0.2220	0.1296	0.0767	0.0154	99.778	0.092	0.053	0.061	0.015
442.4	0.2217	0.1294	0.0765	0.0153	99.778	0.092	0.053	0.061	0.015
506.8	0.1825	0.1020	0.0559	0.0118	99.818	0.080	0.046	0.044	0.012
459.0	0.2116	0.1223	0.0712	0.0144	99.788	0.089	0.051	0.057	0.014
528.6	0.1692	0.0927	0.0490	0.0106	99.831	0.076	0.044	0.038	0.011

As it is aimed to make a comparison between expected costs of retrofitting and as-built options, it is necessary to calculate damage probabilities in the course of expected service period of the structure. For this purpose, probabilities of failure in terms of each limit state have been calculated for 50 years; which is the remaining life-time considered by Padgett and Ghosh (2010) for their studies. This implies that the bridge will give service for the next 50 years and in the moment of earthquake hazard its structural condition will be identical to those used for constructing the relevant FE model.

Calculation of failure probabilities for n years can be performed by the assumption of independence of earthquake events. So, if the probability of failure in terms of a certain limit state in 1 year is equal to P_f , the probability that failure does not occur would be $1 - P_f$. The probability of no failure in n years would naturally be $(1 - P_f)^n$ and finally the probability of failure in n years can be estimated as $1 - (1 - P_f)^n$. Consequences of calculation of failure probabilities by the described method in the course of 50 years

along with relevant damage probabilities have been summarised in Table 4.6 for the set of 10 steel samples of Table 4.5.

Table 4.6 : Life-time probabilities of failure in terms of different limit states and damage probabilities in terms of various damage levels.

s (f_y) (MPa)	P_f ($ls_1 \bar{a}_{rr}, s$) %	P_f ($ls_2 \bar{a}_{rr}, s$) %	P_f ($ls_3 \bar{a}_{rr}, s$) %	P_f ($ls_4 \bar{a}_{rr}, s$) %	P_D ($d_1 \bar{a}_{rr}, s$) %	P_D ($d_2 \bar{a}_{rr}, s$) %	P_D ($d_3 \bar{a}_{rr}, s$) %	P_D ($d_4 \bar{a}_{rr}, s$) %	P_D ($d_5 \bar{a}_{rr}, s$) %
483.1	9.383	5.451	3.126	0.653	90.62	3.93	2.33	2.47	0.65
412.6	11.313	6.859	4.210	0.845	88.69	4.45	2.65	3.37	0.84
454.9	10.160	6.017	3.561	0.730	89.84	4.14	2.46	2.83	0.73
546.7	7.610	4.165	2.138	0.481	92.39	3.44	2.03	1.66	0.48
539.8	7.802	4.305	2.245	0.499	92.20	3.50	2.06	1.75	0.50
441.9	10.517	6.278	3.762	0.765	89.48	4.24	2.52	3.00	0.77
442.4	10.504	6.268	3.754	0.764	89.50	4.24	2.51	2.99	0.76
506.8	8.726	4.974	2.759	0.589	91.27	3.75	2.22	2.17	0.59
459.0	10.048	5.935	3.498	0.719	89.95	4.11	2.44	2.78	0.72
528.6	8.117	4.532	2.420	0.530	91.88	3.58	2.11	1.89	0.54

4.4.6 Annual and life-time failure and damage probabilities in terms of different limit states and damage levels for the retrofitted structure

For an exact estimation of failure and damage probabilities of the retrofitted case, a separate FE model should be constructed for the steel jacketed bridge. Afterwards, the desired probabilities can be calculated by a procedure similar to the one used for the as-built structure. However, this procedure will be shortened in this study using consequences of a research by Padgett and DesRoches (2009). To be more exact, failure probabilities in terms of different limit states will be estimated utilising modification factors introduced in the mentioned study. This approach might be more approximate but, it has the benefit of being convenient and quick to use.

Padgett and DesRoches (2009) have developed fragility curves for four common bridge types (including MSSS concrete bridge class) located in the Central and Southern United States and retrofitted with different techniques including steel jacketing. They have also proposed modification factors which can be applied to the fragility curve of an as-built bridge to obtain fragility curve of the retrofitted structure. In other words, these factors show shifts in fragility curve of the original structure as a result of retrofitting. The mentioned factors vary for different bridge types and retrofitting techniques. Here, only values regarding steel jacketed MSSS concrete bridges are quoted (Table 4.7).

Table 4.7 : Modification factors for steel jacketed MSSS concrete bridges, excerpted from (Padgett and DesRoches, 2009).

	Slight Damage	Medium Damage	Extensive Damage	Complete Damage
Modification Factor (M.F.)	1.05	1.30	1.33	1.41

In this study, factors presented in Table 4.7 are applied to the regression lines fitted to median demand - S_a curves of the FE model made from reinforcing bars with yield strength equal to steel mean yield stress ($f_y = \mu_{f_y} = 472.41 \text{ MPa}$). Afterwards, using resultant shifted demand - S_a curves and relevant a and b constants, annual and life-time failure probabilities in terms of each limit state and annual and life-time damage probabilities in the course of each damage level are calculated. It is assumed that slight, medium, extensive and complete damage levels seen in Table 4.7 are respectively equivalent to Damage Level II, III, IV and V defined in the current study.

Figure 4.4, Figure 4.5, Figure 4.6 and Figure 4.7 exhibit regression lines ($\hat{D} = aS_a^b$) for three of the FE models studied previously and those for the retrofitted structure. As described, regression lines for steel jacketed bridge have been developed using modification factors of Table 4.7. Constant a_{RF} (constant a of regression line of the retrofitted structure) is obtained for each limit state by dividing constant a for the FE model of that limit state by relative modification factor from Table 4.7 ($a_{RF} = a_{(f_y=\mu_{f_y})}/M.F.$). Constant b for the retrofitted structure (b_{RF}) is equal to constant b of the as-built model made of steel with mean yield stress ($b_{RF} = b_{(f_y=\mu_{f_y})}$). It is observed from Figure 4.4 that the regression line related to cracking curvature limit state is diverted only slightly from the original curve. This is due to the small modification factor for slight damage as can be seen in Table 4.7. As a matter of fact, according to findings of Padgett and DesRoches (2009), steel jacketing has only minor impact in case of slight damages. However, due to the mentioned research, for medium and greater damage levels effect of steel jacketing increases as can be understood from modification factors of Table 4.7 and Figure 4.5, Figure 4.6 and Figure 4.7.

In order to estimate failure probabilities using the 2000 SAC/FEMA method, demand dispersion must be also known in addition to a_{RF} and b_{RF} constants. According to Padgett et al. (2010), effect of retrofitting in terms of altering demand dispersion can be considered as minor. Hence, the same values obtained for dispersion of demand - S_a for

the FE model reinforced with steel of mean yield stress were used for calculations of annual failure probabilities. Annual failure probabilities by the described procedure and resultant life-time failure probabilities have been presented in Table 4.8. Annual and life-time damage probabilities calculated using failure probabilities are demonstrated in Table 4.9.

Table 4.8 : Annual and life-time failure probabilities of retrofitted structure in terms of different limit states.

	Cracking Curvature L.S. ² (%)	Yield Curvature L.S. (%)	Spalling Curvature L.S. (%)	Ultimate Curvature L.S. (%)
Annual P_f	0.1951	0.0964	0.0542	0.0104
Life-time (50 Year) P_f	9.305	4.706	2.675	0.518

Table 4.9 : Annual and life-time damage probabilities of retrofitted structure in terms of different damage levels.

	Annual (%)	Life-time (50 years) (%)
$P_D (d_1 a_r)$ %	99.8049	90.695
$P_D (d_2 a_r)$ %	0.0988	4.599
$P_D (d_3 a_r)$ %	0.0422	2.031
$P_D (d_4 a_r)$ %	0.0438	2.157
$P_D (d_5 a_r)$ %	0.0104	0.518

² Limit State

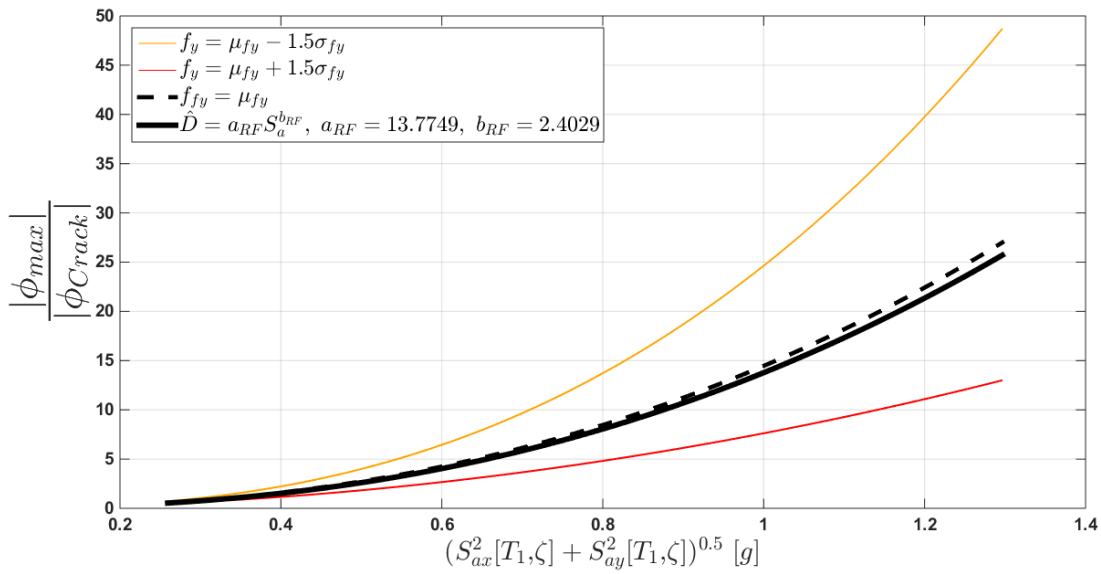


Figure 4.4 : Regression lines for FE models made from three differing steel strengths and steel jacketed model in terms of cracking curvature limit state.

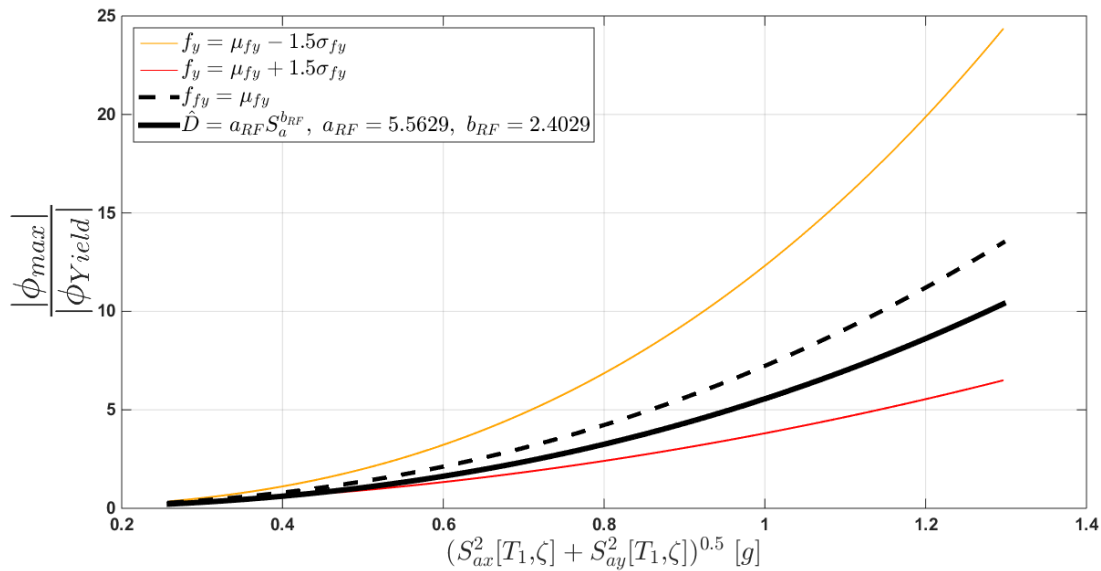


Figure 4.5 : Regression lines for FE models made from three differing steel strengths and steel jacketed model in terms of yield curvature limit state.

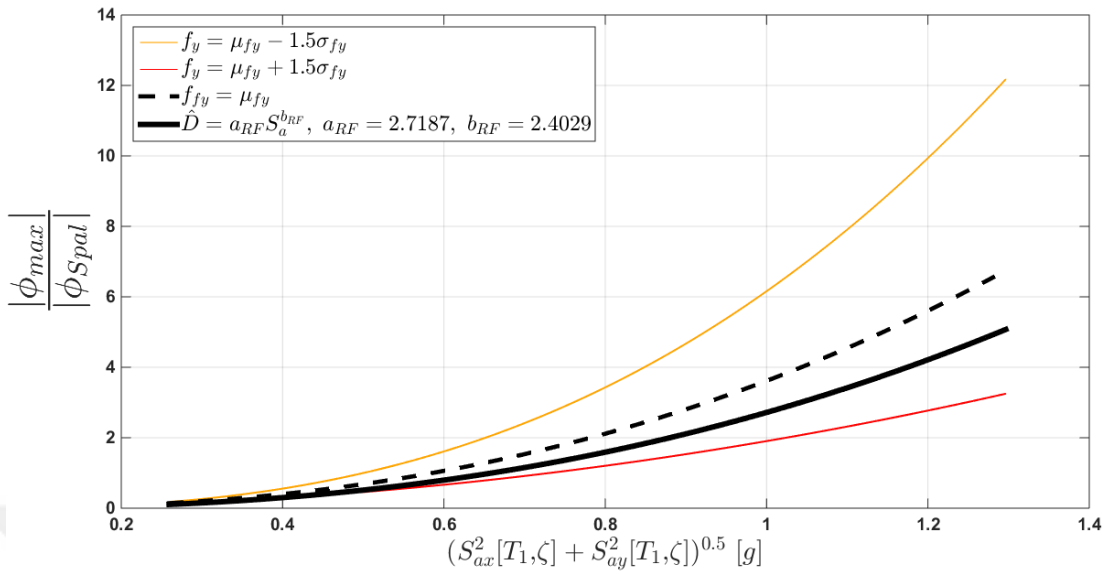


Figure 4.6 : Regression lines for FE models made from three differing steel strengths and steel jacketed model in terms of spalling curvature limit state.

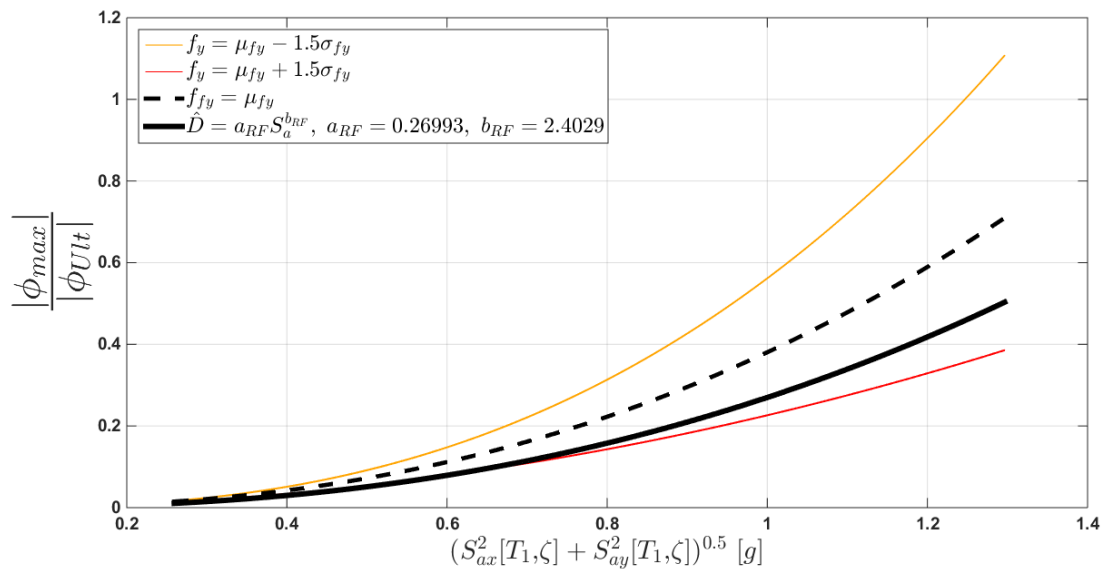


Figure 4.7 : Regression lines for FE models made from three differing steel strengths and steel jacketed model in terms of ultimate curvature limit state.

4.4.7 Expected annual costs and optimal alternative for the non-monitored structure

The money spent on construction of a bridge can be interpreted as the money invested over the period it gives service. Consequently, this investment can be converted into annual instalments by the method used frequently in mortgage payment calculations. The formula used for this purpose is called fixed-rate payment formula and is used for calculating instalments under a fixed interest rate (inflation rate in the course of this study).

$$Annual\ Payment = \left[\frac{R}{1 - (1 + R)^{-N}} \right] Cost \quad (4.10)$$

In equation (4.10), R is the inflation rate, N is the service period of the structure in years and $Cost$ is the amount that needs to be converted to annual payment (annual cost). For instance, if fixed inflation rate (R) is 4.9% (which is the mean inflation rate in construction for the past 50 years according to Turner Cost Index), N is 50 years and initial construction cost is \$1,120,000, *Annual Payment* will be about \$60,410. Annual payment and annual cost have been used interchangeably throughout this study.

Transforming expenses to annual costs has some advantages. For instance, annual cost of maintaining an SHM system can be easily added to the initial cost of installing the system if the initial installation cost has been converted into the annual payment basis. Calculation results of expected annual costs regarded to probabilities of different damage levels and the mean expected cost have been exhibited in Table 4.10 for a structure in its original state. These calculations have been performed assuming an expected service period of 50 years, inflation rate of 4.9%, indirect cost factor of 13 and initial construction cost of \$1,120,000. It is observed that expected annual cost for the non-retrofitted bridge is about \$12,800 which is about 21.2% of its initial construction cost ($12,800/60,410 \cong 21.2\%$).

Table 4.10 : Example of calculating annual expected costs for as-built, non-monitored structure.

$s (f_y)$ (MPa)	E. A. Cost* d_1, \bar{a}_r, s (\$)	E. A. Cost d_2, \bar{a}_r, s (\$)	E. A. Cost d_3, \bar{a}_r, s (\$)	E. A. Cost d_4, \bar{a}_r, s (\$)	E. A. Cost d_5, \bar{a}_r, s (\$)	E. A. Cost \bar{a}_r, s (\$)
483.1	0	926	1,461	4,853	5,131	12,371
412.6	0	1,049	1,664	6,608	6,633	15,953
454.9	0	976	1,543	5,558	5,732	13,809
546.7	0	811	1,273	3,254	3,776	9,114
539.8	0	824	1,294	3,427	3,922	9,467
441.9	0	999	1,580	5,883	6,010	14,472
442.4	0	998	1,579	5,870	6,000	14,447
506.8	0	884	1,392	4,260	4,627	11,162
459.0	0	969	1,531	5,456	5,645	13,602
528.6	0	844	1,327	3,710	4,161	10,043
⋮	⋮	⋮	⋮	⋮	⋮	⋮
					Mean (\$)	12,800
					Normalised	21.2%
					Mean	

*E.A.Cost = Expected Annual Cost

Results of a similar calculation for the retrofitted structure are presented in Table 4.11. Annual cost of steel jacketing has been calculated as about \$1,210 using the amount calculated in Subsection 4.4.3.2 (\$22,380) and employing equation (4.10). Other parameters (expected service life, inflation rate, indirect cost factor and initial construction cost) are the same as those of Table 4.10. It is observed that expected annual cost of the retrofitted bridge approximately is \$11,870 which is about 19.65% of its annual initial construction cost ($11,870/60,410 \cong 19.65\%$).

Comparing annual expected costs for the as-built and retrofitted structures of Table 4.10 and Table 4.11, it is observed that the structure had better get retrofitted regarding to maximum expected monetary gain criterion.

Table 4.11 : Example of calculating annual expected costs for retrofitted, non-monitored structure.

E. A. Cost* d_1, a_r (\$)	$0 + 1,210 = 1,210$
E. A. Cost d_2, a_r (\$)	$1,083 + 1,210 = 2,293$
E. A. Cost d_3, a_r (\$)	$1,276 + 1,210 = 2,486$
E. A. Cost d_4, a_r (\$)	$4,235 + 1,210 = 5,445$
E. A. Cost d_5, a_r (\$)	$4,064 + 1,210 = 5,274$
E. A. Cost a_r (\$)	$10,658 + 1,210 \cong \underline{11,870}$
Normalised Annual Expected Cost	19.65%

Table 4.12 demonstrates results of a study on variations of annual expected costs with initial construction cost, expected service period and significance of the bridge. Significance of a bridge is represented by its indirect cost factor. Column 7 of the table shows if the bridge needs to get retrofitted according to maximum EMV decision criterion. In column 8, the expected annual cost related to the optimal alternative selected between columns 5 and 6 is divided by annual initial construction cost to give normalised annual cost of the non-monitored structure. It is understood from this column that the normalised annual cost increases by the significance of the bridge. It is also observed from this table that as the initial construction cost, expected life period and significance of the bridge increases, the chances of retrofitting grows for being the optimal alternative.

Finally, Table 4.13 demonstrates variations of expected annual costs with number of steel samples. Cases for which non-retrofitting is the optimal alternative have been selected for this study. It is seen that increasing number of samples by 10 folds has a minor effect on the estimated values. Consequently, results by a set of 1,000 samples have been recognised to be sufficient in accuracy for purposes of this study.

Table 4.12 : Annual expected costs of the non-monitored as-built and retrofitted structure as a function of initial cost, life-time and significance.

1	2	3	4	5	6	7	8
Initial construction cost (\$)	Annual initial construction cost (\$)	Expected service period (Year)	Indirect cost factor	Expected annual cost (as-built structure) (\$)	Expected annual cost (retrofitted structure) (\$)	Optimal alternative	Normalised annual cost of the optimal alternative
1,000,000	70,240	25	5.0	2,890	3,980	\bar{a}_r (Branch1)	4.1%
			13.0	7,520	7,830	\bar{a}_r (Branch1)	10.7%
			20.0	11,570	11,200	a_r (Branch2)	15.9%
	53,930	50	5.0	4,400	4,870	\bar{a}_r (Branch1)	8.2%
			13.0	11,430	10,720	a_r (Branch2)	19.9%
			20.0	17,590	15,850	a_r (Branch2)	29.4%
1,120,000	50,400	75	5.0	6,100	6,210	\bar{a}_r (Branch1)	12.1%
			13.0	15,860	14,340	a_r (Branch2)	28.5%
			20.0	24,390	21,450	a_r (Branch2)	42.6%
	78,670	25	5.0	3,240	4,270	\bar{a}_r (Branch1)	4.1%
			13.0	8,430	8,580	\bar{a}_r (Branch1)	10.7%
			20.0	12,960	12,360	a_r (Branch2)	15.7%
60,410	50	5.0	4,920	5,310	\bar{a}_r (Branch1)	8.1%	
		13.0	12,800	11,870	a_r (Branch2)	19.6%	
		20.0	19,700	17,610	a_r (Branch2)	29.2%	
1,250,000	56,440	75	5.0	6,830	6,820	a_r (Branch2)	12.1%
			13.0	17,760	15,930	a_r (Branch2)	28.2%
			20.0	27,320	23,890	a_r (Branch2)	42.3%
	87,800	25	5.0	3,620	4,580	\bar{a}_r (Branch1)	4.1%
			13.0	9,400	9,390	a_r (Branch2)	10.7%
			20.0	14,470	13,610	a_r (Branch2)	15.5%
67,420	50	5.0	5,500	5,780	\bar{a}_r (Branch1)	8.2%	
		13.0	14,290	13,100	a_r (Branch2)	19.4%	
		20.0	21,980	19,510	a_r (Branch2)	28.9%	
62,990	75	5.0	7,620	7,480	a_r (Branch2)	11.9%	
		13.0	19,820	17,640	a_r (Branch2)	28.0%	
		20.0	30,490	26,540	a_r (Branch2)	42.1%	

Table 4.13 : Sensitivity of estimated expected annual cost to number of steel samples.

1	2	3	4	5	6	7
Initial construction cost (\$)	Annual initial construction cost (\$)	Expected service period (Year)	Indirect cost factor	Expected annual cost (1,000 steel samples) (\$)	Expected annual cost (10,000 steel samples) (\$)	Ratio (Col 5/Col 6)%
1,000,000	70,240	25	5.0	2,890	2,920	98.97%
			13.0	7,520	7,590	99.08%
	53,930	50	5.0	4,400	4,440	99.10%
	50,400	75	5.0	6,100	6,150	99.19%
1,120,000	78,670	25	5.0	3,240	3,270	99.08%
			13.0	8,430	8,500	99.18%
	60,410	50	5.0	4,920	4,970	98.99%
1,250,000	87,800	25	5.0	3,620	3,650	99.18%
	67,420	50	5.0	5,500	5,550	99.10%

4.5 Improving the State of Decision Making by Additional Information

In Section 4.2 Maximum Expected Monetary Value (EMV) criterion was introduced. This criterion was used afterwards for choosing between the discussed two alternatives, i.e. retrofitting the structure or leaving it in its as-built condition. The state of decision making might be improved if some information indicating condition of the structure would be available. It is intuitively expected that if the additional information implies a deficiency in the structure -which is use of low strength steel in the course of this study- the chances of choosing the retrofitting alternative must increase. On the other hand, data implying that strength of reinforcing steel is more than its mean value must support chances of choosing to leave the structure in its original state. In other words, the new piece of information influences the prior probabilities used for assessing expected costs related to each alternative. This influence can be reflected into decision making procedure by means of Bayes' theorem which is employed to update prior probabilities by taking advantage of new additional data. A decision analysis which utilises additional information is called a terminal analysis (Ang and Tang, 1984).

The discussed additional information might be of some worth for decision makers as it helps them to decrease uncertainties in part. Nonetheless, acquiring additional information might need certain amount of monetary resources. Moreover, the acquired data might include uncertainties themselves originating from inaccuracies of the

approach used for obtaining them. As a result, it is important to seek an answer to the question that whether the information obtained is worth the financial resources allocated to it or not. A decision analysis in which value of information is assessed prior to acquisition is called a preposterior analysis (Ang and Tang, 1984).

4.5.1 Application of preposterior analysis to the problem

The decision tree demonstrated in Figure 4.1 depicts a typical example of a two-stage preposterior analysis problem. As stated before, preposterior analysis helps decision makers to decide whether or not they should acquire additional information. This additional information which might contribute to reducing uncertainties, could be acquired via laboratory or field tests, research programmes etc. (Ang and Tang, 1984). In the course of this study, data from an SHM system provides the discussed additional information.

Considering the introduced decision tree (Figure 4.1), the problem starts with deciding if the bridge should be equipped by an SHM system. In case it is selected not to monitor the bridge (\bar{a}_m branch), it is decided in the second stage whether or not to retrofit the structure. This alternative (selecting not to monitor the bridge) was studied in previous sections and the optimal alternative for non-monitored case was distinguished by comparing the expected annual costs of retrofitted and original structures in Subsection 4.4.7.

If it is selected to monitor the bridge (a_m), it is again decided in the second stage if the structure should be retrofitted (a_r) or if it should be left in its as-built state (\bar{a}_r). Nonetheless, this time, the decision is influenced by the outcome of the monitoring system (o_1, o_2, \dots, o_k). For each outcome (o_k), the optimal alternative of retrofitting or not retrofitting options (branches 3 and 4) will be determined by a process similar to the non-monitoring decision, i.e. using maximum EMV criterion. If the expected annual cost of the monitored - retrofitted structure given SHM system outcome (o_k) is presented by $E[C|o_k, a_r, a_m]$ and the expected annual cost of the original - monitored structure given SHM system outcome (o_k) is presented by $E[C|o_k, \bar{a}_r, a_m]$, the optimal of the two alternatives ($E[C|o_k, a_r^*, a_m]$) is the minimum of the two values:

$$E[C|o_k, a_r^*, a_m] = \min\{E[C|o_k, a_r, a_m], E[C|o_k, \bar{a}_r, a_m]\} \quad (4.11)$$

This way, the total life-time cost (C_m) for the monitoring alternative is evaluated as:

$$C_m = E[C|a_m] = \sum_{k=1}^m E[C|o_k, a_r^*, a_m] \cdot p_o[o_k] \quad (4.12)$$

In which, m is possible alternative SHM system outcomes.

In the following paragraphs, expected annual cost (C_m) of the structure will be assessed and value of acquired information will be calculated by comparing the expected annual costs for monitoring and non-monitoring options (C_m and $C_{\bar{m}}$).

4.5.2 Formulation of the problem

4.5.2.1 Determining statistical properties of SHM system output

At this stage, it must be decided first what parameter the SHM system is going to measure. As the first trial, it is assumed that the system is only able to acquire information about the actual fundamental period (or frequency) of the bridge (T_1). In this study actual fundamental period of the bridge (T_1) is considered as a random variable. T_1 is assumed to be related to the fundamental period by FE model (T_1') and error ϵ by equation (4.13).

$$T_1 = T_1' \cdot \epsilon \quad (4.13)$$

In equation (4.13), T_1' is defined as a deterministic parameter which is a function of reinforcing steel properties. In order to develop a function for evaluating T_1' , a regression line can be fitted to the data representing variations of fundamental period with steel strength (Table 3.8). Given any arbitrary value for steel strength, this line can be used to estimate the corresponding T_1' value (Figure 4.8).

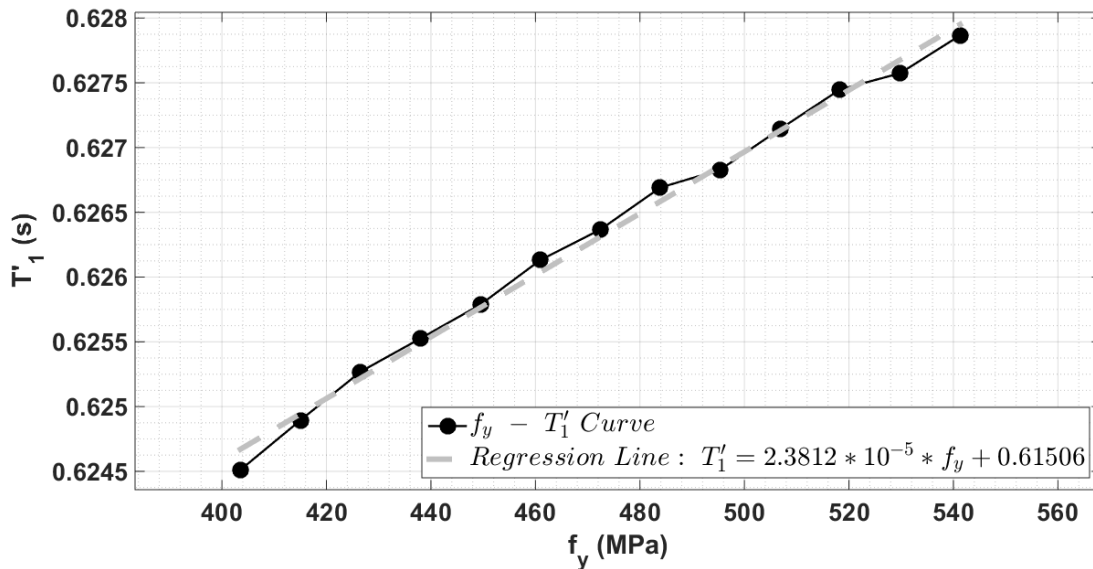


Figure 4.8: $f_y - T_1'$ curve and the regression line.

As an example of what is stated in the above, Table 4.14 has been prepared which demonstrates fundamental periods of FE models (and their natural logarithms) corresponding to a set of 10 (out of 1,000) steel samples presented in Table 4.1 estimated using the regression line shown in Figure 4.8.

Table 4.14 : Sample set of 10 uniformly distributed random numbers, standard normal random values, sample steel strengths, corresponding first modal period from FEM (T'_1) and corresponding natural logarithms of T'_1 .

$0 < u < 1$	z	$s (f_y) (MPa)$	$T'_1 (s)$	$\ln(T'_1)$
0.610	0.280	483.1	0.6266	-0.4675
0.089	-1.347	412.6	0.6249	-0.4702
0.367	-0.340	454.9	0.6259	-0.4686
0.940	1.554	546.7	0.6281	-0.4651
0.923	1.424	539.8	0.6279	-0.4653
0.261	-0.641	441.9	0.6256	-0.4691
0.265	-0.629	442.4	0.6256	-0.4691
0.780	0.773	506.8	0.6271	-0.4666
0.402	-0.248	459.0	0.6260	-0.4684
0.886	1.208	528.6	0.6276	-0.4658

Returning to equation (4.13), origins of error (ϵ) appearing in the equation can be described as follows.

It is a known fact that there are always differences between FE models and real structures. These differences have several origins; e.g., assumptions made for simplifying boundary and support conditions, damping mechanisms, properties of materials, etc. (Olson et al., 2005). Moreover, as any data acquisition instrument has intrinsic inaccuracies, there are always measurement errors which cause measured values to deviate from the true ones. In this study, both inaccuracies originating from FE models and measurement errors are represented by error (ϵ).

Contrary to T'_1 , error (ϵ) is defined as a random variable. Consequently, its distribution and statistical parameters must be defined for further calculations. Liu et al. (2009) have assumed distribution of measurement errors for a steel bridge over Wisconsin River (I-39 Bridge, Northbound) monitored for strain data from July 2004 to November of the same year as normal distribution. They have also assumed the mean value of the error measurement equal to 0.0 and its standard deviation equal to 4%. Nevertheless, during their model sensitivity studies, they have altered standard deviation of error from 2% to 8%.

In this study, error (ϵ) is defined as a lognormal random variable with statistical parameters of $\mu_{\ln \epsilon}$ and $\sigma_{\ln \epsilon}$ which are respectively mean and standard deviation of the associated normal distribution. Mean of natural logarithm of error values ($\mu_{\ln \epsilon}$) is assumed to be zero. Value of error dispersion ($\sigma_{\ln \epsilon}$) will be altered in the subsequent paragraphs with the aim of studying its effects on the estimated information value. Similar to error (ϵ), true fundamental period of bridge (T_1) is also assumed to be a lognormal random variable. Considering the described assumptions and returning to equation (4.13), it is clear that it can be re-written as

$$\ln(T_1) = \ln(T'_1) + \ln(\epsilon) \quad (4.14)$$

It is seen that $\ln(T_1)$ is a linear function of two other variables, i.e. $\ln(T'_1)$ and $\ln(\epsilon)$. Mean of a random variable similar to Y in equation (4.15) which is a linear function of other random variables can be calculated via equation (4.16) (Nowak and Collins, 2000).

$$Y = a_0 + a_1X_1 + a_2X_2 + \dots + a_nX_n = a_0 + \sum_{i=1}^n a_iX_i \quad (4.15)$$

$$\mu_Y = a_0 + a_1\mu_{X_1} + a_2\mu_{X_2} + \dots + a_n\mu_{X_n} = a_0 + \sum_{i=1}^n a_i\mu_{X_i} \quad (4.16)$$

Hence, remembering that $\mu_{\ln \epsilon}$ was assumed to be zero, relation for mean of natural logarithm of T_1 using equation (4.16) can be written as

$$\mu_{\ln T_1} = E[\ln T_1] = \int T'_1(s) f_S(s) ds \cong \frac{1}{n} \sum_{i=1}^n \ln[T'_1(s_i)] \quad (4.17)$$

In equation (4.17), $f_S(s)$ is the lognormal probability density function (PDF) of steel yield stress with statistical parameters presented in Table 3.2. $T'_1(s)$ implies that fundamental period values from FE models are functions of steel strength values. This relation is represented by the regression line shown in Figure 4.8.

In order to solve equation (4.17) in an approximate manner, steel samples produced by Monte Carlo approach and their associated model periods will be used. For example, for the 1,000 steel samples produced in Section 4.3 by Monte Carlo approach and relative T'_1 values presented partially in Table 4.14, $\mu_{\ln T_1}$ is approximated as -0.4678.

After formulating $\mu_{\ln T_1}$, it is needed to establish a relation for dispersion of T_1 ($\sigma_{\ln T_1}$). It is clear from equation (4.13) that if $\epsilon = 1$, $T_1 = T'_1$. Dispersion of fundamental period of structure reported by the SHM system (T_1) can be calculated using the relation for

standard deviation of a random variable which is a linear function of other variables, i.e. equation (3.17) and equation (3.18). This way,

$$\sigma_{\ln T_1} = \sqrt{\sigma_{\ln T'_1|\epsilon=1}^2 + \sigma_{\ln \epsilon}^2} \quad (4.18)$$

As stated before, variance of error ($\sigma_{\ln \epsilon}^2$) and its effect on value of acquired data will be studied later. Variance of the fundamental period of structure reported by monitoring instruments given no error ($\sigma_{\ln T'_1|\epsilon=1}^2$) can be formulated as

$$\sigma_{\ln T'_1|\epsilon=1}^2 = \int [T'_1(s) - \mu_{\ln T'_1}]^2 \cdot f_S(s) ds \cong \frac{1}{n-1} \sum_{i=1}^n (\ln[T'_1(s_i)] - \mu_{\ln T'_1})^2 \quad (4.19)$$

For instance $\sigma_{T'_1|\epsilon=1}$ can be approximated by the described process, using $\ln(T'_1)$ values demonstrated partially in Table 4.14 and considering that $\mu_{\ln T_1} \cong -0.4678$. The approximated value for $\sigma_{T'_1|\epsilon=1}$ is calculated as about 0.0018 by this process.

4.5.2.2 Estimating probabilities of outcomes from the SHM system

Using the assumptions made in Subsection 4.5.2.1, it is now possible to estimate probability of each output. Probabilities calculated at this stage ($p_O[o_k]$) will influence prior probabilities of steel strengths as can be observed schematically in branch 3 of the decision tree (Figure 4.1).

Considering that SHM system outputs have been defined as lognormal variables, they can theoretically vary from 0 to positive infinity. However, probabilities of variables beyond the range of $\exp(\mu_{\ln o} \pm 4\sigma_{\ln o})$ can be considered as minor. As a result, probability of any variable out of this range has been assumed to be zero. Moreover, in order to make things convenient for numerical calculations, this range is divided into a number of intervals (16 intervals). Likelihood of each interval $o_k: \{tl \leq T_1 \leq tl + \Delta tl\}$ can be estimated using equation (4.20). It is clear that $\mu_{\ln o}$ is represented by $\mu_{\ln T_1}$ and $\sigma_{\ln o}$ is represented by $\sigma_{\ln T_1}$.

$$\begin{aligned} p_O[o_k] &= \int_{tl_k}^{tl_k + \Delta tl} \phi_{LN}(t; \mu_{\ln T_1}, \sigma_{\ln T_1}) dt \\ &= \Phi\left(\frac{\ln(tl + \Delta tl) - \mu_{\ln T_1}}{\sigma_{\ln T_1}}\right) - \Phi\left(\frac{\ln tl - \mu_{\ln T_1}}{\sigma_{\ln T_1}}\right) \end{aligned} \quad (4.20)$$

The described process has been illustrated schematically by Figure 4.9 and calculated probabilities have been demonstrated in Figure 4.10. It is seen from Figure 4.10 that probabilities beyond the range of $\exp(\mu_{\ln o} \pm 4\sigma_{\ln o})$ can be safely ignored.

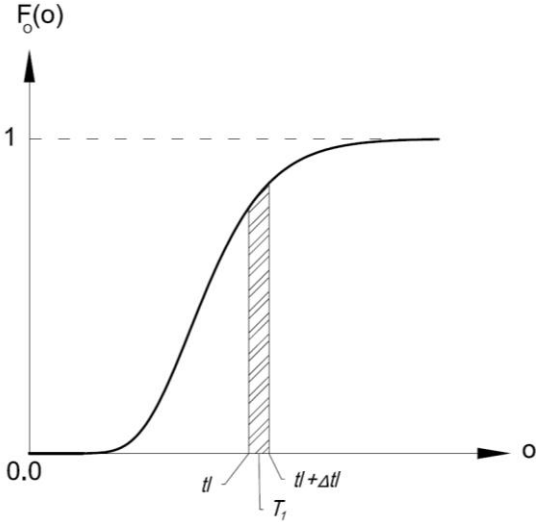


Figure 4.9 : Lognormal cumulative distribution function of SHM system outputs and the process for approximating $p_o[o_k]$.

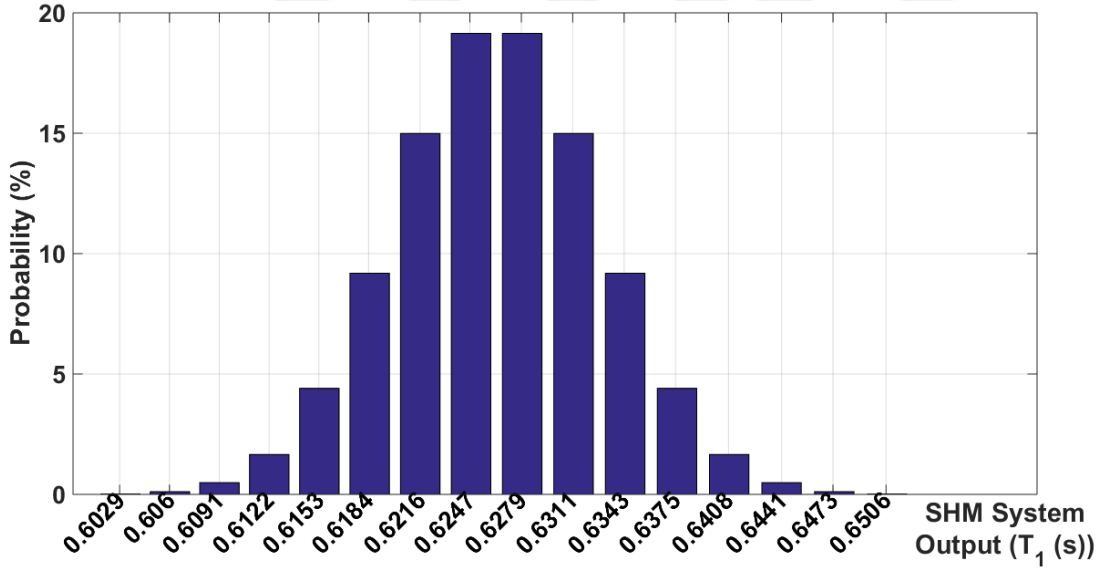


Figure 4.10 : Estimated probabilities of SHM system outputs ($p_o[o_k]$) monitoring fundamental period of structure T_1 .

4.5.2.3 Updating probability distribution functions of steel

Having estimated probabilities of SHM system results, it is possible now to move forward towards branch 3 and update prior probabilities of steel strengths using the additional information ($p_o[o_k]$). This can be done by employing Bayes' theorem which has been discussed in detail in many probability books. A short description has also been

provided by Nowak and Collins (2000). Using Bayes' theorem, updated conditional probability of steel strength can be calculated using equation (4.21):

$$P[S = s_i | O = o_k] = \frac{P[O = o_k | S = s_i] \cdot P[S = s_i]}{\sum_j P[O = o_k | S = s_j] \cdot P[S = s_j]} \quad (4.21)$$

In which $P[S = s_i]$ is the prior steel probability calculated from lognormal probability distribution function of steel. For estimating this probability, steel strength range must be divided into intervals with length of Δs . Afterwards, the probability can be assessed from equation (4.22).

$$P[S = s_i] = \Phi\left(\frac{\ln(s_i + \Delta s) - \mu_{\ln S}}{\sigma_{\ln S}}\right) - \Phi\left(\frac{\ln s_i - \mu_{\ln S}}{\sigma_{\ln S}}\right) \quad (4.22)$$

In which $\mu_{\ln S}$ and $\sigma_{\ln S}$ are logarithmic mean and standard deviation of steel. Conditional probability of SHM system output given steel strength ($P[O = o_k | S = s_i]$) can be calculated using equations (4.23), (4.24) and (4.25).

$$P_i[O = o_k | S = s_i] = \Phi\left(\frac{\ln(tl + \Delta tl) - \mu_{\ln T_1 | s_i}}{\sigma_{\ln T_1 | s_i}}\right) - \Phi\left(\frac{\ln tl - \mu_{\ln T_1 | s_i}}{\sigma_{\ln T_1 | s_i}}\right) \quad (4.23)$$

$$\mu_{\ln T_1 | s_i} = \ln T_1'(s_i) \quad (4.24)$$

$$\sigma_{\ln T_1 | s_i} = \sigma_{\ln \epsilon} \quad (4.25)$$

Equation (4.24) has been established considering the assumption that measurement error variable has a mean value of zero (as a result, error does not appear in the equation). Equation (4.25) which is for conditional dispersion of T_1 ($\sigma_{\ln T_1 | s_i}$) is related only to error dispersion because steel strength has been set as the conditioning parameter. After steel probabilities are updated with regard to an SHM system result (o_k), they get summed up so that the updated CDF of steel could be attained. This is presented by equation (4.26).

$$F_{S|O}(s|o_k) = \sum_{all\ i} P_i[O = o_k | S = s_i] \quad (4.26)$$

Original CDF of steel and updated steel CDFs given 4 (out of 16) SHM system outcomes have been demonstrated in Figure 4.11 assuming 0.01 value for error dispersion.

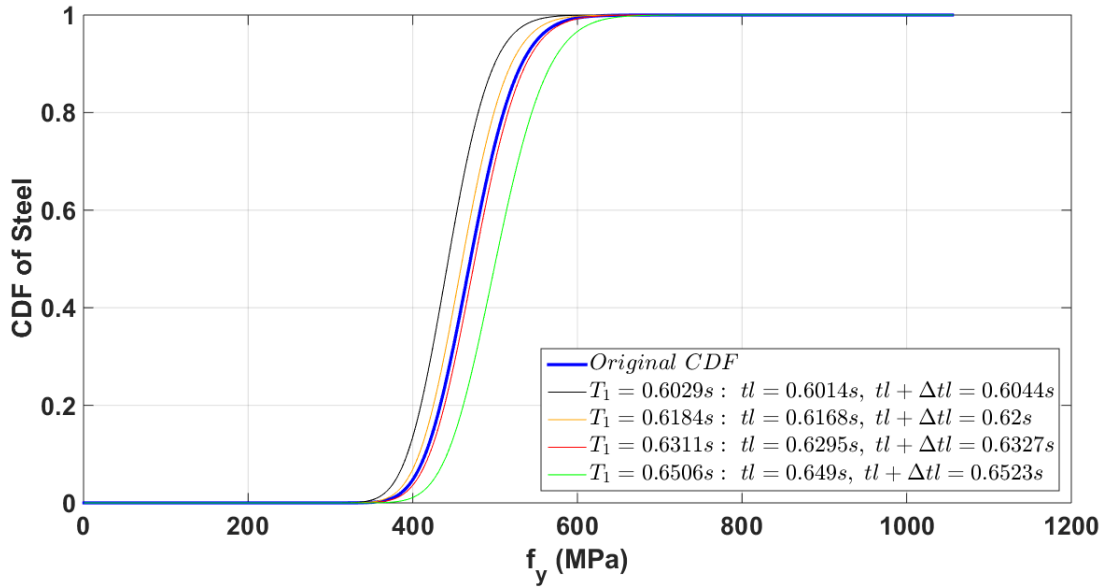


Figure 4.11 : Prior and updated CDFs of steel for different SHM outputs ($\sigma_{\ln \epsilon} = 1.0\%$).

From Figure 4.11 it is observed that for a certain uniformly distributed random variable (u) between 0 and 1, $F_{S|O}(s|o_k = 0.6029 \text{ \& } 0.6184)$ tend to bring about smaller steel strengths than original CDF. On the other hand, for the same value, $F_{S|O}(s|o_k = 0.6311 \text{ \& } 0.6506)$ result in larger steel strengths. Table 4.15 presents the discussed behaviour in a tabular format. Dispersion of error ($\sigma_{\ln \epsilon}$) has been assumed to be only 0.01 for Figure 4.11 and Table 4.15.

Table 4.15 : Prior and updated steel strengths for four different SHM outputs ($\sigma_{\ln \epsilon} = 1.0\%$).

$0 < u < 1$	z	$s(f_y)$ (MPa)	$s(f_y T_1)$	$s(f_y T_1)$	$s(f_y T_1)$	$s(f_y T_1)$
			$T_1 = 0.6029s$ (MPa)	$T_1 = 0.6184s$ (MPa)	$T_1 = 0.6311s$ (MPa)	$T_1 = 0.6506s$ (MPa)
0.610	0.280	483.1	455.0	472.8	488.5	515.2
0.089	-1.347	412.6	390.8	405.1	417.7	438.9
0.367	-0.340	454.9	429.4	445.8	460.2	484.7
0.940	1.554	546.7	512.2	533.3	552.0	584.1
0.923	1.424	539.8	506.1	526.8	545.2	576.6
0.261	-0.641	441.9	417.5	433.2	447.1	470.5
0.265	-0.629	442.4	418.0	433.7	447.6	471.1
0.780	0.773	506.8	476.4	495.4	512.2	540.9
0.402	-0.248	459.0	433.1	449.7	464.3	489.1
0.886	1.208	528.6	496.0	516.1	534.0	564.5

For greater dispersions of error, updated steel CDFs become closer to the original CDF. Figure 4.12 illustrates original and updated CDFs for $\sigma_{\ln \epsilon} = 2.0\%$. It will be observed that as error grows, the additional information by the SHM system loses its value.

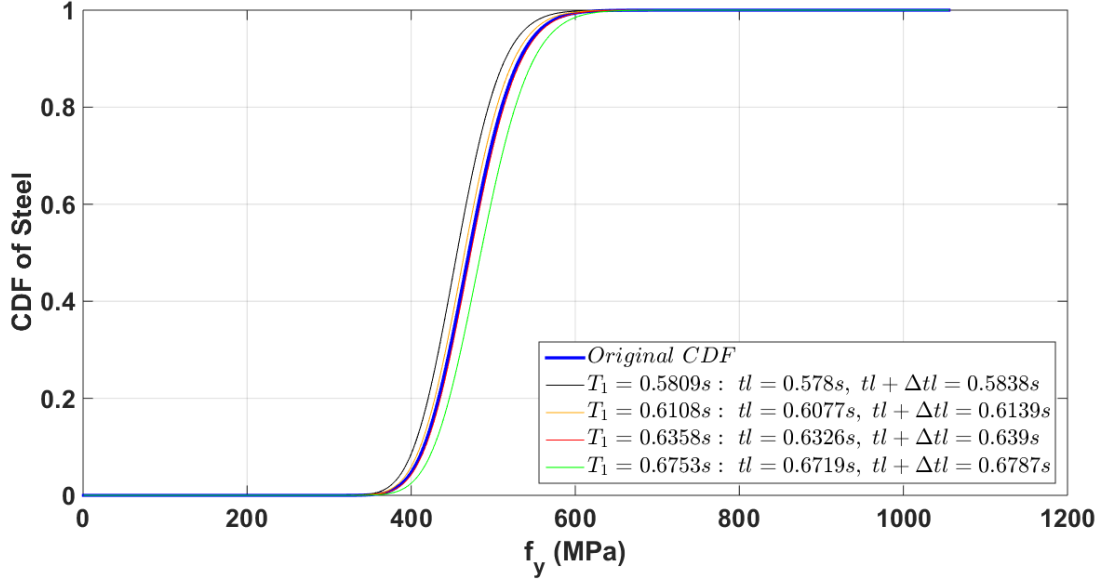


Figure 4.12 : Prior and updated CDFs of steel by different SHM outputs ($\sigma_{nc} = 2.0\%$).

4.5.2.4 Cost of monitoring

Theoretical formulation

Using updated steel strength values, similar to what is shown in Figure 4.11, Figure 4.12 and Table 4.15, failure probabilities for each SHM system output in terms of each limit state ($p_{F|O}[f_j|o_k]$) and probability of damage in the course of each damage level ($p_{D|O}[d_j|o_k]$) can be calculated. The process is the same as the one for a structure without any monitoring, i.e. branch 1 of the decision tree (Figure 4.1). After calculating annual and life-time probabilities of damage, corresponding expected costs can also be calculated. Again, the process is identical to a system without instrumental inspection except that cost of monitoring must be considered as well:

$$E[C|o_k, \bar{a}_r, a_m] = c_m + \sum_{i=1}^5 c_{d_j} \cdot p_{D|O}[d_j|o_k] \quad (4.27)$$

In equation (4.27) c_m is cost of monitoring, c_{d_j} is the cost associated with each damage level (Table 4.3) and $p_{D|O}[d_j|o_k]$ is the likelihood of damage for damage level j given the k^{th} SHM system outcome. This probability can be calculated as:

$$p_{D|O}[d_j|o_k] = \int p_{D|O,S}[d_j|o_k, s] \cdot f_{S|O}(s|o_k) ds \cong \frac{1}{n} \sum_{i=1}^n p_{D|S}[d_j|o_k, s_i] \quad (4.28)$$

In equation (4.28), n is the number of reinforcing steel strength realisations. $p_{D|S}[d_j|o_k, s_i]$ is probability of damage level j given SHM system output k and steel strength i .

For branch 4 of decision tree, which is the retrofitted option of the monitored structure, annual and life-time damage probabilities are not influenced by SHM system outcomes. This is because sensitivity of the retrofitted structure to variations in reinforcing steel strength has been assumed as minor. Hence, expected costs relevant to each damage level will be assessed in the same manner as for the non-monitored bridge; except that cost of monitoring needs to be taken into account as well.

Estimation of costs related to installing and maintaining SHM monitoring systems

Estimation of costs related to installation and maintenance of SHM systems has certain difficulties. This is mainly due to the great variety of SHM systems. Agdas et al. (2016) have reported costs of monitoring for some bridges. For instance, they report that a monitoring system installed for inspecting corrosion of Howard Frankland Bridge in the U.S. costs \$11,900 per pier including both hardware and labour. They also have prepared a price list for some monitoring items for a case study MSSS bridge located in a coastal area. The bridge has three 65' ($\cong 20\text{m}$) spans, 56' ($\cong 17.1\text{m}$) wide deck and has been assumed to have some scouring and corrosion problems. The price list by Agdas et al. (2016), involves items for both wireless and wire-based systems. As the mentioned case study bridge has substantial similarities in geometry and structure with Elek Deresi Bridge³, its SHM system price analysis has been used in this study. Naturally, only items relevant to purposes of this study have been cited and modifications have been made to quantities of some items due to the fact that Elek Deresi Bridge has only two spans (Table 4.16). According to Table 4.16, it is observed that selecting a wireless system instead of a wire-based one results in about 45% reduction in initial costs of monitoring. Consequently, considering advantages of wireless systems over wire-based systems due to deployment convenience and fewer costs, it seems that a wireless system would be the better selection.

Annual expense of a wireless monitoring system can be approximated utilising data presented in Table 4.16 and equation (4.10). Table 4.17 demonstrates such calculations performed for a bridge with three different expected life-times.

³ Elek Deresi Bridge is an MSSS bridge with span length of 20.2m and deck width of 13.7m.

Table 4.16 : Cost of wireless and wire-based SHM systems excerpted from (Agdas et al, 2016).

	Hardware	Unit Cost	Unit	Quantity	Wireless	Wired
Initial	Wireless Processing					
	Unit w/ Embedded Accelerometer	\$600	Node Location	10	\$6,000	-
	Accelerometers	\$750	Sensor	10	-	\$7,500
	Base Station	\$6,500	System	1	\$6,500	\$6,500
	Software License	\$1,000	System	1	\$1,000	\$1,000
	Installation & Power					
	Wired Installation	\$20,000	Bent	1	-	\$20,000
	Wireless Installation	\$8,000	Bent	1	\$8,000	
	Conduit	\$1,020	Span	2	-	\$2,040
	AC Power	\$6,240	Span	2	-	\$12,480
	Solar Power	\$185	Panel	4	\$740	-
				Initial Cost:	\$22,240	\$49,520
Ongoing	Bridge Service					
		Unit Price	Yearly Occurrence		Wireless	Wired
	Data Analysis	\$2,000	1		\$2,000	\$2,000
	Maintenance	\$5,000	2		\$10,000	\$10,000
			Ongoing Cost/Year:		\$12,000	\$12,000

Table 4.17: Annual cost of monitoring for bridges with different life-times.

Expected service period	Annual initial cost	Ongoing cost	Total annual cost
25	\$1,560	\$12,000	\$13,560
50	\$1,200	\$12,000	\$13,200
75	\$1,120	\$12,000	\$13,120

4.5.3 Value of information and value of perfect information

As stated before, value of information (*VI*) is the criterion for choosing whether or not monetary resources should be invested on acquisition of additional data. In the course of

this study, value of information can be expressed as the difference between the expected annual costs of monitoring and non-monitoring alternatives:

$$VI = C_{\bar{m}} - C_m \quad (4.29)$$

If VI is positive, it means that the system had better get monitored because expected annual cost of non-monitoring alternative is higher. In case VI is negative, the system had better left non-monitored as expected monitoring cost is higher than value of information it can provide.

Value of perfect information (VPI) is value of information acquired from a source with 100% reliability (Ang and Tang, 1984). VPI determines the maximum monetary resources that can be spent for acquiring additional data; even if it is absolutely accurate. Considering assumptions made previously, in this study, VPI can be determined from equation (4.29) and assuming a zero value for both $\sigma_{ln\epsilon}$ and monitoring installation and maintenance cost.

Value of perfect information has been estimated in Table 4.18 for some cases. It is observed from this table that VPI is a function of initial construction cost (columns 1 and 2), expected life-time (column 3) and indirect cost factor (column 4). Column 7 shows the maximum amount that can be invested yearly for acquiring additional perfect information. Column 8 shows the maximum amount that can be invested in one instalment for acquiring perfect information. This value has been calculated from equation (4.10) and introducing annual VPI as *Annual Payment*. Normalised VPI (column 9) has been calculated by dividing annual VPI by annual initial construction cost (column 7/column 2). This value can also be calculated by dividing VPI by initial construction cost (column 8/column 1). Comparing annual VPI amounts calculated here with annual expenses of monitoring presented in Table 4.17 shows that a monitoring with specifications described in Subsection 4.5.2.4 cannot be performed even if information with perfect accuracy could be obtained.

In column 10, maximum monetary resources that can be allocated every year to a monitoring with 2.0% error dispersion are presented. In column 11, the maximum money that can be spent in one instalment to the same monitoring is presented. It is observed that no or very little money can be spent on monitoring when $\sigma_{ln\epsilon} = 2.0\%$. Finally, column 12 shows that for the non-monitored case, whether the bridge should be retrofitted or left in its as-built state due to the maximum EMV decision criterion.

Returning to columns 10 and 11, it is seen that value of information drops greatly as error increases. This behaviour can be due to the fact that variation of fundamental period of the bridge with steel properties is very small; as can be observed in Figure 4.8. The observed insensitivity of fundamental period to variations in steel strength is understandable considering the fact that bridge superstructure is almost free to float over the substructure as a result of elastomeric bearings employed. As a result, variations in bent system stiffness cannot influence the fundamental period in a great manner (consulting Figure 2.46a which demonstrates first mode of vibration could be helpful at this stage). As a consequence of this insensitivity, updated steel CDFs get very close to the original steel CDF, making monitoring infeasible (as was seen in Figure 4.12). Considering the observed problem with monitoring for the fundamental period of the structure, it seems to be a good idea to study a parameter with greater sensitivity to changes in steel strength. This could be the fundamental period of the bent system as it is directly influenced by changes in reinforcing steel properties. Moreover, there exist methods for evaluating dynamic properties of bridge substructures. One of these methods is a forced-vibration dynamic test developed for bridge substructures by FHWA. This test will be introduced in the next subsection in a very concise manner.

Table 4.18 : Evaluation of VPI and the maximum allowable budget of monitoring.

1	2	3	4	5	6	7	8	9	10	11	12
Initial construction cost	Annual initial construction cost	Expected service period (Year)	Indirect cost factor	Expected annual cost of non-monitored bridge ($C_{\bar{m}}$)	Expected annual cost of monitored bridge minus monitoring expense	Annual VPI			Maximum Annual Monitoring budget	Maximum Monitoring budget in one instalment	Optimal alternative for non-monitored bridge
						Annual VPI	VPI	Normalised VPI (%)			
						$(\sigma_{In\epsilon} = 0.0\%)$			$(\sigma_{In\epsilon} = 2.0\%)$		
\$1,000,000	\$70,240	25	5.0	\$2,890	\$2,890	-	-	-	-	-	\bar{a}_r (Branch1)
			13.0	\$7,520	\$7,120	\$400	\$5,695	0.57	-	-	\bar{a}_r (Branch1)
		20.0	\$11,200	\$10,530	\$670	\$9,538	0.95	-	-	a_r (Branch2)	
		5.0	\$4,400	\$4,260	\$140	\$2,596	0.26	-	-	\bar{a}_r (Branch1)	
	\$53,930	50	13.0	\$10,720	\$10,200	\$520	\$9,642	0.96	-	-	a_r (Branch2)
			20.0	\$15,850	\$15,240	\$610	\$11,310	1.13	-	-	a_r (Branch2)
		5.0	\$6,100	\$5,710	\$390	\$7,739	0.77	-	-	\bar{a}_r (Branch1)	
		\$50,390	75	13.0	\$14,340	\$13,780	\$560	\$11,112	1.11	-	-
20.0	\$21,450			\$20,780	\$670	\$13,295	1.33	-	-	a_r (Branch2)	
\$1,120,000	\$78,670	25	5.0	\$3,240	\$3,240	-	-	-	-	-	\bar{a}_r (Branch1)
			13.0	\$8,430	\$7,880	\$550	\$7,830	0.7	-	-	\bar{a}_r (Branch1)
		20.0	\$12,360	\$11,690	\$670	\$9,538	0.85	\$10	\$142	a_r (Branch2)	
		5.0	\$4,920	\$4,730	\$190	\$3,523	0.31	-	-	\bar{a}_r (Branch1)	
	\$60,410	50	13.0	\$11,870	\$11,320	\$550	\$10,198	0.91	-	-	a_r (Branch2)
			20.0	\$17,610	\$16,970	\$640	\$11,867	1.06	\$10	\$185	a_r (Branch2)
		5.0	\$6,820	\$6,330	\$490	\$9,723	0.87	\$30	\$595	a_r (Branch2)	
		\$56,440	75	13.0	\$15,930	\$15,340	\$590	\$11,708	1.05	\$10	\$198
20.0	\$23,890			\$23,190	\$700	\$13,891	1.24	-	-	a_r (Branch2)	

Table 4.18 (continued) : Evaluation of VPI and the maximum allowable budget of monitoring.

1	2	3	4	5	6	7	8	9	10	11	12
Initial construction cost	Annual initial construction cost	Expected service period (Year)	Indirect cost factor	Expected annual cost of non-monitored bridge (C_m)	Expected annual cost of monitored bridge minus monitoring expense	Annual VPI		Normalised VPI (%)	Maximum Annual Monitoring budget	Maximum Monitoring budget in one instalment	Optimal alternative for non-monitored bridge
						$(\sigma_{In\epsilon} = 0.0\%)$	$(\sigma_{In\epsilon} = 2.0\%)$				
\$1,250,000	\$67,420	25	5.0	\$3,620	\$3,600	\$20	\$285	0.02	-	-	\bar{a}_r (Branch1)
			13.0	\$9,390	\$8,710	\$680	\$9,681	0.77	\$40	\$569	a_r (Branch2)
			20.0	\$13,610	\$12,920	\$690	\$9,823	0.79	-	-	a_r (Branch2)
			5.0	\$5,500	\$5,230	\$270	\$5,006	0.4	-	-	\bar{a}_r (Branch1)
			13.0	\$13,100	\$12,540	\$560	\$10,383	0.83	\$0	-	a_r (Branch2)
			20.0	\$19,510	\$18,840	\$670	\$12,423	0.99	\$0	-	a_r (Branch2)
			5.0	\$7,480	\$7,000	\$480	\$9,525	0.76	\$10	\$198	a_r (Branch2)
			13.0	\$17,640	\$17,030	\$610	\$12,105	0.97	\$0	-	a_r (Branch2)
\$62,990	75	20.0	\$26,540	\$25,790	\$750	\$14,883	1.19	\$10	\$198	a_r (Branch2)	

4.5.4 Field modal vibration dynamic testing method of bridge substructures by FHWA

Federal Highway Administration (FHWA) started the research project for developing the test in 1995 (Olson et al., 2005). The objective was to develop a non-destructive testing method for identifying deficiencies of bridge substructures (broken piles, scouring events, etc.) from their dynamic properties. In addition, the test must have been able to determine type of footing (shallow or pile) from measured vibrations. This was because at the time, there were thousands of bridges in the U.S. with unknown foundation properties. The report was published in 2005 and describes the testing procedure and results in great detail.

According to the report, three real RC bridges were selected for the experimental investigations. The research team employed a truck-mounted geophysical vibrator (a vibroseis) placed on top of the capbeam for generating forced vibrations. This was because dynamic excitations from other resources (impulse hammers, etc.) were distinguished as insufficient in energy to vibrate the bridge columns in the desired intensity. Vibration responses were measured using vertical and horizontal accelerometers attached to various locations of the bent (capbeam, columns) and a computer-based data acquisition system. The recorded data were analysed later and modal transfer functions (TFs) were derived. TFs can be helpful in distinguishing possible deficiencies. For instance, abnormal variations of the flexibility TF at a node can be a sign of a damaged member, i.e. high flexibility indicates low stiffness and a probable issue with the member. TF results (accelerance TFs) were also used to obtain mode shapes, modal frequencies and damping ratios.

Although the described approach was helpful in detecting broken and scoured pile states, it was distinguished that it lacked sufficient reliability particularly when it was needed to distinguish foundation type. The research team was looking for a method that could detect minor changes of frequencies in a reliable manner. After some delay, they utilised Hilbert-Huang Transform (HHT) Analysis method which has wide applications in monitoring and structural condition assessment. This method managed to successfully and reliably identify local dynamic properties, deficiencies with the bent system and foundation type.

In the following, it is assumed that fundamental period of the bent system has been estimated by the described test (or by any other appropriate approach). Value of

information from such a test will be assessed by the process described in Subsections 4.5.2 and 4.5.2.4. The only difference will be use of fundamental period of the bent as inspection outcome instead of fundamental period of the structure.

4.5.5 Elastic FE model for modal analysis of bent system

Modelling details of the bent system of one of the RC bridges studied by the research team has been discussed in the mentioned FHWA report (Olson et al., 2005). In this subsection, modelling of Elek Deresi Bridge bent system will be followed using those directions.

Details of the bent system for Elek Deresi Bridge have been demonstrated in Figure 2.14. As the bent system is going to be separately modelled, tributary masses from decks are lumped in capbeam nodes. Additionally, mass of the vibroseis truck (22,246 kg) is also added to the mid node of the capbeam (assuming that mid width of the deck is the location that transient loading was applied). As elastomeric bearings can be idealised as roller supports, stiffness contribution from the superstructure was ignored. Figure 4.13 demonstrates the first mode shape of vibration for bent system resulted from eigenvalue analysis.

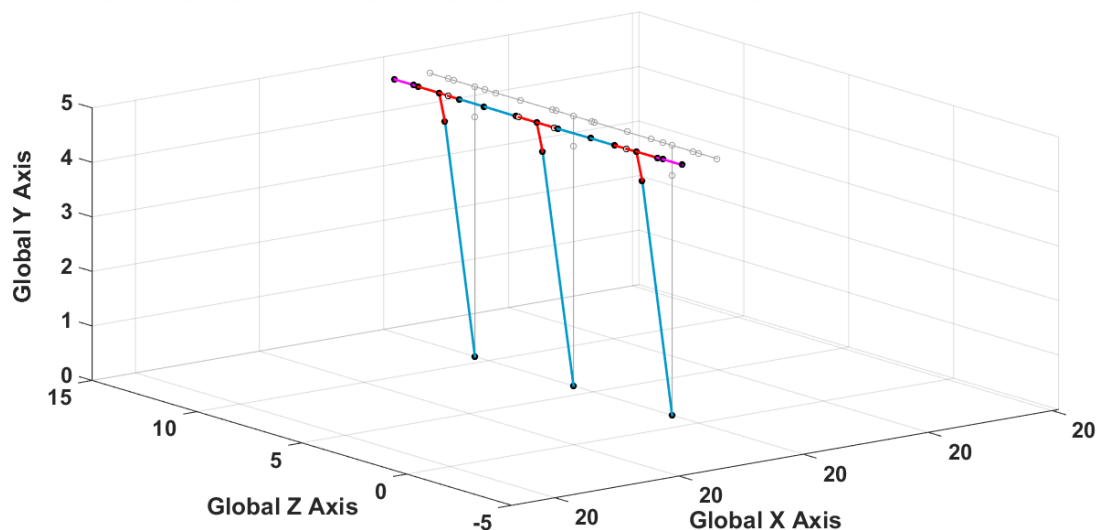


Figure 4.13 : Three dimensional view of the first natural mode shape of bent system.

Similar to the case with the complete structure, 13 FE models with different steel properties have been established. Similar to models of complete structure, variations in confined concrete properties, plastic hinge lengths, etc. by changes in strength of reinforcing steel were taken into consideration. Finally, fundamental periods of bent

system for the FE models were evaluated by modal analyses similar to what has been described in Subsection 3.2.5 for the complete structure (Figure 4.14).

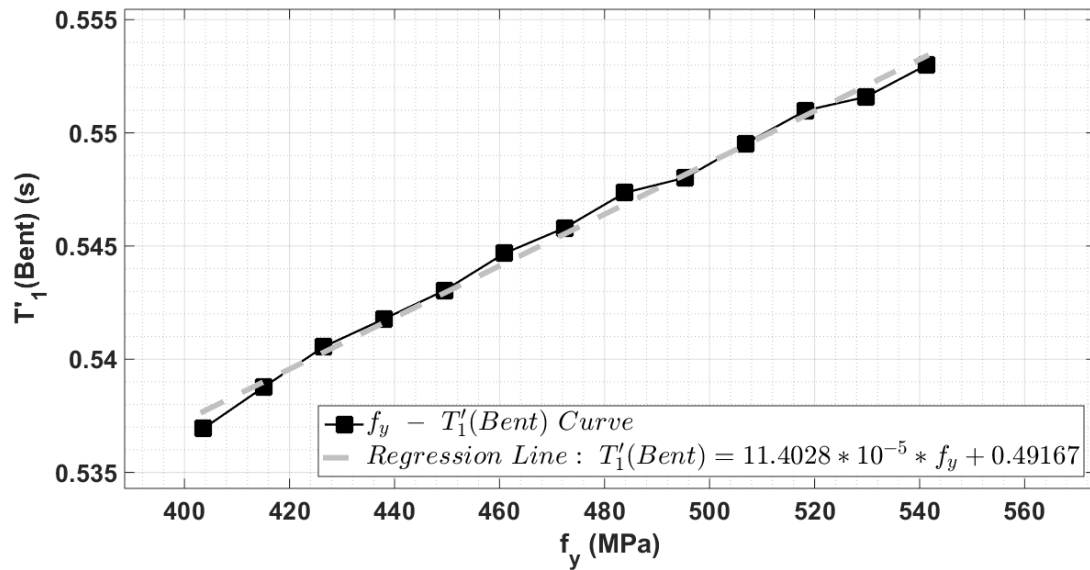


Figure 4.14 : $f_y - T'_1$ curve of the bent system and the regression line.

Comparing Figure 4.14 with Figure 4.8 shows that by changing steel strength from $\mu_{f_y} - 1.5\sigma_{f_y} = 403.5\text{MPa}$ to $\mu_{f_y} + 1.5\sigma_{f_y} = 541.3\text{MPa}$, fundamental period of the bent system grows about 2.9% whereas fundamental period of the complete structure grows only about 0.5%. As a result, it is concluded that fundamental period of the bent system is more sensitive to changes in steel properties.

It is also worth to say that the described modal test by FHWA is best in assessing vertical frequencies and mode shapes. However, as pile foundations and subsurface soil have not been modelled in this study, first mode of vibration has been utilised in the following analyses.

4.5.6 Assessing value of information by monitoring fundamental period of the bent system

In this subsection, value of perfect information and value of information acquired from inspection of fundamental period of the bent system is discussed. The inspection might be via the method described in Subsection 4.5.4.

The procedure is similar to the case of monitoring fundamental period of complete structure. Range of possible outcomes of SHM system has been divided into 16 intervals again. Probabilities of these intervals have been calculated using equation (4.20) and have been illustrated in Figure 4.15.

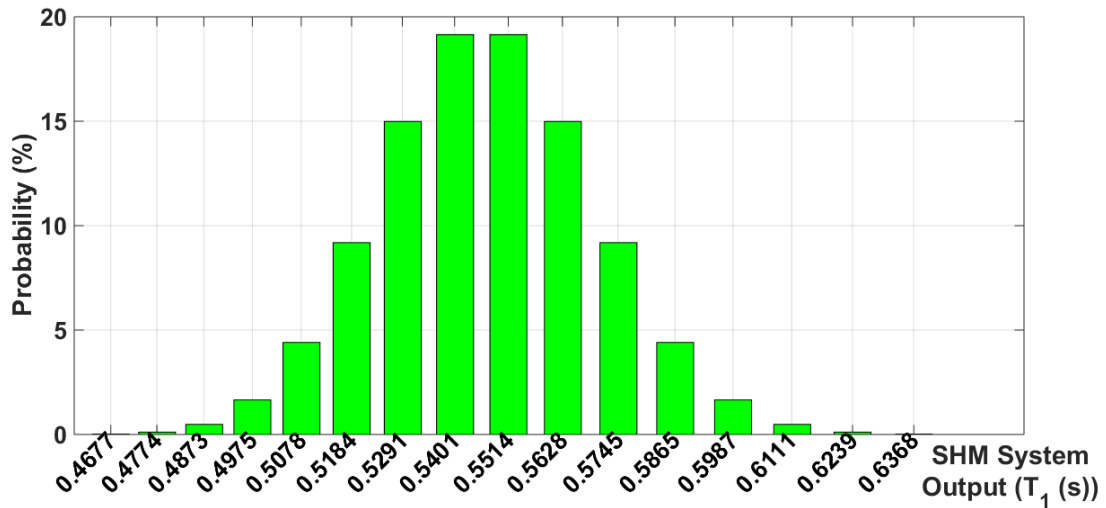


Figure 4.15 : Estimated probabilities of SHM system outputs ($p_o[o_k]$) monitoring fundamental period of bent system.

A table similar to Table 4.18 has been prepared for the bent system monitoring (Table 4.19). Comparing values of columns 7, 8 and 9 of Table 4.19 with those of Table 4.18 shows that apart from some minor differences, values of perfect information are almost identical when a perfect monitoring is performed. However, as error grows, information obtained by monitoring the fundamental period of the bent system proves to have greater value than information acquired from the fundamental period of complete structure (columns 10 and 11 of Table 4.19). The reason for this difference can be understood by observing Figure 4.16 and comparing it with Figure 4.12. It is seen that additional information from the bent system has greater effect on modifying the original CDF of steel.

Table 4.19 : Evaluation of VPI and the maximum allowable budget of monitoring bent system.

1	2	3	4	5	6	7	8	9	10	11	12	
Initial construction cost	Annual initial construction cost	Expected service period (Year)	Indirect cost factor	Expected annual cost of non-monitored bridge ($C_{\bar{m}}$)	(Expected annual cost of monitored bridge minus monitoring price)	Annual VPI	VPI	Normalised VPI (%)	Maximum Annual Monitoring budget	Maximum Monitoring budget in one instalment	Optimal alternative for non-monitored bridge	
												$(\sigma_{In\epsilon} = 0.0\%)$
\$1,000,000	\$70,240	25	5.0	2,890	2,890	-	-	-	-	-	\bar{a}_r (Branch1)	
			13.0	7,520	7,120	\$400	\$5,695	0.57	\$100	\$1,424	\bar{a}_r (Branch1)	
			20.0	11,200	10,530	\$670	\$9,538	0.95	\$220	\$3,132	a_r (Branch2)	
		50	5.0	4,400	4,260	\$140	\$2,596	0.26	\$10	\$185	\bar{a}_r (Branch1)	
			13.0	10,720	10,200	\$520	\$9,642	0.96	\$110	\$2,040	a_r (Branch2)	
			20.0	15,850	15,240	\$610	\$11,310	1.13	\$80	\$1,483	a_r (Branch2)	
	\$50,390	75	5.0	6,100	5,710	\$390	\$7,739	0.77	\$130	\$2,580	\bar{a}_r (Branch1)	
			13.0	14,340	13,780	\$560	\$11,112	1.11	\$80	\$1,587	a_r (Branch2)	
			20.0	21,450	20,780	\$670	\$13,295	1.33	\$70	\$1,389	a_r (Branch2)	
		25	5.0	3,240	3,240	-	-	-	-	-	-	\bar{a}_r (Branch1)
			13.0	8,430	7,880	\$550	\$7,830	0.7	\$190	\$2,705	\bar{a}_r (Branch1)	
			20.0	12,360	11,690	\$670	\$9,538	0.85	\$190	\$2,705	a_r (Branch2)	
\$1,120,000	\$60,410	50	5.0	4,920	4,730	\$190	\$3,523	0.31	\$20	\$371	\bar{a}_r (Branch1)	
			13.0	11,870	11,320	\$550	\$10,198	0.91	\$110	\$2,040	a_r (Branch2)	
			20.0	17,610	16,970	\$640	\$11,867	1.06	\$80	\$1,483	a_r (Branch2)	
	\$56,440	75	5.0	6,820	6,330	\$490	\$9,723	0.87	\$210	\$4,167	a_r (Branch2)	
			13.0	15,930	15,340	\$590	\$11,708	1.05	\$80	\$1,587	a_r (Branch2)	
			20.0	23,890	23,180	\$710	\$14,089	1.26	\$70	\$1,389	a_r (Branch2)	

Table 4.19 (continued) : Evaluation of VPI and the maximum allowable budget of monitoring bent system.

1	2	3	4	5	6	7	8	9	10	11	12
Initial construction cost	Annual initial construction cost	Expected service period (Year)	Indirect cost factor	Expected annual cost of non-monitored bridge ($C_{\bar{m}}$)	(Expected annual cost of monitored bridge minus monitoring price)	Annual VPI	VPI	Normalised VPI (%)	Maximum Annual Monitoring budget	Maximum Monitoring budget in one instalment	Optimal alternative for non-monitored bridge
\$1,250,000	\$87,800	25	5.0	3,620	3,600	\$20	\$285	0.02	-	-	\bar{a}_r (Branch1)
			13.0	9,390	8,700	\$690	\$9,823	0.79	\$290	\$4,129	a_r (Branch2)
		20.0	13,610	12,920	\$690	\$9,823	0.79	\$160	\$2,278	a_r (Branch2)	
		5.0	5,500	5,230	\$270	\$5,006	0.4	\$60	\$1,112	\bar{a}_r (Branch1)	
	\$67,420	50	13.0	13,100	12,540	\$560	\$10,383	0.83	\$100	\$1,854	a_r (Branch2)
			20.0	19,510	18,840	\$670	\$12,423	0.99	\$80	\$1,483	a_r (Branch2)
		5.0	7,480	7,000	\$480	\$9,525	0.76	\$170	\$3,373	a_r (Branch2)	
		\$62,990	75	13.0	17,640	17,030	\$610	\$12,105	0.97	\$70	\$1,389
20.0	26,540			25,780	\$760	\$15,081	1.21	\$80	\$1,587	a_r (Branch2)	

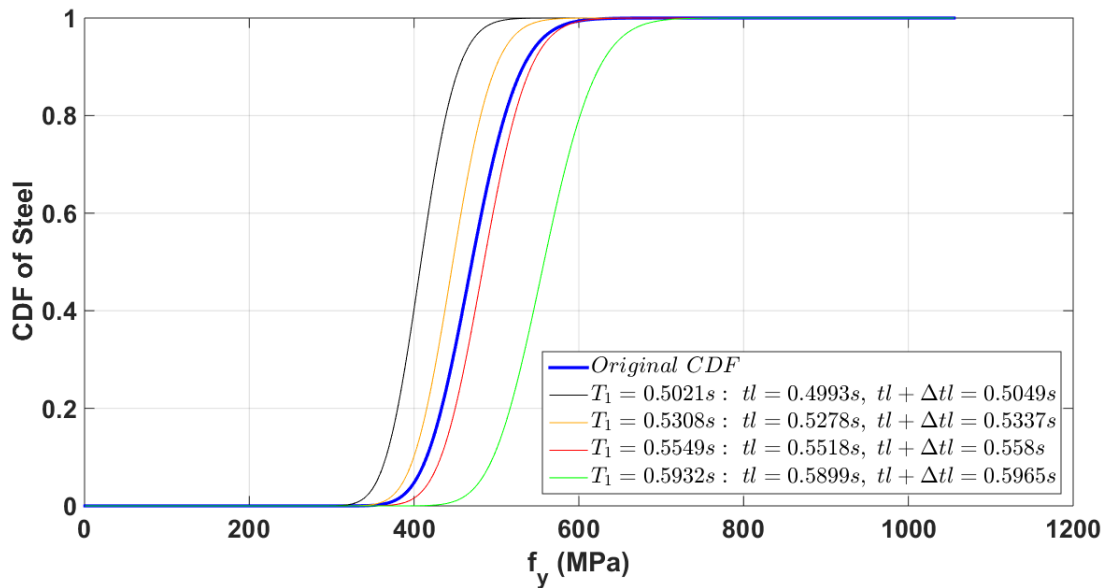


Figure 4.16 : Prior and updated CDFs of steel by different SHM outputs from monitoring the bent system ($\sigma_{inc} = 2.0\%$).

The highlighted rows of Table 4.19 have been selected for a more detailed study. It is seen from those rows that maximum allowable test budget increases with significance of the bridge. Table 4.20 has been established to study reasons of this behaviour. The first and second columns of the table show respectively lower and upper bounds of intervals of SHM system outputs range. Third, fourth and fifth columns show optimal alternatives of the monitored bridge for each interval. For indirect cost factor of 5.0, optimal alternative by monitoring is always the same as the one by non-monitored case (which has been presented in the last row of the table). As a result, information provided by monitoring has no effect on process of decision making. However, for the indirect cost factor of 13.0 and 20.0, it is seen that optimal alternative by monitoring is not always the same as the one for non-monitored case. As a result, additional information from monitoring can influence the decision of retrofitting or not retrofitting the bridge.

Table 4.20 : Comparison of the optimal alternatives selected for the monitored bridge of various significances.

Initial cost = \$1,000,000		Monitored Case		
Expected life-time = 25 years		Indirect Cost Factor		
$\sigma_{ln\epsilon} = 2.0\%$		5.0	13.0	20.0
tl (s)	$tl + \Delta tl$ (s)	$a_r^* T_1(Bent)$	$a_r^* T_1(Bent)$	$a_r^* T_1(Bent)$
0.4993	0.5049	\bar{a}_r	a_r	a_r
0.5049	0.5105	\bar{a}_r	a_r	a_r
0.5105	0.5163	\bar{a}_r	a_r	a_r
0.5163	0.5220	\bar{a}_r	a_r	a_r
0.5220	0.5279	\bar{a}_r	a_r	a_r
0.5279	0.5338	\bar{a}_r	a_r	a_r
0.5338	0.5397	\bar{a}_r	a_r	a_r
0.5397	0.5458	\bar{a}_r	\bar{a}_r	a_r
0.5458	0.5519	\bar{a}_r	\bar{a}_r	a_r
0.5519	0.5580	\bar{a}_r	\bar{a}_r	\bar{a}_r
0.5580	0.5643	\bar{a}_r	\bar{a}_r	\bar{a}_r
0.5643	0.5706	\bar{a}_r	\bar{a}_r	\bar{a}_r
0.5706	0.5769	\bar{a}_r	\bar{a}_r	\bar{a}_r
0.5769	0.5834	\bar{a}_r	\bar{a}_r	\bar{a}_r
0.5834	0.5899	\bar{a}_r	\bar{a}_r	\bar{a}_r
0.5899	0.5965	\bar{a}_r	\bar{a}_r	\bar{a}_r
Non-monitored Case		\bar{a}_r	\bar{a}_r	a_r

Table 4.21 studies effect of error on value of information. The highlighted case in Table 4.19 has been studied. It is observed that the maximum allowable monitoring budget drops as measurement error increases. This behaviour can be understood by observing Figure 4.17 and Figure 4.18 which show original and updated steel CDFs for $\sigma_{ln\epsilon} = 3.0\%$ and $\sigma_{ln\epsilon} = 4.0\%$. It is seen that as error dispersion increases, updated CDFs get closer to the original one. This naturally decreases value of obtained information as results by updated CDFs become closer to the non-monitored case.

Table 4.21 : Effect of error on value of information.

Initial construction cost	Annual initial construction cost	Expected service period (Year)	Indirect cost factor	Expected annual cost of non-monitored bridge ($C_{\bar{m}}$)	(Expected annual cost of monitored bridge minus monitoring price)	Maximum Annual Monitoring budget	Maximum Monitoring budget in one instalment	Optimal alternative for non-monitored bridge	
\$1,000,000	\$70,240	25	$\sigma_{ln\epsilon} = 2.0\%$						
			5.0	2,890	2,890	-	-	\bar{a}_r (Branch1)	
			13.0	7,520	7,120	\$100	\$1,424	\bar{a}_r (Branch1)	
			20.0	11,200	10,530	\$220	\$3,132	a_r (Branch2)	
			$\sigma_{ln\epsilon} = 3.0\%$						
			5.0	2,890	2,890	-	-	\bar{a}_r (Branch1)	
			13.0	7,520	7,480	\$40	\$569	\bar{a}_r (Branch1)	
			20.0	11,200	11,090	\$110	\$1,566	a_r (Branch2)	
			$\sigma_{ln\epsilon} = 4.0\%$						
			5.0	2,890	2,890	-	-	\bar{a}_r (Branch1)	
			13.0	7,520	7,510	\$10	\$142	\bar{a}_r (Branch1)	
			20.0	11,200	11,140	\$60	\$854	a_r (Branch2)	

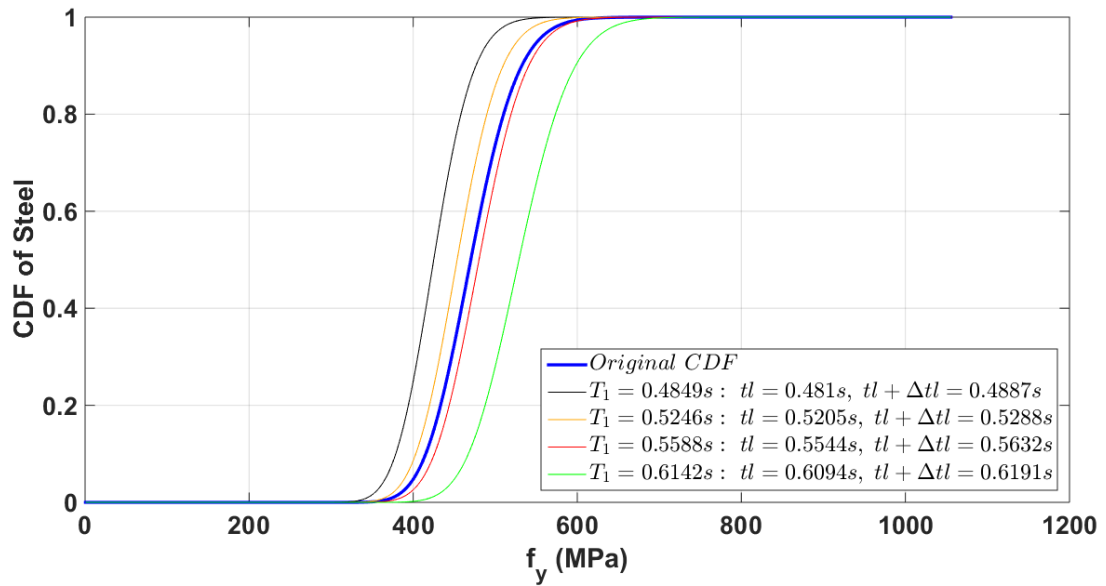


Figure 4.17 : Prior and updated CDFs of steel by different SHM outputs from monitoring the bent system ($\sigma_{nc} = 3.0\%$).

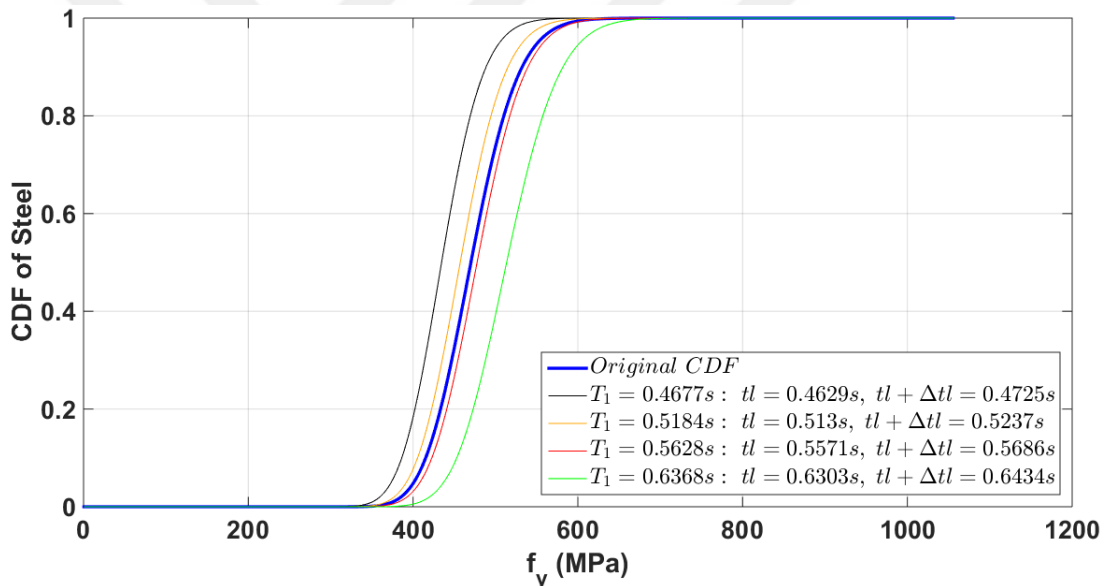


Figure 4.18 : Prior and updated CDFs of steel by different SHM outputs from monitoring the bent system ($\sigma_{nc} = 4.0\%$).

It is important to note that the results presented in this section are obtained for the case of monitoring of the bridge under forced vibrations which result in relatively larger deformations compared to ambient vibrations. Considering Figures 3.6-9 which show variations in cap beam and column moment-curvature diagrams of models for various steel properties, it is obvious that different models behave almost identically for small deformations. However, the difference between moment-curvature analyses outputs of the different models become clearer for larger deformations. Consequently, it is expected that monitoring the bridge for small vibrations (e.g. ambient vibration) will not result in

proper identification of deficiencies in reinforcement steel strength. In the scope of the study, monitoring consists of inferring the modal properties under forced vibration which causes larger deformations. Still however, the proposed approach can be briefly modified to be applicable for the case of small vibrations.



5. CONCLUSIONS AND RECOMMENDATIONS

5.1 Conclusions

The current study on value of information obtained from an SHM system inspecting a two span MSSS concrete bridge led to following results:

1. After establishing finite element model of the bridge in the first chapter, a study was conducted in the second chapter to select the uncertainty random variable for the model.

Two candidate parameters were selected for this purpose: strength of unconfined concrete and yield stress of reinforcing bars.

Several models were constructed using differing values of the two parameters. Afterwards, changes in structural properties due to variations in both parameters were examined. Outputs from moment-curvature analyses showed that moment-curvature results did not differ considerably with changes in concrete strength. Nonetheless, moment-curvature analysis results of samples made from various steel properties showed greater variations. Consequently, yield strength of steel bars was selected as the uncertain model parameter.

2. Models made from varying steel properties were analysed using the 2000 SAC/FEMA method. The objective was to assess failure probabilities of each model in terms of the four limit states defined earlier. It was also meant to see if a relation could be established between yield strength of reinforcing bars and failure probabilities of models made from them. Calculations showed that such a relation existed and a linear regression line could be well fitted to the points of steel strength – failure probability pairs. It was also noticed that probabilities of failure in terms of all limit states were dropping with increase in steel strength value.

3. Chapter 4 mainly addressed two issues. The first issue was to study feasibility of retrofitting the bridge using principles of maximum expected monetary value criterion. Failure probabilities in terms of different limit states calculated in Chapter 3 were utilised for assessing damage probabilities. Direct and indirect expenses associated with damage levels and costs of retrofitting were taken into account. The analyses showed that feasibility of retrofitting is a function of initial construction cost, significance of the

bridge and expected service period of the structure. To be more exact, it was concluded that as initial construction cost, bridge significance and expected life-time increases, retrofitting becomes more feasible.

4. The second issue addressed in Chapter 4 was studying the feasibility of monitoring the bridge based on value of information obtained. It was assumed that the SHM system was only able to monitor one parameter. As the first try, fundamental period of vibration of the bridge was selected as the monitoring parameter and annual monitoring expenses related to such a simple control were estimated. It was observed that value of the acquired information is a function of initial construction cost, significance of the bridge, expected service life of the structure and errors related to modelling and measurement. Particularly, it was realised that value of information decreased significantly as dispersion of error grew. Calculations showed that value of obtained information was much less than the estimated monitoring costs for a monitoring with 2.0% error dispersion. Even value of perfect information from an errorless monitoring was in most cases less than the estimated expenses. The reason for this behaviour was attributed to insensitivity of the fundamental period of the bridge to changes in steel strength.

5. As the second try, fundamental period of the bent system of the bridge was considered as the monitoring parameter. The reason for this selection was the relatively greater changes in the fundamental period of the bent system with steel properties. It was realised that for a certain amount of error dispersion, value of information obtained from monitoring the fundamental period of the bent system was greater than the information value obtained from monitoring the fundamental period of the complete bridge. Value of perfect information obtained from monitoring both parameters showed little differences although it was slightly greater for the case of monitoring the bent system.

6. For a number of cases with different initial construction costs, expected service periods, indirect cost factors and errors, the maximum monetary budget that can be allocated to monitoring was calculated. It was realised that the maximum money distributable on monitoring does not have a direct relation with initial construction cost, expected service period or importance of the bridge. In other words, the maximum distributable budget could be greater for bridges with less construction expenses, shorter life-times and smaller significances. Nonetheless, the maximum allocatable budget and value of obtained information always reduced by increase in dispersion of error.

5.2 Recommendations

1. Pile foundations, subsurface soil, wingwalls and abutment backfill soil were not modelled in this study. A more realistic analysis could be performed if these components are modelled. Particularly, such an analysis could give a better insight about modal properties of the bridge and bridge components.
2. The structure examined in this study is a two span MSSS concrete bridge with elastomeric bearings. It may be interesting if bridges of other classes (MSC steel, etc.) with other types of bearings (fixed, rocker, etc.) are also investigated. Possible variability in value of information obtained from monitoring structural properties of various classes of bridges with different types of bearings could be worth to study.
3. In the context of this study, material properties were considered as model uncertainty variables. However, a wide range of other parameters could be selected as the uncertain model parameter. For instance, an investigation could be performed by taking depth of scouring as the uncertain parameter if information exists about soil and bridge foundation properties.
4. In this study, limit states were defined using normalised curvatures. The maximum value of normalised curvatures over the structure over time was used to control if a certain limit state condition was satisfied. This approach simplifies things; however, it is an approximation as it ignores interdependencies between various components. Consequently, a more advanced study could be conducted considering those interdependencies.



REFERENCES

- Agdas, D., Rice, J. A., Martinez, J. R., & Lasa, I. R. (2016). Comparison of visual inspection and structural-health monitoring as bridge condition assessment methods. *Performance of Constructed Facilities*, 30(3).
- Alampalli, S., & Ettouney, M. (2008). Role of structural health monitoring in bridge security. *Bridge Structures*, 4, 143-154.
- Ang, A. H-S.; Tang, W. H. (1984). *Probability Concepts in Engineering Planning and Design* (Vol. II). Republic of Singapore: John Wiley & Sons.
- Avşar, Ö. (2009). *Fragility based seismic vulnerability assessment of ordinary highway bridges in Turkey*. (Doctoral dissertation). Middle East Technical University, ANKARA.
- Baker, J. W. (2008). *An introduction to probabilistic seismic hazard analysis (PSHA)*. Stanford, USA: Stanford University.
- Barth, F. G. (1993). Engineered demolition of earthquake-damaged bridge structures. *Concrete construction*, 38(7), 480-486.
- California Department of Transportation. (2006). *Visual Catalog for Reinforced Concrete Bridge Damage*. California, USA: California Department of Transportation.
- Caltrans. (2006). *Seismic design criteria version 1.4*. Sacramento, California, USA: California Department of Transportation.
- Cao, J., & Liu, X. (2016). *Wireless sensor networks for structural health monitoring*. Springer International Publishing AG.
- Chen, W. F., & Duan, L. (2014). *Bridge engineering handbook, second edition: Substructure design* (2nd ed.). Boca Raton, Florida, USA: CRC Press.
- Chopra, A. K. (2012). *Dynamics of structures. Theory and applications to earthquake engineering* (Fourth ed.). Boston, USA: Prentice Hall.
- Cornell, C. A., Jalayer, F., Hamburger, R. O., & Foutch, D. A. (2002). Probabilistic basis for 2000 SAC Federal Emergency Management Agency steel moment frame guidelines. *Journal of Structural Engineering*, 128(4), 526-533.

- Diotallevi, P. P., & Landi, L. (2005). On the pushover analysis as a method for evaluating the seismic response of RC buildings. *Earthquake Resistant Engineering Structures*, 81, 203-217.
- Dündar, O., Polat, M., & Tanış, M. (2015). Ülkemiz köprü gözlem ve yöntemi üzerine karşılaştırmalı bir değerlendirme. 7. *Kentsel Altyapı Sempozyumu*. Trabzon, Türkiye.
- European Asphalt Pavement Association (EAPA). (2013). *Asphalt pavements on bridge decks*. Brussels, Belgium: European Asphalt Pavement Association.
- Faber, M. H., & Thöns, S. (2014). On the value of structural health monitoring. *22nd Annual Conference on European Safety and Reliability* (pp. 2535-2544). Wroclaw, Poland: CRC Press.
- Fardis, M. N., & Biskinis, D. E. (2003). Deformation capacity of RC members, as controlled by flexure or shear. *Otani Symposium*. Tokyo, Japan.
- Florida Department of Transportation. (2018). *Structures Design Guidelines*. Structures Design Office.
- Itani, R., & Liao, X. (2003). *Effects of retrofitting applications on reinforced concrete bridges*. Washington: Washington State Transportation Center (TRAC) Civil and Environmental Engineering.
- Jackson, B. (1998). Replacing Oakland's Cypress Freeway. *Public Roads*, 61(5).
- Jones, P. (2011). *Inspection guidance for bridge expansion joints; Part 1 – Reference guide*. Cambridge, England: The Bridge Research Group at Cambridge University.
- Liu, M., Frangopol, D. M., & Kim, S. (2009). Bridge system performance assessment from structural health monitoring: A case study. *Journal of Structural Engineering*, 135(6), 733-742.
- Lupoi, G., Lupoi, A., & Pinto, P. E. (2002). Seismic risk assessment of RC structures with the "2000 SAC/FEMA" method. *Journal of Earthquake Engineering*, 6(4), 499-512.
- Mander, J. B. (1983). *Seismic design of bridge piers*. (Doctoral dissertation). University of Canterbury, Canterbury, New Zealand.
- Mander, J. B., Priestley, M. J., & Park, R. (1988). Theoretical stress-strain model for confined concrete. *Journal of Structural Engineering*, 114(8), 1804 - 1826.
- McKenna, F., Scott, M. H., & Fenves, G. L. (2010). Nonlinear finite-element analysis software architecture using object composition. *Computing in Civil Engineering*, 95-107.

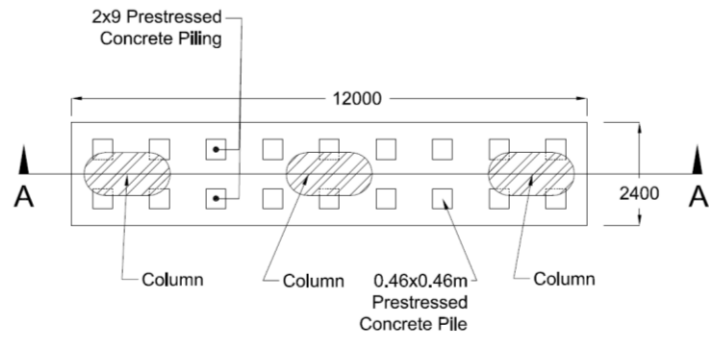
- Nowak, A. S., & Collins, K. R. (2000). *Reliability of structures*. United States of America: McGraw- Hill Higher Education.
- Olson, L. D. et al. (2005). *Dynamic bridge substructure evaluation and monitoring*. U.S. Department of Transportation, Federal Highway Administration. McLean, Virginia, USA: Turner-Fairbank Highway Research Center.
- Omenzetter, P., Limongelli, M. P., & Yazgan, U. (2016). Quantifying the value of seismic structural health monitoring of buildings. *8th European Workshop on Structural Health Monitoring, EWSHM 2016* (pp. 510-519). Bilbao, Spain: NDT.net.
- Padgett, J. E., & DesRoches, R. (2009). Retrofitted Bridge Fragility Analysis for Typical Classes of Multispan Bridges. *Earthquake Spectrum*, 25(1), 117-141.
- Padgett, J. E., Dennemann, K., & Ghosh, J. (2010). Risk-based seismic life-cycle cost–benefit (LCC-B) analysis for bridge retrofit assessment. *Structural Safety*, 32, 165–173.
- Pinto, P. E., & Giannini, R. (2004). *Seismic reliability analysis of structures*. Pavia, Italy: IUSS Press.
- Popov, E. P. (1990). *Engineering mechanics of solids*. (H. W. J., Ed.) Englewood Cliffs, New Jersey, USA: Prentice- Hall International Series in Civil Engineering and Engineering Mechanics.
- Pozzi, M., Zonta, D., Wang, W., & Chen, G. (2010). A framework for evaluating the impact of structural health monitoring on bridge management. In D. Frangopol, R. Sause, & C. Kusko (Ed.), *Proceedings of the 5th international conference on bridge maintenance, safety and management (IABMAS 2010)*. Philadelphia, USA: CRC Press.
- Priestley, M. J., Calvi, G. M., & Kowalsky, M. J. (2007). *Displacement based seismic design of structures* (1 ed.). Pavia, Italy: IUSS Press.
- Priestley, M. J., Seible, F., & Calvi, G. M. (1996). *Seismic design and retrofit of bridges*. United States of America: John Wiley & Sons, Inc.
- Ramberger, G. (2002). *Structural bearings and expansion joints for bridges*. Zurich, Switzerland: International Association for Bridge and Structural Engineering.
- Scott, M. H., & Fenves, G. L. (2006). Plastic hinge integration methods for force-based beam–column elements. *Journal of Structural Engineering*, 244-252.
- Task Group 7.4 of fib, The International Federation for Structural Concrete. (2007). *Seismic bridge design and retrofit – structural solutions*. Stuttgart, Germany: Sprint-Digital-Druck.

- TEC, Turkish Earthquake Code. (2007). *Specification for structures to be built in disaster*. Turkey: Ministry of Public Works and Settlement Government of Republic of Turkey.
- Thöns, S., Döhler, M., & Long, L. (2018). On damage detection system information for structural systems. *Structural Engineering International*, 255-268.
- TSO (The Stationery Office). (2007). *Inspection manual for highway structures* (Vol. 1). London: The Stationery Office.
- Wilson, E. (2002). *Three dimensional static and dynamic analysis of structures*. Berkeley, California, USA: Computers and Structures, Inc.
- Xia, J., Jin, W., Zhao, Y., & Li, L. (2013). Mechanical performance of corroded steel bars in concrete. *Proceedings of the Institution of Civil Engineers-Structures and Buildings*, 235–246.
- Yashinsky, M. (1998). *The Loma Prieta, California, earthquake of October 17, 1989—highway systems*. Washington, USA: U.S. Geological Survey.
- Zhu, L., Fu, Y., Chow, R., Spencer Jr., B. F., Park, J. W., & Mechtov, K. (2018). Development of a high-sensitivity wireless accelerometer for structural health monitoring. *Sensors*, 18(1).
- Zonta, D., Glisic, B., & Adriaenssens, S. (2014). Value of information: impact of monitoring on decision-making. *Structural Control and Health Monitoring*, 21(7), 1043-1056.

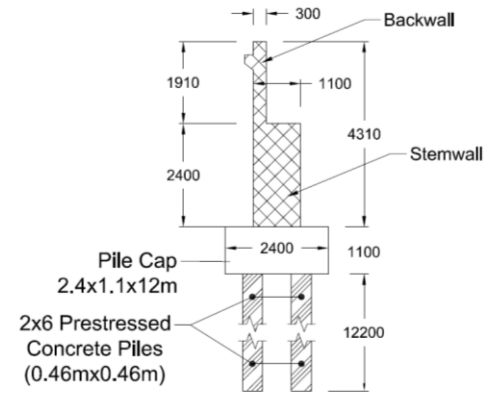
APPENDICES

APPENIX A: Complementary Drawings

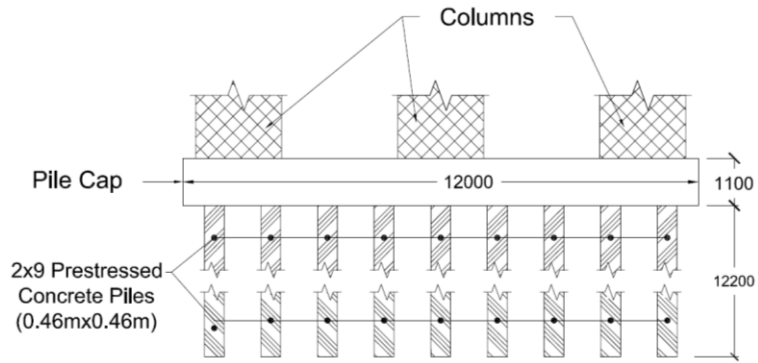




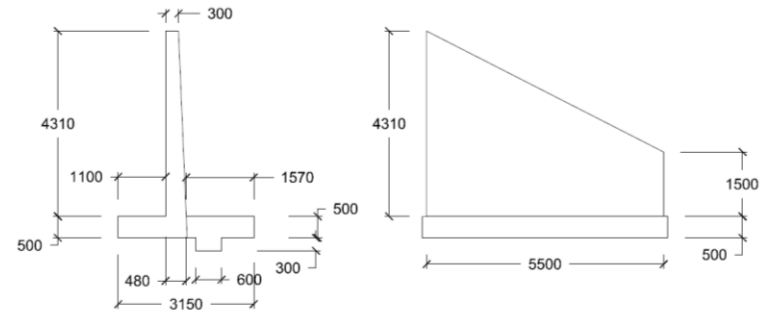
Plan View - Bent System Pile cap



Abutment & Footing Dimensions



Section A - A



Wingwall Dimensions

Note: All dimensions are in mm

Figure A.1: Complementary drawings

CURRICULUM VITAE

Name Surname : Siamak Tahaei Yaghoubi

Place and Date of Birth : Tabriz, Iran 14.09.1980

E-Mail : tahaeiyaghoubi@itu.edu.tr

EDUCATION

B.Sc. : 18.02.2004, Islamic Azad University of Tabriz, Civil Engineering – Civil

M.Sc.: 16.09.2010, Sahand University of Technology, Marine Structures